

**AMORPHOUS SELENIUM FILMS USING CBD:
A NOVEL SELENISATION TECHNIQUE FOR
PREPARING INDIUM SELENIDE AND
COPPER INDIUM SELENIDE THIN FILMS**



**Thesis submitted to
COCHIN UNIVERSITY OF SCIENCE & TECHNOLOGY
for the award of the degree of
DOCTOR OF PHILOSOPHY**

**By
Bindu K.**

**DEPARTMENT OF PHYSICS
COCHIN UNIVERSITY OF SCIENCE AND TECHNOLOGY
COCHIN - 682 022, INDIA**

MAY 2002




Department of Physics
Cochin University of Science and Technology
Cochin – 682 022

CERTIFICATE

Certified that the work presented in this thesis entitled “**Amorphous Selenium films using CBD: A Novel Selenisation technique for preparing Indium Selenide and Copper Indium Selenide Thin Films**” is based on the bonafide research work done by Ms. Bindu K. under my guidance in the Department of Physics, Cochin University of Science and Technology, Cochin – 682 022, and has not been included in any other thesis submitted previously for the award of any degree.

Cochin - 22
03.05.2002


Prof. K. P. Vijayakumar
(Supervising Guide)

DECLARATION

Certified that the work presented in this thesis entitled “**Amorphous Selenium films using CBD: A Novel Selenisation technique for preparing Indium Selenide and Copper Indium Selenide Thin Films**” is based on the original research work done by me under the guidance and supervision of **Prof. K. P. Vijayakumar**, Department of Physics, Cochin University of Science and Technology, Cochin - 22 and has never been included in any other thesis submitted previously for the award of any degree.

Cochin - 22
03.05.2002


Bindu K.

Acknowledgement

With great pleasure I express my sincere gratitude to my supervising guide, Dr. K P Vijayakumar, Professor, Dept. of Physics, Cochin University of Science and technology, for his excellent guidance and constant encouragement. His insight and objective thinking about research problems were an inspiration for me during the course of this work.

I am greatly indebted to Dr. C Sudha Kartha for her advice and keen interest shown in my work.

I am thankful to Prof. Elizabeth Mathai, Head of the Dept. of Physics, Prof. K P Rajappan Nair, Prof. M Sabir, and Prof. K Babu Joseph former heads of the dept. of Physics for providing me the necessary facilities. With pleasure, I thank all the faculty members and all non-teaching staff of the Dept. of Physics for their help.

In the course of the present work, for material characterization we made use of the facility available at Iwate University, through our collaboration with Prof. Y Kashiwaba of the same institute. I am indebted to him and his student, T Abe for helping with XPS measurements. I am grateful to Dr. Yasube, Lecturer, Sendai National College of Technology, Japan for thickness measurement. I am thankful to Director, Sree Chithra Tirunal Institute for medical Sciences & Technology for granting me the permission for SEM analysis, Mr. Sree Kumar for helping me to carry out the analysis. The Head, RSIC Madras for XPS analysis and director, Indian Rare Earths (IRE) for ICP analysis.

I thankfully acknowledge the financial assistance from University Grants Commission (UGC) and Council of Scientific and Industrial Research (CSIR), Govt. of India, in the form of research fellowship. The support from UGC through DSA-COSIST schemes is also gratefully acknowledged. I would like to thank ANERT for providing financial support for the research work.

Words are insufficient to express my gratitude to my colleagues and friends for their support throughout my research career. I am also thankful to my seniors for their moral support.

Last but not least, I thank all my well wishers.

CONTENTS

Preface

List of Publications

CHAPTER 1

THIN FILM PHOTOVOLTAICS: AN INTRODUCTION

1.1 Photovoltaics: An unlimited electrical energy from the sun.....	1
1.2 Performance of a solar cell	3
1.3 Basic material requirements for low cost solar cells	6
1.4 Important thin film solar cell materials.....	9
1.5 CuInSe ₂ – Material for the present investigation	12
1.6 Low cost-hybrid deposition processes opted in the present work	24
1.7 Characterization techniques.....	31
References.....	40

CHAPTER 2

CONVERSION OF COPPER SELENIDE INTO COPPER INDIUM SELENIDE BY DIFFUSING INDIUM: AN ATTEMPT

2.1 Introduction.....	46
2.2. Experimental details	47
2.3 Characterization.....	51
2.4 Conclusion.....	64
References.....	65

CHAPTER 3

AMORPHOUS SELENIUM (a-Se) FILMS USING CBD: DEPOSITION AND CHARACTERIZATION

3.1 Introduction.....	67
3.2 A brief review on a-Se thin films.....	67
3.3 Preparation of a-Se using CBD	69

3.4 Characterization.....	74
3.5 Results and discussions	81
3.6 Conclusion.....	82
References.....	84

CHAPTER 4

PREPARATION OF INDIUM SELENIDE FILMS BY SELENISATION OF INDIUM USING α -Se FILMS

4.1 Introduction.....	86
4.2 Review of works on indium selenide	87
4.3 Experimental.....	88
4.4 Characterization.....	90
4.5 Conclusion.....	115
References.....	116

CHAPTER 5

DEPOSITION OF COPPER INDIUM SELENIDE THIN FILMS THROUGH MULTISTAGE PROCESSES AND CHARACTERIZATION

5.1 Introduction	118
5.2 Part A: SEL process	118
5.2.1 Preparation.....	119
5.2.2 Characterization	120
5.2.3 Discussion.....	153
5.3 Part B: Thermal diffusion of Cu into In_2Se_3 film.....	155
5.3.1 Experimental details.....	156
5.3.2 Characterization	156
5.3.3 Discussion.....	167
5.4 Conclusion	168
References.....	169

CHAPTER 6

RECOVERY AND REUSE OF SELENIUM PRECIPITATE FROM CHEMICAL BATH

6.1 Introduction.....	171
6.2 Experimental.....	172
6.3 Characterization.....	172
6.4. Results and discussions.....	179
6.6 Conclusion.....	180
References.....	181

CHAPTER 7

SUMMARY AND CONCLUSIONS.....	182
------------------------------	-----

Preface

Photovoltaics is one of the most fascinating ways for direct solar energy conversion. Solar cell technology has been undergoing enormous developments for the last few decades, initially providing electrical power for spacecraft and recently for terrestrial systems. Photovoltaics has the potential to become an alternative to the use of fossil fuels if mass production of PV modules on an industrial scale is established. About 90% of today's demand for photovoltaics is met by crystalline silicon based solar cells. In order to produce economically viable PV systems, thin film technology has been developed to achieve substantial reduction in cost, so as to compete in the power market with other conventional and established energy sources.

The main advantage of thin film solar cells is the capability to produce low cost electric power. This is mainly because these types of cells require low quantity of materials even when they have large area. Moreover, large scale fabrication is feasible. Different types of techniques available for thin film deposition make it possible to try new compound semiconductors for better solar cells and this is a unique speciality of thin film cells. Presently through intensive research work, three semiconducting materials have been identified for large scale production of thin film solar cell. They are amorphous silicon, cadmium telluride and copper indium selenide.

Amorphous Si could recently achieve an efficiency of 13.5%. But radiation induced defects (Stabler-Wronsky defect) formation reduces the efficiency during continuous illumination. CdTe based cells have reached a maximum efficiency of 16%. The problems associated with this type of cells are lack of completely optimized manufacturing set up and those related to stability of the cells and usage of poisonous cadmium and tellurium. Cu(Ga,In)Se₂ based solar cells have been achieved the best efficiency more than 18% which results in the extensive research in CIS based cells by several groups all over the world. However, it remains yet to produce large area films at low cost using ecofriendly technique.

In the present work, we describe our efforts to develop device quality CuInSe_2 films through low cost, simple and eco-friendly hybrid techniques. The most important point to be highlighted here is that the method fully avoids the use of poisonous gases such as $\text{H}_2\text{Se}/\text{Se}$ vapour. Instead, selenisation is achieved through solid state reaction between amorphous selenium and polycrystalline metal layers resulting in both binary and ternary selenides. Thin films of amorphous selenium (a-Se) used for this is deposited using Chemical Bath Deposition (CBD). CuInSe_2 films are prepared through the selenisation process. Another PV material, indium selenide (In_2Se_3) thin films are also prepared using this process. The whole work described in this thesis is organized into seven chapters discussed below.

CHAPTER 1 begins with a general introduction on the significance of thin films in photovoltaics. In this chapter there is a brief coverage on important semiconductors for solar cell application, after which an elaborate review on preparation and characterisation of CIS and related alloy thin films and also, CIS based solar cells. Preparation techniques, chemical bath deposition and vacuum evaporation used in the present study are then described. Details of the characterisation techniques used in this work such as Scanning Electron Microscopy for morphological studies, X-ray diffractometry (XRD) for structural analysis, X-ray Photoelectron Spectroscopy (XPS) and Secondary Ion Mass Spectroscopy (SIMS) for elemental analysis are included in this chapter. Details of optical and electrical characterization techniques are also explained at the end of this chapter.

CHAPTER 2 starts with a description on direct deposition of copper indium selenide using CBD. After hinting at difficulties of this technique in controlling the bath parameters, which determines the ternary compound formation, advantages of adopting this method for preparing binary compound is described. The attempt of conversion of binary compound, Cu_2Se into ternary compound, CuInSe_2 by thermal diffusion of vacuum evaporated indium layer is then included. In order to compensate for selenium deficiency of the films

obtained, idea of deposition of selenium using CBD also mentioned in this chapter.

CHAPTER 3 begins with a review of conventional studies on Se thin films. Then the process of preparation and characterisation of amorphous selenium thin films using CBD is described.

In **CHAPTER 4**, includes preparation and characterization of indium selenide thin films by selenisation technique using a-Se film deposited from CBD is included. Selenisation is done by Stacked Elemental Layer (SEL) technique. Structural, compositional, electrical and optical characterisation are included in this chapter. A brief report about the preparation of copper selenide by annealing the bilayer Se/Cu is also described towards the end of this chapter.

Preparation and characterisation of CIS by two different methods are the central theme of the **CHAPTER 5**. This chapter is organized into two sections. First part detailed studies on preparation and characterization of CIS films by annealing multilayer structure, Se/In/Cu deposited sequentially. Second part is preliminary investigations on preparation and characterization of CIS films by diffusion of copper into indium selenide films.

Large scale usage of CBD technique for depositing selenium film, we face into the difficulties dealing with the precipitate available in the bath used for the CBD process. In the present work we developed process for the reuse of selenium precipitate in the bath. Detailed description of the process for recovery of the precipitate formed during selenium film preparation for further deposition process is included in **CHAPTER 6**.

CHAPTER 7 deals with the summary of the work and conclusions from all the studies on all the type of films.

LIST OF PUBLICATIONS

Journal papers

1. Structural, optical and electrical properties of In_2Se_3 thin films formed by annealing chemically deposited Se and vacuum evaporated In stack layers
Bindu K., Sudha Kartha. C, Vijayakumar. K.P, Abe. and Kashiwaba.Y,
Applied surface science (In Press)
2. Amorphous Selenium thin films prepared using CBD: Optimization of the deposition process and Characterization
Bindu. K, Lakshmi. M, Bini. S, Sudha Kartha. C, Vijayakumar. K.P, Abe. and Kashiwaba.Y, *Semiconductor Science and Technology*, 17 (2002) 270
3. Reversible $\text{Cu}_{2-x}\text{Se} \leftrightarrow \text{Cu}_3\text{Se}_2$ phase transformation in copper selenide thin films prepared by chemical bath deposition
Lakshmi M., **Bindu K.**, Bini. S, Vijayakumar. K.P Sudha Kartha. C, Abe. T and Kashiwaba.Y, *Thin Solid Films* 386 (2001)127
4. Chemical bath deposition of different phases of copper selenide thin films by controlling bath parameters
Lakshmi. M, **Bindu. K** , Bini. S, Vijayakumar. K.P Sudha Kartha. C, Abe. T and Kashiwaba.Y, *Thin Solid Films*, 370, (2000) 89
5. Preparation of CuInS_2 thin film using CBD Cu_xS films.
Bini S., **Bindu K.**, Lakshmi M.,Sudha Kartha C., Vijayakumar K.P. Kashiwaba Y, and Abe T , *Renewable Energy*, 20 (2000) 405
6. Study of trap levels by electrical techniques in p-type CuInSe_2 thin films prepared using chemical bath deposition
Zeenath. N. A. Vidyadharan Pillai P K, **Bindu K.**, Lakshmi M and Vijayakumar K. P,
J. of Material Science 35 (2000)1

Conference papers: International/ National

1. Recovery and reuse of selenium precipitate from chemical bath – A new approach for selenisation process to prepare CuInSe₂ thin films
Bindu K., Jayaprasad A., Sudha Kartha. C, Vijayakumar. K.P, Abe. T and Kashiwaba.Y, Accepted for *World Renewable Energy Congress*, Cologne, June 29, 2002
2. A simple and safe selenisation technique of Cu/In multilayer for preparing CuInSe₂ thin films
Bindu. K, Lakshmi. M, Bini. S, Sudha Kartha. C, Vijayakumar. K.P, Abe. T, Kashiwaba.Y, National Symposium on Science and Tehnology of vacuum and thin films (IVSNS-2001)-PP33
3. Structural and Optical absorption changes of chemically prepared Cu_{2-x} Se due to Indium diffusion
K. Bindu, M. Lakshmi, S. Bini, C Sudha Kartha and K. P.Vijayakumar.DAE, Solid State Physics Symposium, IGCAR, Kalpakkam, Dec 20 –24, 1998
4. CBD – A technique to prepare different phases of Copper Selenide
K. Bindu, M. Lakshmi, S. Bini, C Sudha Kartha andK. P.Vijayakumar.DAE. Solid State Physics Symposium, Kurukshetra University, Kurukshetra ,Dec 27 –31,1998
5. CuInS₂ thin film using a new technique
S. Bini, **K. Bindu**, M. Lakshmi, C Sudha Kartha and K. P.Vijayakumar.
DAE, Solid State Physics Symposium, Kurukshetra University,
Kurukshetra Dec 27 –31,1998
6. Preparation of Pyrite (FeS₂) Thin Films Using Chemical Bath Deposition Technique:
An attempt
M.Lakshmi, **K.Bindu**, S.Bini, C.Sudha Kartha, and K.P.Vijayakumar,
ANERT National Conference , Trivandrum, Feb 1999.

CHAPTER I

THIN FILM PHOTOVOLTAICS: AN INTRODUCTION

1.1 Photovoltaics: An unlimited electrical energy from the sun

In today's world of growing energy needs and increasing environmental concern, alternatives for the use of non-renewable and polluting fossil fuels have to be found out. The alternative is solar energy in the form of wind, solar energy, biomass and hydroelectric etc.

Solar energy is simply the energy produced by the sun and collected in different forms, on the Earth. The sun creates energy through thermonuclear fusion process that involves conversion of hydrogen to helium every second. This process liberates a lot of energy in the forms of heat and electromagnetic radiation. The heat remains in the sun and is instrumental in maintaining the thermonuclear reaction. The electromagnetic radiation (including visible light, infra-red light, and ultra-violet radiation) streams out into space in all directions.

Energy requirement of the world can be supplied directly by solar power, which is only a fraction of total energy produced by the sun. Two major advantages of solar power over fossil fuels are the fact that it is completely non-polluting and available for a much longer period.

Photovoltaics (PV) is a high-tech approach to convert sunlight directly into electrical energy. This electricity is direct current and can be directly used, or can be converted to alternating current or can be stored for later use. Conceptually, in its simplest form a photovoltaic device is a solar-powered generator (solar cell) which only consumes solar radiation as fuel. There are no moving parts to wear out; operation is environmentally benign; and if the device is encapsulated, then it has a long life without break down and maintenance. As sunlight is universally available, these can be used anywhere in our planet. Photovoltaic systems are modular, and hence these are suitable for milliwatt and megawatt applications.

PV has the potential to become a major energy source without giving any impact on the global environment. In order to realize this potential, mass production of PV modules on an industrial scale has to be established which must be inexpensive, durable and efficient product.

In 1839, Edmund Becquerel noticed that sunlight absorbed by certain materials can produce small quantities of electricity in addition to heat. Initially, this phenomenon was limited to the use of light detector. Then improved technological advances in material processing and the needs of the emerging space program led to the development of PV cells.

Most of the PV cells in the market today operate at an efficiency of less than 15%; i.e, less than 15% of the radiation falling on the cell is converted to electricity. Maximum theoretical efficiency for a photovoltaic cell is only 32.3% [1, 2], and at this efficiency, solar electricity is very economical. Interestingly most of our conventional techniques of electricity generation are less efficient than this. Unfortunately, the modular efficiency is much lower than 15 %. Even though this may not be quite economical for large scale production, it is fine for indoor applications and lighting. However, hope for bulk solar electricity should not be abandoned as very recently solar cell with an efficiency of 28.2% [2] has been fabricated in a laboratory.

About 90% of today's demand for photovoltaics is met by crystalline silicon solar cells as silicon (Si) semiconductor technology is fairly advanced due to its large scale application in digital/analog electronic industries. Over the past fifty years PV technology along with Si electronics, has become increasingly advanced. However, it is clear that the low optical absorption coefficient ($\approx 10^4 \text{ cm}^{-1}$) and energy band gap of this material (1.1 eV) were not ideal for PV generation, and scientists have been developing materials whose electrical and optical properties are suitable for high conversion efficiency and low cost. Due to advancement of silicon processing technology and availability of technical data, this material is still being used for photovoltaic conversion with increasing success.

In order to produce economically viable PV systems, a new technology, viz., polycrystalline thin film (PTF) technology, has been developed. We now

realize that PTF solar cells have the potential to meet or exceed the performance of a traditional commercial Si technology with a better possibility for power production at low cost. This is mainly because these types of cells require low quantity of materials even when they have large area. Moreover, large-scale fabrication is feasible, through simple and low cost techniques.

1.2 Performance of a solar cell

In order to understand many aspects of photovoltaic devices, one must know the principle. Basic phenomenon behind photovoltaic is the process of generation of electron – hole (e-h) pairs due to the absorption of photon by a semiconducting material. This e-h pair can be separated by an internal built-in electric field and collected at two contacts, which gives rise to a photocurrent, if the two contacts are connected to an external load. A variety of techniques are developed to produce this built in electric field. For the operation of solar cell, the most widely used techniques are pn-homojunction diodes, heterojunction diodes and Schottky diodes.

When a pn-junction is formed, instantaneously positive and negative electrical charges redistribute, establishing internal electric fields that determine, in part, properties of the semiconductor diode. At the instant of junction formation, the concentration of electrons is much larger on n-side while that of holes is higher on the p side. Large difference in carrier concentrations sets up an initial diffusion current resulting a region, near the junction, that is depleted of majority carriers- (i.e, electrons on the n side and of holes on the p side). The region has a space-charge layer with high electric field. Thus in the absence of externally applied potentials, no further current will flow across the junction. The behaviour of the junction under forward and reverse bias, can be described by the ideal-diode equation [3, 4]:

$$I = I_0 \left[\exp\left(\frac{eV}{kT}\right) - 1 \right] \quad (1)$$

Where, I is the external current flow, I_0 is the reverse saturation current, V is the applied voltage, k is the Boltzmanns constant, and T is the absolute temperature. Again, I_0 can be expressed as,

Where, I is the external current flow, I_0 is the reverse saturation current, V is the applied voltage, k is the Boltzmanns constant, and T is the absolute temperature. Again, I_0 can be expressed as,

$$I_0 = I_{s0} \exp\left(-\frac{E_g}{kT}\right) \quad (2)$$

I_{s0} depends on surface recombination velocities and lifetime of carriers. From eq.(2), it is clear that I_0 varies with the temperature of the junction and hence depends on the intrinsic-carrier concentration. This is larger for materials with smaller band gaps than for those with large band gap.

If light impinges on a p-n junction device, the equilibrium conditions are disturbed. Minority carriers-that is, electrons in the p material and holes in the n material-are created in large quantities resulting in a heavy minority current across the junction. This leads to an increase in concentration of electrons in n-side and holes on p-side lowering the potential energy barrier at the junction (as if a forward bias is applied), correspondingly a voltage is established at the external terminals. These excess carriers can flow through the external circuit to do work.

Photovoltaic device can be modeled as an ideal diode parallel to a light-induced current generator I_L , whose magnitude is controlled by the generation of electron-hole pairs by the absorption of incoming light and the collection efficiency of the junction. Equivalent circuit is given in fig.1.1.

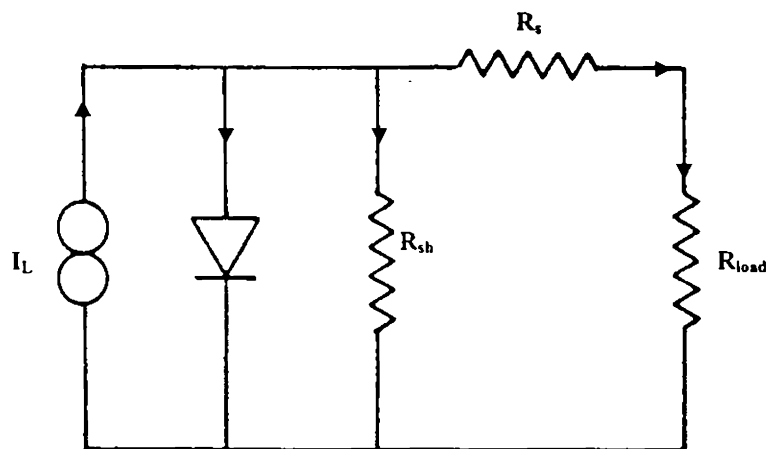


Figure 1.1: Equivalent circuit of a solar cell

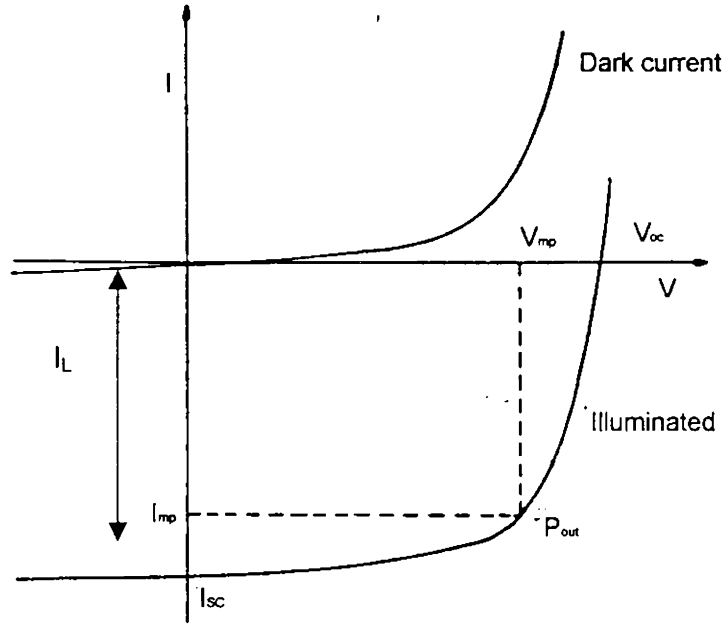


Figure 1.2: I-V characteristic of a solar cell under dark and illuminated conditions

The current and voltage characteristics of the diode are modified by light to [3]

$$I = I_0 \left[\exp\left(\frac{eV}{kT}\right) - 1 \right] - I_L \quad (3)$$

There will be resistive losses due to series (R_s) and shunt resistance (R_{sh}). A current-voltage diagram, shown in fig.1.2 gives the important operational parameters of the cell, which are “short-circuit current” (I_{sc}), “open-circuit voltage” (V_{oc}), and current and voltage at the maximum power point (I_{mp} and V_{mp}) respectively). The maximum power output from a solar cell is simply the product of I_{mp} and V_{mp} . Usually another parameter called fill factor FF is also defined, as

$$FF = \frac{V_{mp} I_{mp}}{V_{oc} I_{sc}} \quad (4)$$

The figure of merit for solar cell performance is the conversion efficiency η , defined as

$$\eta = \frac{V_{mp} I_{mp}}{V_{oc} I_{sc}} \quad (5)$$

Input power P_{in} is

$$P_{in} = A \int_0^{\infty} F(\lambda) \left(\frac{hc}{\lambda} \right) d\lambda \quad (6)$$

Here A is the device area, $F(\lambda)$ is the number of photons incident per square centimeter per second per unit bandwidth incident on the device at wavelength λ , and $\frac{hc}{\lambda}$ is the energy of each photon. The power output is given by

$$P_{out} = V_{mp} I_{mp} = FF V_{oc} I_{sc} \quad (7)$$

and now the expression for fill factor (FF) can be modified as

$$FF \approx \frac{\frac{eV_{oc}}{nkT} - \ln\left(\frac{eV_{oc}}{nkT} + 0.72\right)}{\frac{eV_{oc}}{nkT} + 1} \quad (8)$$

where n is the diode ideality factor. Hence, the fill factor is only one factor in defining the open-circuit voltage V_{oc} . Conversion efficiency η is simply P_{out}/P_{in} . Also, V_{oc} is related to the band gap of the material by the expression given below:

$$V_{oc} = \frac{1}{e} \left[E_g + kT \ln \frac{I_L}{I_{so}} \right] \quad (9)$$

Thus, V_{oc} is material dependent and the efficiency of the cell depends on selection of a suitable material.

1.3 Basic material requirements for low cost solar cells

Thin film solar cells are large area diodes fabricated to enable and maximize the absorption of light within a short distance from the space charge region of a diode. Absorbed photons create e-h pairs as described earlier. Energy of minority carriers is converted to electric energy as these are swept through the barrier field of the diode. In fact the “height of the step” at the junction determines the energy of minority carriers to do work and made to flow through the external circuit.

As a minority carrier device, a solar cell requires properties such as high minority carrier life time and mobility. These can be achieved through good crystallinity, suitable doping, and appropriate band gap. Although there are a variety of solar cells, the following description applies most directly to thin film heterojunction solar cells in which the diode is created by two layers designated as

“window layer” and “absorber layer”. The depletion (space charge or built in field) region is generated at the interface between window and absorber. The material requirements for an efficient solar cell are determined by considering the basic steps involved in the conversion of light into electric power [5].

1.3.1 Light absorption

First requirement is that light reaches the rectifying semiconductor junction through a window layer, which is designed to have minimum absorption before the light reaches the absorber. This is achieved by choosing wide band gap (>2.4 eV) material and making the layer as thin as possible.

Usually absorber material will be a compound semiconductor such as CuInSe_2 , Cu_2S having high absorption coefficient (10^5 cm^{-1}) and results in thin film solar cells with a few (0.5-5.0) μm thickness. Among the well known semiconductors, Si has a low absorption coefficient over the solar spectrum. Hence for Si based cell, thickness has to be of 50-100 μm . Also, the absorption coefficient depends on band gap of the material. Materials with direct band gap have much higher absorption, which reduces the thickness of the absorbing layer. Absorption results in carrier generation and photo-generated carriers exit the absorber region by diffusion process. Since absorber material is characterized by some electrical resistivity, it contributes an internal resistance R_s to solar cell. For all purposes, R_s in cell should be no more than a few tenths of an ohm for each square centimeter of illuminated cell area under one sun conditions. Again it is always better to have, the minority carrier diffusion length at least equal to the effective absorption length [6].

It should be noted that the maximum value of built-in voltage in a junction is limited by the step height or the fermi level difference between p- and n- type materials. From eq. (9) this in fact depends on band gap of the absorber. If the band gap is large, step size will also be larger and hence the cell voltage. On the other hand, photons are absorbed only when their energy is greater than the band gap of the absorber; thus wide band gap materials create less current than narrow band gap materials. Based on these considerations and distribution of energies within the solar spectrum, the optimum band gap energy for an absorber is about 1.5 eV [3].

1.3.2 Generation of minority charge carriers

Sunlight absorbed by the semiconductor generates e-h pairs, i.e., excess charge carriers, in solar cells. Lifetime of these carriers has to be sufficient to enable these carries to reach and cross the built-in field region of the diode used. In most semiconductors electrons have longer lifetime than holes and hence it is advantageous to use p-type semiconductors as absorbers, in which the electrons are minority carriers.

1.3.3 Charge carrier separation by built in electric field

Minority charge carriers gain energy as they travel through the built-in field region, generated by a pn-junction and this energy is used in an external circuit. The absorbing semiconductor must therefore be capable of forming a p-n junction, either as a homojunction or heterojunction. The two materials forming the heterojunction must not only have appropriate electron affinities and energy band gaps to create the internal electric field, but also must have suitable chemical and structural properties so as to have an easy movement for excess minority carriers through the depletion region.

1.3.4 Current output by ohmic contacts

After crossing the built-in field region, the minority charge carrier, becomes a majority carrier and has to leave the solar cell in order to perform useful work. Thus low-loss electrical contacts are required for both p-type and n-type layers. The electrodes required for this are metals or transparent degenerate semiconductors. In practice, low loss contacts are often achieved by producing a thin, heavily doped or degenerate region between the semiconductor and the electrode.

1.3.5 Production technologies for low cost solar cells

In addition to the above requirements of electrical and optical properties solar cells must be made using techniques that permit the production of large area cells at low cost. Hence researchers all over the world are trying to develop techniques as well as materials to suit these requirements. A semiconductor material can be selected for cell fabrication after considering this point also.

Polycrystalline materials are gaining importance under this consideration. Moreover, since there will be large scale production, the technique will also be eco-friendly.

1.4 Important thin film solar cell materials

Presently, through intensive research work, three semiconducting materials have been identified for large-scale production of thin film solar cell to replace crystalline silicon based solar cell for terrestrial applications. They are amorphous silicon (a-Si), cadmium telluride (CdTe) and copper indium selenide (CuInSe₂). Various other materials including copper sulfide (Cu₂S), copper oxide (Cu₂O), cadmium selenide (CdSe) etc., have been studied. But, either due to failure to find out low cost process or due to other disappointing results in efficiency, they are no longer being intensely investigated. CuInS₂ is also a promising candidate for PV applications.

1.4.1 Cadmium Telluride (CdTe)

Cadmium Telluride is an attractive material for solar cell applications because of the nearly ideal direct optical band gap ~ 1.45 eV [7] that makes it suitable for thin film devices. In the case of CdTe, ability to make both n-type and p-type films is another advantage. Difficulty in preparing shallow homojunctions combined with surface recombination losses has challenged the preparation of high efficiency devices. Furthermore, difficulty in preparing low resistivity p-type material has hampered the preparation of low resistance contacts.

Numerous deposition technologies have been developed to produce device quality CdTe films in which the classical deposition process is high vacuum evaporation. Close-spaced sublimation was employed to deposit CdTe film for the first CdTe thin film solar cell to achieve the conversion efficiency of 10% [8]. The present world record of 15.8% was achieved with the same technology using substrate temperature 873 K at 40 mbar [9]. The National Renewable Energy Laboratory [NREL] CdTe team could developed a modified CdTe device structure and fabricated a CdS/CdTe polycrystalline thin film solar cell demonstrating efficiency of 16.4%. [<http://www.ecomall.com/greenshopping/newsolar.htm>].

[<http://www.nrel.gov/>]

One of the most vexing problems associated with this p-type absorber layer is the formation of a low resistance, stable contact. Low resistive contacts could be fabricated by depositing ZnTe, which can be easily doped as p-type.

The major problem associated with CdTe based solar cell is the development of more refined process to deposit device quality films. Environmental safety and health risks associated with use of CdTe are also problems concerned [10]. Cadmium, one of the precursors of CdTe is a highly hazardous material. The acute health effects from inhalation of Cd include pneumonitis, and pulmonary edema. Physical process in which Cd compounds are used or produced in the form of fine fumes or particles cause larger hazards to health due to higher absorption of the material through the lungs than that occur through ingestion [11].

1.4.2. Amorphous silicon (a:Si:H)

Hydrogenated amorphous silicon, a thin film material with properties different from conventional crystalline silicon, offers a new perspective to the photovoltaic technology. Films of this material could be deposited rather easily compared to crystalline Si. Major advantage of this material is that Si and H₂, two important ingredients are abundant. a:Si possesses high optical absorption coefficient ($>10^5 \text{ cm}^{-1}$) over most of the visible spectrum, making thin film devices possible. It could be easily doped by boron and phosphorous for p-type and n-type respectively. Again, optical band gap of the material could be varied between 1.1 eV to 2 eV by alloying with germanium or carbon. Deposition employs low temperature ($<623 \text{ K}$) and could be scaled up to large areas. Stacked, multijunction structures and cell interconnections could be made easily [12].

Amorphous silicon could be prepared by various techniques such as chemical vapour deposition [11], plasma-enhanced chemical vapour deposition (PECVD) or glow discharge (GD) [12] technique. Films obtained, by PEVCD, resulted in low density of states (DOS). It was later discovered that these films contained approximately 10 at. % hydrogen and since then they were referred to

hydrogenated amorphous silicon. Today, most laboratories use the GD technique to prepare a-Si samples.

Amorphous silicon solar cells based on single junction achieved 12.5 % efficiency, multijunction solar cells reached 13.7% efficiency and efficiency of 18.7% was reported for hybrid structure of a-Si:H/Si cell [13].

Major disadvantage with this material is the inherent degradation mechanism, based on the creation of metastable defects during illumination, (Staebler-Wronski effects) which reduces the efficiency of the cell [14].

1.4.3 Copper indium selenide (CuInSe_2)

Copper indium selenide (CIS), one among the Cu-ternary chalcopyrite semiconductors, is probably the most prominent candidate, for PV applications [15]. Extraordinarily high absorption coefficient (10^5 cm^{-1}) of the material makes it suitable for thin film devices. Fundamental optical transition in this material is direct and band gap is 1.04 eV, near to the ideal value for maximum efficiency. Direct band gap relaxes the condition for minority carrier diffusion length. CIS can be prepared in either p-type or n-type which means both homojunction and heterojunction structures are possible. Electron affinity and lattice parameters are comparable with binary semiconductor such as CdS with which heterojunctions are made. It has very high radiation resistance which makes it good for space applications also.

In the early case, thin film CIS cells, at 6.6 % efficiency, were prepared by Kazmerski et al., [16]. Interest in CIS for thin film solar cells increased markedly with the results reported by researchers at Boeing, who demonstrated cells of 10.6% efficiency in 1982 [7]. The use of wider band gap heterojunction partner such as $\text{Cd}_{1-x}\text{Zn}_x\text{S}$, ZnO etc., enhanced both the open-circuit voltage and photocurrent of the device over the previous structures which simply employed CdS. The Boeing group also recognized importance of increasing the optical band gap of the absorber layer as the preferred method of increasing efficiency and introduced the use of alloys. For $(\text{Cu}(\text{In}_{1-x}\text{Ga}_x)\text{Se}_2)$, in which Ga is substituted for In, band gap can be varied within 1 and 1.7 eV continuously. Within this, replacing Se by S, $\text{Cu}(\text{In,Ga})(\text{Se,S})_2$, band gap widens up to 2.7 eV [1]. Using $\text{Cu}(\text{In}_{1-x}\text{Ga}_x)\text{Se}_2$ as

absorber layer, efficiency increased up to 14.3% [17] and recently 18.8% efficiency was achieved with $\text{Cu}(\text{In,Ga})(\text{Se,S})_2$ [18]. The combination of high and low band gap cells to build tandem cells with these materials over a wide range of energy gap opens the way to further increase of efficiencies.

In the present work, we chose the material, CuInSe_2 , which is one of the most promising candidates for photovoltaic applications. We tried to develop device quality CuInSe_2 thin films using low cost and eco-friendly methods.

1.5 CuInSe_2 – Material for the present investigation

CIS belongs to I-III-VI chalcopyrite compounds, which are three-element analog of extensively studied II-VI semiconductors. Recently CIS and related alloys gained significant importance in basic and applied research especially in the area of photovoltaics. As mentioned earlier this material has nearly ideal parameters for maximum efficiency.

1.5.1 Basic properties

Stable crystal structure of CIS is a subset of the adamantine class and is named after the mineral chalcopyrite, CuFeS_2 . Characteristics of the adamantine structure is a tetragonal arrangement of atoms in which each atom has four nearest neighbours. In general, various compound crystal structures are derived from the basic diamond close-packed structure. It has a sub-lattice of anion in cubic close-packing as in zinc blend (sphalerite) structure or in hexagonal close packed type as in the Wurtzite structure. In chalcopyrite compounds (γ -phase), a slight shift of the anion sites results in the tetragonal symmetry with c-axis nearly twice the original axis (zinc blend structure). CIS crystallizes in this form (fig. 1.3) at room temperature and reverts to the sphalerite structure (δ -phase) above 1073 K [19].

In general for a three component system, there is only a limited information on phase stability. Figure 1.4 shows the pseudo-binary phase diagram for CIS systems reported by Moller [3]. In the figure, the two-dimensional phase diagram is along $\text{Cu}_2\text{Se-In}_2\text{Se}_3$ tie line.

Interest in CIS and related compounds is mainly due to the extremely high absorption coefficient and low band gap, as mentioned earlier. For thin films, band gap is slightly higher than that of crystalline material due to extremely high absorption, compositional variation and grain size effects depending on the method of preparation.

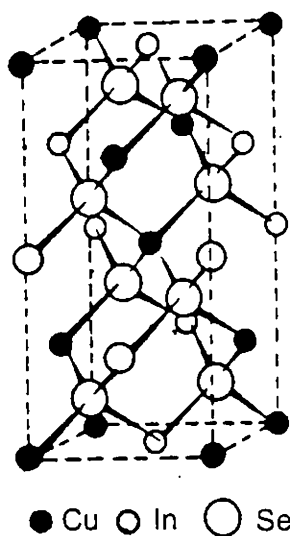


Figure 1.3: Chalcopyrite structure of CuInSe_2

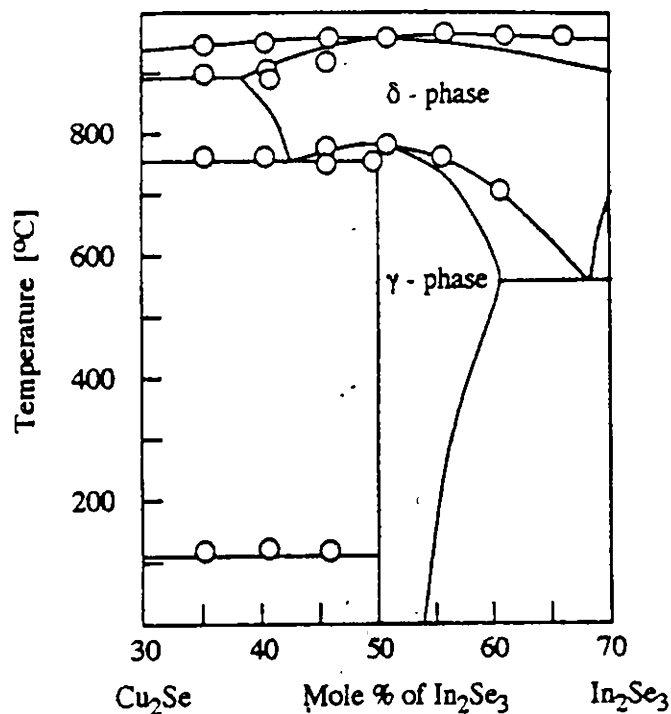


Figure 1.4: Pseudobinary phase for CuInSe_2 based on $\text{Cu}_2\text{Se}-\text{In}_2\text{Se}_3$

In I-III-VI compounds, off-stoichiometry is more complex than in the II-VI materials. In the latter, off-stoichiometry means simultaneous atomic and valance effect. In general, this deviation is limited within a fraction of atomic percent.

According to Neumann [20] for the nearly stoichiometric compound $\text{Cu}_a\text{In}_b\text{Se}_c$ ($a \approx 1$, $b \approx 1$ and $c \approx 2$), deviation of its actual composition from the ideal formula CuInSe_2 can be described by two parameters, viz., the deviation from molecularity (Δm) and the deviation from stoichiometry (Δs). These are defined as,

$$\Delta m = \frac{\text{Cu}}{\text{In}} - 1 \quad (10)$$

$$\Delta s = \frac{2[\text{Se}]}{[\text{Cu}] + 3[\text{In}]} - 1 \quad (11)$$

where $[\text{Cu}]$, $[\text{In}]$ and $[\text{Se}]$ are total concentrations of Cu, In and Se atoms respectively. This kind of approach on the basis of defect chemistry model was proposed by other researchers [21].

A distinguishing feature of this type of materials is that both n and p-type can be prepared. This is achieved by adjusting Δm and Δs during preparation [22]. $\Delta m > 0$ means Cu-rich films and $\Delta m < 0$ denotes In-rich films. $\Delta s > 0$ indicates there is an excess selenium and $\Delta s < 0$ indicates deficiency in selenium. Hence analysis of these parameters reveals that if $\Delta m > 0$ and $\Delta s > 0$, the films are p-type and if $\Delta s < 0$ films are n-type.

1.5.2 Review of studies on CIS thin film and related compounds

Being a leading candidate in the area of thin film photovoltaics, many interesting studies have been reported for the last a few decades in CuInSe_2 . New methods were developed for deposition of thin film CIS. Structural, electrical, optical and other related studies were carried out using novel techniques by various research group all over the world.

Interest in CuInSe_2 dates back to the work of Wagner et al [23] who demonstrated a 12% conversion efficiency using single crystals. Extremely high absorption coefficient of the material makes thin film photovoltaic devices practical, although a band gap of 1.04 eV is usually considered too low for

optimum conversion efficiency of the solar cell. Kazmerski et al., [16] prepared CIS films by a method of simultaneous evaporation of three sources. After this achievement, advanced studies were going on to analyse the material properties with the intention of modifying the material parameters to increase the efficiency of the device. Subsequently many methods were being developed to prepare CIS films and analyses were also in progress.

In 1979, Fray et al prepared p-type chalcopyrite CuInSe_2 by vacuum evaporation and discussed their electrical and optical properties [24]. Immediately after, Bates et al. reported method of spray pyrolysis of solution containing InCl_3 , CuCl and N,N –dimethylselenourea. Optimum conditions were suggested from thermodynamical calculations using free energy minimization computer program applied to the existence of CuInSe_2 which favoured the existence of Cu_2Se with increase in copper concentration [25]. Cammy et al., showed the kinetic effects in CIS formation in the same method using the solution containing similar ingredients [26]. They observed that formation of Cu_{2-x}Se was favoured by reducing copper concentration and substrate temperature in contradiction with Bates' report.

During next few years research gained much momentum in the development of this material for device application. Szot et al [27] prepared chalcopyrite CIS films having a band gap of 1.02 eV, by co-evaporation of the elements (Cu, In and Se) using an electron beam heating technique. In 1986, Isomura et al reported preparation of both p-type and n-type CIS thin films using d.c sputtering and vacuum evaporation from bulk material [28]. Gary et al., discussed electrodeposition of Cu-In-Se systems and Cu-In alloy followed by annealing in Se-atmosphere to obtain CIS films [29]. Morphological, compositional and photo-electrochemical behaviour of these layers were also included.

Large grain and near stoichiometric films were prepared by selenisation of vacuum evaporated or electrodeposited Cu-In precursor in H_2Se atmosphere, as reported by Chu et al., [30]. Neelkanth et al. [31] deposited chalcopyrite p-type films of CIS by vacuum evaporation of the constituent elements by the 'three-temperature' method. Electrical transport properties of co-evaporated films were

studied by Garacia-Cuenca et al. The films were p-type and the conductivity activation energy ranged from 0.03 to 0.5 eV in the range 300-400 K. Grain boundary trapping models were considered in the analysis of the results [32]. In the same year, Kristensen et al. prepared stoichiometric CIS films and analysed by microprobe, X-ray, scanning and transmission microscopy [33]. They tested photoactivity of the films in photoelectrochemical cells (PEC) with configuration Mo/n-CIS/T, I₃⁻/C which gave photocurrents up to 10 mA cm⁻² and photovoltage of 200 mV under illumination intensity of 85 mWcm⁻².

In 1990's much developments were reported in the preparation and analysis of the material. Structural, electrical and optical properties of n-type CIS films having band gap 1 eV produced by rf sputtering from a stoichiometric target in an Ar/O₂ atmosphere were reported by Toshiyuki Yamaguchi et al. [34]. They found that growth rate decreased with increasing O₂ content and SeO₂, CuO and In₂O₃ coexist together on the surface. At the same time, a novel single step electrodeposition process was described by Garg et al., [35]. Thin polycrystalline films were obtained by Khare et al using this method [36]. Films were having preferred orientation (112)_U (chalcopyrite) and (111)_F sphalerite with some binary phases.

Chemical process, well suited for large area deposition, gained much pace in the next few years. Brown et al. performed detailed examination of the morphology of CIS films prepared using chemical spray pyrolysis [37]. Guillen et al prepared Se rich chalcopyrite CIS films having E_g 0.99 eV, by cathodic electrodeposition from aqueous citric acid plating baths [38]. Same group reported detailed analysis on optical properties of these films in the wavelength range 400-200 nm [39]. As-deposited CIS film was found to possess an allowed direct transition with E_{ga}=0.96 eV and forbidden direct transition with E_{gf} = 1.38 eV. Heat-treated films at 673 K showed E_{ga} = 1.00 eV, but no forbidden transition was observed.

Tembhurkar et al. observed similar types of transitions for the films deposited by spray pyrolysis using aqueous solution of CuCl, In₂Cl₃ and selenourea on substrates at temperature 623 K. Two dominant intrinsic acceptor like levels,

selenium interstitial at 70 meV and copper vacancies at 30 meV were obtained from conductivity measurements, for p-type films [40].

Kumar et al prepared CIS films by rapid thermal annealing stacked (Cu-In)/Se layers consisting of electro deposited Cu-In and evaporated Se [41]. Rapid thermal annealing at 623 K yielded a strongly oriented chalcopyrite phase.

Padam et al deposited CIS films using chemical bath deposition (CBD) [42] and described the influence of vacuum/air annealing and Cu:In ratio on defects produced in these films. They found that on annealing in air, V_{Cu} increases leading to increase in p-type nature and also, phases like Cu_2Se , SeO_2 and In_2O_3 were formed. Two years later, Vidyadharan et al, reported their preliminary results on preparation of p-type Cu rich films using CBD, at room temperature [43].

Photoelectrical properties of solution grown films were analysed by Manohar Lal et al. using steady state and transient photoconductivity measurements taken as a function of temperature. They suggested a bimolecular recombination mechanism in $CuInSe_2$, from the results of variation of photocurrent with increase in light intensity which obeyed power law [44].

Other advanced techniques for the growth and analysis of CIS films were developed along with conventional techniques. Mikihiro Nishitani et al., developed Molecular Beam Epitaxy to prepare CIS films by co-evaporation of the elements. They showed that at substrate temperature 773 K there was a critical In-flux intensity for the fabrication of stoichiometric CIS films [45]. Shigemi et al [46] employed UV photoelectron spectroscopy to study electron acceptor levels at surfaces of chalcopyrite structure CIS films prepared by MBE. Surface Fermi level pinning was observed for Cu-rich films and shallow acceptor levels ascribable to Cu_{In} and V_{Cu} were observed for near stoichiometric and In-rich films.

Photoluminescence (PL) studies of CIS films of Cu/In ratio ranging from 0.81 to 1.81 grown using MBE were reported by Shigeru et al. [47]. PL properties were found to be sensitive to the growth parameters such as Cu/In ratio or substrate temperature. This kind of studies were reported by Tanda et al for CIS films by selenising Cu/In stack layers with solid-or vapour-phase selenium [48]. Further, the

origin of PL peaks and its behaviour were studied through the dependence of PL spectra on the temperature and excitation intensity [49].

In the same year, with the intention of preparing high mobility p-type CIS films, Ashida et al. successfully introduced 'quasi-flash-evaporation method' without poisonous gases such as Se vapour or H_2Se . They used two methods; one was sequential evaporation of first Cu_2Se and then In_2Se_3 and subsequent annealing; second was evaporation of powdered mixture of Cu_2Se and In_2Se_3 and annealing [50].

Many groups started to develop different sputtering methods to deposit precursor for $CuInSe_2$ films due to high uniformity offered by the process. Parretta et al reported CIS film preparation by selenization of sputtered metal precursors and the surface morphology, phase composition and adhesion at Mo/glass substrate were correlated to the structure of the precursors [51].

Chalcopyrite CIS films having direct band gap in the range, 0.96-1.01 eV and with strong (112) orientation was produced using selenisation of co-sputtered Cu-In films with selenium vapour [52]. In this paper Schmidt et al found that Cu-rich films were p-type and In-rich films were n-type. Also, they reported a thermally activated conductivity for higher temperature and the variable range hopping mechanism in the lower temperature range.

Masaharu Terauchi et al. prepared CIS films by selenization of rf-magnetron sputtered and laser ablated Cu-In-O precursor in H_2Se atmosphere. CIS films obtained by selenizing former precursor resulted in chalcopyrite single phase films while the later contained In_2O_3 phase [53].

Menna et al prepared CIS film in a two-stage process: by sputtering Cu, In layers followed by selenization by vacuum evaporation. Films were analysed by EDX and XRD. The chalcopyrite ordered vacancy compound, $CuIn_3Se_5$ (OVC) was formed as secondary phase [54].

Microstructural studies on $CuInSe_2$ thin films produced by rapid annealing of elemental layers of Cu, In, and Se was done using scanning tunneling

microscopy, in constant current mode, by Riedl et al. [55]. The polarity of the current is a measure of the conductivity type and the observation of leakage currents at small bias voltages allows the identification of gap states around the Fermi level. Intra- and inter-granular non-uniformities of the conduction type are observed.

Local structure of CIS thin films was studied by Yuji Kuwahara et al. [56] using extended X-ray absorption (EXAFS) on the CuK and SeK edges employing synchrotron radiation. They found that as Cu increased, Cu-Se and In-Se bond length deviated from that of stoichiometric crystal, which was attributed to the chemical disorder of the cation sites and the formation of anion vacancies in the chalcopyrite lattice.

Effect of etching on the surface morphology and grain boundary parameters of Cu-rich CIS films prepared using three source evaporation was discussed by Pal et al., [57].

In 1995, Adurodija et al reported solid-liquid reaction mechanism involved in the formation of CIS films by annealing stacked elemental layers (SEL) technique. Reaction chemistry was analysed after annealing Cu-In-Se stacked layer and Cu-Se, In-Se and Cu-In layers at different temperatures using XRD, EDX and SEM. Studies of the time progressive reaction at 723 K showed that chalcopyrite CuInSe_2 films were formed after a reaction time of 60 s [58]. Similar studies on reaction chemistry and growth dynamics of CuInSe_2 film grown by physical vapour deposition was carried out along the reaction path leading from the $\text{Cu}_x\text{Se}:\text{CuInSe}_2$ (two-phase region to single-phase CuInSe_2) by Tuttle et al. [59].

Nishitani et al demonstrated a distinct study of In-situ composition monitoring method of Cu/In ratio in the bilayer deposition process of CIS film. The principle of this method was based on the idea that the hole concentration changed abruptly at the stoichiometric composition while the film composition gradually changed from Cu-rich to In-rich through stoichiometry during the deposition process [60].

In the same year, Sebastian et al., reported the formation of CIS films combining two low cost and large area techniques viz. electroless process for $\text{Cu}_{11}\text{-In}_9$ alloy and followed by selenisation at 673K employing CVTG [61]. Guillen et al. used same technique to co-deposit Cu, In and Se thin films to prepare CuInSe_2 in one-step. Heat treatment at 673 K in flowing argon, removed the excess Se and the subsequent KCN treatment eliminated Cu_2Se phase [62].

Linear and nonlinear optical properties of tetragonal CIS thin films grown epitaxially on GaAs (001) was studied by Bottomley et al. as a function of temperature [63].

A sequential deposition process for CIS leading to highly efficient device was described by Zweigart et al.[64]. First InSe_x precursors were deposited either by co-evaporation of In and Se or by evaporation of In_2Se_3 . In subsequent step, Cu and Se were added in order to form CuInSe_2 . A model for Cu rich and Cu-poor growth was introduced in the report.

Selenisation of different types of precursors became the main technique for the subsequent years. Basol et al. reported growth of CIS film by selenizing evaporated Cu-In alloy precursors in H_2Se atmosphere at 673 K [65].

Recently, Schon et al. prepared CIS films by selenising electron beam evaporated Cu/In layers in $\text{H}_2\text{Se}/\text{Ar}$ atmosphere. They found that In-rich films were of small grain size and Cu-rich films were possessed by larger grains [66].

Nakada et al developed an apparatus for a sequential sputtering/selenisation technique to minimize the metal target contamination, for the growth of CuInSe_2 . [67]. The apparatus consists rotating drum holding substrates and three horizontally interconnected fibers for Cu, In and Se fluxes. Here a very thin Cu/In layer deposited was selenized at each rotation and polycrystalline CIS films were formed after repeating this process.

Due to the simplicity and suitability for large area deposition, solution grown techniques were in rapid progress. Stratieva et al. studied the structural and electrical properties of electrodeposited CuInSe_2 layers from a thiocyanate electrolyte with a complexing agent [68]. They obtained Cu-rich films and

annealing in Ar ambient improved the crystallinity. The band gap was 1 eV for 823 K annealed films.

CIS films were prepared by one-step electro-deposition process from an electrolyte containing Cu^+ , In^{3+} and Se^{4+} ions and thiocyanate as complexing agent [69]. Morphological and structural studies revealed that annealing in Se ambient was more effective than annealing in Ar.

Nomura et al., deposited CuInSe_2 films by Pulse-plated electrodeposition process from an aqueous solution of CuCl_2 , InCl_3 and SeO_2 . The optimum annealing conditions were discussed using XRD and Raman Spectra [70].

Manjunath et al. prepared CIS films by electroless method from aqueous solutions of copper chloride, indium chloride, selenous acid and lithium chloride, at a pH of 2.2 [71]. The films were In-rich at the surface and Cu-rich in the bulk which was attributed to a possible Cu diffusion towards the substrate.

Recently, a novel method of ionized cluster beam deposition was developed by Kenichi et al. [72]. From the effect of nozzle diameter, it was found that the energy of Cu clusters played a very important role in the crystal growth of CIS.

Another new technique of Metal organic chemical vapour deposition was reported by Artaud et al, using hexafluoroacetylacetonato copper ($\text{Cu}(\text{hfa})_2$) as Cu precursor [73]. Band gap obtained was 1 eV. Cu-rich films were composed of Cu_{2-x}Se and on In-rich side CuIn_3Se_5 phase was appearing. This kind of observation was also reported by Calixto et al in the case of electrodeposited films [74]. A thin layer of CuIn_3Se_5 is advantageous for the device performance as this n-layer forms a 'pseudo-homojunction' with p-CIS layer.

Sung Chan Park et al. [75] prepared CuInSe_2 films by sequentially evaporating In_2Se_3 and Cu_2Se at room temperature and subsequent annealing in Se atmosphere. CuIn_3Se_5 layer was formed at the surface by co-evaporating of In_2Se_3 and Se at 823 K.

Guenoun et al. reported [76] an improvement in closed-vapour transport method to deposit CIS films in a closed vertical tube. High optical-quality

polycrystalline and epitaxial CuInSe₂ thin films were grown by a simultaneous-feeding or alternative-feeding physical vapour deposition method, by Chichibu et al., [77].

For the last two years, there are many reports on various types of studies on this material using advanced techniques. Optical and electrical properties of flash-evaporated amorphous CuInSe₂ films were presented by Sakata et al. [78]. They obtained direct band gap energy of 1.21 –1.41 eV.

Kenji et al., carried out Piezoelectric photoacoustic (PPA) measurements in samples grown on GaAs (001) using MBE, to investigate non-radiative carrier recombination in processes in comparison with PL measurements [79]. Three PPA signal peaks obtained were corresponding to band gap energies of the CIS and the GaAs substrate. They obtained two peaks due to intrinsic defects which are Cu vacancy (V_{Cu}) and interstitial In (In_i) in In-rich sample.

Raman spectra of spray pyrolysed polycrystalline films CIS were investigated by Shirakata et al. They observed Γ_1 Raman peak at 174 cm⁻¹ in Cu-rich and stoichiometric films, and a peak at 182 cm⁻¹ in In-rich films [80].

Polarized Raman spectra were measured at room temperature from the (001)- and (112)- oriented CIS heteroepitaxial layers grown on (001)- and (111)- oriented Si substrates by Vorlicek. [81]. The analysis of the results proved the expected orientation and good crystalline quality of the (001) layers. No special orientation was identified along (112) plane.

One of the major problems associated with CuInSe₂ film was reduced V_{oc} due to low band gap of the material. It was found that the band gap of the material could be increased to the optimum value of 1.5 eV by substituting Ga into some of In sites, resulting the quaternary material - CuIn_xGa_{1-x}Se₂ [82]. This could also reduce the built-in-back surface field due to bandgap tailoring. Masse et al deposited CuInSe₂, Cu(In,Ga)Se₂ and CuIn(Se,S)₂ films on SnO₂ using a close-spaced vapour transport in closed tube with iodine. They observed strong (100) or (001) preferred orientation [83].

There are many other reports on the growth and characterization of these quaternary alloys. A novel process consisting of two-selenization of magnetron sputtered metallic precursors using Se vapor and a method for Ga incorporation using a single Cu-Ga alloy target for the growth of $\text{CuIn}_x\text{Ga}_{1-x}\text{Se}_2$ films was developed by Neelkanth et al. [84].

Friedfeld et al reported the electrodeposition of $\text{CuIn}_x\text{Ga}_{1-x}\text{Se}_2$ thin films with various Ga/In ratios [85]. Process was the deposition of Cu-Ga precursor film onto a molybdenum substrate, followed by the deposition of Cu-In-Se thin film and subsequent annealing.

Graded band gap CuInGaSe_2 thin films were prepared using a three-stage process. In the first stage, In, Ga and Se were co-evaporated at $T_s \sim 533$ K to form the $(\text{In,Ga})_2\text{Se}_3$ precursor and then Cu-Se at 823 K followed by codeposition of In, Ga and Se [86].

Further increase in band gap and thus leading to improved efficiency of CIS based device was reported by many authors due to substitution of Se by S leading to the formation of $\text{CuIn}(\text{S}_x\text{Se}_{1-x})_2$ or $\text{CuIn}_x\text{Ga}_{1-x}(\text{S}_x\text{Se}_{1-x})_2$. Walter et al. developed a sequential process for the fabrication of polycrystalline $\text{CuIn}_x\text{Ga}_{1-x}(\text{S}_x\text{Se}_{1-x})_2$ thin films using $(\text{In,Ga})_x(\text{S,Se})$ precursors [87].

1.5.3 Review on CuInSe_2 based solar cells

Most of the solar cells based on CIS is CdS/CIS heterojunction in which CIS is the absorber layer (p-type) and CdS (n-type) is the window layer. This is because, CdS has very good lattice match with CuInSe_2 . The extra ordinarily high absorption coefficient of the material makes thin film devices practical, although band gap of 1.04 eV is usually considered too low for optimum conversion efficiency of the solar cell. Kazmerski et al., [16]. prepared thin film solar cell with 6.6 % efficiency, as cited earlier. After that lot of modifications were developed by several research groups in order to improve the material parameters as well as the device structure, to increase the efficiency of the cell and large area production. As a result a record efficiency of 18.8 % was achieved for $\text{Cu}(\text{In,Ga})\text{Se}_2$ based solar cells. This is the highest efficiency reported among all other cells [20], already

mentioned sec. 1.4.3. This was reported by Contreras et al., from National Renewable Energy Laboratory (NREL), USA. Some of the reported devices based on CIS and related alloys are listed in the table 1.1.

Preparation methods used for the absorber layers, window layer and electrodes are also specified in the table. Efficiency and other cell parameters are separately illustrated.

1.6 Low cost-hybrid deposition processes opted in the present work

A wide variety of experimental techniques have been developed over the last fifty years for the deposition of thin films, specifically for solar cell applications [88].

Any thin film deposition process involves the following three steps:

- i. creation of atomic/molecular/ionic species,**
- ii. transport of these species through a medium and**
- iii. condensation of these species on a substrate**

Depending on the way in which these species are created, we can broadly classify the deposition techniques as Physical methods and Chemical methods [89].

In Physical methods, material to be deposited is first transferred to gaseous state and then condenses to thin films. This method can be classified as vacuum evaporation and sputtering.

In chemical methods film deposition takes place either by gas phase or liquid phase chemical processes. This method can be again classified as electroless or solution growth, electrochemical deposition and chemical vapour deposition (CVD).

Details of these techniques and the properties of films prepared using each technique are described in detail in literature [90].

Cell structure	Preparation method		Cell parameters				Reference	Remarks if any
	Absorber	Window	η (%)	J_{sc} mA/cm ²	V_{oc} mV	FF (%)		
Glass/ITO/CIS/ CdZnS	CIS-spray pyrolysis	CdS-spray pyrolysis	3.14	8.25	440	27.8	Rajaram et al. (1985) [91]	
Glass/Mo/CIS/CdS/ITO	CIS-three source evaporation	CdS- evaporation	10.8	34.3	67.6		Birkmire et al. (1986) [92]	Heat treatment at 200 °C
Glass/Mo/CIS/CdS/Al	CIS-reactive sput.	CdS- evaporation	5.5	24.8	370	60	Lammasson et al (1987) [93]	
Glass/Mo/CIS/CdS/Al	CIS- electrodep	CdS- evaporation	4	30	300	50	Shih et al. (1987) [94]	
Glass/Mo/CIS/CdZnS/Al	CIS-SEL proc.	CdZnS-evaporation	3.5	25	260	45	H. Oumous et al (1987) [95]	
Glass/Mo/CIGS/CdZnS/ZnO	CIGS co-evap	CdZnS-wet chem. Proc	11.1	31.1	542	65.9	Devaney atl (1990) [96]	Area- 4cm ² , Ga:(In+Ga)-0.28 Eg-1.15 eV
Glass/ITO/ZnO/CdS/CIGS/ Au - superstrate	CIS- co evap	CdS-evap	6.3	32	332	60	Nigami et al. (1994) [97]	CdS was annealed in air at 200 °C

Table 1.1: Review of solar cell devices based on CIS thin film

Glass/Mo/CIS/CdS ITO /ZnO	CIS-Selenis.evap. Cu/In/Se stack Ir.	CdS - CBD	10.3	39	427	61.9	Katsumi Kushiya et al (1994) [98]	ZnO- MOCVD
Glass/Mo/CIGS/ In _x (OH,S) _y /ZnO/ MgF	CIGS- evaporation	In _x (OH,S) _y - CBD	15.7	35.5	594	74.6	Hariskos et al. (1996) [99]	In _x (OH,S) _y - from a soln. InCl ₃ and thioacetamide
Glass/Mo/CIS/CdS /ZnO	CIS- selenis. EB evap. Se/In/Cu	CdS- CBD	8.7	36.2	417	57.5	Basol et al. (1996) [100]	Substrate- flexible 50 μm thick KAPTON polyimide sheet
Glass/Mo/CIGS/CdS/ZnO/M gF ₂ /Al – sub module	CIGS – co-evap	CdS-CBD	16	31.96	678	75.8	Contreras et al. (1996) [101]	Graded band gap str. η increased from 13.2% to 16.4 %
Glass/Mo/CIS/CdS/ZnO	CIS-ED	CdS - CBD	6.3	42	330	57	Qui et al. (1997) [102]	ZnO- rf sputt
Glass/Mo/CIGS/CdZnS/ZnO	CIGS co-evap	CdS – CBD	13.7	36.3	546	68.4	Chen et al. (1998) [103]	Area-0.8995 m ² Cu/(In+Ga)= 0.89
Glass/Mo/CIS/In _x Sc _y /ZnO/IT O/Al	CIS-co-evap of In +Se,co-evap.Cu+ Se	In _x Sc _y – co-evap. In+Se	8.46	35.1	423	57	Ilan Kown et al., (1998) [104]	

Glass/SbO ₂ /CIS/CdS/Im (ALL-CBD) Cell	CIS-CBD	CdS-CBD							Vidyadharan Pillaimet al [105]	
Glass/Mo/CIGS/CdS/ZnO/M gF ₂ /Al	CIGS - ED	CdS-CBD	15.4	30.5	666	66..87			Bhattacharya et al. (2000) [106]	ZnO- rf sputt. Final composition was adjusted by adding In, Ga and Cu by PVD
Glass/Mo/CIGS/CdS/ZnO/M gF ₂ /Al	CIGS ~ Cu- In(Ga)-Se-Dc sputt + Ann.	CdS- BD	13	34.65	536	70.08			Markus et al. (2000) [107]	.
Glass/Mo/CIGSS/ CdS/ZnO/EVA/Glass module	CIGSS-SEL proc. Ann. SEL in H ₂ S	CdS- BD	14.7	35..35	695	71.7			Franz H. Karg et al. (2001) [108]	

When one is dealing with deposition of thin films for solar cell fabrication, it is essential to use techniques that are simple, low cost and capable of controlled deposition to produce large area films with well defined properties. All the techniques have their own advantages and limitations. When solar cell application is considered one has to use a single or combination of techniques. In the present work, we used combination of chemical bath deposition and vacuum evaporation so that the whole process is low cost and eco-friendly for large area fabrication. These two techniques are described briefly below.

1.6.1 Chemical Bath Deposition (CBD)

CBD is solution growth process used for depositing compound thin films and is rarely used for deposition of elemental semiconductor. In the present work, we could deposit thin films of elemental selenium [109] CBD is a technique in which thin semiconductor films are deposited on substrates immersed in solutions containing ions of the required compound semiconductor [110]. There are many reports from different research groups, regarding the preparation of large number of compound thin films such as PbS [111], PbSe [112], Sb₂S₃, CdS, CdSe, Cu_xS [113, Cu_{2-x}Se [114] used for different applications.

For the last ten years, Thin Film Photovoltaic Division, Cochin University of Science and Technology has been investigating preparation of semiconducting thin films such as CuInSe₂, CuInS₂, Cu_xS, CdS, CdSe Cu_{2-x}Se and Cu₃Se₂ for solar cell applications. The first ALL CBD solar cell based on CIS, i.e CIS/CdS cell was fabricated in this laboratory, though the efficiency was low [107]. In this case, both CuInSe₂ and CdS films were prepared using CBD.

In the present work, initially this technique was used to deposit Cu_{2-x}Se as precursor to prepare CuInSe₂. Also, CBD technique was used to deposit selenium thin film and later we could develop a novel selenisation process for preparing CIS using this selenium thin film.

1.6.1.1 Principle of CBD

In CBD process, precipitation of solid phase occurs due to the super saturation in the reaction bath. At a given temperature, when the ionic product

exceeds the solubility product, precipitation occurs and otherwise, the solid phase produced will dissolve back to the solution resulting no net precipitation. In a typical CBD process, substrates are immersed in a solution containing the cations and the anions and controlled precipitation leads to the formation of thin film.

1.6.1.2 Process of thin film deposition

There are two possibilities for thin film deposition in CBD. First is the “ion-ion process” in which the ions condense on the substrate surface to form the film (heterogeneous precipitation). The second is the “cluster by cluster” process in which colloidal particles of the compound that are formed in the solution gets adsorbed at the substrate surface to form thin layers (homogeneous precipitation).

1.6.1.3 Factors influencing the deposition process

Parameters on which this process depends are nature of the complexing agent and reactants, temperature, pH value, concentration of ions, the nature of the substrate and duration of reaction.

i. Nature of the reactants

Nature of the reactants may affect the composition of the products. Rate of deposition and thickness of the sample depends on the ionic concentration. Increase in concentration of complexing agent will reduce the release of metal ions. As a result the rate of reaction decreases which will increase the terminal thickness of the film.

ii. Temperature and pH of the reaction bath

As temperature of the bath increases, the rate of reaction increases which increases terminal thickness of the film. The pH of the solution influences the solubility product of the metal ions or chalcogenide ions, which may effect the condition of precipitation.

iii. Nature of substrates and duration of reaction

Crystallinity of the films depends on the duration of reaction. Generally the growth of good crystalline quality film proceeds at a slow rate.

The reaction kinetics and adhesion of the films depends on nature of the substrate. Hence surface of the substrate should be perfectly cleaned. Higher deposition rates and terminal thickness are observed if the substrates used have same lattice parameters as that of the material to be deposited [112].

1.6.1.4 Advantages and Disadvantages

a. Advantages

CBD technique is probably the simplest and cost-effective of all the deposition techniques. The arrangement is very simple: a beaker containing glass substrates dipped in it. It should also be noted that the process is carried out in atmospheric pressure and relatively low temperature. High purity chemicals are not essential in this process. All these facts make the process low cost. Also, the incorporation of impurity from the reaction bath to the films deposited on substrates is less probable. If the precipitate remained in the reaction is recovered to use as precursor for other techniques or as starting chemical for new deposition process, then there is minimum environmental hazards. Also, this reduces material wastage to minimum.

b. Disadvantages

It is difficult to dope the semiconductor with external dopants using CBD. If ternary or multinary films are deposited using this method, then it is not easy to control the stoichiometry of the films formed. Choice of substrates is restricted as it should not react with solutions in the bath. Also, in the case of multilayer deposition during solar cell fabrication, the possibility of reaction of the initially deposited layer should be carefully considered.

1.6.2 Vacuum Evaporation

Deposition of thin films using vacuum evaporation is simple, convenient and is the most widely used technique. Here, sufficient amount of heat is given to the evaporant in vacuum (usually of the order of 10^{-6} mbar) to have vapour pressure necessary for evaporation. Evaporated material is allowed to condense on a substrate kept at suitable temperature and convenient distance from the evaporant. Generally, the techniques employed to supply heat of evaporation for the material are resistive heating, flash evaporation, electron beam evaporation and laser evaporation.

In the present work, we adopted resistive heating method. In this method, the evaporant material is taken in a source, which is resistively heated so that the material gets evaporated and are transported through vacuum to condense on

substrate. Source materials should have negligible vapour pressure at the vapourisation temperature of the material and it should not react with the evaporant. Shape of the source should be such that it should be possible to hold the material in the available form like, wire, foil or powder. The material used for making sources is refractory material such as W, Mo, Ta etc., and source can be in the form of foils or filaments.

This technique is mainly used for the preparation of metallic layers such as Cu, In and Al during material deposition and electrode coating in the present studies.

1.7 Characterization techniques

In order to prepare device quality film, the optimization of preparation conditions is the main task. This is to be done on the basis of suitable morphological, structural, compositional, optical and electrical properties of the films obtained in each condition. Characterization of the films is a primary requirement to optimize for good quality films. In the following sections, the techniques used in the present investigation are described briefly.

1.7.1 Morphology

Microstructure and thickness have a significant influence on the properties of the films. In the case of solar cells, the absorber layer should have large grain size and approximately 2 μm thickness.

1.7.1.1 Measurement of thickness

Film thickness may be measured either by in-situ monitoring of the rate of deposition or after the film is taken out from the deposition bath or chamber. In the present investigation different methods were used for thickness measurement depending on method of film preparation.

Gravimetric method was used to estimate thickness of films prepared using CBD. In this method a cleaned substrate was weighed using a microbalance and then film of required thickness (single dip or multiple dip) was deposited on it. After deposition the substrates were weighed, from which weight of the film was

found out. Knowing the dimensions of the film, and assuming bulk density, the film thickness was estimated.

In-situ measurement of thickness for samples deposited by vacuum evaporation was done using a quartz crystal thickness monitor (model CTM200). Here, quartz crystal was also exposed for deposition along with the substrates during vacuum evaporation. As a result, frequency of oscillation of the crystal changes. Then, the in-situ value of thickness of the deposited material is automatically displayed by the unit if the density of the material is already fed into the unit.

In some cases thickness was measured using Stylus method. This method involves physically traversing the surface (film+substrate) with a fine stylus suspended from an electro-magnetically sensitive spring. At the region of the film, the stylus moves in the upward direction. Vertical movement of the stylus (needle like diamond probe) is amplified electronically and recorded on paper by a spark pen. The machine used here is SURFCOM 1400A (ACCRETECH (Tokyo Seimitsu Co., LTD.))

1.7.1.2 Surface morphology

Scanning Electron Microscope (SEM) is the most widely used instrument for obtaining microstructural and surface features of thin films. A finely focused electron beam is scattered over the surface of the specimen and the secondary electrons generated from the specimens are used for Z-modulation in a corresponding raster on an oscilloscope or TV screen. In order to avoid charging problems, a thin layer of gold is deposited on the specimen without altering the surface features. The secondary electron mode is generally preferred for topographical feature determination since these electrons generate only from about 10 Å or less from the film surface and hence the picture obtained is a faithful reproduction of the surface features. The magnification can be varied up to 10^5 . From the micrograph, information about columnar structure, grain size and film thickness etc., are obtained.

In the present investigation, a JEOL scanning electron microscope was employed for studying the surface morphology of the films. Morphological changes of the films due to post deposition treatments were clearly studied using SEM.

1.7.2 Structural Characterisation

Electrical and optical properties of a material are influenced by the crystallographic nature of the films. In the present work, crystallographic studies are carried out using X-ray diffractometer (XRD). Transmission spectroscopy (TEM), Laser Raman Spectroscopy are other techniques generally used for structural studies.

1.7.2.1 XRD

XRD is one of the most useful methods for exploring the nature of material. XRD is used to determine the phase content in many minerals and materials. As a result, it is used by researchers in a wide range of disciplines. It requires no elaborate sample preparation and is essentially non-destructive. Generally, it gives a whole range of information about the crystal structure, orientation, crystallite size, composition (with the help of standards), defects and stresses in thin films. Experimentally obtained diffraction pattern of the sample is compared with Joint Council Powder Diffraction (JCPDS) data for standards. This gives information of different crystallographic phases, the relative abundance and preferred orientations. From the width of the diffraction peak, average grain size in the film can also be estimated.

Interplanar spacing d was calculated from the X-ray diffraction profiles using the formula,

$$2d\sin\theta = n\lambda \dots\dots\dots (12)$$

where θ is the Bragg angle and n is the order of the spectrum, λ is the wavelength of X-rays. Using the d - values the set of lattice planes (hkl) were identified from the standard data and the lattice parameters are calculated using the following relations.

For the tetragonal systems

$$\frac{1}{d^2} = \frac{(h^2 + k^2)}{a^2} + \frac{1}{c^2} \dots\dots\dots (13)$$

and for hexagonal systems,

$$\frac{1}{d^2} = \frac{4}{3} \frac{(h^2 + hk + k^2)}{a^2} + \frac{1}{c^2} \dots\dots\dots(14)$$

where a and c are lattice parameters. The grain size (L) was evaluated using Scherrer's formula,

$$L = \frac{k\lambda}{\beta \cos\theta} \dots\dots\dots (15)$$

Where k is a constant ~ 1 and β , the width usually measured in radians at an intensity equal to the intensity of half the maximum intensity of the peak.

In this work, we used XRD to identify different phases of films formed at various preparation conditions. XRD measurements were taken using $\text{CuK}\alpha_1$ ($\lambda=1.5405 \text{ \AA}$) radiation and a Ni filter operated at 30 kV and 20 mA (Rigaku (D.Max.C) X-ray diffractometer).

1.7.3 Compositional analysis

Chemical composition analysis of thin films cannot be done using standard chemical methods, as the quantity of material is very low. Hence we have to use sophisticated analytical techniques for the chemical analysis of thin films.

Analytical techniques that are generally used for chemical analysis of thin films are Inductively Coupled Plasma (ICP), X-ray Photoelectron Spectroscopy (XPS) and Secondary Ion Mass Spectroscopy (SIMS), Rutherford Back Scattering (RBS), Proton Induced X-ray Emission Technique (PIXE) and Energy Dispersive X-ray Analysis (EDX). In the following sections we describe ICP, XPS and SIMS, which were used in the present studies.

1.7.3.1 ICP

Inductively coupled plasma atomic emission is a technique for elemental analysis which utilizes plasma as the atomization and excitation source. Plasma is an electrically neutral, highly ionized gas that consists of ions, electrons and atoms. The energy that maintains an analytical plasma is derived from electric or magnetic field. The sample to be analysed is usually first dissolved in a suitable solvent and then mixed with water before being fed into plasma. Atoms in the plasma emit

light with characteristic wavelength for each element. This light is recorded by one or more optical spectrometers. Intensity of lines will be a measure of the quantity of the elements present in the sample. For quantitative analysis, intensity of light emitted from a standard sample is recorded and is compared with that of the sample to be analysed.

In the present work, this technique was used for the elemental analysis of films prepared using CBD and for comparison of stoichiometry of films prepared in different conditions.

1.7.4.2 XPS analysis

When a molecule or atom is bombarded with high energy X-rays, emission of inner core electrons from the sample atom takes place. Kinetic energy of the photoelectron (E_k) is then measured using an energy analyzer. Binding energy (E_b) of core electron relative to Fermi level can be computed from the relation

$$E_b = h\nu - E_k - \phi \quad (16)$$

where $h\nu$ is the energy of the exciting photon, ϕ is the work function. The energy of the ejected electrons is thus the characteristics of the atoms involved and their chemical environment. The binding energy of the core electrons are affected by the valance electrons and therefore by the chemical environment of the atom. When atomic environment of an atom changes, it alters the local charge surrounding the atom. This charge, in turn, reflects itself as a variation in the binding energy of all the electrons of the atom. Thus not only the valance electrons but also the binding energy of the core electrons experiences a characteristic shift. Hence the shift in the binding energy can give important information regarding the valance states/compound formation of the atom in the sample and one can use this technique to find out whether an element present in a sample is in pure or in compound form [115]. XPS technique is generally a surface analysis technique. However, with facility for physically etching using sputtering technique, depth profile is also achieved.

In the present study, XPS spectra were recorded using an ULVAC-PHI unit (model:ESCA-5600CIM) employing Argon ion sputtering (Voltage = 3 kV, Raster size=3×3 mm², pressure 10⁻⁸ mbar). Depthwise elemental presence and

compositional analysis was done using the spectra, for all the samples prepared using CBD and vacuum evaporation.

1.7.3.2 SIMS

Bombardment of a sample surface with a primary ion beam followed by mass spectrometry of the emitted secondary ions constitutes secondary ion mass spectrometry (SIMS). This technique uses the principle of ion sputtering to detect elements on sample surfaces or to create in-depth profiles from 20 to 2000 nm below the sample surface. In fact, quantitative depth profiling with high detection sensitivity and depth resolution is the most powerful capability of SIMS. Sputtering of secondary ions happens when energetic particles bombard on a sample surface. This makes this method of analysis destructive because the sample is actually eroded, or etched.

When the primary ion strikes the sample there is a momentum transfer to the target atom. This occurs because the primary ion penetrates the sample surface, travels into it for some distance, and then collides with the target atom. Collisions repeat until the energy transfer is insufficient to displace any more target atoms. Some of the primary ions get embedded into the surface while others are ejected along with secondary ions. The ionised debris will then be transferred to the mass spectrometer for analysis. Depth profiling using SIMS is an important technique that is useful to determine concentration of an element in a material as a function of depth.

We used this technique for the elemental analysis as a function of depth.

1.7.4 Optical characterization

Optical measurements constitute an important means of determining the band structures of semiconductors. Photon induced electronic transition can occur between different bands which lead to the evaluation of energy band gap.

Band gap of thin film sample is determined from the absorption spectrum. Near the absorption edge the absorption coefficient α can be expressed as [116]

$$\alpha = A(h\nu - E_g)^2 \quad (17)$$

where A is constant, $h\nu$ is the photon energy, E_g is the band gap and γ is a constant which determines nature of the transition. A plot of $(\alpha h\nu)^{1/\gamma}$ as a function of $h\nu$ gives a straight line with an intercept on the $h\nu$ axis equal to the band gap of the material. In one electron approximation, $\gamma=1/2$ and $3/2$ for allowed direct transition and forbidden direct transition respectively. Value of γ for indirect allowed transitions where phonons are involved is two and for forbidden indirect transition it is three.

In this work, investigations on optical properties are confined to the wavelength dependence of optical absorbance and transmittance of the films. Band gap of the films is the main parameter evaluated from the spectrum recorded using UV-VIS-NIR Spectrophotometer (Hitachi U-3410 model).

1.7.5 Electrical properties

Knowledge of electrical properties of semiconductor materials is necessary for understanding the factors affecting the performance of solar cells. Lifetime and mobility of the minority carriers have been identified as the main electrical parameters of the material controlling the performance of solar cells. In the present investigation, electrical characterization was done by electrical conductivity measurements under dark and illumination conditions, and hall measurements.

1.7.5.1 Electrical conductivity

For the development of device quality films, it is necessary to investigate electrical conductivity under dark and illumination. Also, in thin films, impurities, grain boundaries and interfaces influence the electrical properties. These effects can be understood by analyzing the temperature dependence of both dark and photoconductivity.

In the present work, dependence of conductivity on temperature was measured in the range 50-300 K. Current and voltage were measured using a source measure unit (SMU) (Model:Keithly 236) interfaced by GPIB card and ICS software. Low temperature was achieved using liquid helium cryostat having autotuning temperature controller (Lakeshore 321 model). Further details of measurements are given in following chapters.

1.7.5.2 Hall measurement

Conductivity type, mobility and density of charge carriers of samples were investigated using Hall measurement set up. These parameters were evaluated using Vander Pauw method by four probe measurement technique [117]. In this case measurement of current and voltage are illustrated in fig. 1.5.

In this method, conductivity of the symmetric thin film samples is given by,

$$\rho = \frac{\pi d(R_A + R_B)}{\ln 2} f(R_A/R_B) \quad (18)$$

for symmetric contact, $f(R_A/R_B)=1$

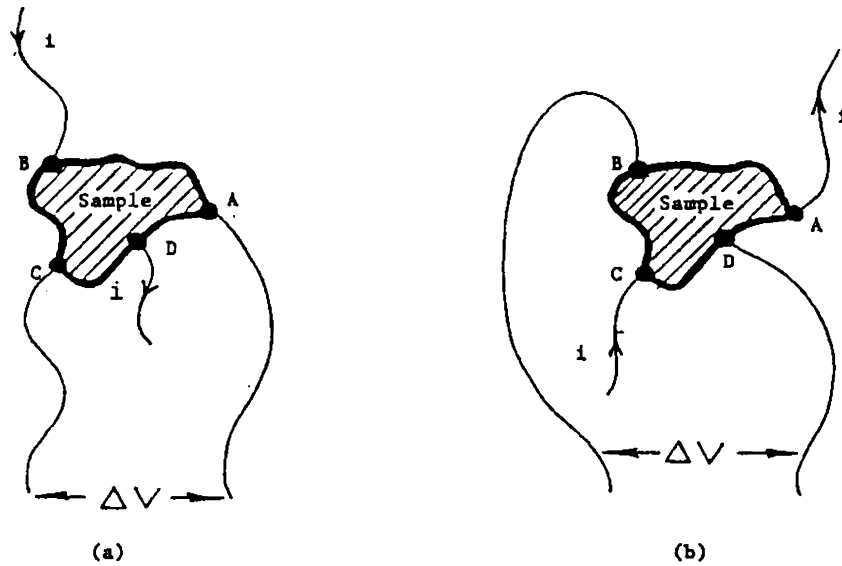


Figure 1.5: vander Pauw method of four probe measurement

The hall mobility (μ), carrier density (n) and Hall coefficient (R_H) are given by.

$$\mu = \frac{(\Delta R_C + \Delta R_D) d}{2 \rho B} \quad (19)$$

$$n = \frac{1}{\rho e \mu} \quad (20)$$

$$R_H = \rho \mu \quad (21)$$

where, $R_C = \frac{V_C - V_A}{i}$ and $R_D = \frac{V_D - V_B}{i}$ as illustrated in fig. ΔR_C and ΔR_D are change in resistance due to reversing the magnetic field and d is the thickness of the sample. In this work, measurements were carried out using Hall measurement set up supplied by MMR Technologies Inc. having MP350 power supply to vary magnetic field and K50 temperature controller.

References

- [1] B. Dimmer and H.W. Schock, *Prog. Photovolt. Res. Appl.*, 6 (1998) 193
- [2] N. Gocsen and J.J. Loferski, *Sol. Energy Mater.*, 1 (1979) 271
- [3] Hans Joachim Moller, *Semiconductors for Solar Cells*, Artech House, Boston, London 1993
- [4] M.S. Thyagi, *Introduction to Semiconductor Materials and Devices*, John Wiley & Sons, 1991
- [5] Dieter Bonnet and Peter Meyers, *J. Mater. Res.*, 13 (1998) 2740
- [6] Stephen. J. Fonash, *Solar Cell Device Physics*, Academic Press 1981
- [7] A .Catalano, *Solar Energy Mater and Sol. Cells*, 41/42 (1996) 205
- [8] Y-S. Tyan and E. A. Perez-Albuerne, *Proc. 16th Photovoltaic Specialist Conf., 1982*, 794
- [9] C. Fekides, J. Britt, Y. Ma. and L. Killian, *Proc. 23rd IEEE Photovoltaic Specialists Conf.*, 1993, 389
- [10] Asema. E and van. B. C. W Engelenburg; *Proc. 11th EC Photovoltaic Solar Energy Conference, Montreux, Switzerland,1992*, Harwood Academic Publishers, Chur, Switzerland, 1993, p-995
- [11] V. M Fthenakis and Moskowitz; *Prog. Photovolt.: Res. Appl.*, 3 (1995) 295
- [12] C. Yang Jeffry; *Prog. Photovolt.: Res. Appl.*, 6 (1998) 181
- [13] W. H Bloss, F. Pfisterer, Schubert. M and T.Walter; *Prog. Photovolt. Res. Appl.*, 3 (1995) 3
- [14] D. L Steabler and C. R. Wronski, *Appl. Phys. Lett.*, 31 (1977) 292
- [15] L. L. Kazmerski; *Current Topics in Photovoltaics*, Academic Press, London (1985) 41
- [16] L. L Kazmerski, P. J Iveland, P. R White and R. B. Cooper; *Proc. 13th IEEE Photovoltaic Specialists Conf.*, Washington, DC, 1978, p-18
- [17] Tokio Nakada, Hiroki Ohbo, Takayuki Watanabe, Hidenobu Nakazawa, Masahiro Matsui and Akio Kunioka, *Solar Energy Materials and Solar Cells* 49 (1997) 285
- [18] M.A. Contreras, B. Egaas and K. Ramanathan, *Prog. Photovolt.* 7 (1999) 311

-
- [19] John. D. Meakin, *SPIE-photovoltaics*, 543 (1985) 108
- [20] H. Neumann, *Solar Cells*, 16 (1986) 317
- [21] H.J. Von Bardeleben, *Solar Cells*, 26 (1986) 381
- [22] Neelkanth. G. Dhere, M. Cristina Lourenco and Ramesh G. Dhere, Lawrence. L. Kazmerski, *Solar Cells*, 16 (1986) 369
- [23] S. S Wagner, J. L Shay, P. Migiliorato, and H. M. Kasper, *Appl. Phys. Lett.*, 25 (1974) 434
- [24] A.F. Fray and P. Lloyd, *Thin Solid Films*, 58 (1979) 29
- [25] Clayron W. Bates, JR., Kim F. Nelson and S. Atiq Raza, John B. Mooney, Jutta M. Recktenwald, Loren Macintosh and Robert Lamoreaux, *Thin Solid Films*, 88 (1982) 279
- [26] Cammy. R, Abernathy, Clayton W. Bates, Jr., Anaba A. Anani and Belgacemhaba, *Thin Solid Films*, 115 (1984) L41
- [27] J. Szot and D. Haneman, *Sol. Energy Mater.*, 11(1984) 289
- [28] S. Isomura, A. Nagamatsu, K. Shinohara and T. Aono, *Solar Cells*. 16 (1986) 143
- [29] Gary Hodes and David Cahen, *Solar Cells*, 16 (1986) 245
- [30] T. L. Chu, Shirley S. Chu, S. C. Lin and J. Yue, *J. Electrochem. Soc: Solid State Sci. Technol.*, 131 (1984) 2182
- [31] Neelkanth G.Dhere, M. Cristina Lourenco and Ramesh Dhere, *Solar Cells* 16 (1986) 12
- [32] M.V. Garacia-Cuenca, M. Manchon, M. Varela, A. Lousa and J. L. Moenza, *Sol. Energy Mater.*, 17 (1988) 347
- [33] R.D. L Kristensen, S. N. Sahu and D. Haneman, *Sol. Energy Mater.* 17 (1988) 329
- [34] Toshiyuki Yamaguchi, Jiro Matsufusa, Hideki Kabasawa and Akira Yoshida, *J. Appl. Phys.* 69 (1991) 7714
- [35] Pankaj Garg, J. C. Garg and A.C. Rastogi, *IEEE Photovoltaic Specialist Conference*, Florida, 1990, 471
- [36] N. Khare, G. Razzini and L. Perldo Bicelli, *Thin Solid Films*, 186 (1990) 113

-
- [37] Brian. J Brown, Clayton W. Bates and Jr., *J. Appl. Phys.*, 68 (1990) 2517
- [38] C. Guillen, E. Galiano and J. Herrero, *Thin Solid Films*, 195 (1991) 137
- [39] J. Herrero and C. Guillen, *J. Appl. Phys.* 69 (1991) 429
- [40] Y.D. Tembhurkar and J.P. Hirde, *Thin Solid Films*, 215 (1992) 65
- [41] S.R. Kumar, R.B. Gore and R.K. Pandey, *Thin Solid Films*, 223 (1993) 109
- [42] G.K. Padam, G.L. Malhotra and S.K. Gupta, *Sol. Energy Mater.*, 22 (1991) 303
- [43] P.K. Vidyadharan Pillai, K.P. Vijayakumar and P.S Mukherjee, *J. Mater. Sc. Lett.* 13 (1994) 1725
- [44] Manohar Lal, Navadeep Goyal and Anil Vohra, *Thin Solid Films*, 227 (1993) 177
- [45] Mikihiko Nishitani, Takayuki negami, Masaharu Terauchi and Takashi Hirao, *Jpn. J. Appl. Phys.*, 31 (1992) 192
- [46] Shigemi Kohiki, Mikihiko Nishitani, Tkayuki Negami, Takahiro Wada, Hideaki Monjushiro, Iwao Watanabe and Yu Yokoyama, *Thin Solid Films*, 238 (1994) 195
- [47] Shigeru Niki, Yunosuke Makita, Akimasa Yamada, Akira Obara, Osamu Igarashi, Syunji Misawa, Michihiro Kawai, Hisayuki Nakanishi, Yutaka Taguchi and Noboru Kutsuwada, *Sol. Energy Mater. Sol. Cells.*, 35 (1994) 141
- [48] Mayasayuki Tanda, Susumu Manaka, Jorge R. Encinas Marin, Katsumi Kushiya, Hideki Sano, Akira Yamada, Makoto Konagai and Kiyoshi Takahashi, *Jpn. J. Appl. Phys.*, 31 (1992) L753
- [49] Mayasayuki Tanda, Susumu Manaka, Akira Yamada, Makoto Konagai and Kiyoshi Takahashi, *Jpn. J. Appl. Phys.*, 32 (1993) 1913
- [50] A. Ashida, Y. Hachiuma, N. Yamamoto, T. ITO and Y. Cho, *J. Mater. Sc. Lett.*, 13 (1994) 1181
- [51] Antonio Parretta, Maria Luisa Addonizio, Antonio Agati, Michele Pellegrino, Luigi Quercia, Francesco Cardellini, J. Kessler and H. W. Schock, *Jpn. J. Appl. Phys.* 32 (1993) 32
- [52] J. Schmidt, H.H Roscher and R. Labusch, *Thin Solid Films*, 251 (1994) 116

-
- [53] Masaharu Terauchi, Takayuki Negami, Mikihiko Nishitani, Mitsusuke Ikeda, Hiroko Wada and Takahiro Wada, *Sol. Energy Mater. Sol. Cells* 35 (1994) 121
- [54] P. Menna, A. Parretta, M. Pellegrino, L. Quercia and M.L. Addonizio, *Sol. Energy Mater. Sol. Cells*, 35 (1994) 165
- [55] W. Riedl, J. Rimmasch, V. Probst, F. Karg and R. Guckenberger, *Sol. Energy Mater. Sol. Cells*, 35 (1994) 129
- [56] Yuji Kuwahara, Hiroyuki Oyanagi and Hirotaka Yamaguchi, Masakazu Aono, Sho Shirakata and Shigeri Isomura, *J. Appl. Phys.*, 76 (1994) 7864
- [57] R. Pal, K.K Chattopadhyay, S. Chaudhari and A.K Pal, *Thin Solid Films* 254 (1995) 111
- [58] F.O. Adurodija, M.J. Carter and R. Hill, *Sol. Energy Mater. Sol. Cells* 37 (1995) 203
- [59] J.R. Tuttle, M. Contreras, M.H. Bode, D. Niles, D.S. Albin, R. Matson, A.M. Gabor, A. Tennant, A. Duda and R. Noufi, *J. Appl. Phys.*, 77 (1995) 153
- [60] Nishitani. M, Negami. T and Wada. T, *Thin Solid Films*, 258 (1995) 313
- [61] P.J. Sebastian, A.M. Fernandez and A. Sanchez, *Sol. Energy Mater. Sol. Cells*, 39 (1995) 55
- [62] C. Guillen and J. Herrero, *Sol. Energy Mater. Sol. Cells* 43 (1996) 47
- [63] D. J. Bottomley, A. Mito, S. Niki and A. Yamada, *J. Appl. Phys.*, 82 (1997) 817
- [64] S. Zweigart, S. M. Sun, G. Bilger and H. W. Schock, *Sol. Energy Mater. Sol. Cells*, 41/42 (1996) 219
- [65] Bulent M. Basol, Vijay K. Kapur, Craig R. Leidholm, Arvind Halani, Kristen Gledhill, *Sol. Energy Mater. Sol. Cells*, 43 (1996) 93
- [66] H. Schon, V. Alberts and E. Bucher, *Thin Solid Films*, 301 (1997) 115
- [67] Tokio Nakada and Akio Kunioka, *Jpn. J. Appl. Phys.*, 37 (1998) L1065
- [68] N. Stratieva, E. Tzvetkova, M. Ganchev, K. Kochev and I. Tomov, *Sol. Energy Mater. Sol. Cells*, 45 (1997) 87
- [69] E. Tzvetkova, N. Stratieva, M. Ganchev, I. Tomov, K. Ivanova, K. Kochev, *Thin Solid Films*, 311 (1997) 101

-
- [70] Shigetaka Nomura, Kazuhiko Nishiyama, Kenji Tanaka, Motoya Sakakibara, Masatoshi Ohtsubo, Nobuyuki Furutani and Saburo Endo, *Jpn. J. Appl. Phys.*, 37 (1998) 3232
- [71] Manjunatha Pattabi, P. J. Sebastian, X. Mathew and R.N. Bhattacharya, *Sol. Energy Mater. Sol. Cells*, 63 (2000) 315
- [72] Kenichi Kondo, Hiroyuki Sano and Katsuaki Sato, *Thin Solid Films*, 326 (1998) 83
- [73] M.C. Artaud, F. Ouchen, L. Martin, S. Duchemin, *Thin Solid Films*, 324 (1998) 115
- [74] M.E. Calixto and P.J. Sebastian, *Sol. Energy Mater. Sol. Cells* 63 (2000) 335
- [75] Sung Chan Park, Doo Youl Lee, Byung Tae Ahn, Kyung Hoon Yoon, and Jinsoo Song, *Sol. Energy Mater. Sol. Cells* 69 (2001) 99
- [76] K. Guenoun, K. Djessas and G. Masse, *J. Appl. Phys.*, 84 (1998) 589
- [77] S.Chichibu, T. Shioda, T. Irie and H. Nakanishi, *J. Appl. Phys.* 523 (1998) 522
- [78] H. Sakata and H. Ogawa, *Sol. Energy Mater. Sol. Cells*, 63 (2000) 259
- [79] Kenji Yoshino, Hirosumi Yokoyama, Kouji Maeda and Tetsuo Ikari, Atsuhiko Fukuyama, Paul. J. Fons, Akimasa Yamada and Shigeru Niki, *J. Appl. Phys.*, 60 (1999) 4354
- [80] Sho Shirakata, Hitoshi Kubu, Chihiri Hamaguchi and Shigehiro Isomura, *Jpn. J. Appl. Phys.*, 36 (1997) L 1394
- [81] V. Vorliceck, V. Zelenzny, A.N. Tiwari, M. Krejci and H. Zogg, *J. Appl. Physics*, 82 (1997) 5484
- [82] M.A. Contreras, A.M. Gabor, A.L. Tennant, S. Asher, J.R. Tuttle and Noufi, *Prog. in Photovolt: Res. and Appl.*, 2 (1994) 287
- [83] G. Masse, K. Djessas, K. Guenoun and A. Smith, *Thin Solid Films*, 278 (1996) 82
- [84] Neelkanth. G. Dhere and Kelvin W. Lynn, *Sol. Energy Mater. Sol. Cells*, 41/42 (1996) 271
- [85] R. Friedfeld, R. P. Raffaele, and J.G. Mantovani, *Sol. Energy Mater. Sol. Cells*, 58 (1999) 375

-
- [86] Andrew M. Gabor, John R. Tuttle, Michael H. Bode, Amy Franz, Andrew L. Tennant, Miguel A. Contreras, Rommel Noufi, D. Garth Jensen and Allen M. Hermann, *Sol. Energy Mater. Sol. Cells*, 41/42 (1996) 355
- [87] T. Walter, D. Braunger, H. Dittrich, Ch. Koble, R. Herberholz and H.W. Schock, *Sol. Energy Mater. Sol. Cells*, 41/42 (1996) 355
- [88] K. L. Chopra and S. R Das, *Thin Film Solar cells*, Plenum Press, New York (1983) p- 195
- [89] Joy George, *Preparation of Thin Films*, Marcel Dekker, Inc., New York (1992) p-353
- [90] L. I Maissel, R. Glang; *Hand Book of Thin Film Technology*, Mc Graw Hill, New York (1970)
- [91] Poolla Raja Ram, R. Thangaraj, A. K. Sharma and O.P Agnihotri; *Solar Cells*, 14 (1985) 123
- [92] R.W. Birkmire, L.C. Dinetta, P.G. Lasswell, J.D. Meakin and J.E. Phillips, *Solar Cells*, 16 (1986) 419
- [93] T.C. Lommasson, H. Talieh, J.D. Meakin and John A. Thorton, *IEEE Photovoltaic Specialists Conf.* 1987, 1285.
- [94] Shih and C.X. Qiu, *IEEE Photovoltaic Specialists Conf.* 1987, 1201
- [95] H. Oumous, A. Knowles, M.H. badawi, M.J. Carter and R. Hill, *IEEE Photovoltaic Specialists Conf.* 1987, 477
- [96] W.E. Devaney, J.M. Stewart, W.S. Chen, *IEEE Photovoltaic Specialists Conf.* 1990, 535
- [97] Takayuki Negami, Mikihiko Nishitani, Mitsusuke Ikeda and Takahiro Wada, *Sol. Energy Mater. Sol. Cells*, 35 (1994) 215
- [98] Katsumi Kushiya, Hideki Hakuma, Hideki Sano, Akira Yamada, Makoto Konagai, *Sol. Energy Mater. Sol. Cells*, 35 (1994) 223
- [99] Dimitri Hariskos, Martin Ruckh, Ulfert Ruhle, Thomas Walter, Hans Werner Schock, Jonas Hedstrom and Lars Stolt, *Sol. Energy. Mater. Sol. Cells* 41/42 (1996) 345
- [100] Bulent M. Basol, Vijay K. Kapur, Craig R. Leidholm, Arvind Halani, Kristen Gledhill, *Sol. Energy. Mater. Sol. Cells* 43 (1996) 93

-
- [101] Miguel A. Cotreras, John Tuttle, Andrew Gabor, Andrew Tennant, Kannan Ramanathan, Sally Asher, Army Franz, James Keane, L. Wang and Rommel Noufi, *Sol. Energy Mater. Sol. Cells*, 41/42 (1996) 231
- [102] S.N. Qiu, W.W. Lam, C.X. Qiu, I. Shih, *Appl. Surface Sci.*, 113 (1997) 764
- [103] Wen S. Chen, J. M. Stewart, W.E. Devaney, R.A. Devaney, R.A. Mickleson and B. J. Standbery, *IEEE Photovoltaic Specialists Conf.*, 1993, 422
- [104] Se Han Kwon, Byung Tae Ahn, Seok Ki Kim, Kyung Hoon Yoon and Jinsoo Song, *Thin Solid Films* 323 (1998) 265
- [105] P. K. Vidyadharan Pillai and K.P. Vijayakumar, *Sol. Energy Mater. Sol. Cells*, 51 (1998) 47
- [106] R.N. Bhattacharya, W. Batchelor, K. Ramanathan, M.A. Contreras and T. Moriarty, *Sol. Energy Mater. Sol. Cells*, 63 (2000) 367
- [107] Markus E. Beck, Amy Swartzlander-Guest, Rick Matson, James Keane and Rommel Noufi, *Sol. Energy Mater. Sol. Cells*, 64 (2001) 135
- [108] Franz H. Karg, *Sol. Energy Mater. Sol. Cells*, 66 (2001) 645
- [109] K. Bindu, M Lakshmi, S. Bini, C. Sudha Kartha, K.P Vijayakumar, T. Abe and Y. Kashiwaba, *Semiconductor Science and Technology*, 17 (2002) 270
- [110] P. K Nair, M. T. S Nair, V. M. Garcia, O. L Arenas, Y. Pena, A. Castillo, I. T. Ayala, O. Gomezdaza, A. Sannchez, J. Campos, H. Hu, R. Surez and M. E Rincon, *Sol. Energy Mater. Sol. Cells*, 52 (1998) 313
- [111] D.E. Bode, in:G. Hass and R.E. Thun (Eds.), *Physics of Thin Films*, Academic Press, New York 3 (1996) 275
- [112] O. Savadogo and K.C. Mandal, *Appl. Phys. Lett.*, 63 (1993) 12
- [113] K.L. Chopra, R.C. Kainthla, D.K. Pandya, A.P. Thakoor, in:G. Hass, M.H. Francombe, J.L. Vossen, (Eds), *Physics of Thin Films*, Academic Press, New York, 12 (1982) p-201
- [114] K.L. Chopra and S.R. Das, *Thin Film Solar Cells* Plenum Press, New York, (1983)]
- [115] John.F. Moulder, William F. Stickle, Peter E. Sobol, Kenneth D. Bomben, Perkin Elmer Corporation, U.S.A (1992) p-20
- [116] R.A. Smith, *Semiconductors*, Academic Publishers (1989)
- [117] L.J. van der Pauw, *Philips. Res. Rep.*, 13 (1958) 1

CHAPTER 2

CONVERSION OF COPPER SELENIDE INTO COPPER INDIUM SELENIDE BY DIFFUSING INDIUM: AN ATTEMPT

2.1 Introduction

There are several methods reported for the preparation of device quality CuInSe_2 films, either in one-step or multi-step processes and some of those are reviewed in the last chapter. In one-step processes, CuInSe_2 film is grown by codeposition of Cu, In and Se simultaneously. Techniques for film deposition in this case are physical evaporation, chemical deposition or electrodeposition [1]. Physical evaporation involves three source evaporation of Cu, In and Se with proper control of flux of each element [2]. However, for large area fabrication this technique is not suitable. Chemical deposition include spray pyrolysis [3,4] and chemical bath deposition [5,6]. In both cases molarity and/or pH of the solution containing Cu, In and Se ions are appropriately controlled to get nearly stoichiometric CuInSe_2 films. In spray pyrolysis temperature of the substrate and in CBD the temperature of the reaction bath are also controlling parameters affecting formation of single phase CuInSe_2 . In electrodeposition, principle is electrolysis of ionic solution containing Cu, In and Se ions. Electrode potential, molarity, pH of the solution etc., are the parameters to be controlled in this case [7].

For large area fabrication, chemical methods are much better options compared to physical evaporation methods. In spray pyrolysis, sophisticated arrangements for handling residual evaporants like Se and the use of high purity chemicals make the process much expensive. Of all techniques, solution growth processes are the most simple, low cost and hence well suited for large area deposition of semiconducting thin films. Vidyadharan Pillai et al, fabricated 'All-CBD' $\text{CuInSe}_2/\text{CdS}$ solar cell [8]. However, the major problem associated with this process was the deposition of other binary phases like Cu_2Se and CuSe along with CuInSe_2 phase, unless otherwise controlled.

The multi-step process involves deposition of binary compounds as precursor films in the first step and then convert the binary into ternary compound. For example, deposition of precursor In-Se in the first step Cu-Se in the second step and annealing in the final step or Cu-In layer in first step followed by selenisation. Zweigart et al reported a sequential process starting from In_xSe and converting into CuInSe_2 by diffusing Cu and subsequent selenisation [9]. $\text{Cu}(\text{In,Ga})\text{Se}_2$ films were prepared by Nakada et al., in a multi-step process [10]. In the first step, they deposited CuGaSe layer and then Cu-rich CIGS layers along with Na_2Se at substrate temperature $550\text{ }^\circ\text{C}$. In the final step, In, Ga and Se were evaporated at the same substrate temperature. Usually the binary precursors are deposited by physical evaporation or sputtering.

Bhattacharya et al prepared In-Se, Cu-Se and Cu-In-Se thin films by electrodeposition and subsequent annealing led to CuInSe_2 formation [1]. Brien et al., reported a process to convert Cu_{2-x}Se into CuInSe_2 . They deposited copper selenide by electroless deposition from selenous acid bath containing copper sulphate and indium sulphate and then In was incorporated into the film by a galvanostatic cathodic polarization [11].

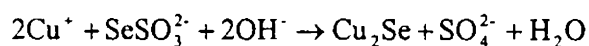
In the present work, we tried a multi-step process in which the precursor is Cu_{2-x}Se on which an indium layer was deposited and diffused by annealing process leading to the formation of CuInSe_2 .

2.2. Experimental details

CBD is potentially stable process for deposition of binary precursor. In the present investigation, we adopted CBD process for growing copper selenide precursor and tried to convert it into CuInSe_2 compound through indium diffusion. Here we adopted a multi-step process which consists of three consecutive stages. In the first step, Cu_{2-x}Se film was deposited and in the second step indium layer was evaporated on the Cu_2Se layer using vacuum evaporation. Third stage involved annealing the bilayer consisting of $\text{Cu}_{2-x}\text{Se}/\text{In}$ in high vacuum.

2.2.1 Preparation of Cu_{2-x}Se using CBD

Deposition of copper selenide thin films involved a controlled reaction between copper ions and selenium ions present in a reaction bath, leading to deposition on the surface of substrate placed in the bath. The reaction can be written as [12],



Release of copper and selenium ions depends on pH and temperature of the reaction bath and concentration of reactant solution. Nature of films deposited also depends on substrate. Hence, growth of good quality Cu_{2-x}Se film requires appropriate choice of substrate and optimized conditions of reaction bath. In the following section a detailed description of these points is given.

2.2.1.1 Preparation of substrates

Substrates used for the depositing Cu_{2-x}Se as precursor for CuInSe_2 is SnO_2 coated glass slides of dimension $2.5 \times 4.5 \times 0.2 \text{ cm}^3$ and this resulted in better adhesion. [6]. SnO_2 was prepared using spray pyrolysis [13] on well-cleaned glass substrate. Cleaning was found to be very important, as it is one of the factors determining the composition and grain size of the film. We adopted solvent cleaning described as follows: Glass slides were first dipped in freshly prepared chromic acid for 3 h, to remove oil content on the glass substrates. Then the slides were washed with running water followed by soap solution (Extran). These were again washed with running water. Finally all the slides were rinsed with distilled water and then dried before coating Cu_{2-x}Se .

Then, 50 ml of 0.5 M alcoholic solution of SnCl_4 was sprayed on these cleaned glass substrates kept at 673 K for 1 h, using air as carrier gas. Pyrolytic decomposition of SnCl_4 droplets resulted in deposition of SnO_2 at that temperature. After SnO_2 coating also, it was cleaned using distilled water and dried

2.2.1.2 Preparation of reactant solutions

In this work, Cu_{2-x}Se deposition involved the controlled release of Cu ions from copper trisodium citrate complex and the ion by ion condensation along with the selenium ions present in the solution, on to the substrate [14]. Chemicals used for the preparation were LR grade (Merck) copper sulfate ($\text{CuSO}_4 \cdot 5\text{H}_2\text{O}$), trisodium citrate (TSC) ($\text{Na}_3\text{C}_6\text{H}_5\text{O}_7 \cdot 2\text{H}_2\text{O}$), sodium sulphite (Na_2SO_3) and sodium

hydroxide (NaOH). Selenizing agent used was Na_2SeSO_3 solution prepared using finely powdered selenium pellets (99.99 %).

Na_2SeSO_3 solution was prepared by dissolving selenium powder in Na_2SO_3 solution kept at 363 K subjected to constant stirring for 1 h. Here, 0.2 M (200 ml) the solution was prepared by dissolving weight of Se corresponding to 0.2 M Se (4.6 g) in excess of aqueous solution of Na_2SO_3 [(0.3 M) (15 g)]. On cooling the solution traces of Se was precipitated which was filtered out. 1 M CuSO_4 , TSC and NaOH solutions were prepared to use for the deposition process.

2.2.1.3 Deposition of Cu_{2-x}Se as precursor

In the first trial, the bath parameters chosen were those optimized by Vidyadharan Pillai et al, for the deposition of CuInSe_2 film [6]. They used 7.5 ml of 0.2 M CuSO_4 solution in a 100 ml beaker mixed with same volume of TSC along with 25 ml of 0.2 M solution of indium citrate. To this solution containing Cu and In ions, 20 ml of 0.1 M Na_2SeSO_3 was added and pH of the resultant solution was adjusted to 6.5 by adding NaOH drops. Same conditions were followed for the preparation of Cu_{2-x}Se film with the difference that indium citrate was not added. Four SnO_2 coated glass substrates were dipped vertically in the solution kept at room temperature for 1 h. Film formed at the surface of the substrate facing the wall of the beaker was chosen and the other side was cleaned using dil. HCl. Uniform films of reddish brown colour were obtained from this bath.

Later the reaction bath was modified as follows: In a 50 ml beaker 10 ml of 0.2 M CuSO_4 solution was taken to which 10 ml of TSC was added. Then 10 ml of 0.2 M Na_2SeSO_3 was added to this solution with stirring. pH of the solution before adding Na_2SeSO_3 solution was adjusted to 4.5 using NaOH drops so that the resultant solution had a pH 6.5. SnO_2 coated glass substrates were vertically dipped in the transparent green solution bath, kept at room temperature. After 10 min, the bath turned to brown and reddish brown films were formed after 1 h of deposition.

In order to improve the uniformity and thickness of the film, different trials were carried out varying molarity of the reactant solutions and temperature of the bath keeping pH of the final solution ~ 6.5.

First deposition was done for different molarity of CuSO_4 solution keeping all the other parameters same as above. 0.1 M and 0.4 M solution of CuSO_4 were tried for 0.2 M Na_2SeSO_3 . It was found that in the first case immediate precipitation resulted in non-uniform films and the second case resulted in uniform films.

Then, molarity of Na_2SeSO_4 solution was varied as 0.05 and 0.1 M keeping all the other conditions as that of first trial. It was observed that reaction rate was slow when the molarity was 0.05 and hence thickness was low after 1 h deposition. Good films were obtained for 0.1 M solution.

Thus from the visual observation of the nature of reaction and uniformity of the films, the following parameters were fixed for room temperature deposition as 0.2 M (10 ml) CuSO_4 , 0.1 M Na_2SeSO_3 (10 ml) and the pH of the resultant solution was fixed at ~ 6.5 . Then, the experiment was repeated at different temperatures in the range 278-343 K. When temperature of the bath was lowered to 278 K keeping in ice bath, the rate of deposition was very slow. As temperature of the bath was raised above room temperature, faster rate of reaction resulted in non-uniform films.

From all the trials and observations, optimized conditions for the preparation of good quality Cu_{2-x}Se films is as follows: 10 ml (0.2 M) CuSO_4 solution was mixed with 0.2 M 10 ml TSC in a 50 ml beaker and stirred well and NaOH was added drop by drop so that the pH of the bath is ~ 4.5 . Then 10 ml (0.1 M) Na_2SeSO_4 was added making pH of the bath 6.5. The solution was stirred well and kept at room temperature. After 1 h of deposition, uniform reddish brown films were obtained. Triple dipped films of (thickness $\sim 1\mu\text{m}$) Cu_{2-x}Se were chosen as the precursor for the preparation of CuInSe_2 .

2.2.2 Diffusion of Indium into Cu_{2-x}Se film

The final step for preparing of CuInSe_2 was the diffusion process of indium into Cu_{2-x}Se film. This involved vacuum evaporation of indium layer on Cu_{2-x}Se film and annealing the bilayer, $\text{Cu}_{2-x}\text{Se}/\text{In}$ in high vacuum. Diffusion annealing process was tried for different indium layer thickness on same Cu_{2-x}Se film until the composition analysis resulted $\text{Cu}:\text{In} \sim 1$.

For the evaporation process, Cu_{2-x}Se (deposited on SnO_2 coated glass substrates) were loaded in a vacuum chamber at a distance of 14 cm above the molybdenum boat. Calculated weight of indium (40 mg) to get 400 Å was taken in the boat and the chamber was evacuated to a pressure of 10^{-5} mbar using diffusion pump. Then the boat was resistively heated until indium was evaporated to condense on the substrates.

These bilayer samples were subjected to high vacuum (10^{-5} mbar) annealing in a borosil glass tube winded with tungsten wire, at 573 K for 1 h. The heating rate was 3 K/min, using the temperature controller (Digicon). It was found that after annealing, indium fully diffused into Cu_{2-x}Se layer. Then another layer of indium of thickness 300 Å (~30 mg) was deposited on the annealed sample and again subjected to annealing in the same conditions. This diffusion annealing was repeated in steps of 300 Å so that the total thickness of indium layer diffused was equal to 1300 Å (400+300+300+300 Å). Diffusion process was terminated at this thickness after the compositional analysis using XPS indicated Cu:In ratio to be 1. This will be described in characterization part.

As-prepared Cu_{2-x}Se sample was labeled as CS. Then at each step of annealing the sample was renamed as CIS400, CIS700, CIS1000, CIS1300 according to thickness of indium layer diffused. Hereafter the samples are known by these labels.

2.3 Characterization

Structural, compositional and optical properties of the films after indium diffusion, were analysed using different techniques. Structural studies were done using XRD and composition of the film was determined using XPS. Optical properties of the films were studied by UV-Vis-NIR spectrophotometer.

2.3.1 XRD

Crystallographic studies of as-prepared Cu_{2-x}Se sample and changes in the structure of this film due to indium diffusion were analysed by comparing XRD patterns of as-prepared and indium diffused samples after different stages of annealing. However, XRD of samples which showed significant change in optical

absorption is only presented here. Figure 2.1 shows the XRD pattern of as-prepared Cu_{2-x}Se sample (CS). Scan conditions were 2θ between 20° and 60° with scan speed $15^\circ/\text{min}$. Figure shows two peaks at $2\theta=27.5^\circ$ and 44.7° , corresponding to d-values 3.34 \AA and 2.03 \AA . These two peaks are identified as reflections from (111) and (220) planes of cubic Cu_{2-x}Se phase, with reference to JCPDS-0680 and other reports [15, 13,16]. After diffusing indium layer of thickness $\sim 1300 \text{ \AA}$ in various steps as described in section 2.2.2, the XRD pattern obtained is given in fig. 2.2. This pattern consists of distinct peaks and the respective 2θ values and d- values are given in table 2.1. Identified phases are also indicated in the table from which, it is clear that there are new peaks due to indium diffusion in addition to substrate peaks and Cu_{2-x}Se peaks. According to the JCPDS data, these peaks are due to reflections from corresponding planes of $\gamma\text{-In}_2\text{Se}_3$ and CuInSe_2 indicated in fig 2.2. There are certain peaks that are overlapped by CuInSe_2 , Cu_{2-x}Se and SnO_2 which are also marked in the figure. d- values of Cu_{2-x}Se peak slightly increases after annealing probably as a result of variation in x due to escape of Se from the film during annealing [16]. Also, the height of peak is a quantitative measure of corresponding phase. Small peaks of CuInSe_2 show that only small amount of CuInSe_2 is formed. Thus XRD analysis reveals that indium diffusion into Cu_{2-x}Se resulted in a mixed phase consisting of CuInSe_2 , Cu_{2-x}Se and In_2Se_3 .

Sample	2 θ (degrees)	d-value (Å)	Identified Phase	(hkl)
CS	26.5	3.36	SnO ₂	(110)
	27.0	3.33	Cu _{2-x} Se	(111)
	33.7	2.65	SnO ₂	(101)
	44.7	2.02	Cu _{2-x} Se	(220)
	51.6	1.77	SnO ₂	(211)
CS1300	26.5	3.36	SnO ₂ /Cu _{2-x} Se	(110)/(111)/(112)
	27.5	3.24	Cu _{2-x} Se/CuInSe ₂	(006)
	29.0	3.07	γ -In ₂ Se ₃	(200)
	29.5	3.02	γ -In ₂ Se ₃	(201)
	30.5	2.92	γ -In ₂ Se ₃	(202)
	33.5	2.67	γ -In ₂ Se ₃	(101)
	35.5	2.52	SnO ₂	(211)
	37.5	2.38	CuInSe ₂	(200)
	42.0	2.15	SnO ₂	(105),
	44.0	2.06	CuInSe ₂	(220)/(204),(220)
	51.5	1.79	Cu _{2-x} Se/CuInSe ₂	(211)
	52.5	1.74	SnO ₂	(311)/(116),(312)
	65.5	1.42	Cu _{2-x} Se/CuInSe ₂ SnO ₂	(112)

Table 2.1: XRD details of CS and CS1300

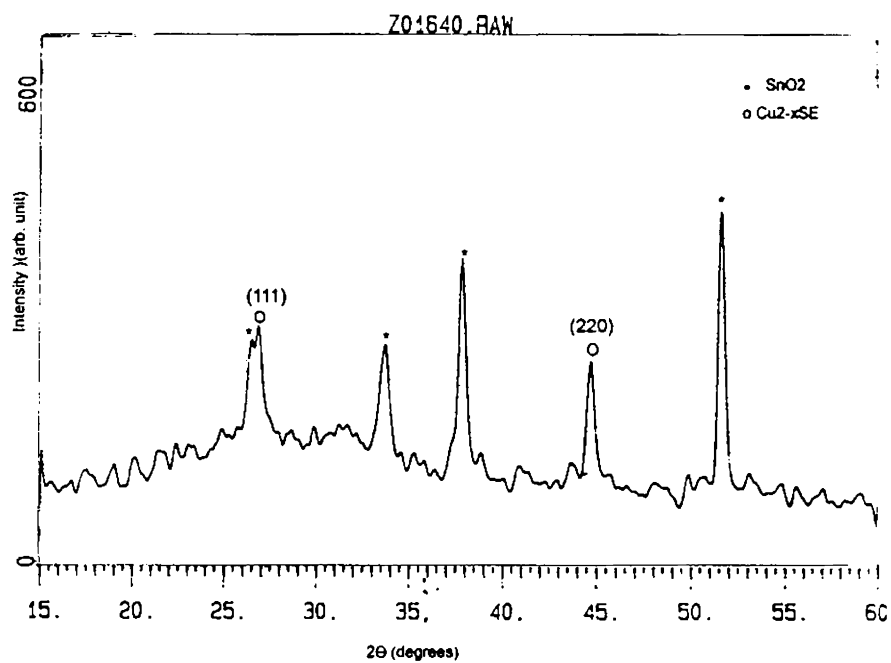
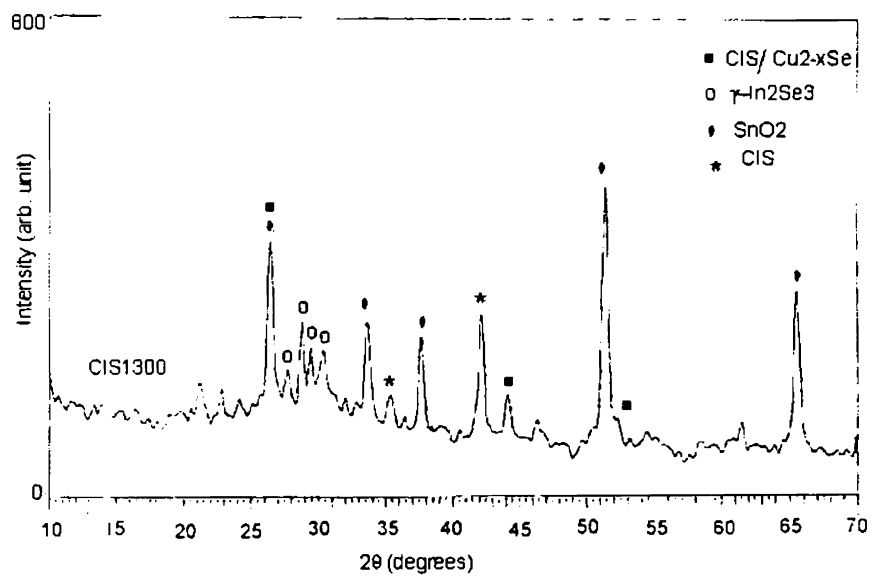
Figure 2.1: XRD pattern of as-prepared Cu_{2-x}Se on SnO₂

Figure 2.2: XRD pattern of CIS1300

2.3.3 Optical properties

Wavelength dependence of optical absorption of CS sample is given in fig.2.3 in the range 1200-400 nm. At longer wavelength absorption is high due to the presence of free carriers [12]. A rapid increase in absorbance (αt) is observed below 600 nm, which corresponds to interband transition. The optical band gap of the material is found out as 2.17 eV from the plot of $(\alpha t h\nu)^2$ vs. $h\nu$, by extrapolating the graph on $h\nu$ axis as given in fig.2.4. The linear nature of the graph indicates that the fundamental transition in Cu_{2-x}Se film is direct.

Changes in absorbance of Cu_{2-x}Se film due to indium diffusion are illustrated in fig. 2.5 for various indium layer thickness. It is obvious from the figure that the optical absorbance at lower wavelength corresponding to interband transition, enhanced significantly with increase with indium diffusion. Specifically, absorbance near 1200 nm, which is the fundamental absorption edge of CuInSe_2 , increased with increase in quantity of indium diffused and maximum change occurs when indium thickness is 1300 Å.

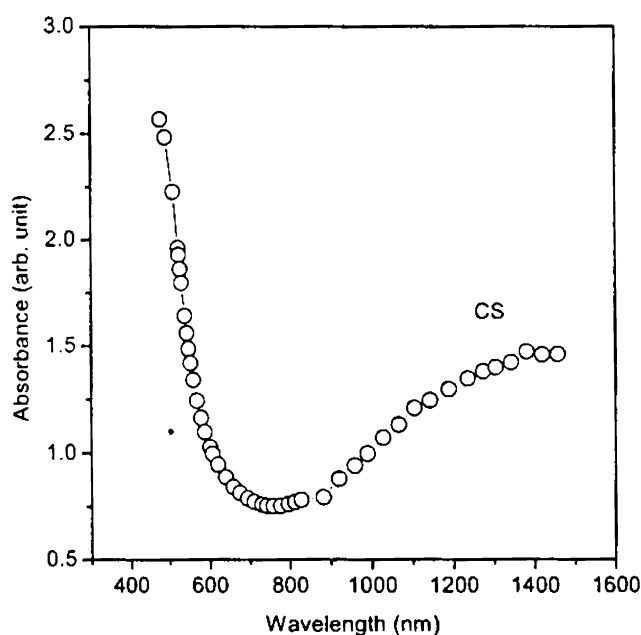
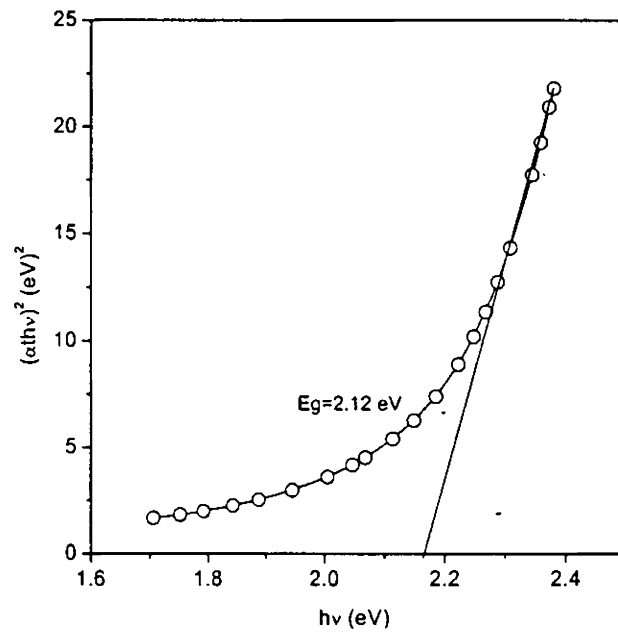
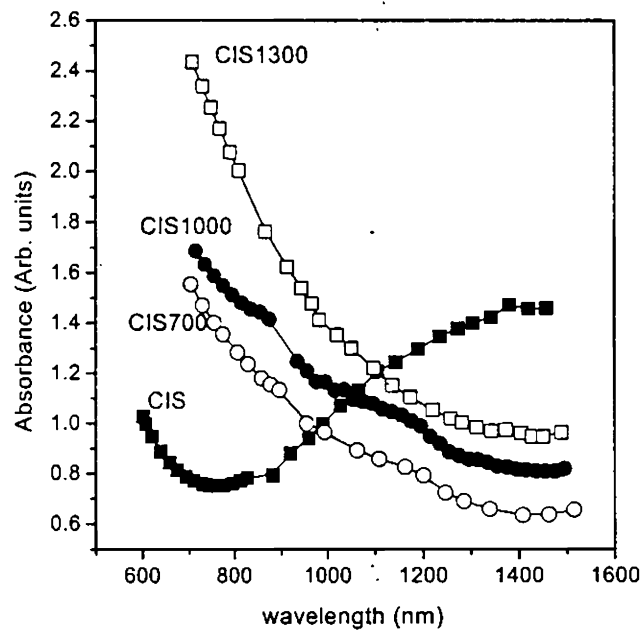


Figure 2.3: Optical absorption spectrum of CS

Figure 2.4: Plot of $(\alpha h\nu)^2$ vs. $h\nu$ of CS sampleFigure 2.5: Optical absorption spectrum of Cu_{2-x}Se sample after each stage of indium diffusion

2.3.2 XPS

Compositional analysis was done on indium-diffused samples, which had higher optical absorbance at wavelengths corresponding to the fundamental absorption edge of CuInSe_2 . Thus XPS spectra was recorded for sample CS1300 and compared with that of CS film. XPS profile montage of as-prepared Cu_{2-x}Se i.e, sample CS is shown in fig. 2.6. Depth profile was done for 30 cycles equivalent to 150 minutes sputtering. Each cycle corresponds to 3 minute sputtering and the approximate depth achieved in each cycle is 100 Å. In the spectra, the peak at characteristic binding energy denotes the presence of corresponding element in the specimen. In the figure, carbon, C1 (1s) peak is checked to correct shift in energy due to instrumental error. The standard value of C1s peak is 284.5 eV and any shift from this value shows requirement of correction for peaks corresponding to different elements. Since the film is deposited on conducting substrate, SnO_2 , shift due to charging effect was avoided. From the spectra, BE of Cu $2p_{1/2}$ and $2p_{3/2}$ levels are 952.2 and 932.5 eV respectively. Similarly, BE of Se $3d_{5/2}$ level is 54 eV. In the elemental state, corresponding energies of Cu levels are 952.4 and 932.6 eV [17] and that of Se $3d_{5/2}$ level is 55.5 eV [18] There is no significant shift in BE for Cu levels from metallic state. However, Se $3d_{5/2}$ level shows a shift 1.5 eV from the elemental state, which indicates compound formation. We could not find from literature, the shift in BE for Se $3d_{5/2}$ or Cu $3p_{3/2}$ in Cu_{2-x}Se state. Cahen et al., reported the respective values of 52.9 eV and 932.5 eV in Cu_2Se and Kazmerski et al., reported 54.5 eV for Se $3d_{5/2}$ level in Cu_xSe [19, 20].

Thus by noting BE values obtained from the sample and using XRD pattern, the compound is identified as Cu_{2-x}Se . At the surface, traces of oxygen are present, which might be due to the exposure of sample to the atmosphere. From the surface to the substrate, the presence of Cu and Se with constant energy reveals the uniformity of the film across its thickness. Two layers, Cu_{2-x}Se and SnO_2 are clearly distinguishable in the figure. SnO_2 layer starts appearing at 20th cycle from the surface.

Depth profile of atomic concentration of Cu and Se shows the ratio Cu/Se is 4 (fig. 2.7). This is due to preferential sputtering of Se. In order to rectify this

Cu:Se ratio was measured in a standard sample of CuSe powder. The correction factor for Se was found to be 2 and after the correction, Cu:Se ratio became as 2:1 in the film.

XPS spectra of sample CIS1300 is shown in figure 2.8. BE of Cu and Se levels have no appreciable change compared to those from sample CS. Two peaks of In at 444 eV and 452 eV are corresponding to BE values of In $3d_{5/2}$ and In $3d_{3/2}$ levels. In elemental state, BE value of In $3d_{5/2}$ which is more intense than the other, is 443.6 eV [21]. Slight shift in BE value of In is due to compound formation in the film. From the value of In $3d_{5/2}$ from the film, the possible compounds formed may be In_2Se_3 and CuInSe_2 in addition to the Cu_{2-x}Se already present in the film [20]. However, BE of Cu $2p_{3/2}$ in CuInSe_2 is 931.8 eV, which is less than that detected from the sample. Also, there is a possibility of formation of In_2O_3 [22]. Traces of oxygen was also observed in the graph, which may be due to the presence of In_2O_3 . Correlating with XRD, the phases formed are In_2Se_3 , traces of CuInSe_2 and In_2O_3 and also, un-reacted Cu_{2-x}Se .

Depth profile of atomic concentration is shown in fig. 2.9. Here, it is observed that the ratio of Cu:In is ~ 1 , but selenium content is very less compared to the Cu/In ratio. However, the indium layer deposited at the surface of Cu_{2-x}Se is uniformly diffused into the depth due to annealing.

Thus it is obvious that by simply diffusing indium into copper (I) selenide, it is difficult to get stoichiometric copper indium selenide films without additional selenisation process.

ESCA PROFILE 1/16/98 START=2, END=32, NFN=1
FILE: CIS102 4

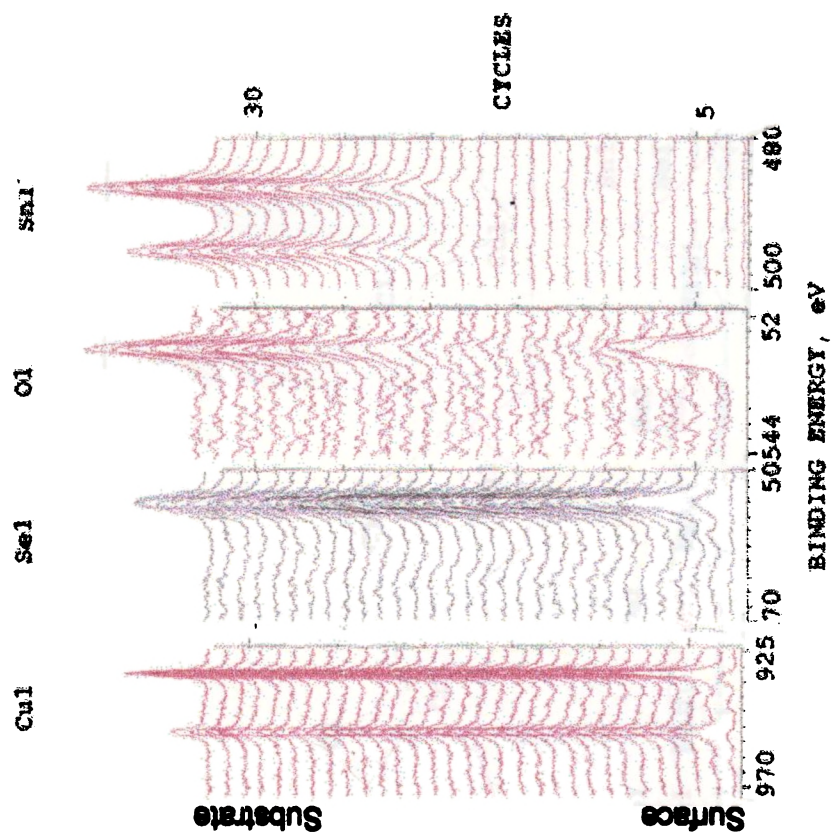


Figure 2.6: XPS profile montage of sample CS

ESCA Profile Alt. 16 Jan 98 Area: 1 Region: 8(Cl) 45 degrees
File: CIS102 4
Sputter Time: 150.00 min
Scale: 0.100 kc/s Offset: 0.000 kc/s Al 400 W Ep: 3.00 kV

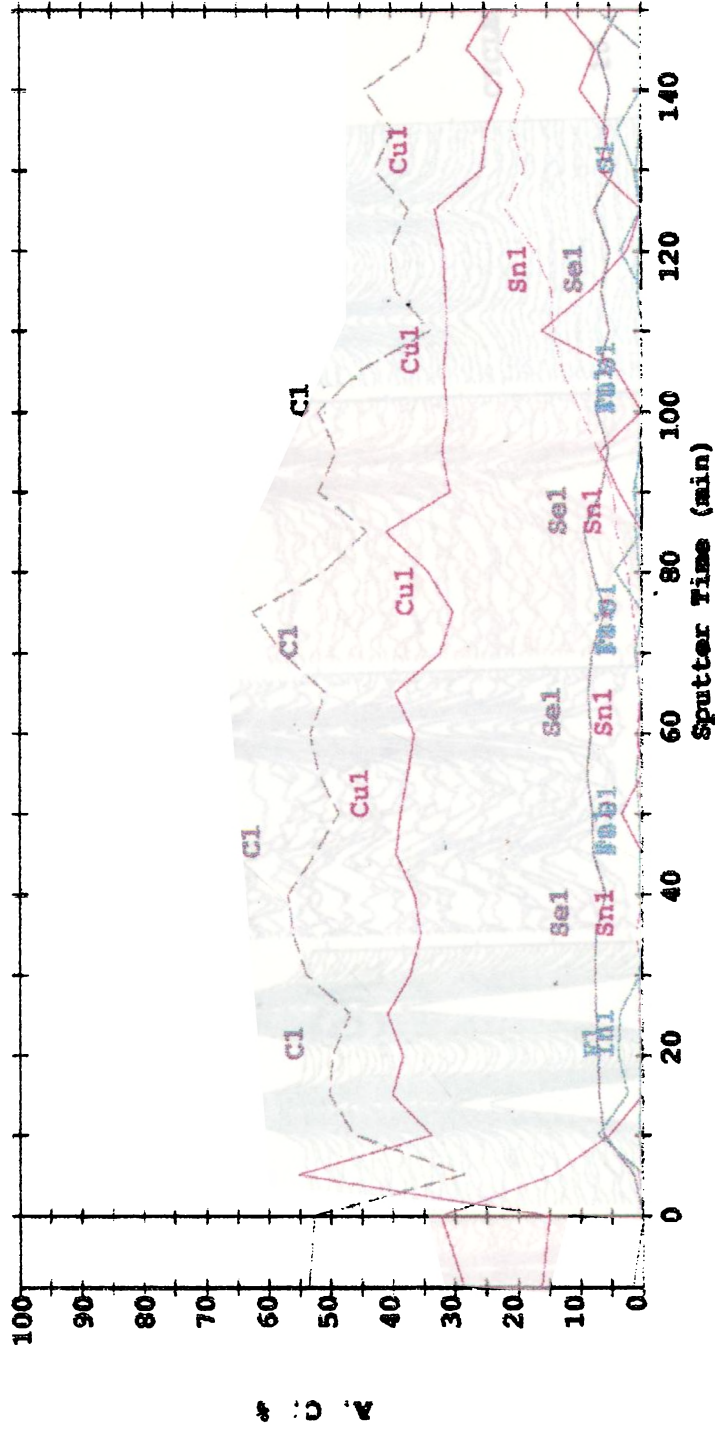


Figure 2.7: Depth profile of percentage atomic concentration of sample CS

ESCA PROFILE 9/19/99 START=1, END=52, NTH=1
FILE: CIS77 (1) CuInSe2

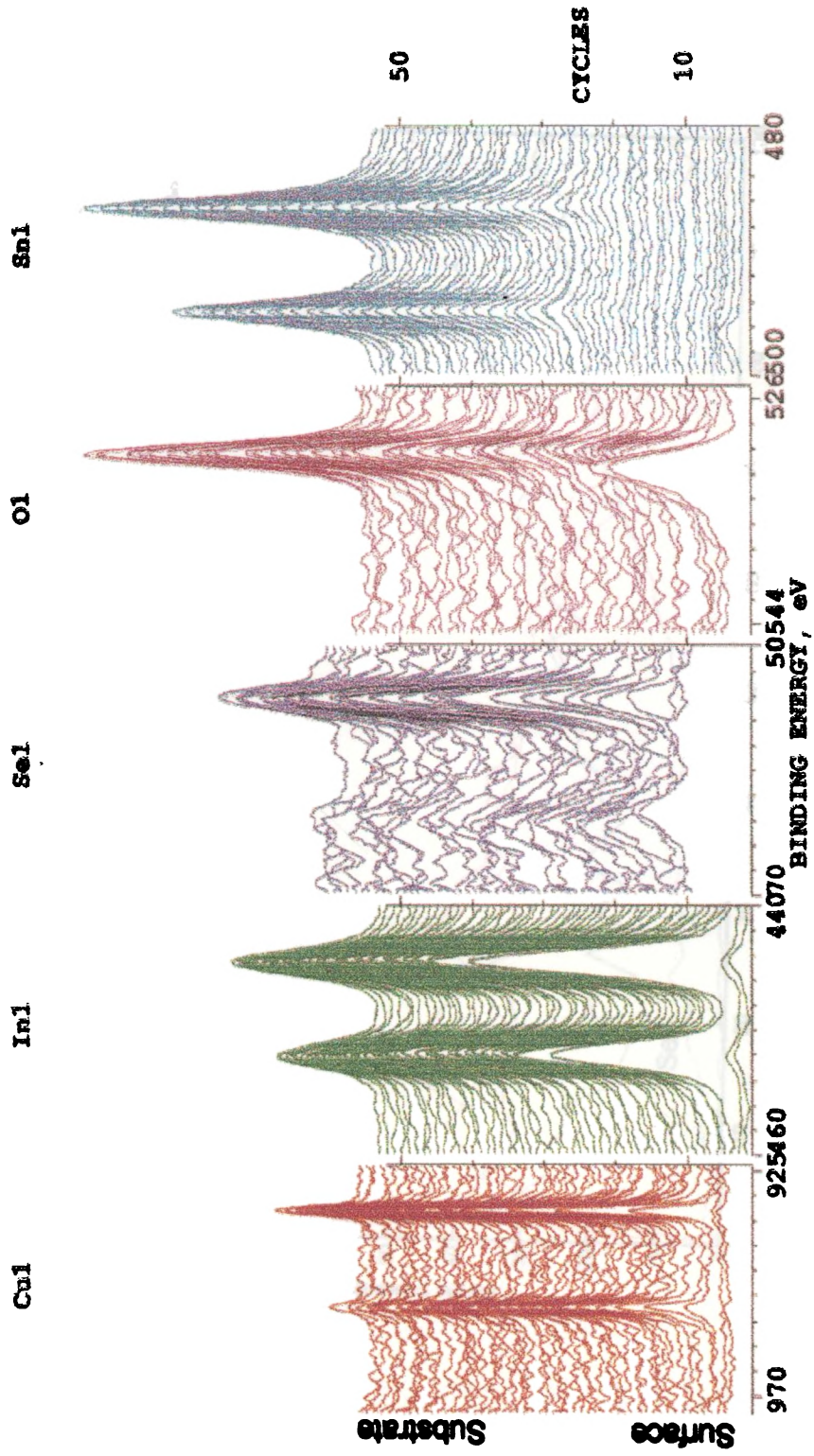


Figure 2.8: XPS profile montage of sample CIS1300

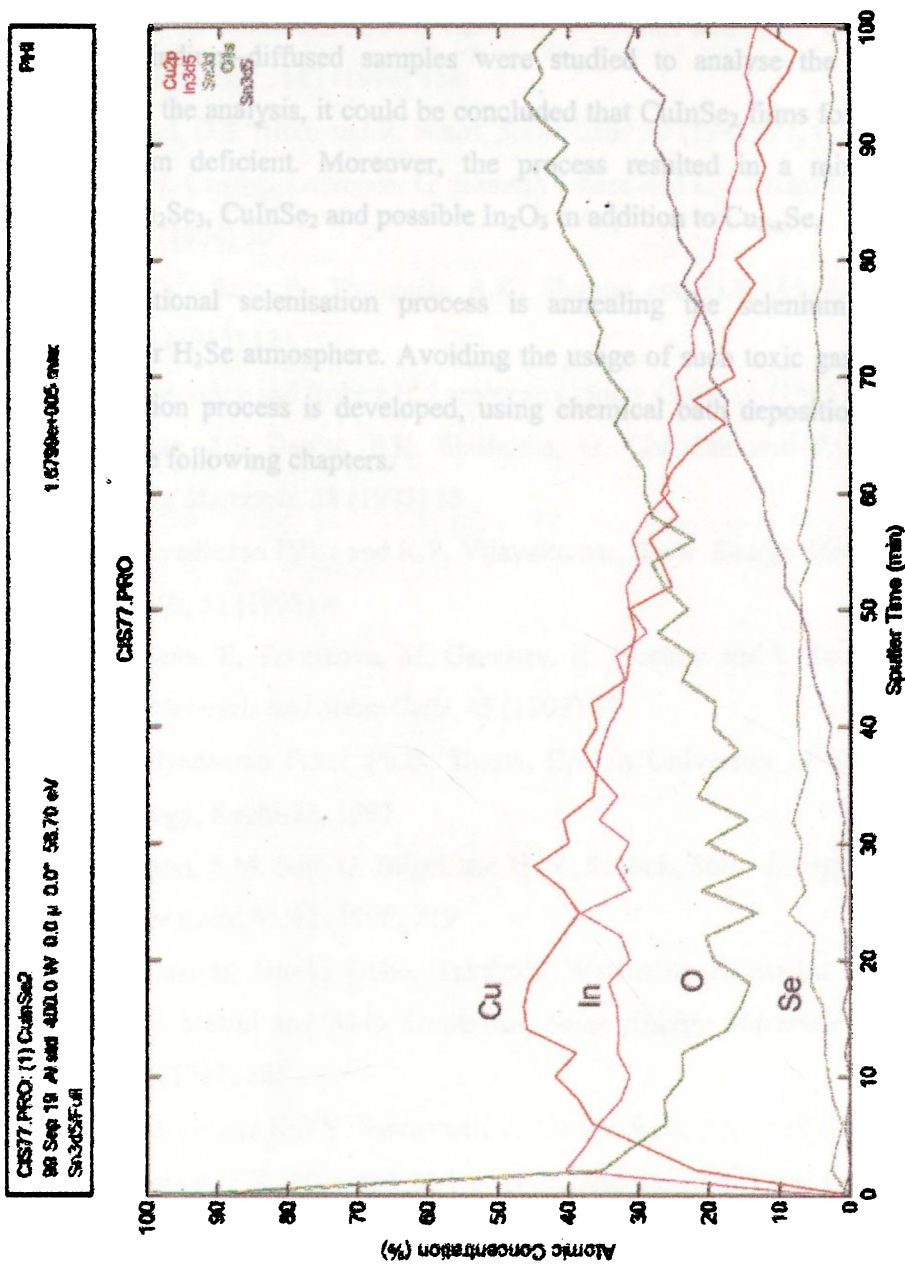


Figure 2.9: Depth profile of percentage atomic concentration of sample CIS1300

2.4 Conclusion

A multi-step process for the preparation of CuInSe₂ film was attempted starting from Cu_{2-x}Se prepared using CBD. The process was diffusion annealing of vacuum deposited In into Cu_{2-x}Se film. Structural, compositional and optical properties of indium-diffused samples were studied to analyse the formation CuInSe₂. From the analysis, it could be concluded that CuInSe₂ films formed were highly selenium deficient. Moreover, the process resulted in a mixed phase consisting of In₂Se₃, CuInSe₂ and possible In₂O₃ in addition to Cu_{2-x}Se.

Conventional selenisation process is annealing the selenium deficient sample in Se or H₂Se atmosphere. Avoiding the usage of such toxic gases, here a novel selenisation process is developed, using chemical bath deposition. This is described in the following chapters.

References

- [1] R.N. Bhattacharya, A.M. Fernandez, M.A. Contreras, J.Keane, A.L. Tenmant, K. Ramanathan, J.R. Tuttle, R. N. Noufi and A.M. Hermann. *J. Electrochem. Soc.*, 143 (1996) 854
- [2] J.R. Tuttle, D.S. Albin and R. Noufi, *Solar Cells* 30 (1991) 21, G. Neelkanth Dhere, M. Cristina Lourenco, G. Ramesh Dhere and L. L. Kazmerski, *Solar Cells* 13 (1984) 59
- [3] Poola Raja Ram, R. Thangaraj, A.K. Sharma and O.P. Agnihotri, *Solar Cells*, 14 (1985) 123
- [4] John B. Mooney and Robert H. Lamoreaux, *Solar Cells*, 16 (1986) 211
- [5] A. Kumar, A.L Dawar, P.K. Shishodia, G. Chauhan and P.C. Mathur, *Journal of Materials*, 28 (1993) 35
- [6] P.K. Vidyadharan Pillai and K.P. Vijayakumar, *Solar Energy Materials and Solar Cells*, 51 (1998) 4
- [7] N. Stratieva, E. Tzvetkova, M. Ganchev, K. Kochev and I. Tomov, *Solar Energy Materials and Solar Cells*, 45 (1997) 87
- [8] P.K. Vidyadharan Pillai, Ph.D. Thesis, Cochin University of Science and Technology, Kochi-22, 1997
- [9] S. Zweigart, S.M. Sun, G. Bilger and H.W. Schock, *Solar Energy Materials and Solar Cells*, 41/42 (1996) 219
- [10] Tokio Nakada, Hiroki Ohbo, Takayuki Watanabe, Hidenobu Nakazawa, Masahiro Matsui and Akio Kunikioka, *Solar Energy Materials and Solar Cells* 49 (1997) 285
- [11] R.N. O'Brien and K.S.V. Santhanam, *J. Electrochem. Soc.*, 139 (1992) 434
- [12] V.M. Garcia, P.K. Nair and M.T.S. Nair, *Journal of Crystal Growth*, 203 (1999) 113
- [13] Sunny Mathew, Ph. D. Thesis, Cochin University of Science and Technology, Kochi, India (1994)
- [14] M. Lakshmi, K. Bindu, S. Bini, K.P. Vijayakumar, Kartha C. Sudha, T. Abe, and Y. Kashiwaba, *Thin Solid films*, 370 (2000) 89
- [15] H. Komura, T. Matsumae and R. Makabe, *Thin Solid Films*, 71 (1980) 53

-
- [16] M. Lakshmi, PhD Thesis, Cochin University of Science and Technology, 2001
- [17] W. Gaarenstroom and N. Weinograd, *J. Chem. Phys.*, 67 (1977) 3500
- [18] C.D. Wagner, W.M. Riggs, L.E. Davis, J.F. Moulder and G.E. Muilenberg, Handbook Of X-Ray Photoelectron Spectroscopy, Perkin-Elmer Corporation, Physical Electronics Division, Eden Prairie, Minn. 55344 (1979)
- [19] D. Cahen, P.J. Ireland, L.L. Kazmerski and I.A. Thiel, *J. Appl. Phys.*, 57 (1985) 4761
- [20] L.L. Kazmerski, O. Jamjoum, J. Ireland, S.K. Deb, R.A. Mickelsen and W. Chen, *J. Vac. Sci. Technol.*, 19 (1981) 467
- [21] P.A. Bertrand, *J. Vac. Sci. Technol.*, 18 (1981) 28
- [22] V.I. Nefedov, D.Gati, B.F. Dzhurinskii, N.P. Sergushin and Y.V. Salyn, *Zh. Neorg. Khim.*, 20 (1975) 2307

CHAPTER 3

AMORPHOUS SELENIUM (a-Se) FILMS USING CBD: DEPOSITION AND CHARACTERIZATION

3.1 Introduction

Selenisation is the process of incorporating elemental selenium into metallic layers to prepare binary or ternary selenides. Conventional technique involves annealing the required metallic layer in an atmosphere of hydrogen selenide or selenium vapour, which are extremely toxic gases. This requires highly sophisticated arrangements for complete safety and protection, which makes the set up much expensive. Moreover, this will become a problem in large-scale production. When one considers cost effectiveness as well as avoiding toxic gases, CBD is the best option for selenisation.

In the present investigation, we adopted CBD for the preparation of selenium (a-Se) in the form of thin films. Structural analysis of the films showed that the films are amorphous in nature.

3.2 A brief review on a-Se thin films

Selenium is 34th element in the periodic table with two unsatisfied bonds in its outer orbital structure. It can exist in crystalline form but the amorphous form (a-Se) is of interest for different technological applications. Density of a-Se is 4.2 g/cc and it is believed to be an inorganic polymer consisting of covalently bonded chains. Although it is not a crystalline structure an effective band-gap of 2.2 eV can be ascribed to it. Resistivity of a-Se is exceedingly high (about 10^{16} ohm cm) making the material a very good insulator. However it is a photoconductor and if an electric field is present to separate the photogenerated electrons and holes, it can generate significant currents [1].

Amorphous selenium has been widely investigated over the decades because of the many scientific and technological interests. Earlier it was the xerographic material of choice for a long time, and is now being considered for

digital x-ray imaging [2]. Even though in the present work, we are not studying such applications, some of the recent research works on this material in this direction are reviewed here.

In a review report on amorphous semiconductors, David Adler described different suggestions made by many researchers on the structure of a-Se [3]. In that review, they proposed a combination of molecular Se_8 rings and polymeric chains to be consistent with all structural studies. Recently, Caprion et al showed that a-Se consists of interconnected chains and rings with a mean coordination number of 2.1 [4].

Structural changes from amorphous phase to crystalline phase (c-Se) are reported in recent studies. Laser induced crystallization is reported for a-Se films due to irradiation by linearly polarized He-Ne or Ti:Sapphire (630 -750 nm) laser beams with sample temperature at and slightly above the glass transition temperature. They prepared a-Se thin films using thermal evaporation of gray selenium. After laser exposure, both β -monoclinic and hexagonal crystalline phases were detected [5].

Light-induced changes in a-Se films (prepared using pulsed laser evaporation) were investigated by Hansen et al. [6]. They explained this as light induced relaxation of void-filled short-chain selenium film into a denser equilibrium state of long polymer chain film which does not readily wet glass or silicon substrate. Peled et al reported photodeposition of a-Se films by continuous-wave argon ion lasers. When laser light was allowed to pass through a-Se colloid-Se ion solution. [7], they observed an increase in rate of redox reaction leading to the formation of $\text{Se}^{(0)}$ from Se^{4+} .

Dependence of crystallization of films on temperature and time of aging was investigated by Zienab et al. They calculated optical bandgap energies for different allotrops of selenium as 1.65 eV for black Se, 1.6 eV for monoclinic and 2.05 eV for amorphous Se [8]. Crystallization process was also found to depend on the deposition procedure. Parameters such as deposition rate, film thickness, substrate temperature and nature of substrate have marked effects on the structure

of the film [9,10]. Fleury et al., used conductivity studies to analyse kinetics of structural change taking place in flash evaporated a-Se films [11].

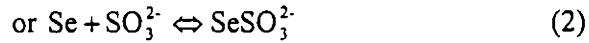
In the applications of a-Se thin films, only a few important reports are listed here. In X-ray imaging, X-ray sensitivity of the film was investigated by Kasap et al., [12]. Holographic recording in ultra thin a-Se film was performed by Ballesteros et al. [13].

In the following sections, preparation of a-Se thin film using CBD and characterization of these samples using different techniques are described.

3.3 Preparation of a-Se using CBD

3.3.1 Principle

Principle of this technique is described in detail by Kitaev et al. [14]. They considered the formation of Na_2SeSO_3 by dissolving selenium in the aqueous solution of Na_2SO_3 , which is represented as



Principle of selenium deposition is based on the fact that concentration of sulphites and hence solubility of selenium depends on pH of the solution. This could be explained as follows. For the reaction (2), equilibrium constant of this reaction is given by

$$K_{\text{SeSO}_3^{2-}} = \frac{[\text{SeSO}_3^{2-}]}{[\text{SO}_3^{2-}]} \quad (3)$$

where, $[\text{SeSO}_3^{2-}]$ and $[\text{SO}_3^{2-}]$ are equilibrium concentration of the SeSO_3^{2-} and SO_3^{2-} respectively. Considering hydrolysis of sodium sulphite, the fractional concentration of SO_3^{2-} , $\alpha_{\text{SO}_3^{2-}}$ is given by

$$\alpha_{\text{SO}_3^{2-}} = \frac{[\text{SO}_3^{2-}]}{[\text{H}_2\text{SO}_3] + [\text{HSO}_3^-] + [\text{SO}_3^{2-}]} \quad (3)$$

$$= \frac{K_{\text{H}_2\text{SO}_3}}{[\text{H}^+]^2 + K_1[\text{H}^+] + K_{\text{H}_2\text{SO}_3}} \quad (4)$$

where K_1 is the first dissociation constant of the reaction,

$\text{H}_2\text{SO}_3 \rightleftharpoons \text{HSO}_3^- + \text{H}^+$ and is given by

$$K_1 = \frac{[\text{HSO}_3^-][\text{H}^+]}{[\text{H}_2\text{SO}_3]}$$

and $K_{\text{H}_2\text{SO}_3}$ is total dissociation constant given by

$$K_{\text{H}_2\text{SO}_3} = K_1 \times K_2 \quad (5)$$

where, K_2 is the second dissociation constant of the reaction,

$\text{HSO}_3^- \rightleftharpoons \text{SO}_3^{2-} + \text{H}^+$ and is given by

$$K_2 = \frac{[\text{SO}_3^{2-}][\text{H}^+]}{[\text{HSO}_3^-]}$$

From eq. (4) it is clear that as a result of hydrolysis of Na_2SO_3 , concentration of $[\text{SO}_3^{2-}]$ ions is defined not only by concentration of sodium sulphite salt in the solution but also the value of pH. Kitaev et al., determined the value of $\alpha_{\text{SO}_3^{2-}}$ by substituting the value of $K_1 = 1.3 \times 10^{-2}$ and $K_{\text{H}_2\text{SO}_3} = 8.2 \times 10^{-10}$ as given in the table below.

PH	1	2	3	4	5	
$\alpha_{\text{SO}_3^{2-}}$	9.1×10^{-7}	3.6×10^{-6}	5.7×10^{-5}	6.3×10^{-4}	6.3×10^{-3}	
PH	6	7	8	9	10	11
$\alpha_{\text{SO}_3^{2-}}$	5.9×10^{-2}	0.33	0.87	0.98	.99	1.0

Table 3.1: Fractional dissociation constant of SO_3^{2-} at different pH

As seen from the table 3.1, the concentration of SO_3^{2-} is equal to that of Na_2SO_3 in the solution, only at $\text{pH} \geq 10$. Hence, if pH of Na_2SO_3 solution is < 9 , the concentration of SO_3^{2-} is,

$$[\text{SO}_3^{2-}] = \alpha_{\text{SO}_3^{2-}} \times [\text{Na}_2\text{SO}_3] \quad (6)$$

From the known amount of Na_2SO_3 the equilibrium constant of eq. (2), which expresses the precipitation of Se, becomes,

$$K_{\text{SeSO}_3^{2-}} = \frac{[\text{SeSO}_3^{2-}]}{[\text{Na}_2\text{SO}_3] - [\text{SeSO}_3^{2-}]} \quad (7)$$

From eq. (7) equilibrium concentration of SeSO_3^{2-} can be calculated as,

$$[\text{SeSO}_3^{2-}] = \frac{\alpha_{\text{SO}_3^{2-}} \times K_{\text{SeSO}_3^{2-}}}{1 + \alpha_{\text{SO}_3^{2-}} \times K_{\text{SeSO}_3^{2-}}} + [\text{Na}_2\text{SO}_3] \quad (8)$$

In the logarithmic form, this equation can be written as

$$p[\text{SeSO}_3^{2-}] = p \frac{\alpha_{\text{SO}_3^{2-}} \times K_{\text{SeSO}_3^{2-}}}{1 + \alpha_{\text{SO}_3^{2-}} \times K_{\text{SeSO}_3^{2-}}} + p[\text{Na}_2\text{SO}_3] \quad (10)$$

where,

$$p[\text{SeSO}_3^{2-}] = -\log[\text{SeSO}_3^{2-}]$$

Eq. (8) describes the solubility of Se in Na_2SO_3 solution of the given concentration. This can be illustrated in the plot of $p[\text{SeSO}_3^{2-}]$ vs. pH for $[\text{Na}_2\text{SO}_3]$ of 1 mole/l at 25 °C, as given in the figure 3.1. The graph reveals the solubility of Se in Na_2SO_3 increases with increase in the pH of the solution as $p[\text{SeSO}_3^{2-}]$ gives inverse of solubility.

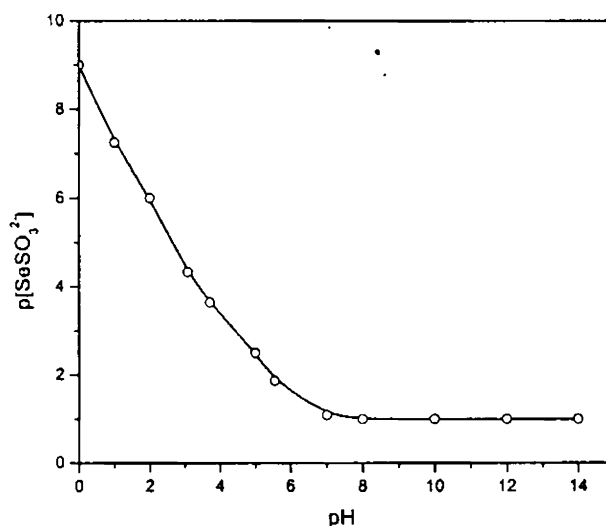


Figure 3.1: Variation of solubility of selenium in the Na_2SO_3 with pH of solution (conce. of Na_2SO_3 is 1 mole/l)

Above mentioned calculations indicate the value of pH of the medium to be employed in the synthesis of Na_2SeSO_3 solution should be $\text{pH} \geq 10$. Thus selenium can be precipitated by reducing the pH of selenosulphate solution to more acidic values.

In the present work, pH of Na_2SO_3 and Na_2SeSO_3 solutions were greater than 10. Rate of selenium precipitation is controlled by reducing pH of the selenosulphate solution to a value in the range 4.2-4.5, so as to form thin films. Effect of temperature and molarity of the solution was also studied experimentally.

3.3.2 Experiment

A stock solution of 0.2 M sodium selenosulphate (Na_2SeSO_3) was prepared by dissolving selenium powder of weight equivalent to 0.2 M (99.99% pure) in aqueous solution of excess sodium sulphite kept at 363 K, subjected to constant stirring as described in sec. 2.2. pH of as-prepared Na_2SeSO_3 solution was ~ 10.5 .

Well-cleaned glass slides of dimension $2.5 \times 4.5 \times 0.2 \text{ cm}^3$ with and without SnO_2 coating were used as substrate for the deposition process. Cleaning process of the slides was described in sec. 2.2. Preparation of SnO_2 coated glass substrates was also cited in the same section. In the case of glass substrates, these were heated to 673 K over which ethanol was sprayed and cooled down to room temperature. After cooling, these substrates were well-cleaned using soap solution and then in distilled water followed by drying in heater at 373 K.

Deposition was carried out in a 25 ml beaker to minimize the consumption and wastage of solution, even during initial trials. Three substrates were dipped vertically in the beaker so that three samples of area 5.5 cm^2 could be prepared at a time. Film deposited on the substrate surface facing the wall of the beaker was chosen as good film as mentioned in chapter 1.

As-prepared 0.2 M Na_2SeSO_3 solution (pH ≈ 10.5) was stable. However, acidification of the above solution resulted in selenium precipitation as described in the theory. In order to obtain selenium in the form of thin film, the precipitation was controlled by varying molarity, pH and temperature of the bath containing Na_2SeSO_3 solution. Volume of the solution was kept constant as 20 ml, the maximum volume that could be conveniently handled in a 25 ml beaker.

3.3.3 Parameters affecting the deposition

Growth of the selenium film depends on the rate of precipitation of selenium from the Na_2SeSO_3 solution, which in turn, depends on various factors such as pH, molarity, temperature of the bath and nature of the substrate as mentioned in introductory chapter. Here, experimental observations during growth process and nature of the films obtained at different conditions are described in the following paragraph.

i. Molarity

Initially, the deposition was carried out at different concentrations of Na_2SeSO_3 solution. For that, different molar solutions were prepared by dilution of the 0.2 M stock solution. The made up solutions were 0.006 M, 0.0125 M, 0.025 M, 0.05 M and 0.075 M, for trials. pH of all the solutions were adjusted to 4.5 (an arbitrary value) with 50% dilute acetic acid, keeping the bath at room temperature (300 K). Uniform films were obtained for 0.006 M solution after 3 hrs of deposition. Time of deposition was chosen on the basis the reaction rate. When molarity is increased from 0.006 M, immediate precipitation (colloidal), red in colour, was observed. Thus, for further trials, concentration was selected at 0.006M Na_2SeSO_3 .

ii. pH value

In order to study the effect of pH value, this parameter (of the 0.006 M solution) was varied from 3.00 to 7.2 at room temperature. Then it was seen that at lower pH values (3, 3.2, 3.5 etc.) precipitation was fast and hence no film was deposited. When it was in the range 4.2-4.7, uniform films were obtained. As pH value was made higher than this range, precipitation became slower and films were deposited in the form of 'patches'. When the pH of the solution was neutral or alkaline, there was no visible change for the solution, since it is stable according to the theory. Thus the pH was always kept at 4.5 for the deposition of Se films.

iii. Temperature

Furthermore, the deposition process was carried out at various temperatures using (0.006 M solution) (pH 4.5) viz at 278 K (keeping in the ice bath), 300 K, 323 K, 333 K and 343 K (keeping in hot air oven). At temperatures, higher than 300 K, the precipitation was fast and colour of the precipitate was gray. It was found that at 278 K, deposition time was 8 hrs to obtain uniform film of enough

thickness. At 300 K, uniform films were formed as described earlier. So the optimum temperature for the film formation was found to be 300 K.

iv. Nature of the substrate

It was found that the uniformity of the films strongly depends on nature of surface of glass substrates. Three types of differently treated glass substrates were used for the deposition process. One type was bare glass slides. Second type was alcohol sprayed glass slides as mentioned earlier. SnO₂ coated glass slides were the third type. Films deposited on SnO₂ coated glass substrates and alcohol sprayed glass substrates, were found to be more adhesive than those formed on untreated glass substrates.

From the above discussion, the best samples were those prepared at 300 K from 0.006 M Na₂SeSO₃ solution at pH value 4.5 and therefore further analyses were done on this type of samples. The film was annealed to improve the structural, optical and electrical properties at different temperatures viz., 308 K, 323 K, 343 K and 373 K in high vacuum for 1h.

3.4 Characterization

After the preliminary visual observation of physical appearance of the films, morphological, structural, compositional, optical and electrical properties were analysed using different techniques. Morphology was analysed using SEM. Crystallinity was studied using XRD. XPS and SIMS were used for the depth-wise elemental analysis. The XPS spectra were recorded for 500 cycles for which each cycle corresponds to Argon ion sputtering for 1 min. ICP was used for bulk elemental analysis and. Optical properties were studied from optical absorption spectrum. Electrical characterization was done using I-V characteristics measured by SMU.

3.4.1 Visual observations

The as-prepared films were orange red in colour, uniform and smooth. It was found that due to aging, it was converted to gray form. The gray films were not uniform, but it was powdery. The conversion was relatively faster when the films were kept in open air rather than in dried conditions in desiccator. Also, films prepared on bare glass slides were less stable than that on alcohol sprayed or SnO₂

coated glass substrates. The film after annealing appeared as thinner, non-uniform and gray in colour. Damage during annealing occurs even at 313 K.

3.4.2 Thickness

Thickness of films was measured by stylus profilometer. Figure 3.2 shows the profile of the measurement. Thickness of the triple dipped films was measured as 5000 Å.

3.4.3 SEM

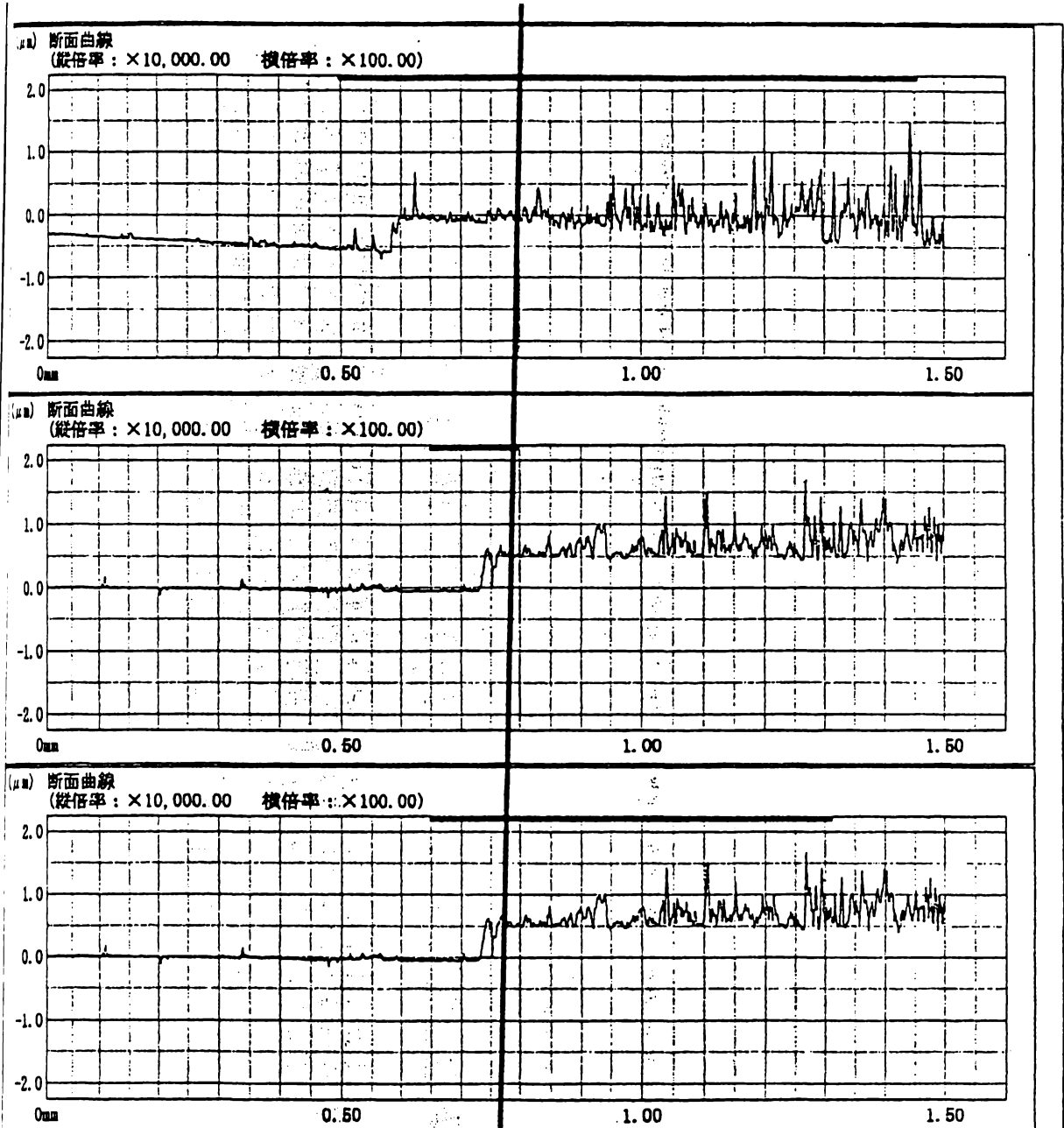
Surface nature of the films was studied using Scanning Electron Micrograph. Fig. 3.3(a) and fig 3.3(b) shows the morphology of selenium film deposited on glass and SnO₂ coated glass substrate respectively. This indicates the effect of substrate on the morphology of the films. On glass continuous lateral growth is observed while on SnO₂ coated glass, growth is granular type. This type of growth nature was reported by Kitaev et al., for amorphous selenium films [13].

3.4.4 XRD

Structural analysis of the films was carried out using XRD. The scan rate was 2 °/min in the range 2θ between 14 and 50 °. Figure 3.4 shows the pattern of Se film deposited on glass. The figure clearly shows amorphous nature of the films. When the film was annealed, no improvement in crystallinity was observed as the film was damaged.

3.4.5 XPS

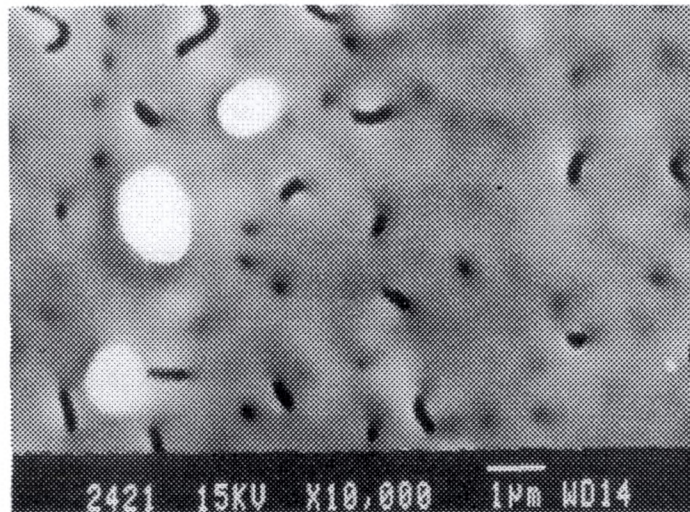
XPS spectra of samples gave the composition of the films. Depth profile of the films deposited on SnO₂ coated glass substrate is shown in fig. 3.5. This reveals presence of selenium with binding energy at 55.5-56 eV [15], which corresponds to the elemental state. Traces of oxygen and tin are also detected at the front surface, which are diffused from the tin oxide coated glass substrate to selenium film. Oxide formation is ruled out as the binding energy of SeO₂ is 58.85 eV [16]. Presence of Na is also checked since there is a possibility of incorporation of Na from the Na₂SeSO₃ solution. The depth profile shows Na signal only in the region of glass substrate.



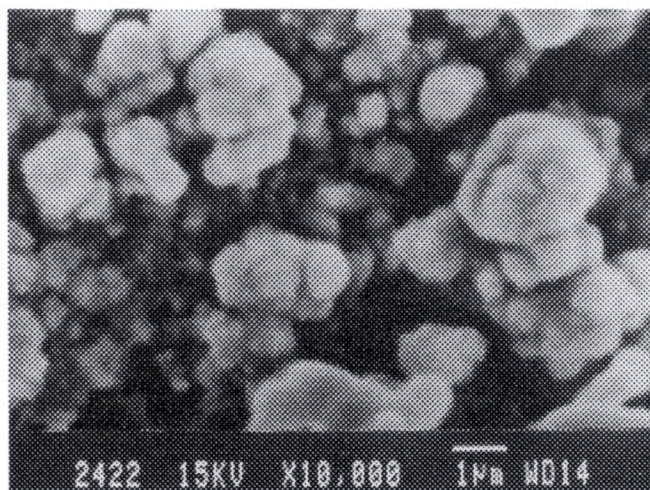
試料情報1 試料情報2 日付 測定者名 出力単位 極性 ピックアップ ピックアップ 算出規格 測定種別 測定長さ カットオフ波長 測定倍率 測定速度 カットオフ種別 傾斜補正 移動・戻り速度 リターン設定 予備駆動長さ 1s カットオフ比 1s カットオフ波長 評価長さ	③ Se 008 01/09/01 Y. Kashiwaba mm, μm 正転 高倍率ピックアップ JIS-B 82規格 断面測定 1.5mm × 50K 0.06mm/s 後半補正 1.50mm/s 通常測定 カットオフ波長 / 3 × 2 2.5 μm 0.9577mm	時間 ロット番号 サンプル番号 自動保存ファイル名 自動測定ファイル名 解析条件ファイル名 SPC出力ファイル名	12:50:57 68 WORK68.RST TEACH001.TAH CALCOND.ana SPCFILE.csv	Rmax 2.1706 μm
		時間 ロット番号 サンプル番号 自動保存ファイル名 自動測定ファイル名 解析条件ファイル名 SPC出力ファイル名	12:52:43 71 WORK71.RST TEACH001.TAH CALCOND.ana SPCFILE.csv	Rmax 0.7300 μm
		時間 ロット番号 サンプル番号 自動保存ファイル名 自動測定ファイル名 解析条件ファイル名 SPC出力ファイル名	12:53:10 72 WORK72.RST TEACH001.TAH CALCOND.ana SPCFILE.csv	Rmax 1.7332 μm

Fig.3.2: Thickness of selenium thin film

②



(a)



(b)

Figure 3.3: Scanning electron micrograph of a-Se films on
(a) glass substrate (b) SnO₂ glass substrate

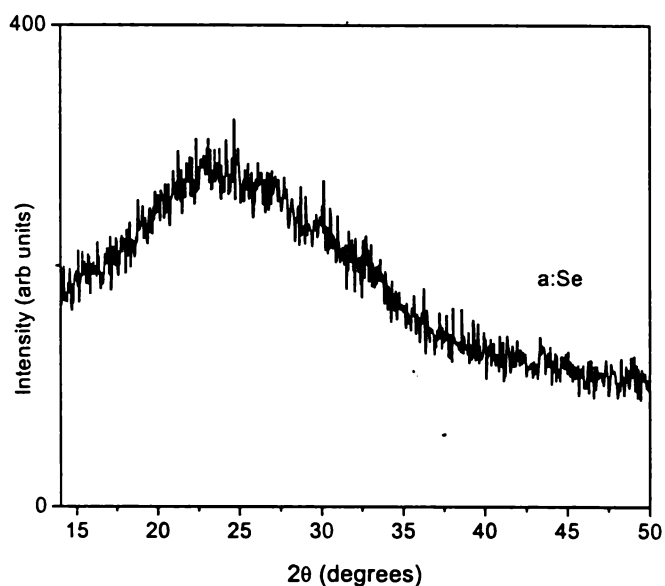


Figure 3.4: XRD pattern of a-Se film deposited on glass substrate

3.4.6 SIMS

Depth-wise elemental analysis was confirmed by SIMS analysis as illustrated in figure 3.6. At the surface selenium and traces of sodium are present. Even though oxygen or sulphur was not observed in the spectrum, Na was detected in this analysis throughout the depth up to SnO₂-Glass interface. Towards the region of SnO₂- Glass amount of Na is more compared to that on the surface.

3.4.7 ICP

In this technique, film was dissolved in concentrated HNO₃ and very diluted solution of which is sprayed into plasma state. Emission line intensity corresponding to the ions was measured, which in turn proportional to the amount of element present in the solution. It was found that emission line consists of only selenium. Sodium or tin was not detected in the flame.

ESCA PROFILE 8/18/01 START=2, END=502, NTH=2
FILE: Se008 No.3 Se film on NESA

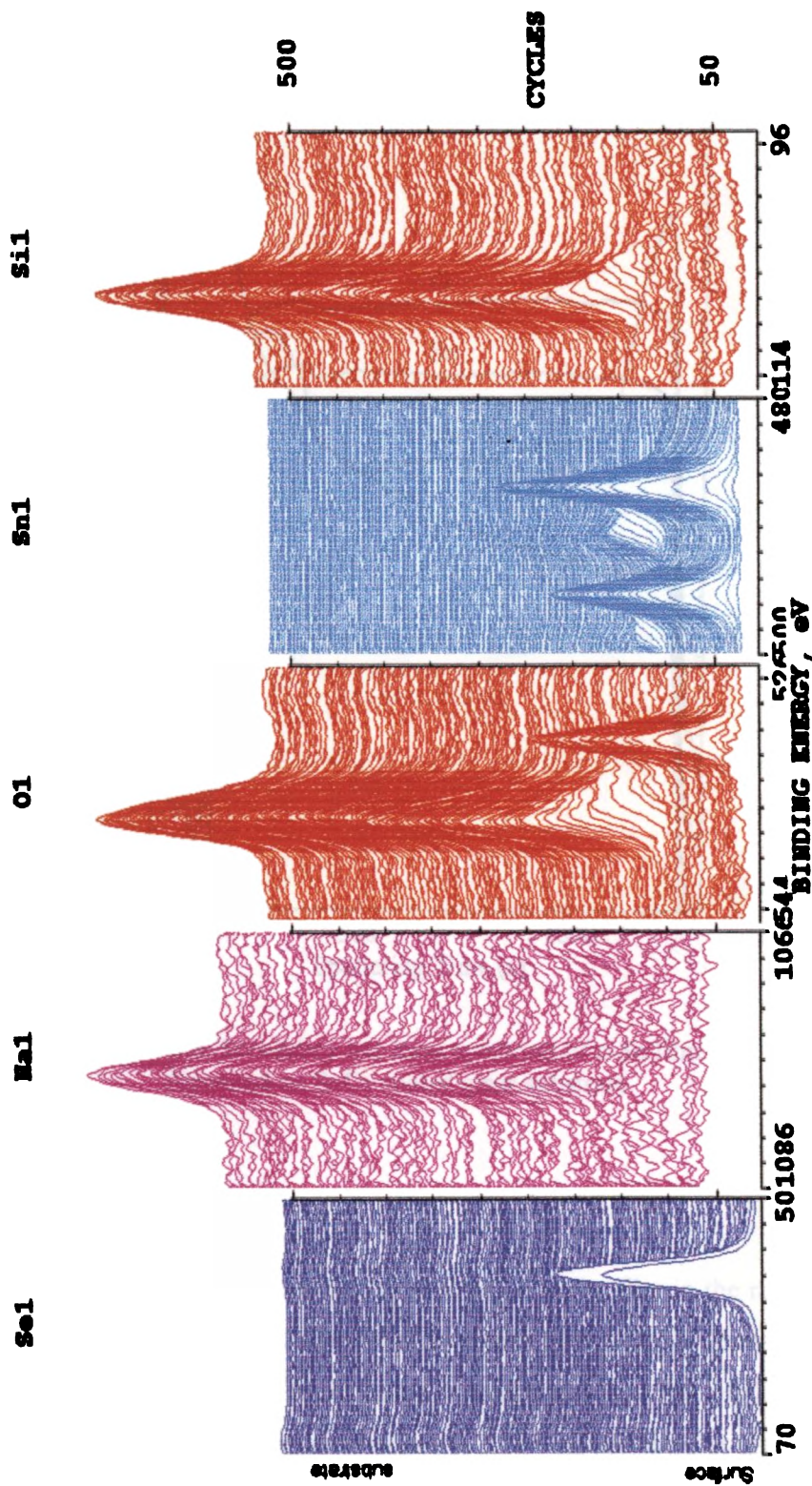


Figure 3.5: XPS profile montage of a-Se deposited on SnO₂ coated glass substrate

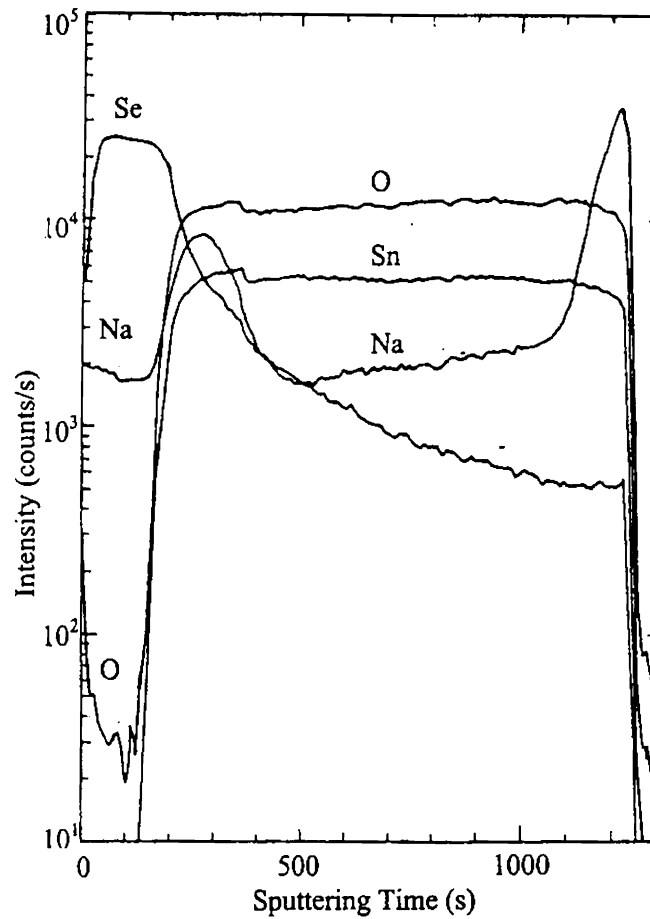


Figure 3.6: Secondary ion mass spectrum of a-Se film deposited on SnO₂ coated glass substrate

3.4.8 Optical properties

Wavelength dependence of optical absorption of the film in the range 450-700 nm is shown in fig.3.7. The spectral dependence of absorption shows that the film has direct band gap (E_g). The E_g value is determined from the plot of $(\alpha h\nu)^2$ vs. $h\nu$ as given in fig. 3.8. The value obtained is 2.1 eV as indicated in the plot and is in agreement with the reported value for amorphous selenium [8].

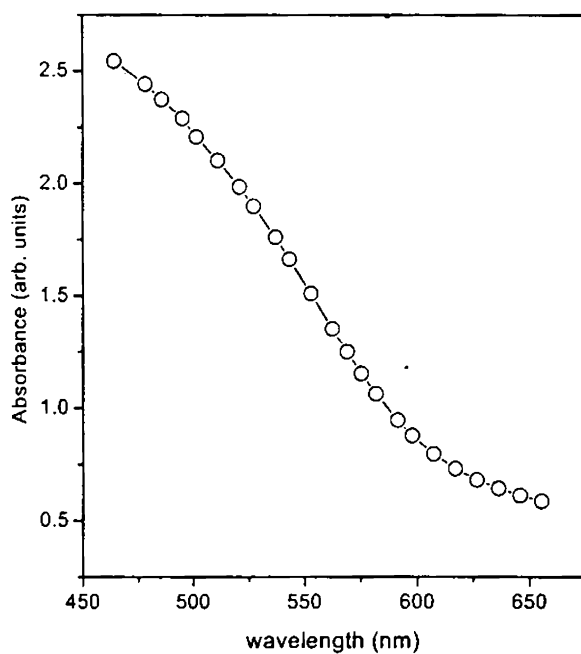


Figure 3. 7: Wavelength dependence of optical absorption of a-Se film

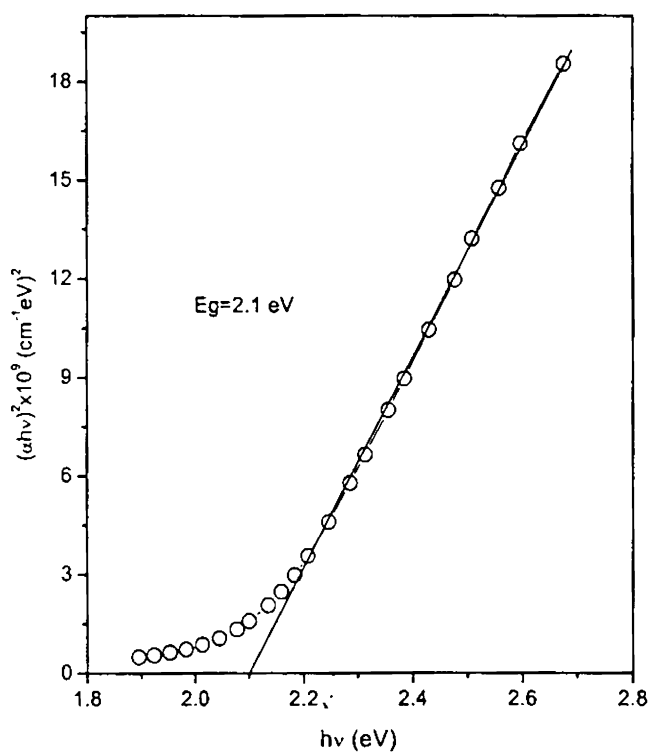


Figure 3.8: $(\alpha h\nu)^2$ Vs $h\nu$ plot for a-Se film

3.4.9 Electrical characterization

Resistance of the film was evaluated from the I-V characteristic given in fig. 3.8. Measurements were taken across two magnanine wire leads pasted on two terminals coated on the surface of the film with separation of 5mm. Electrodes were Au layer evaporated on the film. The resistance evaluated from the graph is 1.2×10^{10} ohm. It shows the film is electrically an insulator. Under illumination no change in resistance was observed.

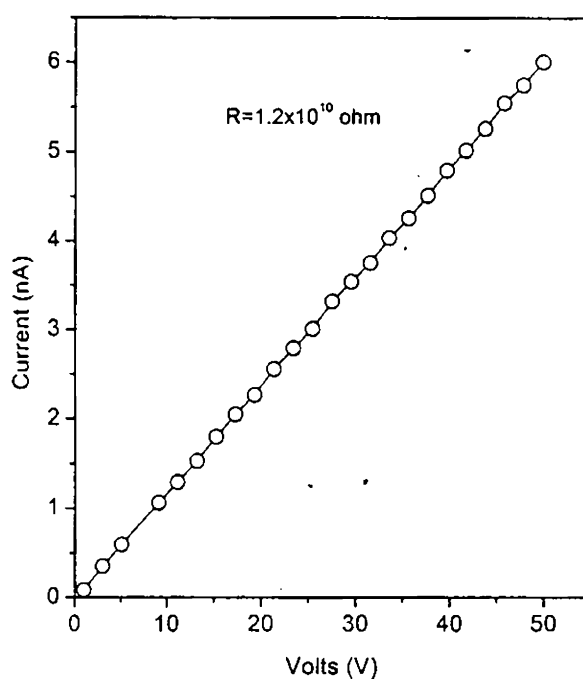


Figure 3.9: I-V characteristics of a-Se at room temperature

3.5 Results and discussions

a-Se thin films were prepared by lowering pH value of Na_2SeSO_3 solution to ~ 4.5 . Morphological studies (fig.3.3(a) and (b)) of the films show that surface of the film has spreading of liquid drop like appearance, which is characteristics of amorphous material. Due to aging the red coloured film was converted to gray form and was found that in the open air, conversion was more effective. Also, less adhesive films were easily undergoing transformation. Hansen et al [6] described these structural changes as due to the presence of voids and dangling bonds in the films. Due to illumination or annealing, these atoms become more mobile and fill

the voids and attain a low energy configuration. They also observed formation of mottled films under room temperature storage for several days. In the present case, XRD could not identify the crystalline nature of gray form.

Both the as-prepared and gray coloured films are dipped in CS₂. The gray form was found to be insoluble and this shows it is the hexagonal form of selenium [6]. It is well known that CS₂ dissolves amorphous selenium while not affecting crystalline selenium. Since our aim was not in the detailed study of selenium thin films, further studies on conversion process were not carried out.

The presence of selenium film on the top of SnO₂ was confirmed using SIMS (fig. 3.6), XPS (fig. 3.5) and ICP. In SIMS analysis the Na level in the film and SnO₂ layer is more or less same and increases to more than one order at the glass face. This Na may be from the soda lime glass substrate, which contains 15% Na₂O as it is very clear from the XPS analysis [17]. Traces of Na from the glass may be ejected due to sputtering and detected during depth profiling, as SIMS is highly sensitive to sodium (10¹⁴ atoms/cc). High sensitivity of Na to this technique is due to its low ionization potential and extremely high ionization cross-section of the element [18].

However, ICP analysis could not detect sodium in the film. If Na detected in SIMS analysis is from the film, it should have been detected in ICP analysis also, which is more sensitive than SIMS (10¹³ atoms/cc). Hence the only possibility of detecting sodium (from SIMS) is from the substrate.

From the studies optical absorption, a-Se was found to possess a direct band gap of 2.1 eV. Electrically a-Se is found to be an insulator.

3.6 Conclusion

Amorphous selenium films could be deposited using CBD from sodium selenosulphate solution by adjusting the pH at 4.5, at room temperature. Thickness of tripple-dipped films was 5000 Å. Morphological studies were performed by SEM. Structural and elemental analyses were done using XRD, XPS and SIMS. These studies reveal that the films obtained were pure amorphous selenium. Thus deposition of an element in the form of thin film could be achieved using CBD, the simple and low cost process. Optical band gap evaluated from the spectral

dependence of absorbance was 2.1 eV. Very high value of resistance revealed that the film was nearly electrically insulator.

Selenium, which is extremely toxic in its vapour state, is available in the non-toxic form and can be used for preparation of binary and ternary selenides. In the proceeding chapters, selenisation process using this selenium film is described.

References

- [1] (<http://www.sunnybrook.utoronto.ca:8080/~hunter/selenium.html>)
- [2] H.Z. Song, G.J. Adriaenssens, E.V. E.V. Emelianova and V.I. Arkhipov, *Physical Review B*, 59 (1999) 10607
- [3] David Adler, *Amorphous Semiconductors*, The Chemical Rubber Co. 1972, p-42
- [4] D. Caprion and H.R Schober, *Physical Review B*, 62 (2000) 3709
- [5] V.K. Tikhomirov, P. Hertogen, G.J. Adriaenssens, C. Glorieux and R. Ottenburgs, *J. Non-Cryst. Solids*, 227-230 (1998) 732
- [6] S.G. Hansen and T.E. Robitaille, *Thin Solid Films*, 151 (1987) 111
- [7] A. Peled, A.A. Friesem and K. Vonokur, *Thin Solid Films*, 218 (1992) 201
- [8] S. Zienab and ElMandouh, *Fizika A*, 2 (1993) 35
- [9] A. Munoz, F.L. Cumbrea, A. Conde and R. Marquez, *Thin Solid Films* 149 (1987) L73,
- [10] B. Petretis, H. Rogass and A. Statas, *Phys. Stat. Sol.*, (a) 30 (1975) K3
- [11] G. Fleury, A. Hamou, C. Viger and C. Vacter, *Phys. Stat. Sol.*, (a) 64 (1981) 311
- [12] S.O. Kasap, V. Aliyah, B. Polischuk and A. Ballie, *J. Appl. Phys.*, 83 (1998) 2879
- [13] J.M. Ballestors, R. Hernandez, J.M. Herreros, C.N. Afonso, A.K. Petford-Long and R.C. Doole, *Applied Physics A Materials Science & Processing*. 65 (1997) 463
- [14] G. A. Kitaev and G.M. Fofauov, *Zh. Prikl. Khim.*, (Leningrad) 43 (1970) 169
- [15] C.D.Wagner, W.M. Riggs, L.E. Davis, J.F Moulder and G.E. Muilenberg, *Handbook Of X-Ray Photoelectron Spectroscopy*, Perkin-Elmer Corporation, Physical Electronics Division, Eden Prairie, Minn. 55344 (1979)
- [16] L. L. Kazmerski, O. Jamjoum, P.J. Ireland, S. K. Deb, R. A Mickelsen and W. Chen, *J. Vac. Sci. Techn.*, 19 (1981) 467
- [17] M. Ruckh, D. Schmid, M. Kaiser, R. Schaffler, T. Walter and H.W. Schock, *Solar Energy Mater. Sol. Cells*, 41/42 (1996) 335

-
- [18] S. Zweigart, S.M. Sun, G. Bilger and H.W. Schock, *Solar Energy Mater. Sol. Cells*, 41/42 (1996) 219

CHAPTER 4

PREPARATION OF INDIUM SELENIDE FILMS BY SELENISATION OF INDIUM USING a-Se FILMS

4.1 Introduction

Amorphous selenium thin film, prepared through CBD is used as the source for the preparation of binary selenides. Here Stacked Elemental Layer (SEL) technique is applied for selenisation process. Among the selenides, indium selenide (In_2Se_3) has been the subject of recent studies [1, 2]. We selected this material, as this compound has valuable electrical and optical properties and is of great interest for photovoltaic applications, in the thin film form. Several deposition and annealing techniques have been used by different research groups for the preparation of this film [1, 2, 3]. In most of the reports, elemental Se layer was deposited using vacuum evaporation. This involves Se vapour, which is highly poisonous. In the present technique, a-Se deposition using CBD is totally pollution free since it avoids the usage or release of any toxic gas or vapour.

SEL structure adopted here is Glass/a-Se/In. Indium selenide is formed by the solid-state reaction between Se and In, constituting the bilayer, and this is induced by annealing [4]. Detailed studies on structural, morphological, optical and electrical properties of the films formed at different temperatures are carried out in the present investigation.

In order to prove that the a-Se thin film can be used as the selenium source for the preparation of any binary selenide, we also, present a brief note on the preparation and characterization of copper selenide thin films. The SEL structure for the formation of copper selenide is Glass/a-Se/Cu.

As we are concentrating deeply in studies on indium selenide, a few of the recent works on various aspects of this material are reviewed here.

4.2 Review of works on indium selenide

Indium selenide (In_2Se_3) is a compound semiconductor which belongs to III-V family. It crystallizes in layered structure in which each layer consists of five atomic sheets, Se-In-Se-In-Se bound by strong forces. Interaction between adjacent layers is much weaker and is believed to be Van der Waals type [5]. This compound shows at least three modifications denoted by α , β and γ with transition temperatures of 473 K and 823 K, respectively for $\alpha \rightarrow \beta$ and $\beta \rightarrow \alpha$. Both α - and γ - forms of In_2Se_3 are found stable at room temperature, while β -form is obtained only above 473 K [6].

There are many reports on crystal structures and phase transformation in In_2Se_3 compound. Structural investigation of In_2Se_3 crystals grown from the melt by Bridgman-Stockbarger method was performed by both selected area and convergent beam electron diffraction techniques. They identified two phases of hexagonal and rhombohedral structures [7].

Recently, Jiping et al., carried out phase transformation studies using electron diffraction, high resolution electron spectroscopy, XRD together with optical absorption studies [8]. They reported, that there exist only two phases, viz, low- and high-temperature phases in In_2Se_3 as per the time-temperature-transformation (TTT) diagram and the transformation temperature is 853 K. Low temperature phase was having vacancy ordered in screw form (VOSF) structure and the high-temperature phase was having layered structure. Both possessed semiconducting optical properties.

Emziane et al., studied the influence of substrates on crystalline quality of thin films of $\gamma\text{-In}_2\text{Se}_3$ grown by sequential thermal evaporation of In and Se [9]. Substrates used were soda lime glasses, mica sheets, SnO_2 -coated and gold-coated glasses. They concluded that films deposited on SnO_2 -coated glass substrates were having significantly better preferential orientation along the direction perpendicular to substrate surface than those films deposited on Au-coated glass or mica sheets. Texture of the films formed on Au-coated glass substrates was relatively better than that of the films on mica sheets. However, the phase was independent of

nature of substrate. Thomas et al reported the formation of α -phase by the same method, at different annealing conditions [10].

Studies on temperature dependence of fundamental absorption edge of α -, β - and γ -phases of In_2Se_3 was made by Julien et al. They observed that the fundamental absorption was associated with direct transition. E_g values were 1.35, 1.3 and 1.81 eV respectively, at room temperature and decreased with increase in temperature [11]. Later they analysed far-infrared spectra of In_2Se_3 crystal over a temperature range 10-500 K and observed formation of intermediate phases, from the spectra [12].

Herrero et al., prepared In_2Se_3 films by annealing alternate electrodeposited layers of Se and In from separate baths [13]. Influence of annealing temperature on properties of the films was examined using XRD. Photoactivity of the films was tested in a photoelectrochemical cell with a sulfite/sulfate redox couple. Marsillac et al, deposited In_2Se_3 layer either by direct evaporation of the compound in powder form or by annealing the sequentially deposited In and Se layers [14]. They found that thin films of single phase and high orientation could be obtained when the ratio between In and Se was 2:3 and annealed in selenium atmosphere for 24 h at 573 K. Same group later reported that by annealing in flowing Ar monophased, stoichiometric and homogeneous films could be prepared irrespective of deposition conditions [15].

Very recently, epitaxial growth of γ - In_2Se_3 was investigated by Tomohiko Oshsuka et al [16]. They deposited the film with defect wurtzite structure on GaAs (111)B substrate and the films were having vacancy-ordered crystal structure.

4.3 Experimental

Procedure for deposition of indium selenide and copper selenide thin films by selenising the corresponding metallic layers consists of different stages. This involves preparation of metallic precursor and incorporation of Se into it. As mentioned earlier, we adopted SEL technique for the preparation of these metal chalcogenide films.

4.3.1 Preparation of Indium selenide thin films

SEL structure was grown using chemical bath deposited a-Se film and vacuum evaporated indium thin films. Whole process of film preparation of In_2Se_3 involved two steps. First step was the preparation of Se-In stack layers while second stage involved the process of annealing the stack layers.

Substrates used were micro-glass slides, which were well cleaned using commercial detergent (Extran) followed by washing in distilled water as described in Chapter 2. In order to get good adhesion for the film, substrates were sprayed using alcohol as cited in chapter 3, for a-Se film preparation.

In-Se stack layer preparation consists of two steps. In the first step, selenium thin film was deposited using CBD as explained in the last chapter. Briefly the procedure is as follows: 0.0125 M (20 ml) Na_2SeSO_3 solution was taken and the pH of the solution was adjusted to ~ 4.5 by adding a few drops of dilute acetic acid with stirring. Substrates were then placed vertically in the bath kept at room temperature. Orange-red films were obtained after 3 h of deposition. For the preparation of indium selenide films, triple dipped selenium films of thickness $\sim 5000 \text{ \AA}$ having an area 5.5 cm^2 were chosen. The area was selected by masking the substrate using teflon tape, wrapped very tightly to the glass slide so that the required area for deposition was exposed to the solution. Masking by this method was found to be very successful.

The a-Se film was dried in open air at room temperature and loaded in the vacuum chamber (Box coater- BK350), to carry out the second step. A layer of indium of thickness 350 \AA (5N purity) was deposited using thermal evaporation on the selenium layer such that Se/In atomic ratio was higher than 1.5. Approximate weight of indium to be evaporated to get 350 \AA layer was calculated as 40 mg, assuming the substrates at a distance of 15 cm from the Mo boat.

Thickness of indium layer was monitored using a quartz crystal thickness monitor (PIME HIVAC CTM 200). In the final stage, the samples were taken from the chamber and loaded in the annealing tube which is then subjected to high vacuum (10^{-5} mbar) annealing for 1hr. In order to investigate the properties of

films formed at different temperatures, the stack layers were annealed at temperatures viz., 373 K, 423 K, 473 K, 573 K, 673 K and 723 K. Heating rate was 3 K/min, using the temperature controller (Digicon). Hereafter the annealed films were labeled as IS100, IS150, IS200, IS300, IS400 and IS450 respectively in accordance with temperature. In all the samples, thickness of a-Se and In was same.

4.3.2 Preparation of Copper selenide thin films

Here procedure was exactly similar to that of preparation of indium selenide except that the SEL structure deposited was Glass/a-Se/Cu. Only one type of sample was prepared to analyse the nature of the films formed due to solid-state reaction between Cu and Se during annealing. Annealing temperature was 473 K for 1h. Thickness of copper film was 200 Å and corresponding weight taken for evaporation was 30 mg. In this case also, selenium films used were triple dipped films of thickness 5000 Å.

4.4 Characterization

Both indium selenide and copper selenide films were characterized using different techniques. Detailed studies were done on indium selenide while copper selenide films were characterized structurally and optically.

4.4.1 Characterization of Indium selenide

General appearance of the annealed films was first analysed visually. Surface topography of the films was examined using SEM. Structural studies of samples were performed using XRD and compositional analysis was done using XPS. Optical properties were studied using optical absorption spectrum and Electrical characterization was done by conductivity and Hall measurements.

4.4.1.1 Visual appearance

After unloading from annealing chamber, samples were checked that whether there were any scratches present due to handling etc. Then films without any scratch were carefully examined by naked eye to observe the presence of pinholes and other non-uniformities. Uniform samples free from pinholes were selected for further analysis. IS100 was deep red in colour and films formed at

higher temperature were golden yellow. Also, transparency of the films increased with increase in temperature.

4.4.1.2 Thickness

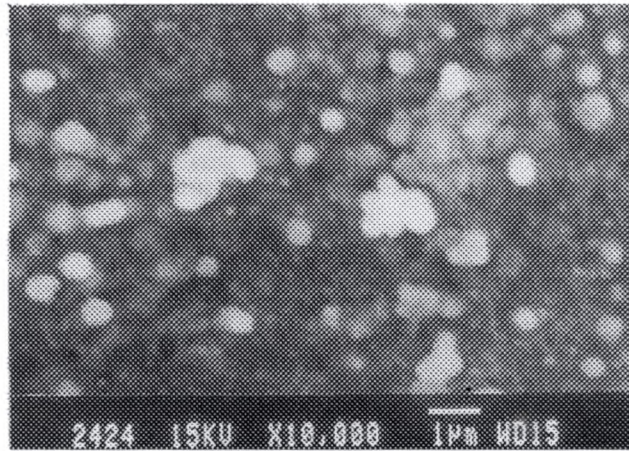
Thickness of the films IS100 and IS400 was measured using stylus method. These two films were selected for the measurement on the basis of structural and optical studies. Thickness of IS100 was on the average 0.8 μ . The stylus profile showed a fluctuating signal on the surface of the film indicating that the surface was not uniform. In the case of IS400, thickness was \sim 0.4 μ having uniform surface.

4.4.1.3 SEM

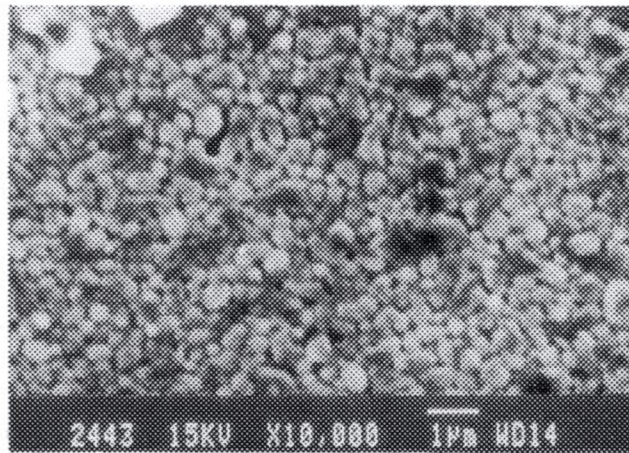
Analysis of surface topography using SEM was done on films of good structural properties, as verified from XRD. The samples selected were IS100, IS200 and IS400 and corresponding micrographs are shown in figures 4.1 (a), (b) and (c) respectively. All are taken in the same magnification; \times 10,000. Granular shaped grains are very clear in the case of IS100. In the case of IS200, laterally spread liquid drop like microcrystallites are observed. IS400 shows spherical shaped grains. Average grain size estimated from the micrographs is about 0.2 μ m in the case of IS100 and IS400.

4.4.1.4 XRD

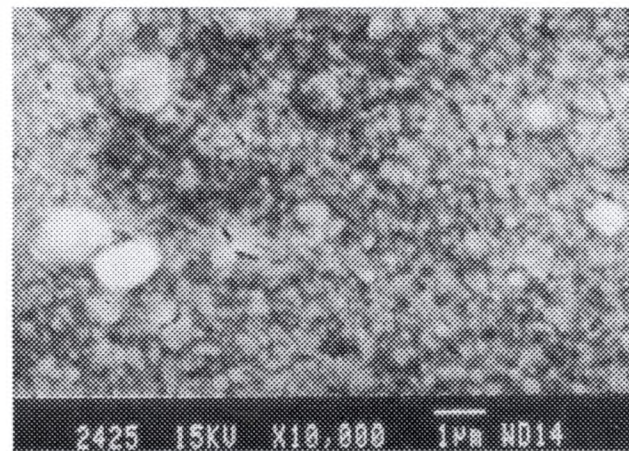
Results of structural analysis of the films formed at different temperatures are given in fig. 4.2. Scan range for 2θ values was from 15-50° at a rate of 5°/min. XRD pattern of as-deposited Se-In stack layers shows (fig. 4.2 (a)) only a single peak corresponding to In layer at $2\theta=32.8^\circ$ ($d=2.72$ Å) [JCPDS 5-646] and the selenium film is amorphous in nature, as mentioned in chapter 3. However, IS100 and IS150 have two peaks at $2\theta=23.3^\circ$ ($d=3.80$ Å) and $2\theta=29.6^\circ$ ($d=3.01$ Å) corresponding to planes (101) and (204) of γ -In₂Se₃ as seen in fig. 4.2(b) and (c) respectively [JCPDS 40-1407]. No distinct peaks are present in IS200 and IS300 as evident from fig. 4.2(d) and (e) and XRD pattern of IS400 and IS450 are illustrated in fig. 4.2 (f) and (g) respectively. They show well-defined peaks at $2\theta=16.9^\circ$



(a)



(b)



(c)

Figure 4.1: Scanning Electron Micrograph of (a) IS100; (b) IS200; (c) IS400

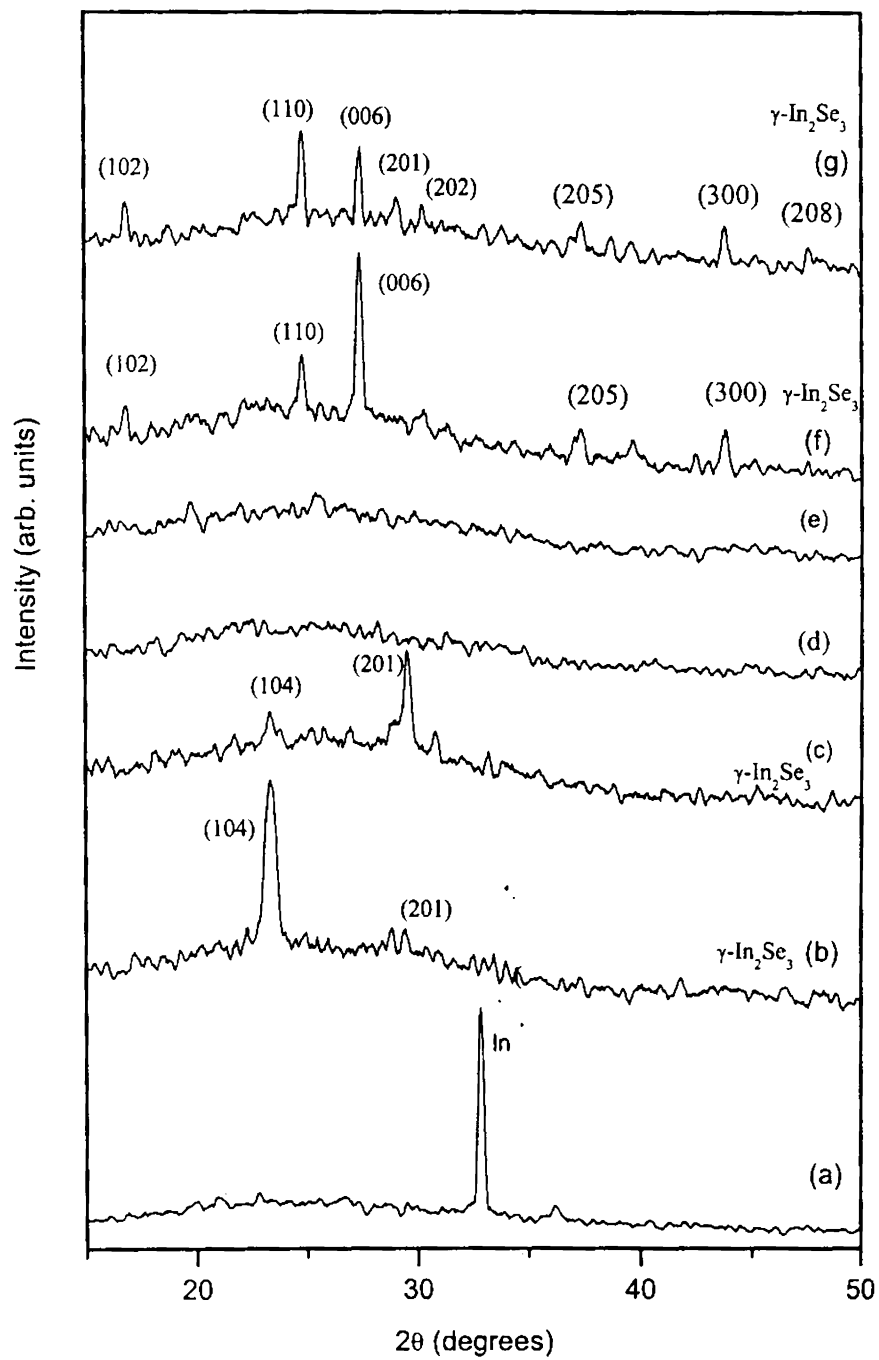


Figure 4.2: XRD pattern of (a) un-annealed Se-In stack layers; (b) IS100; (c) IS150; (d) IS200; (e) IS300; (f) IS400; (g) IS450

All these observations are summarized in the table given below:

Sample	2 θ (degrees)	d-value (Å)	(hkl)	Identified phase	Reference
In-Se as prepared	32.8	2.72	(100)	In	JCPDS 5-646
IS100 and IS150	23.3 29.6	3.80 3.01	(101) (204)	γ -In ₂ Se ₃	JCPDS 40-1407
IS200 and IS300	No distinct peaks observed				
IS400 and IS450	16.9 24.6 27.5 29.2 30.3 37.5 43.9 47.6	5.24 3.61 3.24 3.05 2.94 2.39 2.06 1.95	(102) (110) (006) (201) (202) (205) (300) (208)	γ -In ₂ Se ₃	JCPDS 40-1407

Table 4.1: XRD analysis of as-prepared and annealed In-Se stack layers

($d=5.24$ Å), $2\theta=24.6$ ($d=3.61$ Å), $2\theta=27.5$ ($d=3.24$ Å), $2\theta=29.2$ ($d=3.05$ Å), $2\theta=30.3$ ($d=2.94$ Å), $2\theta=37.5$ ($d=2.39$ Å), $2\theta=43.9$ ($d=2.06$ Å), $2\theta=47.6$ ($d=1.95$ Å). These peaks are coinciding with that of γ -In₂Se₃ phase. Planes corresponding to these d-values are (102), (110), (006), (201), (202), (205), (300) and (208) respectively [JCPDS 40-1407] [17].

4.4.1.5 XPS

XPS profile montage of IS100, IS150 and IS400 are shown in fig. 4.3(a), 4.4(a), 4.5(b) respectively. Spectra for all the samples were recorded for 25 cycles, which is equivalent to Ar⁺ sputtering time of 25 minutes. Each cycle corresponds to etching of 100 Å layer of the film. In all the spectra, binding energies (BE) of In 3d_{5/2} and Se 3d_{5/2} levels are at 445 eV and 54.8 eV respectively. BE of Se (3d_{5/2} electron) in elemental state and In₂Se₃ states are 55.5-55.6 eV and 54.8 eV respectively. Similarly, BE of In (3d_{5/2} electron) in elemental and In₂Se₃ states are 443.8 eV and 444.8 eV [18]. From the values of BE obtained in XPS analysis, it is clear that the films formed at different temperatures are In₂Se₃. Depth profile of the film proves that the presence of In and Se peaks of from surface to substrate region is more or less uniform. This is inferred from the uniform height of the respective

ESCA PROFILE 8/25/01 START=2, END=27, NTR=1
FILE: InSe024 1 IS100 Se/In on MESA

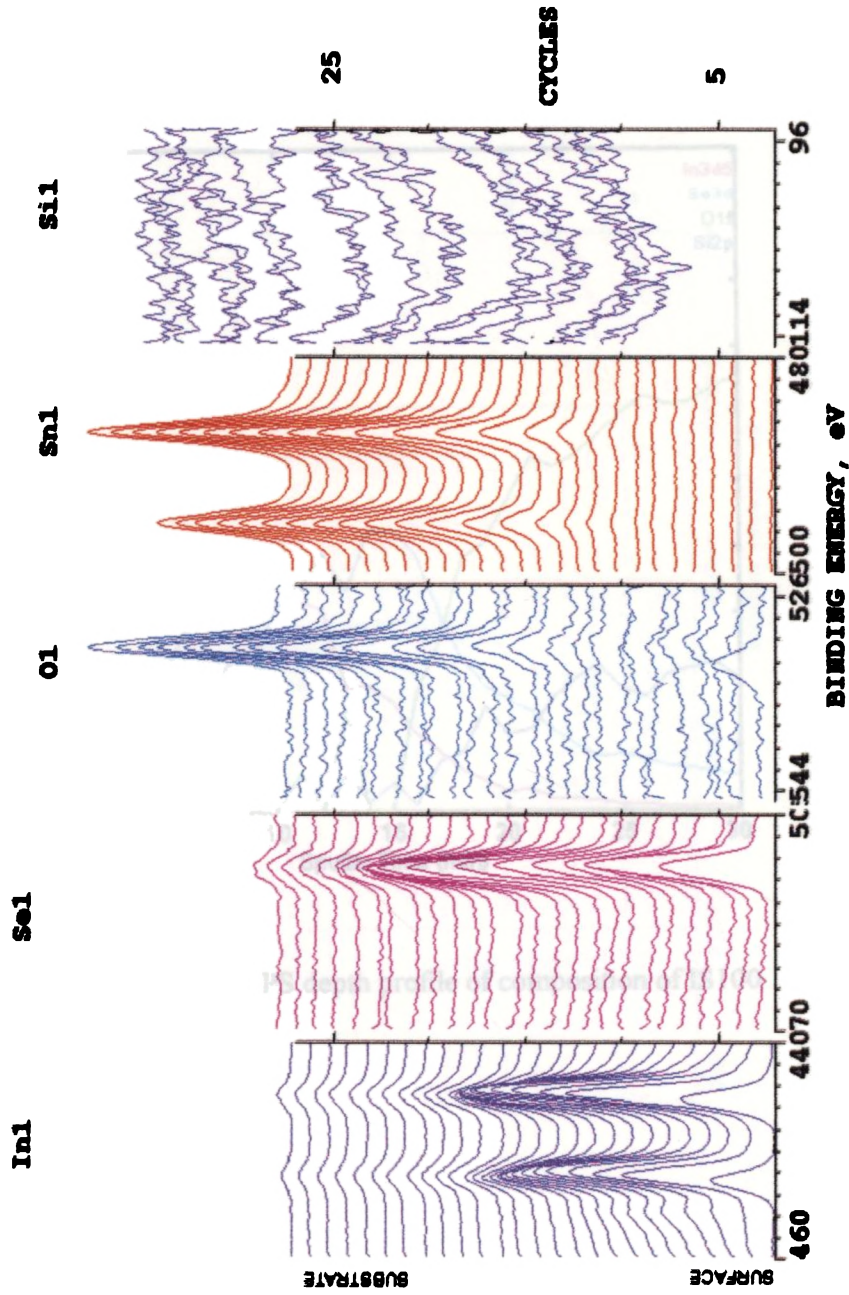


Figure 4.3(a): XPS profile montage of sample IS100

Chapter 4

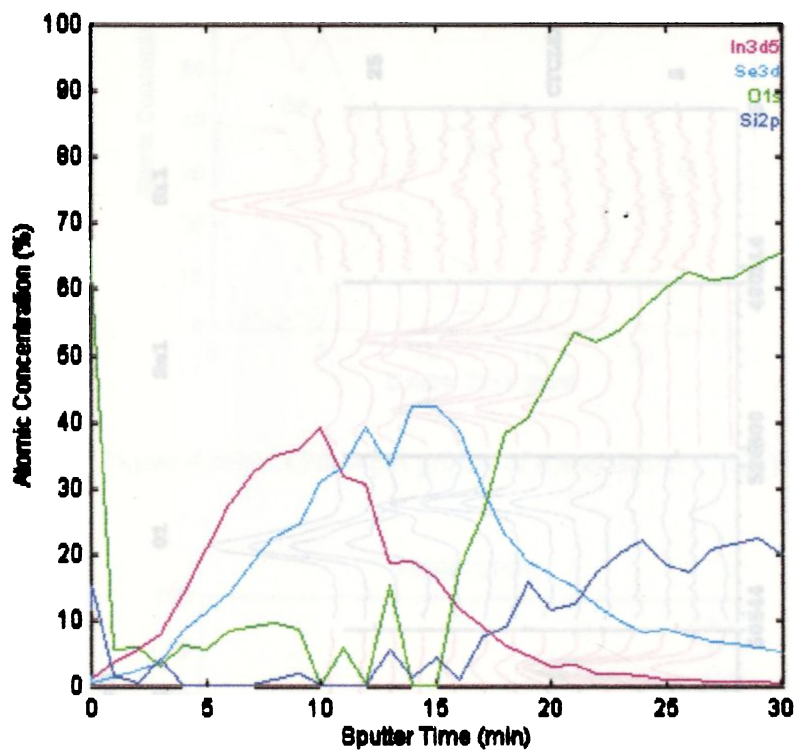


Figure 4.3(b): XPS depth profile of composition of IS100

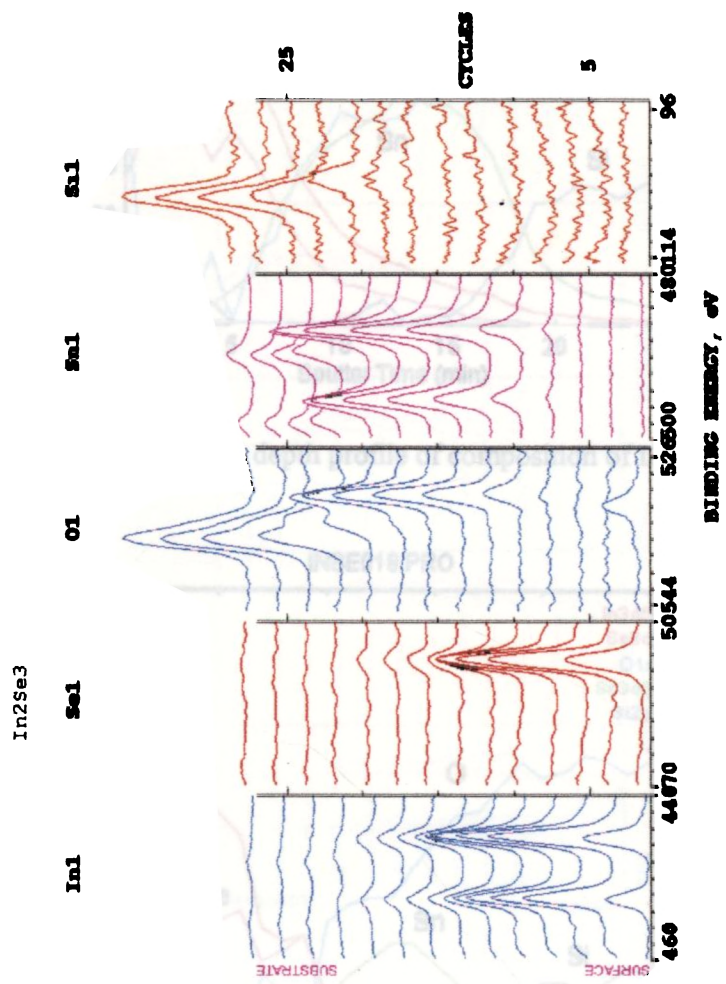


Figure 4.5(a): XPS profile montage of sample IS1.50

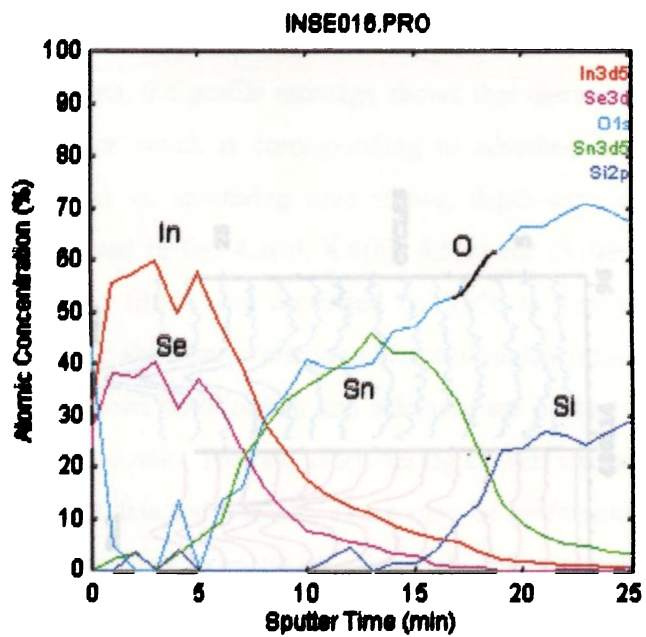


Figure 4.4(b): XPS depth profile of composition of IS150

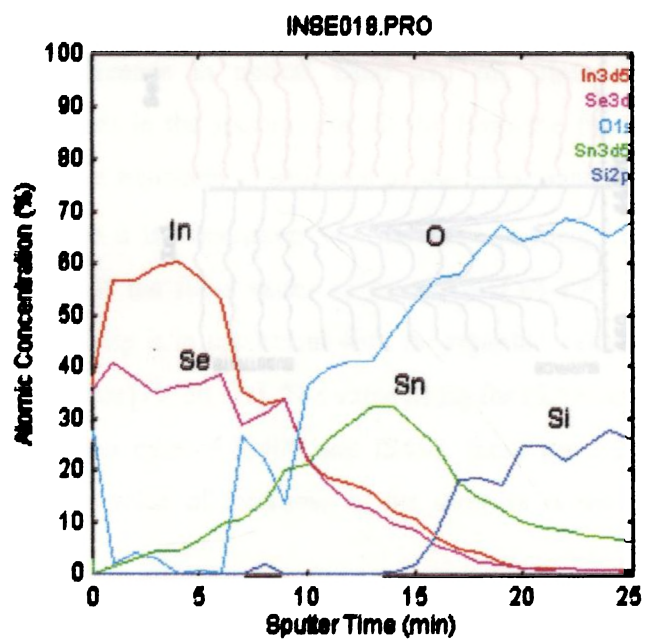


Figure 4.5(a): XPS depth profile of composition of IS400

T398

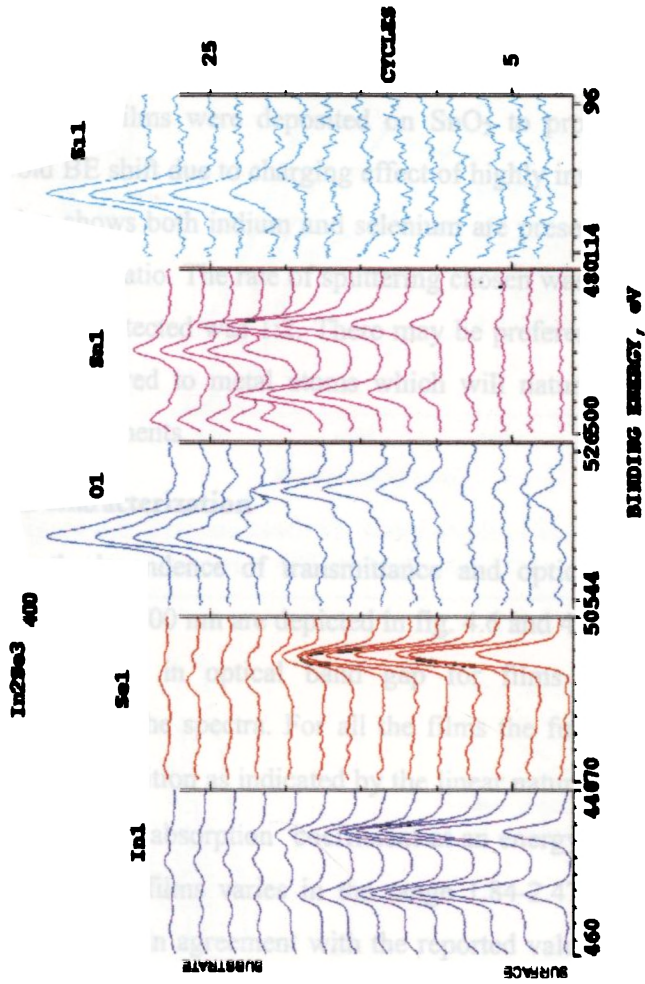


Figure 4.5(b): XPS profile montage of sample IS400

peaks. In all the films, the profile montage shows that there is no oxygen present except at the surface which is corresponding to adsorbed oxygen. The plot of atomic concentration vs. sputtering time shows, depth-wise composition of the films and are depicted in fig. 4.3(b), 4.4(b), 4.5(a) for IS100, IS150 and IS400 respectively. All the films were deposited on SnO₂ to provide a low resistive substrate to avoid BE shift due to charging effect of highly insulating glass. Depth-wise composition shows both indium and selenium are present uniformly through the depth, in the same ratio. The rate of sputtering chosen was with respect to SiO₂ so that ratio of Si:O detected was 1:2. There may be preferential sputtering of VI group elements compared to metal atoms which will naturally results in lower percentage of those elements.

4.4.1.6 Optical characterization

Wavelength dependence of transmittance and optical absorption of the films in the range, 400-1500 nm are depicted in fig. 4.6 and 4.7 respectively. There is significant difference in optical band gap for films formed at different temperatures as seen in the spectra. For all the films the fundamental absorption edge is due to direct transition as indicated by the linear nature of plot of $(\alpha h\nu)^2$ on $h\nu$ (fig. 4.8), where α is absorption coefficient at an energy of $h\nu$ deduced from fig.4.7. E_g value of the films varies in the range 1.84-2.47 eV. For IS100 and IS150 the value of E_g is in agreement with the reported values in the range 1.8-2 eV, for γ -In₂Se₃ films [19, 20, 21]. The value of E_g for IS200 and IS300 are 2.41 eV and 2.35 eV. In the case of IS400 and IS450, these are 2.25 eV and 2.09 eV respectively. Here, value of thickness of the samples is not considered, for the calculation.

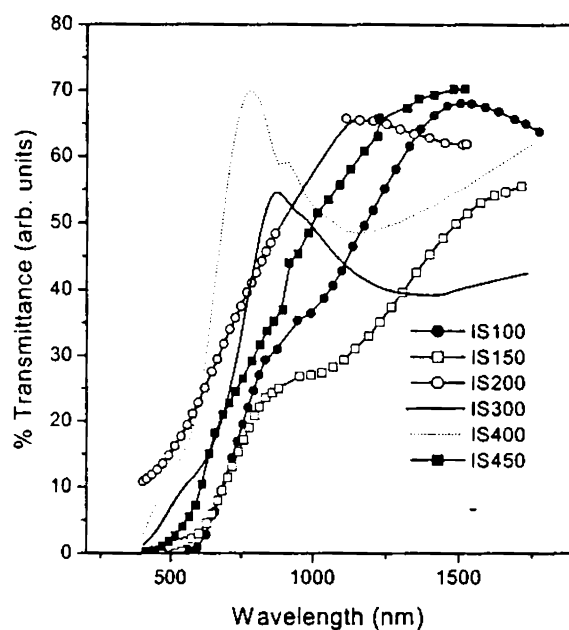


Figure 4.6: Transmittance vs. wavelength of In_2Se_3 films formed at different temperatures

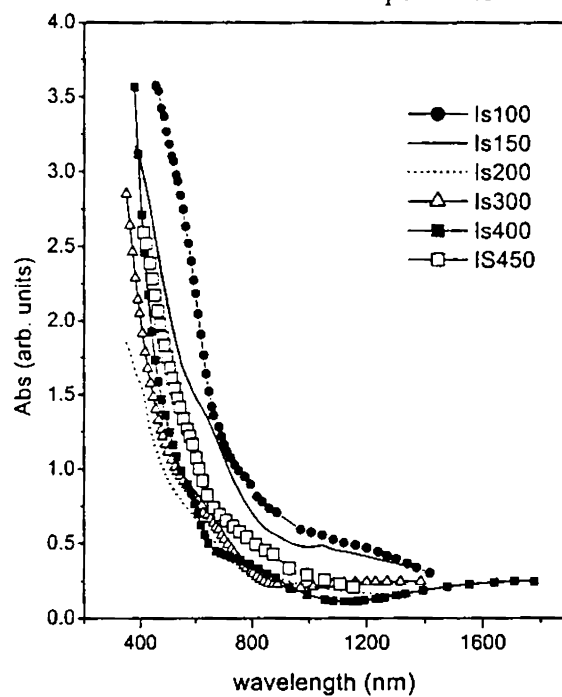


Figure 4.7: Spectral dependence of absorbance of In_2Se_3 films formed at different temperatures

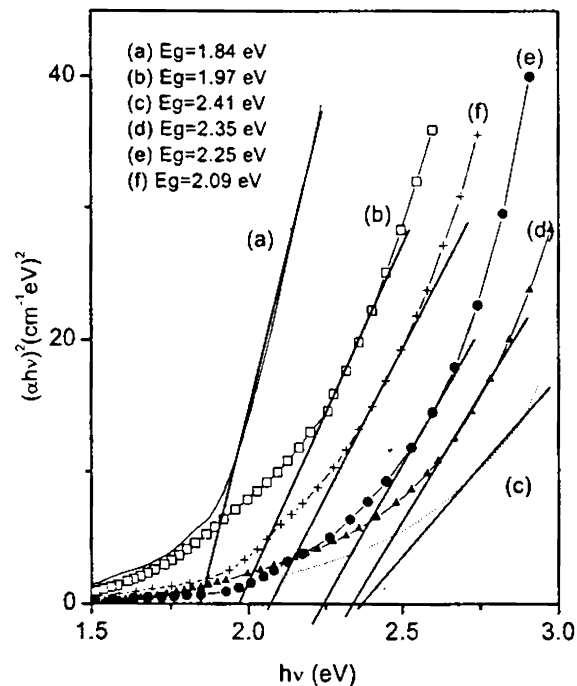


Figure 4.8: Plot of $(\alpha hv)^2$ vs. $h\nu$ of (a) Is100; (b) IS150; (c) IS200; (d) IS300; (e) IS400; (f) IS450

4.4.1.7 Electrical characterization

Electrical studies involved measurement of temperature dependence of dark conductivity, steady state photoconductivity and Hall measurements.

i. Dark conductivity

As mentioned earlier, dark conductivity for all the films is measured as a function of temperature in the range 50 K-300 K. For that, the films were prepared on glass substrates. Electrical contact is made using silver paint in the form of two end contacts, with a separation such that the film area for the measurement was 5 mm \times 5 mm. Sample was placed in a liquid helium cryostat, using thermal grease to avoid any thermal gradient along or across the sample. Output was measured across two magnanin wire leads pasted on the electrodes coated on the sample, using silver paste. Ohmic contact of silver for In_2Se_3 film was checked by I-V characteristics measurement. Cryostat was evacuated to a pressure of 10^{-5} mbar. Sample was cooled down to 50 K and then slowly heated to 300 K at a rate of 2.5

$^{\circ}\text{K}/\text{min}$. Value of current at different temperatures was measured for a constant applied voltage (20 V).

Variation of conductivity with inverse temperature is plotted in fig. 4.9. Since thickness of all samples could not be measured, we plotted current instead of absolute value of conductivity assuming both have same variation. Hereafter, variation of current is taken as variation of conductivity itself. From the plot, it is evident that the nature of variation of conductivity with temperature is similar for all samples except IS400 and IS450. Conductivity increases very slowly with temperature in low-temperature range ($T < 160$ K), but in high-temperature range ($T > 180$ K) the increase is rather sharp. This is a general behaviour of polycrystalline and amorphous semiconducting thin films [22]. The two types of behaviours in low and high temperature region can be due to two different mechanisms. The high-temperature mechanism is attributed to thermal excitation of charge carriers across the potential barrier at grain boundaries. Experimental data for this range ($T > 180$ K) can be fitted to a law in the form [21],

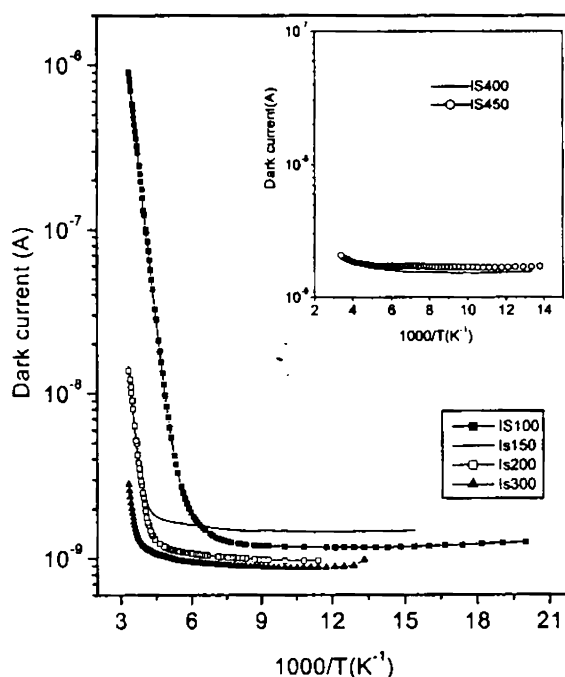


Figure 4.9: Plot of dark conductivity vs. $1000/T$ for In_2Se_3 films formed at different temperature

$\sigma = \sigma_0 \exp -\frac{E_a}{kT}$, where E_a is the activation energy and T is the absolute temperature. Values of E_a were evaluated from Arrhenius plot of conductivity (in log scale), $\log(\sigma)$ vs. $1000/T$ (fig. 4.9) and are given in table 4.2.

Low-temperature ($T < 160$ K) conduction process involves variable range hopping mechanism with tunneling between states which are close in energy [23]. This is a low activation energy process. In this case, the experimental curve can be fitted with $\sigma = \sigma_0 T^{1/2} \exp -\left(\frac{T_0}{T}\right)^{1/4}$, where the value of T_0 is related to the degree of disorder of the semiconductor. Conductivity data are represented in fig. 4.10 as $\ln(\sigma T^{1/2})$ vs. $T^{-1/4}$. Value of T_0 for each film was evaluated and is given in table 4.2.

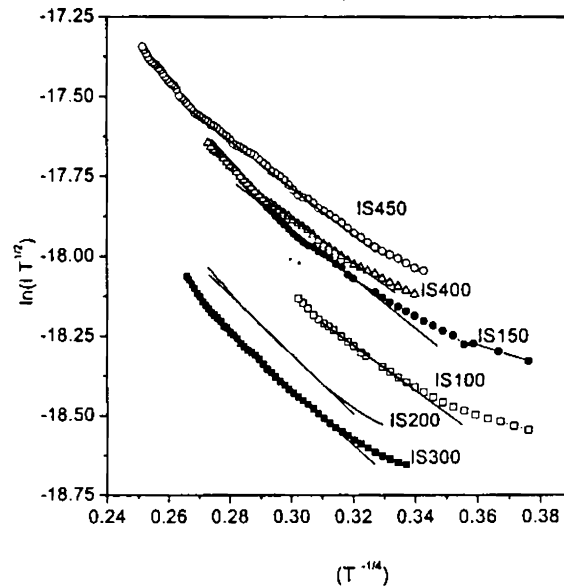


Figure 4.10: Plot of $\ln(\sigma T^{1/2})$ vs. $T^{-1/4}$ for In_2Se_3 films formed

At different temperatureSample	E_a (eV)	T_0 (K) (10^4)
IS100	0.25 ($T > 180$)	0.27
IS150	0.27 ($T > 268$)	0.29
IS200	0.27 ($T > 270$)	0.80
IS300	0.25 ($T > 290$)	0.76
IS400	-	0.35
IS450	-	0.30

Table.4.2 Values of E_a and T_0 for In_2Se_3 films formed at different annealing temperatures

ii. Photoconductivity

In order to evaluate the photovoltaic application of the material, the electrical behaviour of the films under illumination is studied in the steady state conditions.

Dependence of conductivity with temperature under illumination was investigated in comparison with that in dark condition. First the sample was cooled to 50 K and then illuminated by light radiation of intensity 15 mW/cm^2 . The current value gradually increased and then attained a steady value after one minute of illumination. At this steady state, the sample was heated at the same rate as that in dark condition and corresponding current measurements were taken, for a constant applied voltage, 20 V.

Variation of conductivity with inverse temperature under illumination is illustrated in fig. 4.11, in comparison with dark current. On irradiation, conductivity increases considerably from the dark value for all samples and behave almost in a similar manner with increase in temperature as in dark condition. At low temperature, conductivity under illumination exceeds the dark value by a few orders in the case of all films except IS400 and IS450 as seen in the figure.

Variation of photosensitivity ($\Delta I/I$), which is the ratio between change in current due to illumination and dark current at each temperature, is depicted in fig. 4.12. All samples show same variation except IS400. At low temperatures, IS100 has maximum photosensitivity and becomes minimum at room temperature compared to other films. At room temperature better photosensitivity is for IS150.

iii. Hall measurements

Hall measurements were carried out to evaluate the type of conductivity carrier density and mobility of charge carriers of the films. Experimental details are given in chapter 1. A rectangular piece of sample of area 1 cm^2 was cut and four point-contacts were made nearest to the corners (circumference) for electrical connection, using silver paste. Then magnanine wire leads of the four-probe set up were pasted at the four terminals, using silver paste. Measurement was performed at room temperature, in high vacuum with a magnetic field applied was 2000 Gauss. It was observed that films IS100 and IS150 exhibit n-type conductivity while others show weakly p-type with low carrier concentration. The measured parameters are given in the table.

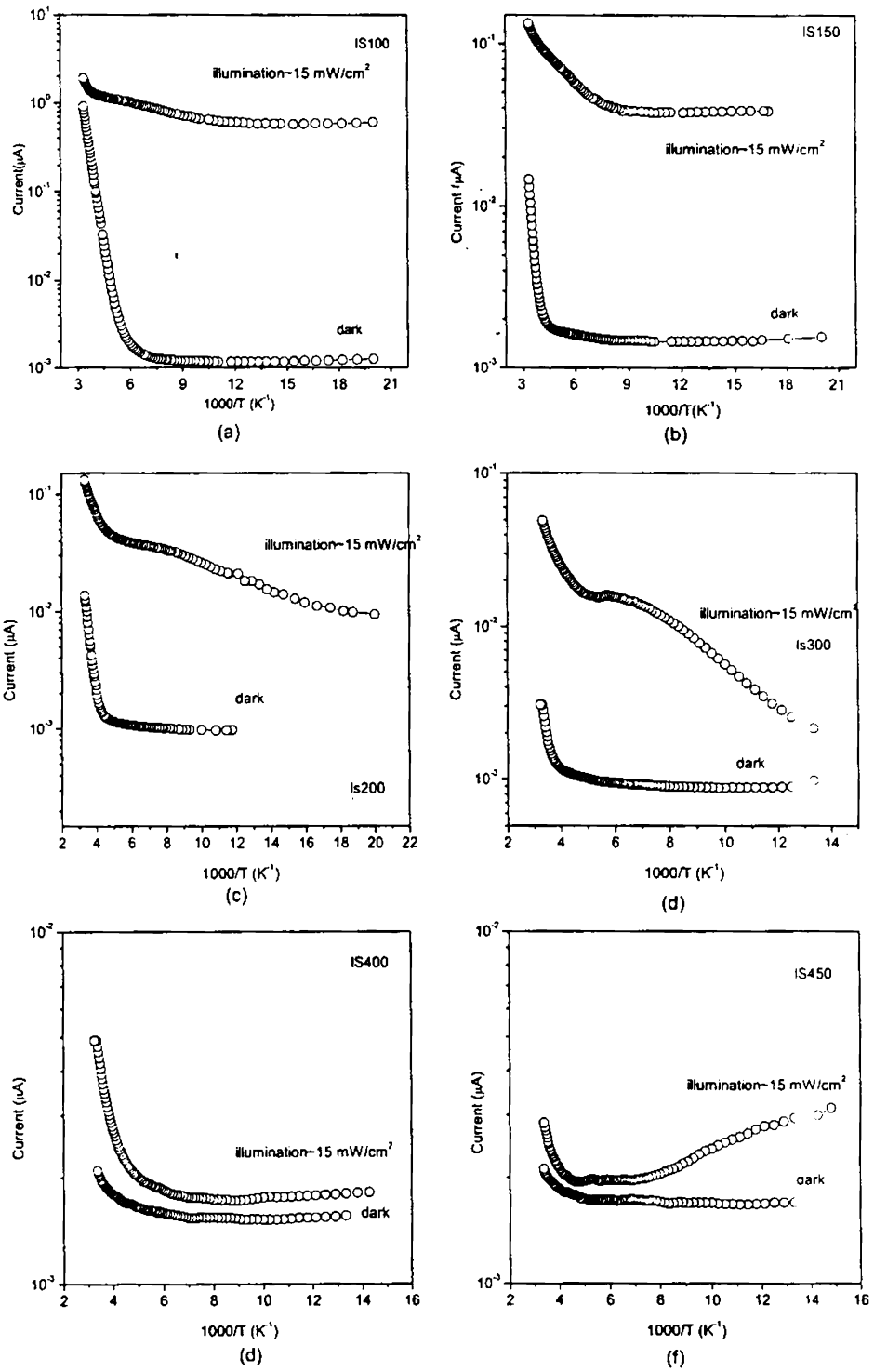


Figure 4.11: Comparison of dark conductivity and steady state conductivity under illumination vs. $1000/T$
 (a) IS100; (b) IS150; (c) IS200; (d) IS300; (e) IS400; (f) IS450

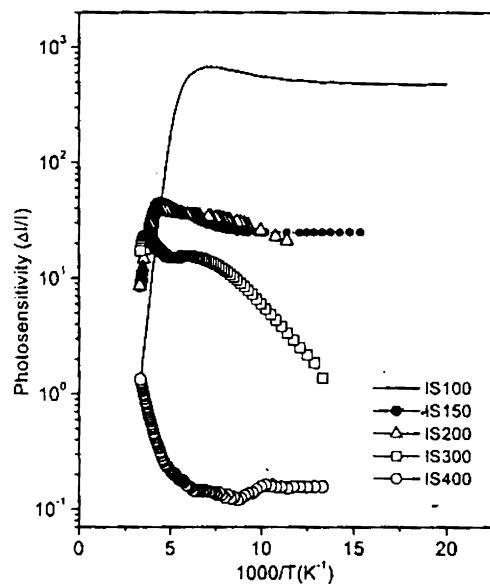


Fig. 4.12: Variation of photosensitivity with temperature for In_2Se_3 samples formed at different temperature

Sample	Resistivity (ρ) $\Omega \text{ cm}^{-1}$	Mobility (μ) cm^2/Vs	Hall coeff. cm^3/C	Carrier density (cm^{-3})	Type of carriers
IS100	1.47×10^3	26	3.7×10^4	4.9×10^{14}	electrons
IS150	5.5×10^5	9.8	5.38×10^6	1.16×10^{12}	electrons
IS200	1.1×10^6	85	6.7×10^{10}	9.24×10^7	Holes
IS300	8.46×10^5	53	1.35×10^{11}	4.48×10^7	Holes
IS400 IS450	Measurement was not possible due to still higher resistance				

4.4.2 Discussion on In_2Se_3

After annealing the Se-In stack layers in high vacuum, no traces of indium was visually observable on the surface, for all types of samples. Before annealing, white layer of In was seen on the surface and was opaque. Even, due to annealing at 373 K, below the melting point of In, undiffused layer of indium could not be observed at the surface. As the annealing temperature was increased the films became more transparent, with golden yellow colour. Film formed at 373 K is more thick compared to those formed at 673 K. This shows that there is gradual

decrease in thickness with increase in annealing temperature due to the evaporation of both indium and selenium at higher temperatures [24].

Crystallographic studies show that the phase formed at all temperatures is hexagonal γ - In_2Se_3 . Fig.4.2 shows that γ - In_2Se_3 formed at 373 K consists of (104) plane. At 423 K, (201) plane grows with expense of (104) plane. At 673 K and 723 K, all planes except those present at 373 and 423 K are distinguishable. Amorphous nature of films formed at 473 K and 573 K can be considered as the intermediate state of reorientation of grains, which leads to the growth of all planes at high temperature at the expense of those present at low temperatures. SEM of IS200 also supports the intermediate process of reorientation at 473 K and 573 K (fig. 4.1).

Compositional analyses shows that, In:Se ratio approximately remains the same at all temperature except at 373 K. BE of $\text{In}3d_{5/2}$ and $\text{Se}3d_{5/2}$ levels are coinciding with that of In_2Se_3 , in all the films. XPS profile montage and depth-wise compositional analysis, (fig. 4.3, 4.4 and 4.5), supports that interlayer mixing of Se and In and subsequent solid-state reaction between them induced by annealing results in the formation of In_2Se_3 films uniformly.

Optical characterization explicitly shows a shift in band gap for the films formed at different annealing temperatures. This can be correlated to the structural differences of the films. Eg value, (1.8 eV) for film formed at 373 K, coincides with the reported value of polycrystalline γ -phase. For the films formed at 473 and 573 K, band gap is higher (fig. 4.8). This may be due to the poor crystallinity of the films as seen in XRD leading to quantum size effect [25]. It is also observed that absorbance value varies according to crystallinity of the films. Eg value of IS400 and IS450 are slightly higher than that of IS100. This increase may be corresponding to decrease of localized states near the mobility edge due to improvement in crystallinity at high temperature [26].

Temperature dependence of dark conductivity (fig. 4.9) indicates two mechanisms for the conduction process in the measured range of temperature. Low-temperature ($T < 180$ K) mechanism is attributed to variable range hopping between localized states as described earlier. The disorder parameter T_0 (Table.

4.2), increases with decrease in crystallinity, in agreement with XRD analysis. In samples formed at 673 K and 723 K, the main conduction process is hopping mechanism as seen in inset of fig. 4.9, in the measured range of temperature. The high-temperature process is attributed to thermally activated conduction across the grain boundaries. The activation energy for all the films is approximately 0.25 eV, for IS100, IS150, IS200 and IS300 showing that same mechanism is contributing for the high-temperature conduction process. It is well known that the electrical properties of polycrystalline semiconductor films are affected by potential barrier scattering at grain boundaries. Trapping of charge carriers by interface states at boundaries sets up potential barriers which cause band bending. As a result, current flow is limited by thermionic emission over the barrier at high temperature [27]. From hall measurements, carrier concentration decreases with increase in annealing temperature, which increases the grain boundary potential barrier width. Hence thermally activated conduction process occurs in such samples at higher temperature. This supports shift of high-temperature mechanism towards the higher temperature with increase in annealing temperature (Fig. 4.10).

n-type nature of In_2Se_3 may be attributed to the presence of excess indium or interstitial indium atoms [28]. In the case of IS100, the low temperature annealing may result in slightly higher concentration of In near the surface. This excess indium may be remaining as interstitial making it n-type. In the case of other samples, indium is evaporated from the film due to annealing and also, diffusion process is more effective at high temperature. As a result, the ratio In:Se decreases towards the depth which is clear from fig. 4.5(b) and 4.6(a). Hence, n-type nature decreases with annealing temperature and films show slightly p-type nature due to indium vacancies. Reduced thickness for films IS400 may also be due to evaporation of indium. Redistribution of gap states at higher temperatures may also increase resistivity of films. Highly insulating nature of $\gamma\text{-In}_2\text{Se}_3$ polycrystalline films of all distinct peaks was already reported earlier [28].

From the studies on photosensitivity, sample IS150 has maximum photosensitivity at room temperature.

4.4.3 Characterisation of copper selenide

Structural, compositional and optical properties of the annealed Se/Cu stack layers were analysed using XRD, XPS and absorption and transmission spectra.

4.4.3.1 XRD

Crystallographic change taking place due to annealing process in Se/Cu bilayer is illustrated in fig. 4.13. Fig 4.13(a) and (b) show XRD patterns of Se/Cu layers before and after annealing respectively. Figure 4.13 (a) has a very small peak at $2\theta=30.7^\circ$ ($d=2.88 \text{ \AA}$). This corresponds to (100) plane of Cu [JCPDS 4-0836]. In the case of annealed sample, two peaks at $2\theta=26.9^\circ$ ($d=3.32 \text{ \AA}$) and $2\theta=44.65^\circ$ ($d=2.03 \text{ \AA}$) correlated to the cubic phase of Cu_{2-x}Se [JCPDS 6-0680] [29]. Planes corresponding to these d-values are (111) and (220) as indicated in the figure.

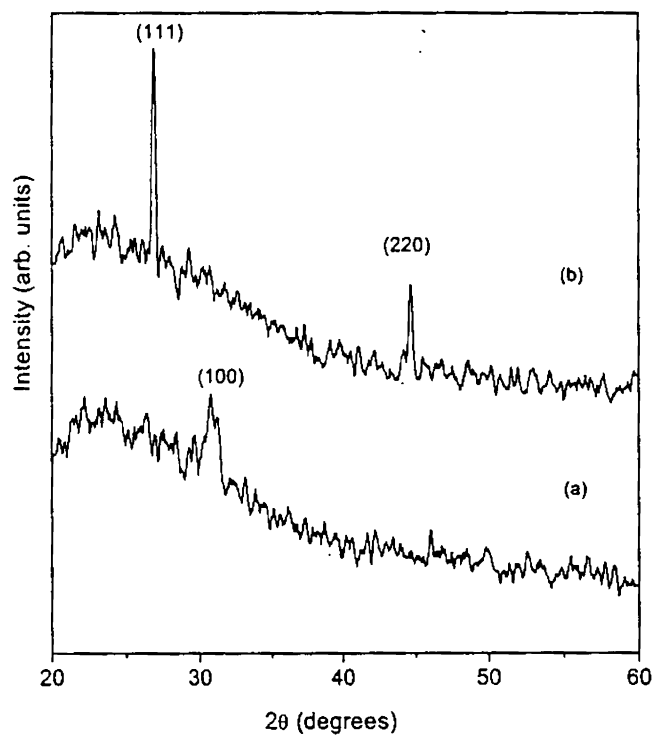


Figure 4.13: XRD pattern of Se-Cu stack bilayer
(a) before annealing (b) after annealing

ESCA PROFILE 8/25/01 START=2, END=202, NTR=2
FILE: CuSe025 2 CuSe Se/Cu on MESA

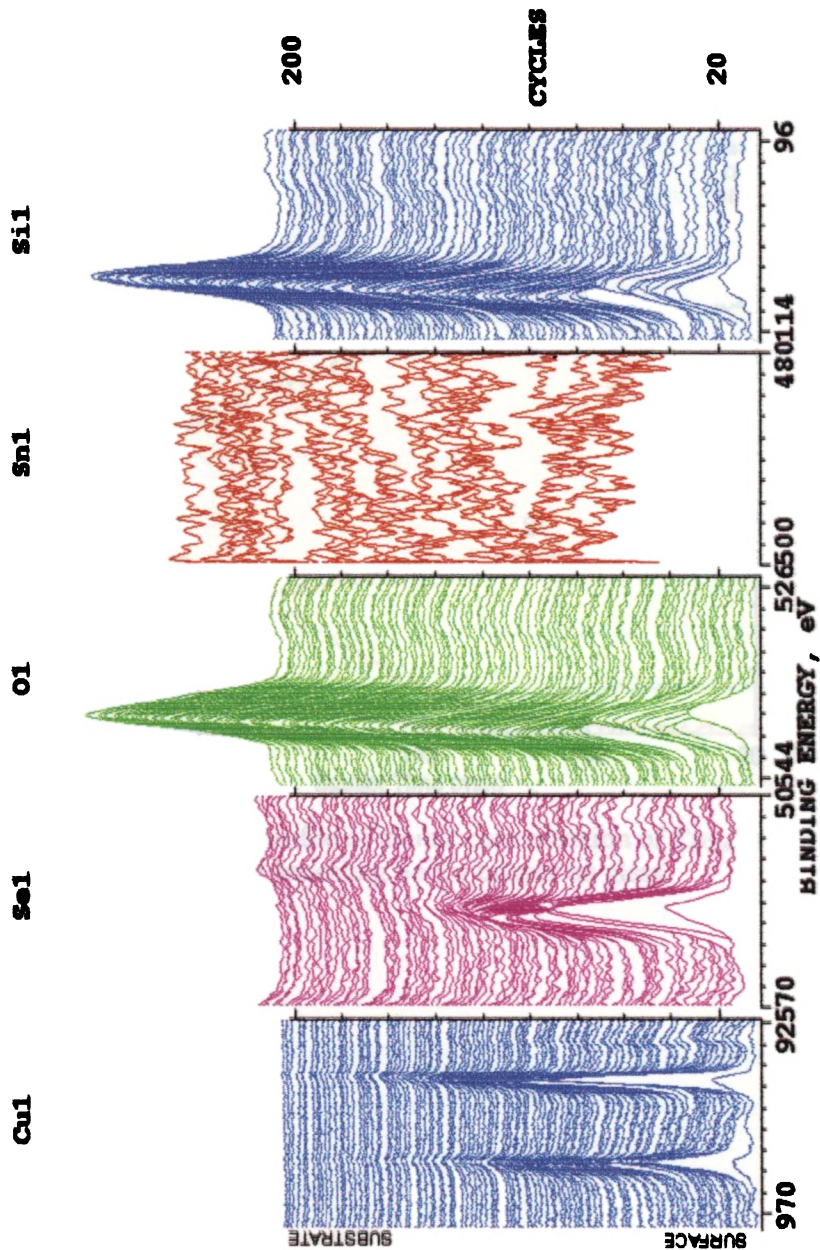


Figure 4.14(a): XPS profile montage of sample Se/Cu annealed at 473 K

Chapter 4

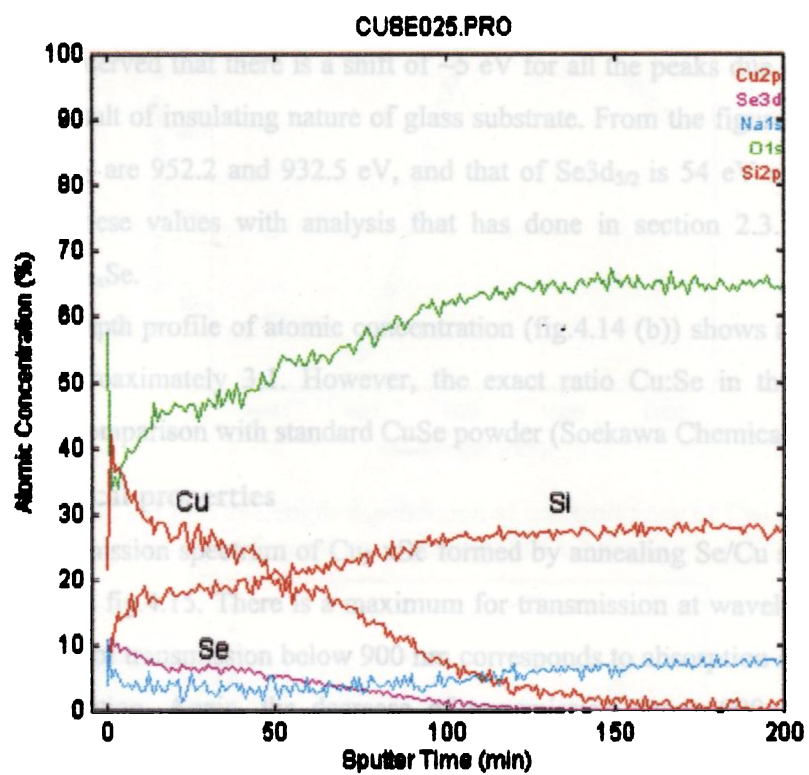


Figure 4.14(b): Depth profile of atomic concentration of Cu_{2-x}Se film formed by annealing Se/Cu bilayer on glass

4.4.3.2 XPS

This technique was used to find out the composition of the films formed by annealing Se/Cu stack layers. XPS profile montage of the film is given in fig 4.14 (a). It was observed that there is a shift of ~ 5 eV for all the peaks due to charging effect as a result of insulating nature of glass substrate. From the figure, BE of Cu $2p_{1/2}$ and $2p_{3/2}$ are 952.2 and 932.5 eV, and that of Se $3d_{5/2}$ is 54 eV respectively. Comparing these values with analysis that has done in section 2.3.3, the film formed is Cu_{2-x}Se .

The depth profile of atomic concentration (fig.4.14 (b)) shows that ratio of Cu/Se is approximately 3:1. However, the exact ratio Cu:Se in the film was analysed by comparison with standard CuSe powder (Soekawa Chemical) as 2:1.

4.4.3.3 Optical properties

Transmission spectrum of Cu_{2-x}Se formed by annealing Se/Cu stack layers is as shown in fig.4.15. There is a maximum for transmission at wavelength ~ 900 nm. Decrease of transmission below 900 nm corresponds to absorption due to band to band transition. Again, the decrease of transmission above 900 nm can be attributed to free carrier absorption [30]. From spectral dependence of optical absorbance, $(\alpha h\nu)^2$ is found out and plotted against $h\nu$ as depicted in fig. 4.16. Linear nature of the plot indicates that the fundamental transition is direct. The band gap (E_g) evaluated from the plot is 1.78 eV, which is slightly less than the reported value obtained for chemical bath deposited Cu_{2-x}Se [30]. This can be attributed to the variation of 'x' with respect to preparation conditions. Also, since the films were formed at higher temperature which may lead to better crystallinity. This can reduce band gap value [31].

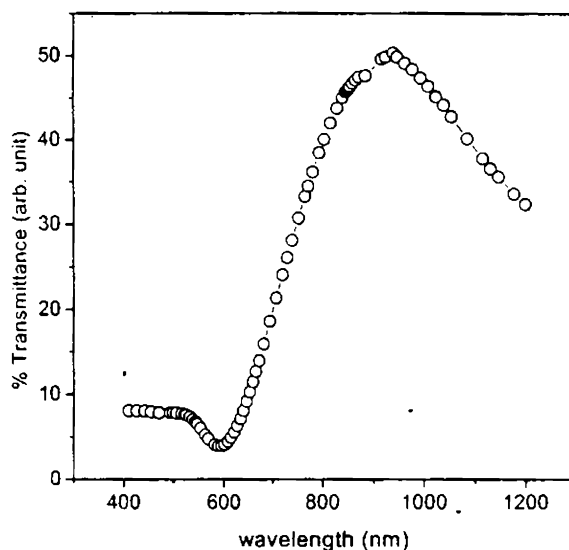


Figure 4.15: Wavelength dependence of transmittance of Cu_{2-x}Se film formed by annealing Se/Cu bilayer

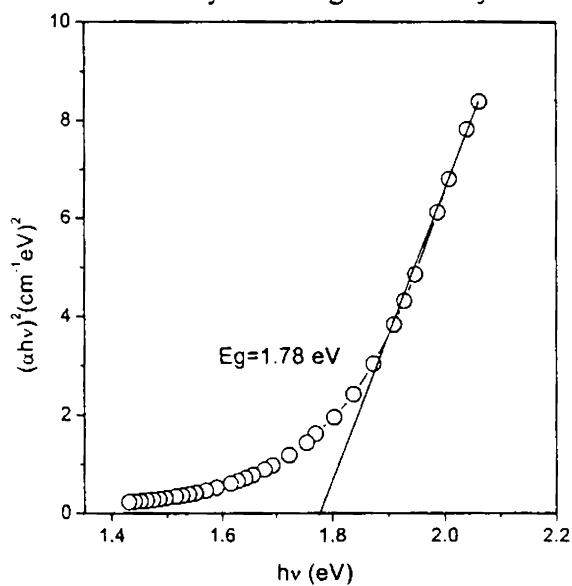


Figure 4.16: Plot of $(\alpha h\nu)^2$ vs. $h\nu$ for Cu_{2-x}Se film formed by annealing Se/Cu bilayer

4.4.4 Discussion on Cu_2Se

In the case of copper selenide, XRD studies (fig.4.13) reveal that it is formed through solid-state reaction between Cu and Se induced by annealing at 473 for 1hr. XPS analysis also supports the inter layer diffusion process, uniformly across the thickness of the sample.

Deviation of band gap value (1.8 eV) from the reported value may be due to the variation non-stoichiometric index 'x' for the films formed by this method from that of those formed by other techniques.

4.5 Conclusion

In₂Se₃ films were successfully prepared by annealing stack layers consisting of chemically deposited Se and vacuum evaporated In. Structural, morphological, compositional and optical properties of films formed at different annealing temperatures were studied. Structural studies revealed that γ -In₂Se₃ films containing (104) and (201) planes are formed at 373 K and 423 K while same phase consists with other planes were formed at higher temperatures. XPS depth profile shows that there is uniform interlayer mixing of In and Se induced by annealing. Dark conductivity was found to be maximum for those films. Depending on the annealing temperature, the films exhibit p-type and n-type conductivity. Films formed at 423 K were found to be good for PV application.

Copper selenide thin films were also successfully prepared using chemical bath deposited a-Se by SEL technique. Structural, compositional and optical characterization of films formed due to annealing Se/Cu stack layer at 473 K were analysed. It could be inferred that the a-Se from CBD can be used for preparation of binary selenides by SEL technique.

References

- [1] J. Weszka, Ph. Daniel, A. Burian. A.M. Burian, A.T. Nguyen, *J. Non-Crystalline Solids* 265 (2000) 98
- [2] Herrero, J. Ortega, *Solar Energy Materials* 16 (1987) 477
- [3] M.A. Afifi, N. A. Hegab and A.E. Bekheet, *Vacuum* 148 (1995) 431
- [4] K. Bindu, C. Sudha Kartha, K.P. Vijayakumar, T. Abe and Y. Kashiwaba, *Appl. Surf. Sci.*, (in press)
- [5] C. Julien and M. Eddrief, *Materials Science and Engineering B*13 (1992) 247
- [6] C. Julien, A. Chevy and D. Siapkak, *Phys. Stat. Sol. (a)* 118 (1990) 553
- [7] C. De Blasi, D. Manno, G. Micocci and A. Tepore, *Journal of Crystal Growth* 96 (1989) 947
- [8] Jiping Ye, Sigeo Soeda, Yoshio Nakamura and Osamu Nittono, *Jpn. J. Appl. Phys.* Vol 37 (1998) 4264
- [9] M. Emziane and R Le Ny, *J. Phys. D: Appl. Phys.* 32 (1999) 1319
- [10] B. Thomas *Appl. Phys. A* 54 (1992) 293
- [11] C. Julien, A. Chevy and D. Siapkak, *Phys. Stat. Sol. (a)* 118 (1990) 553
- [12] C. Julien and M. Eddrief, *Materials Science and Engineering B*13 (1992) 878
- [13] J. Herrero and J. Ortega, *Solar Energy Materials* 16 (1987) 477
- [14] S. Marsillac, J. C. Bernede, R. Le Ny and A. Conan, *Vacuum* 46 (1995) 1315
- [15] M. Emziane, S. Marsillac, J. Querfelli, J. C. Bernede and R. Le Ny, *Vacuum* 48 (1997) 878
- [16] Tomohiko Osthuka, Kazayuki Nakanishi, Tamotsu Okamoto, Akira Yamada, Makoto Konagai and Uwe Jahn, *Jpn. J. appl. Phys.* 40 (2001) 509
- [17] M. Emziane, R. Le Ny, *J. Phys:D, Appl. Phys* 3 2 (1999) 1319
- [18] L. L Kazmerski, O. Janjoun, P. J Ireland, S. K. Deb, R. A. Mickelsen, W. Chen, *J. Vac.Sci. Technol.* 19 (1981) 467
- [19] S.N. Sahu *Thin solid Films* 261 (1995) 98
- [20] C. Jullien, A. Chery and D. Siapkak, *Phys. Stat. Sol. (a)* 118 (1990) 553

-
- [21] T. P Sharma, S.K. Sharma, R. Kumar, Garima Jain and S.C.K Misra. *Indian J. of Pure & Appl. Physics* 28 (1990) 486
- [22] C. Gullen, J. Herrero, *J. Appl. Physics*. 71 (1992) 5479
- [23] Ichiro Watanabe, Toshiyuki Sekiya *Journal of Non-Crystalline Solids* 97:98 (1987) 667
- [24] S. N. Sahu *Thin Solid Films* 261 (1995) 98
- [25] L. Brus, *J. Chem. Phys.* 90 (1986) 2555
- [26] G. Micocci, A. Tepore, R. Rella and P. Siciliano, *Phys. Stat. Sol. (a)* 148 (1995) 431
- [27] M. V. Garcia-Cuenca, M. Manchon, M. Varela, A. Lousa and J. L. Morenza, *Solar Energy Materials* 17 (1998) 347
- [28] Brahim-Otsmane, Emery. J. N, Eddrief. M, *Thin Solid Films*, 237 (1994) 291
- [29] R.B. Shafizade, I. V. Ivanova, M. M. Kazinets, *Thin Solid Films* 55 (1978) 211
- [30] V.M. Gracia, P.K. Nair, M.T.S. Nair *Journal of Crystal Growth* 203 (1999) 113
- [31] P.K. Nair, M.T.S. Nair, V.M. Garcia, O.L. Arenas, Y. Pena, A. Castillo, I.T Ayala, O. Gomezdaza, A. Sanchez, J. Campos, H. Hu, R. Suarez and M.E. Rincon, *Solar Energy Materials and Solar Cells* 52 (1998) 313

CHAPTER 5

DEPOSITION OF COPPER INDIUM SELENIDE THIN FILMS THROUGH MULTISTAGE PROCESSES AND CHARACTERIZATION

5.1 Introduction

Even though the importance of CuInSe_2 film in the field of photovoltaics is well accepted, a convenient method of preparation which can be used for large scale production has not yet been evolved. In this chapter we are presenting simple selenisation process, using chemical bath deposited amorphous selenium thin films for the preparation of CuInSe_2 films. Here, we tried to avoid the usage of selenium vapour or H_2Se gas, which are extremely toxic. Instead, the selenium layer is deposited using simple chemical process in which no gases are used. We developed different methods to deposit CIS films using hybrid processes. In all these processes, selenisation is done using selenium film deposited from chemical bath. Two methods are described here in detail. One method is Stacked Elemental Layer (SEL) technique of annealing the multilyer having structure Se/In/Cu . Second method is thermal diffusion of Cu into In_2Se_3 film.

5.2 Part A: SEL process

SEL technique involves induced solid-state reaction between elements constituting the stacked layers by inter layer diffusion process. There are several reports on the preparation of thin films binary and ternary selenides using this technique. Adurodija et al [1] reported CIS preparation by annealing vacuum evaporated Se/In/Cu stacked layers. They analysed in detail the reaction mechanism involved during CuInSe_2 formation. Here, structural and optical properties of the as-deposited elemental stack layers are compared with that of annealed Se/In/Cu stack layers at different temperatures to analyse growth process of CuInSe_2 . Also, the process is analysed with variation in Cu/In ratio in the film formed at optimized annealing temperature using the above techniques.

5.2.1 Preparation

Substrates used were preheated and well-cleaned micro glass slides. Procedure for cleaning and other details are described in earlier chapter 3.

The whole process of CIS film preparation in the present work involved three steps. In the first step, selenium films of required thickness (here, 5000 Å) were deposited as described in section 3.3.2. Thickness of selenium layer was chosen such that CIS film formed will be nearly stoichiometric with Cu:In:Se ratio 1:1:2. In the second stage, indium layer of thickness, 350 Å and copper layer of thickness, 200 Å were vacuum evaporated sequentially on the selenium layer such that the ratio, $(\text{Cu}+\text{In})/\text{Se} \sim 1$ in the sample. Structure of the elemental stack layers obtained was Se/In/Cu with selenium forming the lower layer on glass or SnO₂ coated glass substrate. In the final stage, the stack layers were annealed in vacuum at different temperatures for 1 h. The rate of heating was always kept at 3 K/min and annealing temperatures were 423 K, 473 K, 573 K and 673 K. During annealing, sample was kept at 423 K for 1hr, near the melting point of indium, before reaching the final temperature. This may cause the formation of Cu-In alloy [2] and subsequent selenisation by the Se layer at higher temperatures leading to the formation of CIS films. This intermediate annealing at 423 K helped to prevent indium globules formation. The same problem could also be reduced by deposition of Cu on indium to some extent [3]. High vacuum (10^{-5} mbar) was maintained during annealing process. Films formed at different temperatures were analysed using various techniques. The annealed films at different temperatures are named as CIS150, CIS200, CIS250, CIS300 and CIS400. In this study the Cu/In ratio was fixed at 1.3 (assuming slightly greater than 1).

In order to analyse compositional dependence on growth process, films were prepared by varying Cu/In ratio in the stack layers. This was done by changing the thickness of Cu layer keeping thickness of indium layer the same at 350 Å. The ratio was calculated knowing the values of density and molecular weight of Cu (8.9 g/cc and 63.54 respectively) and In (7.3 g/cc and 114.8 respectively) and distance from the source to substrate is 15 cm.

Amount of indium was 40 mg in Mo boat. The calculated Cu/In ratio for different weights of Cu were 10 mg (0.5), 20 mg (0.9), 25 mg (1.1), 30 mg (1.3), 35 mg (1.6) and 40 mg (1.8) for evaporation. Hereafter, these samples were labeled as CIS0.5, CIS0.9, CIS1.1, CIS1.3, CIS1.6 and CIS1.8 respectively. Films having Cu/In ratio >1 are called Cu-rich films and when the ratio is <1 , In- rich films. Cu/In stack layers was deposited on to three substrates (coated with selenium) simultaneously.

Morphological, structural and compositional changes taking place in the multilayer, Se/In/Cu during annealing leading to the formation of CIS were analysed using different techniques. Also, SEL process was tried with multilayer structure Se/Cu/In with Cu/In~ 1.3 and analysed using XRD.

A few samples were prepared on SnO₂ coated glass substrate since some techniques require conducting substrates for avoiding charging effect due to highly insulating nature of glass substrate. Films having Cu/In ≥ 1.3 show semi-metallic nature. These films were treated with NaCN solution and structural, optical and electrical properties the films were studied.

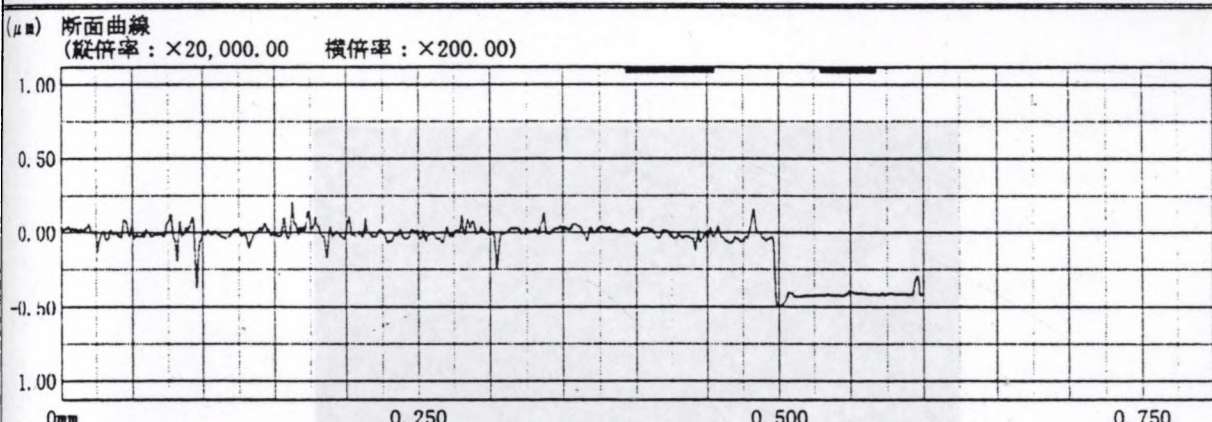
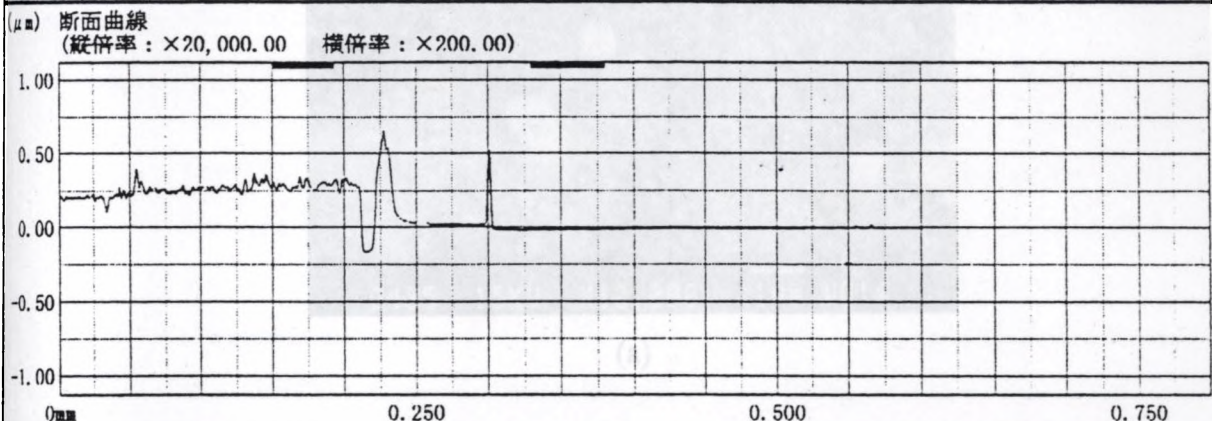
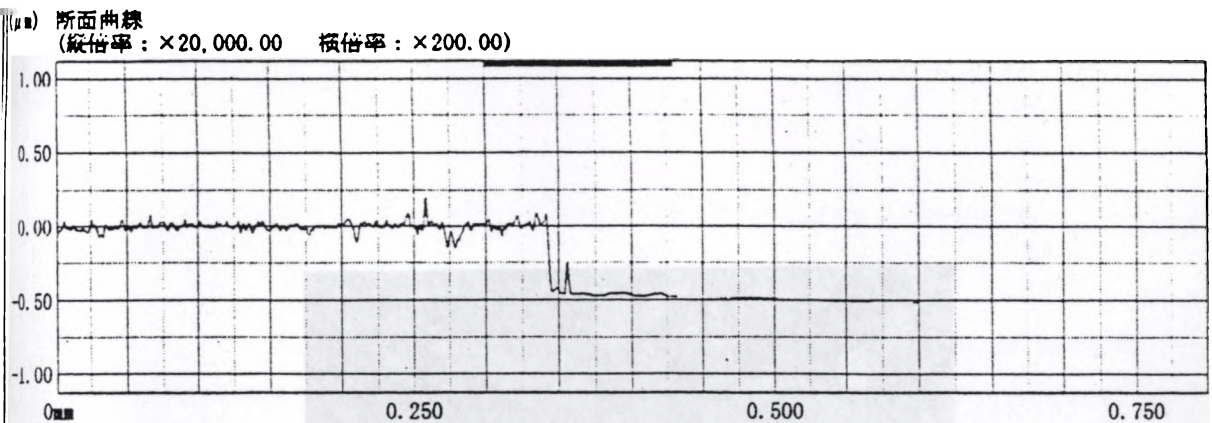
5.2.2 Characterization

5.2.2.1 Thickness

Thickness of a representative sample CIS1.3 was measured using surface profilometer. Measured thickness was 0.5 μm as shown in fig.A

5.2.2.2 Morphology

Surface morphology of CIS1.3 film deposited on glass substrate and SnO₂ coated glass substrate are given in figure 5.1(a) and 5.1(b) respectively. Granular shaped grains are clear in these films. A few void-like structures are observed in these films, which is present during selenium deposition as depicted in fig 3.2 in section 3.4.3. On SnO₂ no such voids are present. As far as device fabrication is concerned, presence of voids is not at all desirable. Furthermore, in the device fabrication, CuInSe₂ films will be deposited on transparent conducting oxides such as SnO₂ or ITO. This implies that presence of voids in films on glass is not very important when the quality of film for device fabrication is concerned.

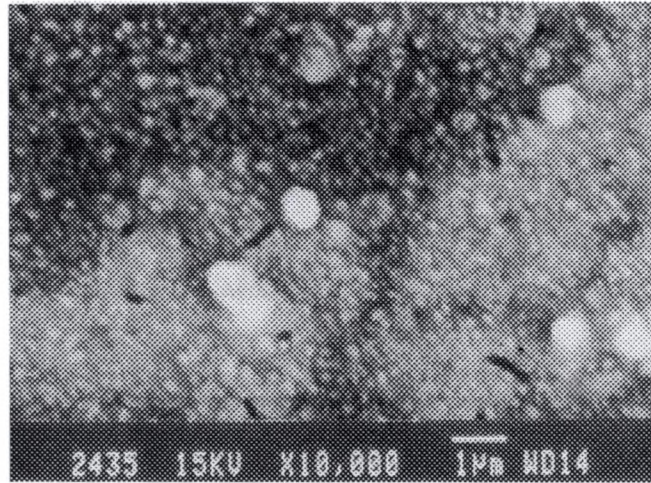


試料情報1	膜を一部削った	時間	18:47:11	Rmax	0.5660 μm
試料情報2	CISCu25	ロット番号			
日付	02/01/23	サンプル番号	60		
測定者名	Yasuhiro Kashiwaba	自動保存ファイル名	WORK60. RST		
出力単位	mm, μm	自動測定ファイル名	TEACH001. TAH		
極性	正転	解析条件ファイル名	CALCOND. ana		
ピックアップ	高倍率ピックアップ	SPC出力ファイル名	SPCFILE. csv		
量出規格	JIS-'82規格	時間	18:49:11	Rmax	0.3606 μm
測定種別	断面測定	ロット番号			
測定長さ	0.6mm	サンプル番号	63		
カットオフ波長		自動保存ファイル名	WORK63. RST		
測定倍率	×50K	自動測定ファイル名	TEACH001. TAH		
測定速度	0.06mm/s	解析条件ファイル名	CALCOND. ana		
カットオフ種別		SPC出力ファイル名	SPCFILE. csv		
傾斜補正	前半補正	時間	18:51:44	Rmax	0.4650 μm
移動・戻り速度	1.50mm/s	ロット番号			
リターン設定	通常測定	サンプル番号	68		
予備駆動長さ	カットオフ波長/3×2	自動保存ファイル名	WORK68. RST		
λsカットオフ比		自動測定ファイル名	TEACH001. TAH		
λsカットオフ波長	2.5 μm	解析条件ファイル名	CALCOND. ana		
評価長さ	0.1296mm	SPC出力ファイル名	SPCFILE. csv		

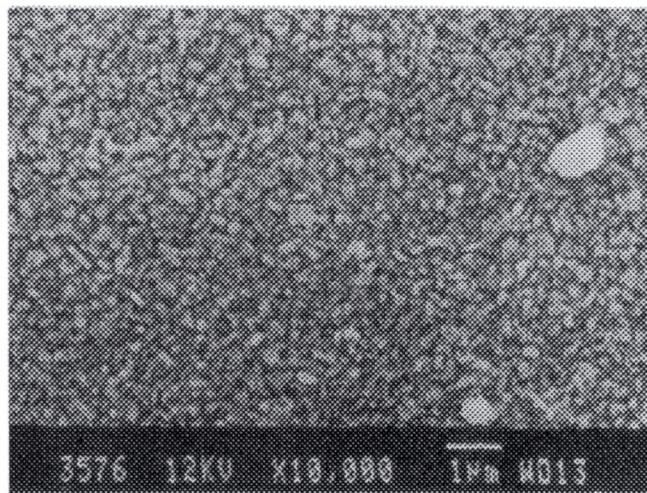
(Scraped sample) CIS Cu25 3/4

Fig.A: Thickness of CIS film

Chapter 5



(a)



(b)

Figure 5.1 Scanning Electron Micrograph of
(a) CIS1.3 on glass substrate (b) CIS1.3 on SnO₂ coated glass

Important when the quality of films for device fabrication is concerned.

5.2.2.3 Structure

Figure 5.2 shows XRD patterns of Se/In/Cu stack layers annealed at different temperatures, drawn with same intensity scale. XRD spectrum of unannealed Se/In/Cu film (fig. 5.2(a)) exhibits the peaks corresponding to (101) plane ($d=2.72 \text{ \AA}$) of metallic In [JCPDS 5-646]. Absence of peaks of Cu or Se, implies that as-prepared Se and Cu layers were amorphous in nature. Fig.5.2 (b) shows that film CIS150 consists of peaks corresponding to phases of crystalline Se, Cu_9In_4 alloy and In_2Se_3 . The XRD peak at $2\theta = 28.05^\circ$ ($d=3.17 \text{ \AA}$), $2\theta, 29.2^\circ$ ($d=3.05 \text{ \AA}$) and 31° ($d=2.88 \text{ \AA}$) coincide with that of Cu_9In_4 alloy [JCPDS 2-1178, 42-1476]. A relatively weak peak at $d = 3.05 \text{ \AA}$ is also present due to the formation of In_2Se_3 , as mentioned in the sec.4.4. Hence, in fig.5.2(b) the strong peak at $d = 3.05 \text{ \AA}$ can be attributed due to the presence of Cu_9In_4 alloy and In_2Se_3 phases. For the sample, CIS200 (fig.5.2(c)), peaks corresponding to chalcopyrite CuInSe_2 at 2θ values 26.55° ($d=3.34 \text{ \AA}$) and 44.1° ($d=2.04 \text{ \AA}$) along with Cu_9In_4 are present [(JCPDS 23-206), 4, 5, 6]. In the case of films CIS250, CIS300 and CIS400 additional peak of CuInSe_2 at $2\theta = 52.5^\circ$ ($d=1.74 \text{ \AA}$) is present along with other peaks as depicted in figures 5.2(d), 5.2(e) and 5.2(f) respectively. For all the phases formed at different temperatures, planes of orientation are marked in the figure.

XRD spectrum of the multilayer Se/Cu/In annealed at 673 K is shown in figure 5.3, which shows the presence of CuInSe_2 and CuIn alloy.

Growth of CuInSe_2 film with increase of Cu/In ratio is depicted in fig. 5.4. For the film CIS0.3, XRD shows a small peak corresponding to d value of 3.34 \AA , which is the most prominent peak of CIS film in chalcopyrite phase as given in fig. 5.4(a). Also, there is an indication of peak at $d = 2.04 \text{ \AA}$. All the three peaks corresponding to CuInSe_2 phase are present in the film CIS0.5 as seen in fig. 5.4(b). In the case of CIS0.9, CIS1.1, CIS1.3 and CIS1.6, as Cu/In ratio increases, intensity of all the peaks increases as shown in figures 5.4(c), (d), (e) and (f) respectively. For film CIS1.8, peak intensity decreases, which is evident in fig. 5.4(g) (All the plots are drawn for same intensity scale). Variation of grain size

with Cu/In ratio is illustrated in table 5.1 by comparing FWHM values corresponding to (112) planes of the respective films obtained from the XRD.

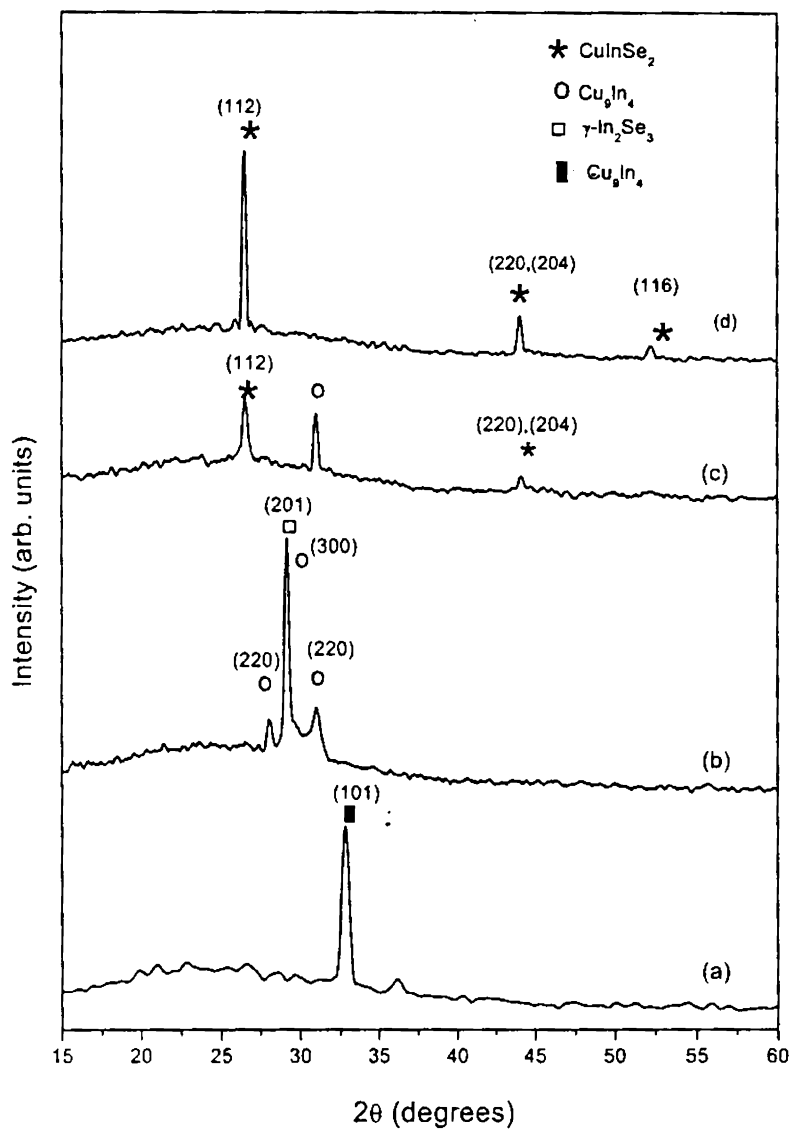


Figure 5.2: XRD pattern of (a) un-annealed Se/In/Cu multilayer Cu/In~1.3; (b) CIS150; (c) CIS200; (d) CIS250 (same intensity scale)

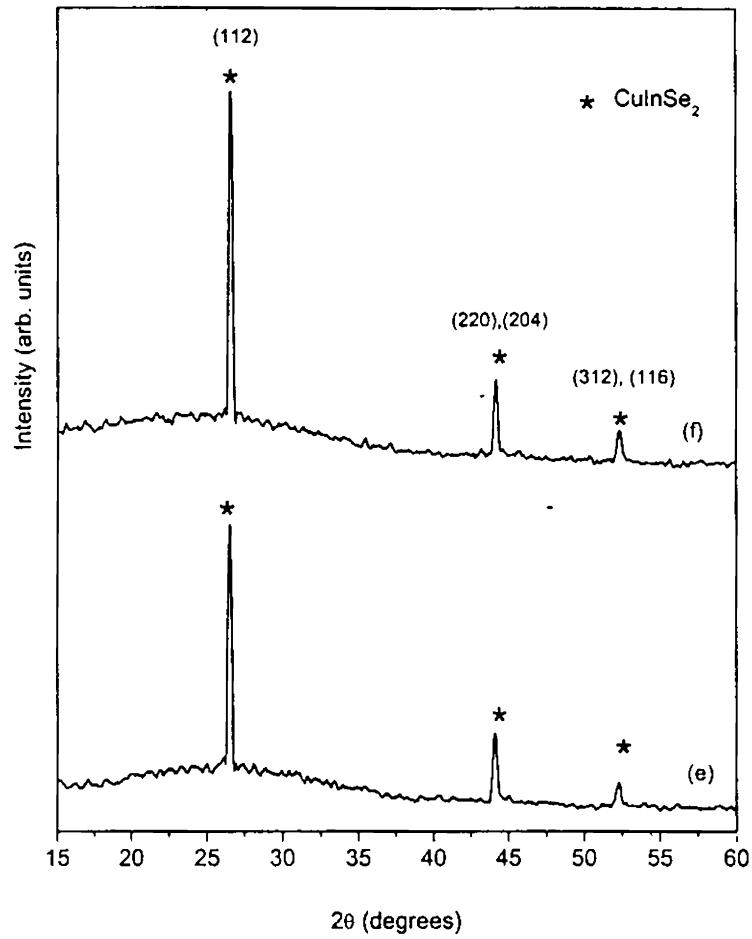


Figure 5.2: XRD pattern of (e) CIS300 (f) CIS400

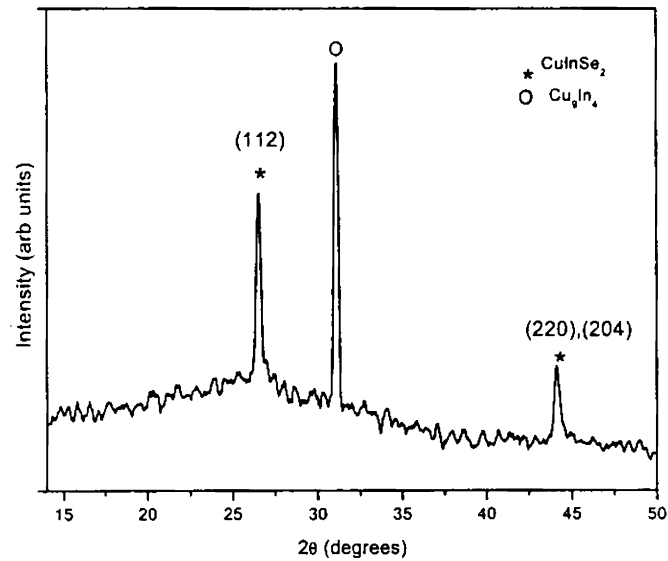


Figure 5.3: XRD pattern of Se/Cu/In annealed at 673 K for 1 hr

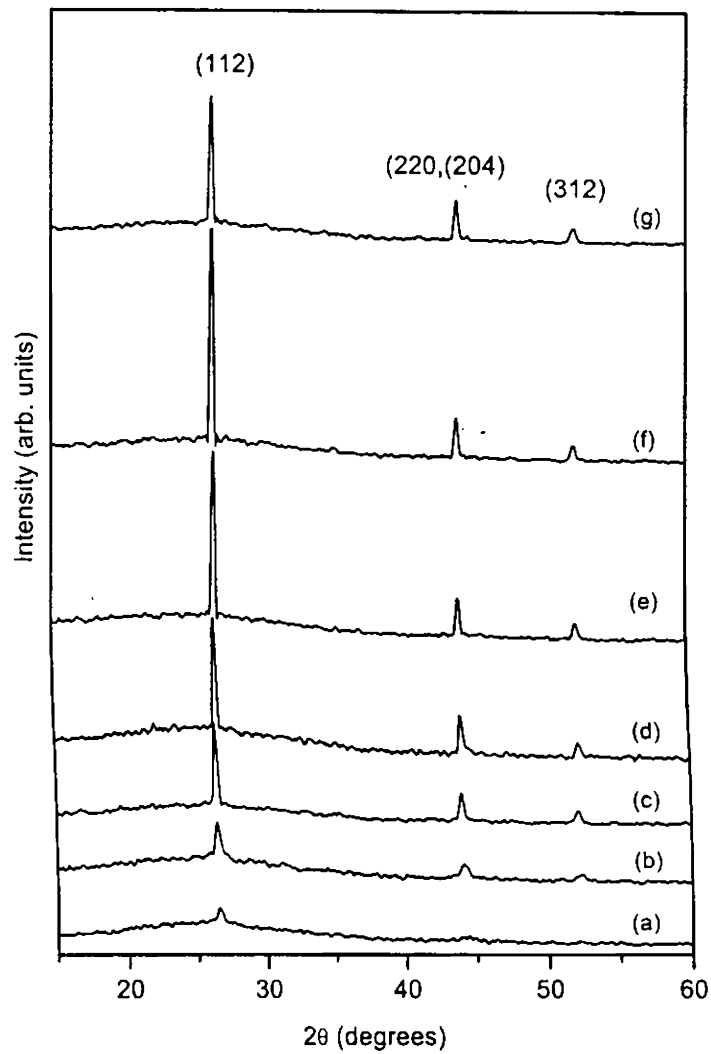


Figure 5.4: XRD pattern of CIS films formed at 673 K having different Cu/In ratio
 (a) CIS0.3; (b) CIS0.5; (c) CIS0.9; (d) CIS 1.1; (e) CIS 1.3
 (f) CIS 1.6; (g) CIS 1.8 (same intensity scale)

Sample	Cu/In	FWHM	Grain size (Å)
CIS0.3	0.3	0.646	72.2
CIS0.5	0.5	0.583	79.8
CIS0.9	0.9	0.524	88.9
CIS1.1	1.1	0.521	89.34
CIS1.3	1.3	0.520	89.51
CIS1.6	1.6	0.516	90.207
CIS1.8	1.8	0.526	88.49

Table 5.1 Comparison of FWHM values with Cu/In ratio

5.2.2.4 Compositional analysis

From the above analysis, CuInSe₂ film growth is significant when the ratio is greater than 0.5. Hence compositional studies were confined in samples CIS0.9, CIS1.1 and CIS1.3. XPS technique was used for depth-wise compositional analysis. Experimental details are described elsewhere in earlier chapters.

Profile montage of as-prepared Se/In/Cu (un annealed CIS1.3) stack layers is given in fig. 5.5(a). BE of Cu 2p^{3/2}, In 3d^{5/2} and Se 3d^{5/2} are 932.8, 444.7 and 55.5 eV which corresponds to the respective elemental state [7]. Three distinct layers of Cu, In and Se are clearly observed in the spectrum. Depth profile of atomic concentration of the sample also shows Cu/In/Se layers from the surface to the substrate as seen from fig. 5.5(b). Copper is found to be diffused slightly into the depth even in the as-prepared conditions. Selenium concentration in the sample is always less due to preferential sputtering effect as mentioned in preceding chapters.

Figure 5.6(a) shows the profile montage for sample CIS0.9. Here, BE of Cu 2p^{3/2} and In 3d^{5/2} have no appreciable shift from the value in elemental state. However, BE of Se 3d^{5/2} level is lowered by 1 eV to value 54.5 eV which corresponds to BE value in CuInSe₂ [7]. Similar case is reported for amorphous CuInSe₂ films prepared using flash evaporation, by Sakata et al., [8]. Figure 5.6(b) giving depth profile of composition reveals that Cu and In diffuse into Se layer leading to the formation of CuInSe₂ film due to annealing. Cu/In ratio obtained from the plot is about 0.8, which is nearer to that of the gravimetric calculation.

For the films having Cu/In ratio 1.1, XPS profile montage and depth profile of atomic concentration is expressed by figures 5.7(a) and 5.7(b) respectively. The ratio of Cu/In ratio from the graph is ~1.16.

Similar behavior is observed in the case of films having Cu/In ratio 1.3 as expressed in figures 5.8(a) & (b). Diffusion of Cu, In and Se are uniform through the depth and the ratio is almost same as 1.3.

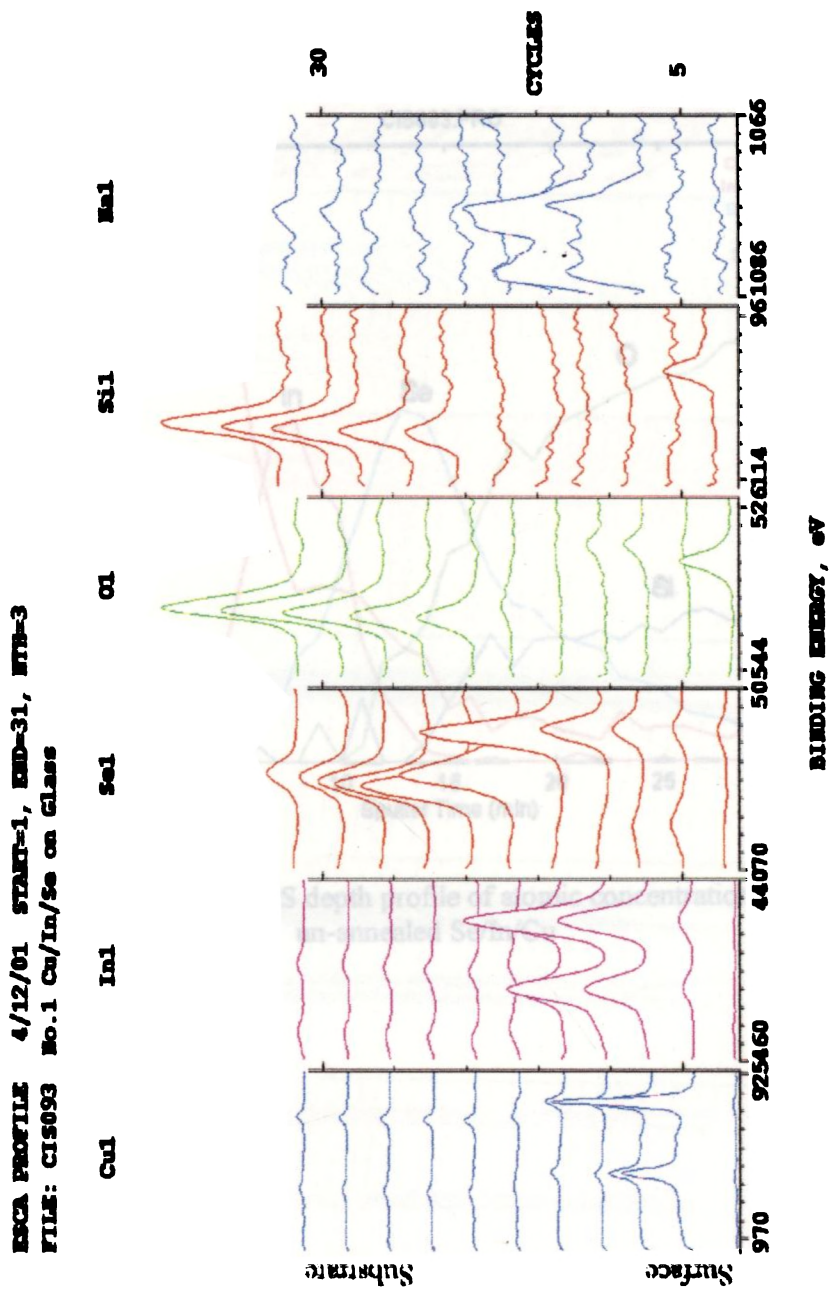


Figure 5.5(a): XPS depth profile of Se/In/Cu --un-annealed CSII.3

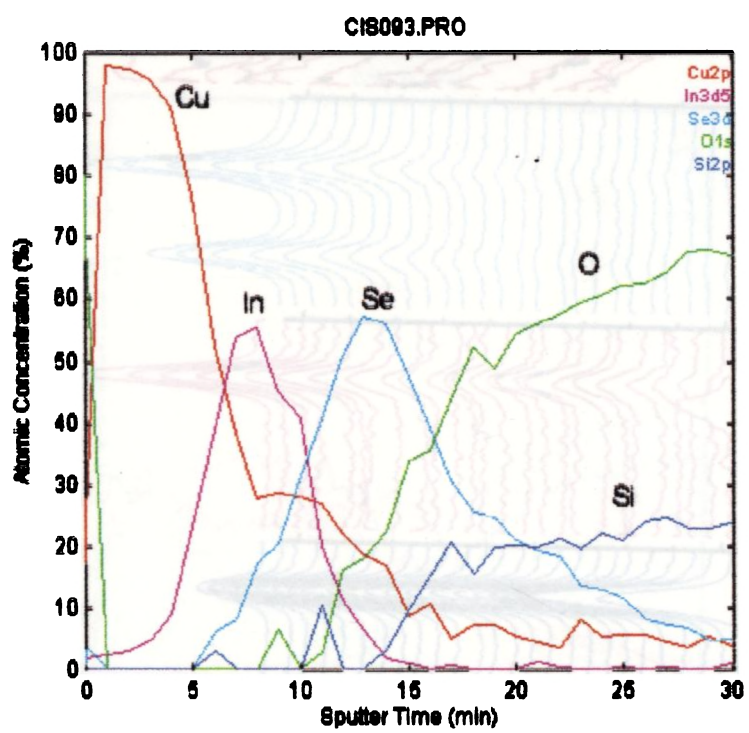


Figure 5.5(b): XPS depth profile of atomic concentration of un-annealed Se/In/Cu

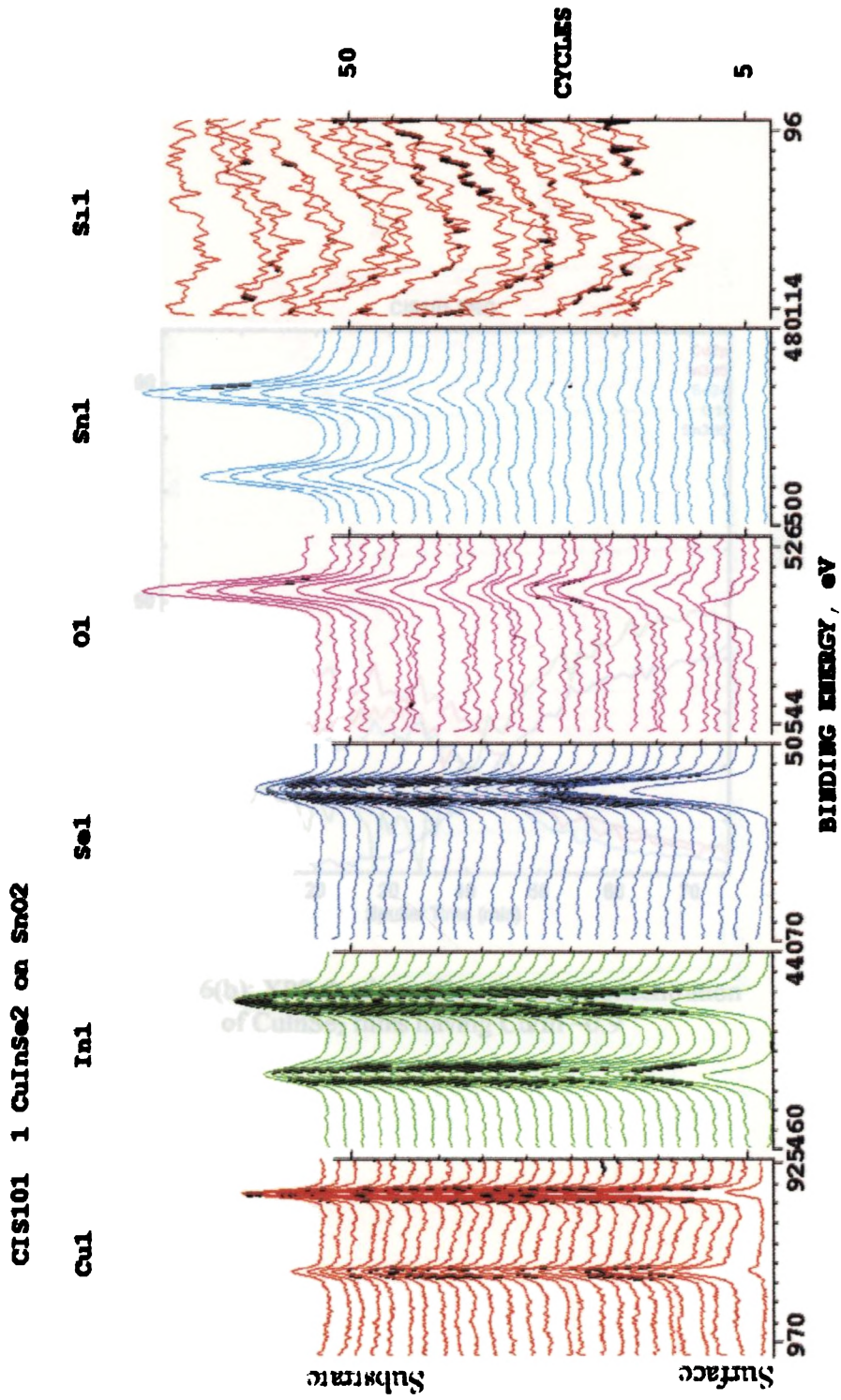


Figure 5.6(a): XPS depth profile of CIS0.9

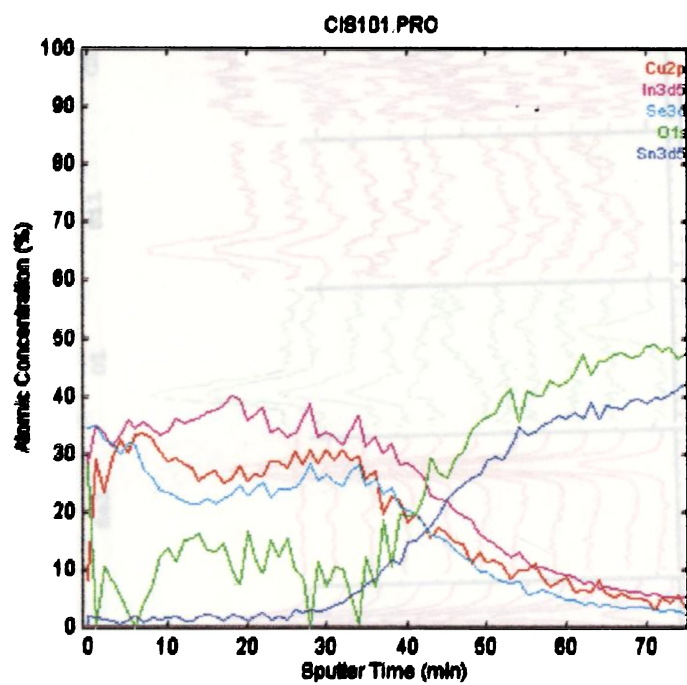


Figure 5.6(b): XPS depth profile of atomic concentration of CuInSe₂ films having Cu/In ~0.9

ESCA PROFILE 1/5/02 STAIR-2, MD-52, MM-5
FILE: CISE133 3 CISE025 CUISE02 FILM

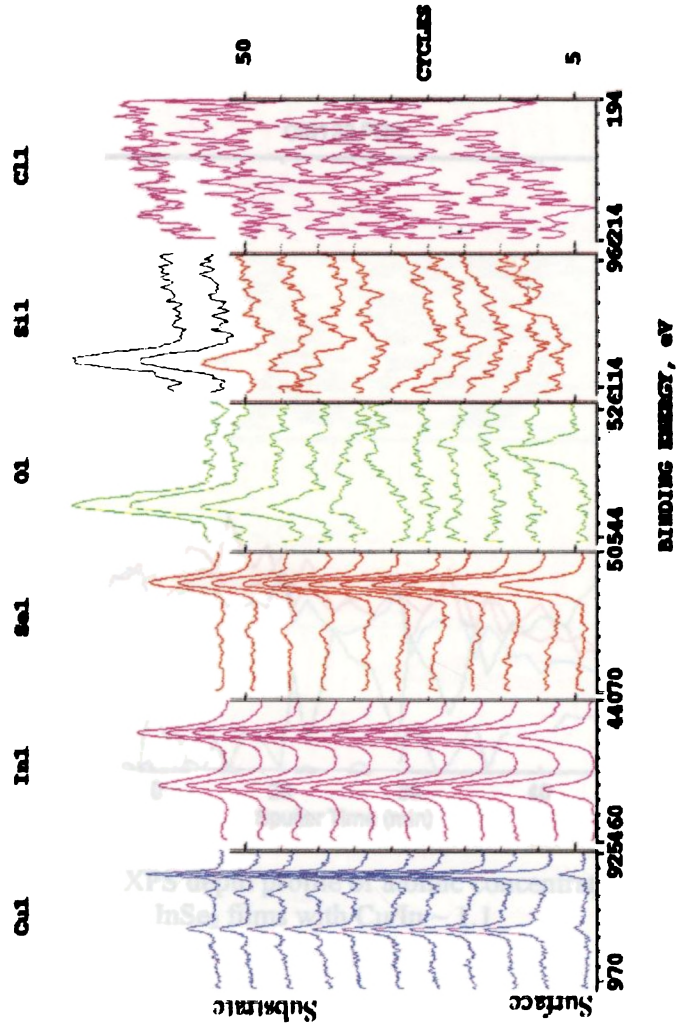


Figure 5.7(a): XPS depth profile of CIS1.1

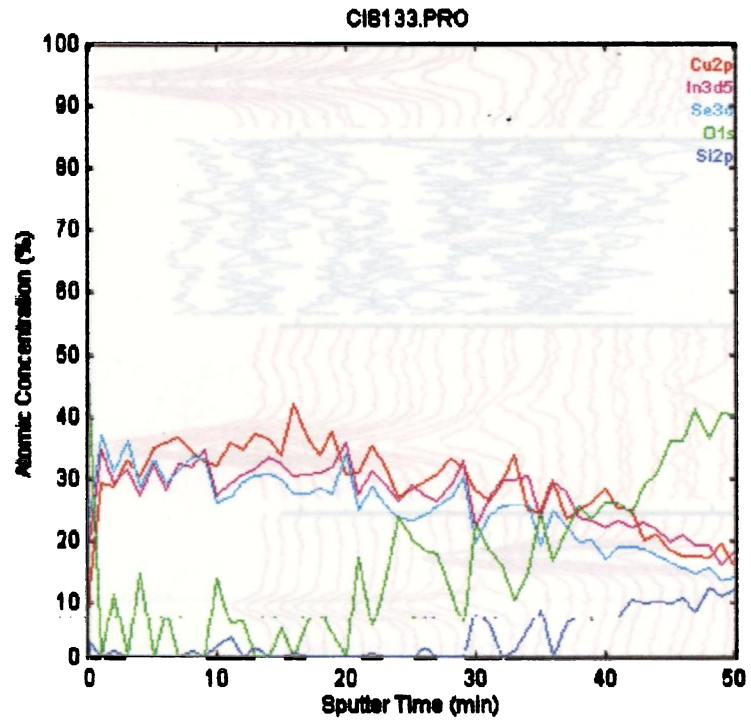


Figure 5.7(b): XPS depth profile of atomic concentration of CuInSe₂ films with Cu/In ~ 1.1

ESCA PROFILE 8/26/01 STAGE=2, END=52, NTH=2
 FILE: CIS117 3 CIS Se/In/Cu on MESA

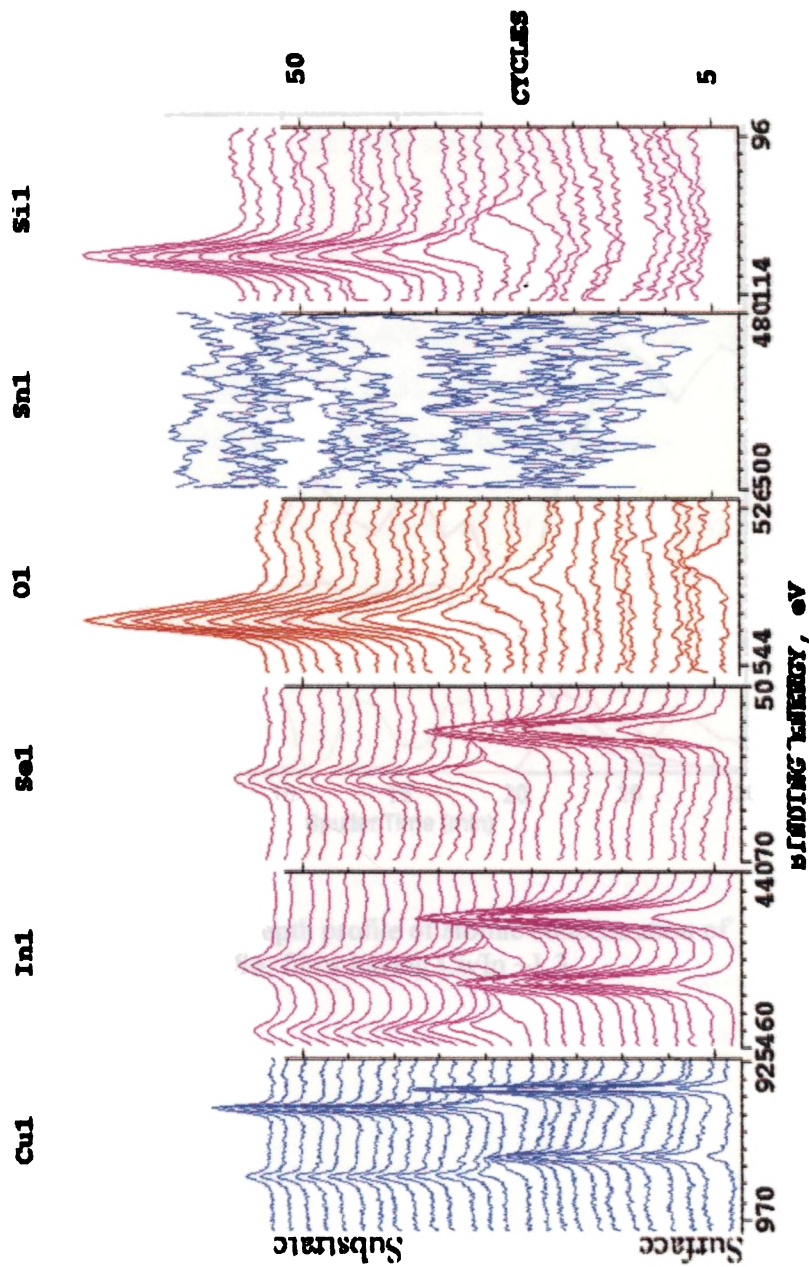


Figure 5.8(a): XPS depth profile of CIS1.3

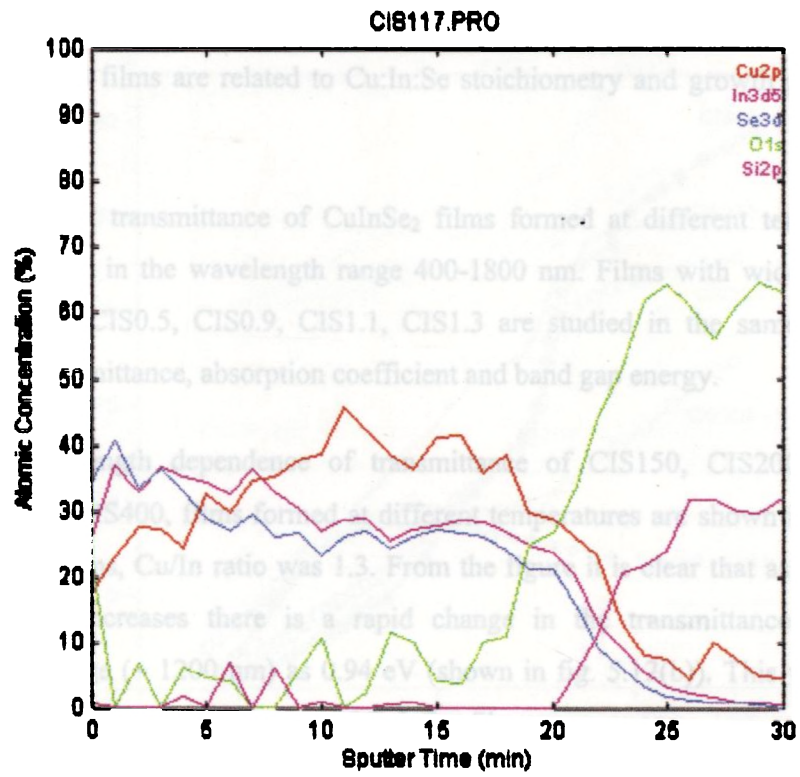


Figure 5.8(b): XPS depth profile of atomic concentration of CuInSe₂ films having Cu/In ~1.3

5.2.2.5 Optical characterization

The optical properties of polycrystalline thin films can vary due to grain boundary and compositional effects. In recent years, optical properties of CuInSe₂ films near and above fundamental absorption edge were studied by many groups [9, 10]. Spectral dependence of the absorption coefficient and the band gap energy values of CIS films are related to Cu:In:Se stoichiometry and growth parameters [9, 10, 11].

Optical transmittance of CuInSe₂ films formed at different temperatures were analysed in the wavelength range 400-1800 nm. Films with wide range of composition, CIS0.5, CIS0.9, CIS1.1, CIS1.3 are studied in the same range to evaluate transmittance, absorption coefficient and band gap energy.

Wavelength dependence of transmittance of CIS150, CIS200, CIS250 CIS300 and CIS400, films formed at different temperatures are shown in fig. 5.9. For all the films, Cu/In ratio was 1.3. From the figure it is clear that as annealing temperature increases there is a rapid change in the transmittance near the absorption edge (~ 1200 nm) as 0.94 eV (shown in fig. 5.12(b)). This value is in agreement with the reported value of CuInSe₂ film.

Compositional dependence of transmission and absorption spectra of CIS films are illustrated in fig. 5.10 and fig. 5.11 respectively. For all the films there is a rapid decrease in transmittance value near the absorption edge. Also, it is very clear that % transmittance of films gradually decreases while α increases with increase in Cu/In ratio.

Eg value for all the samples are evaluated from the plot of $(\alpha h\nu)^2$ vs. $h\nu$ and marked in the fig. 5.11. Linear dependence of $(\alpha h\nu)^2$ on $h\nu$ near the band edge shows that CIS is a direct band gap material. Eg values for In-rich films, CIS0.5, CIS0.9 are 1 and 0.97 eV respectively. In the case of Cu-rich films, CIS1.1 and CIS1.3, the values are 0.96 and 0.94 eV respectively. These values are close to the reported values for Cu-rich and In-rich films [11, 12, 13].

From the figure, it is observed that E_g value decreases with increase in Cu/In ratio. Band gap tailoring due to high defect density is observed for Cu/In ratio 1.1 and this becomes more significant for the ratio 1.3.

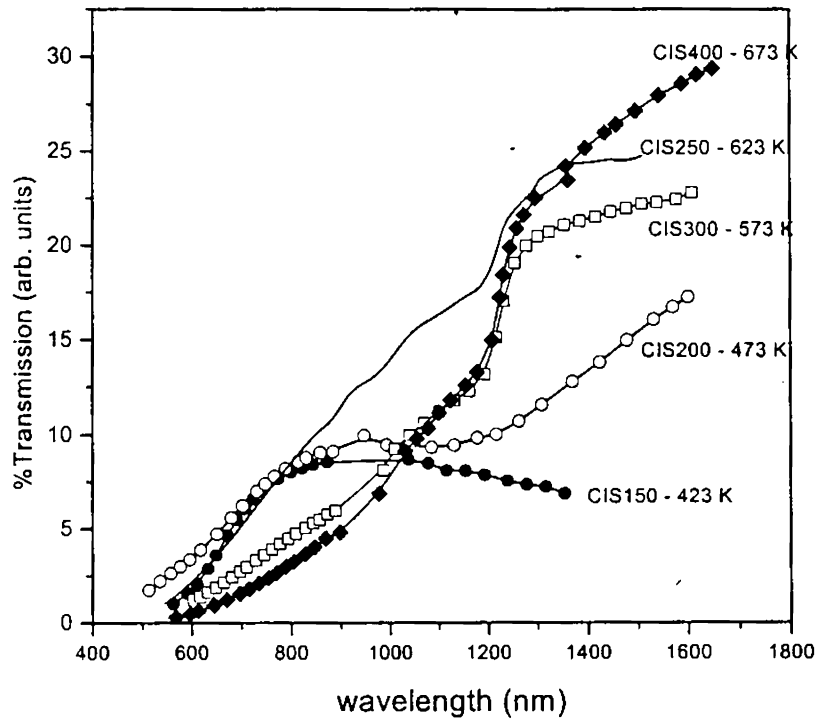


Figure 5.9: Wavelength dependence of Transmittance of CIS films formed at different annealing temperature (Cu/In~1.3)

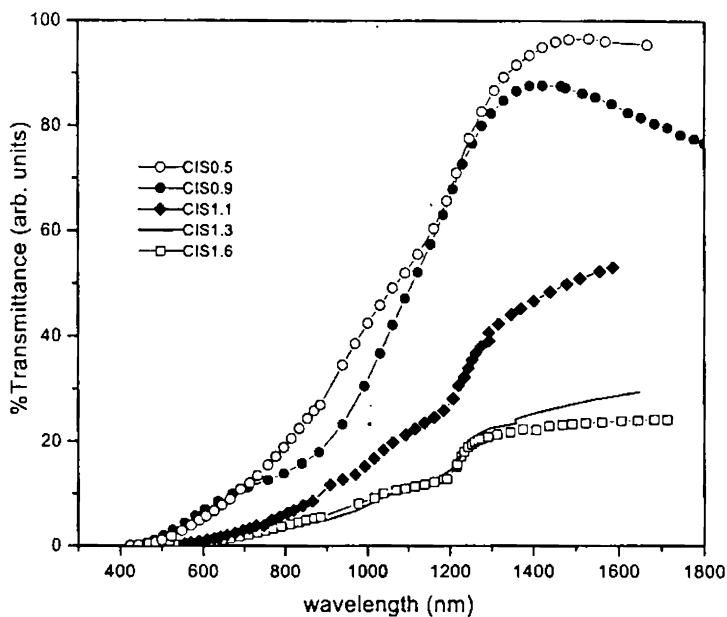


Figure 5.10: Wavelength dependence of Transmittance of CIS films having various Cu/In ratio (annealing temperature – 673 K)

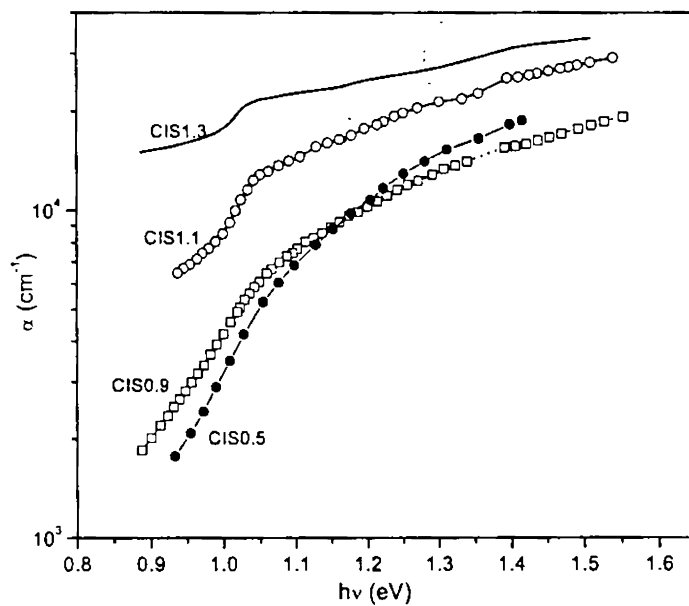


Figure 5.11: Absorption coefficient (α) vs. photon energy for CIS samples various Cu/In ratio

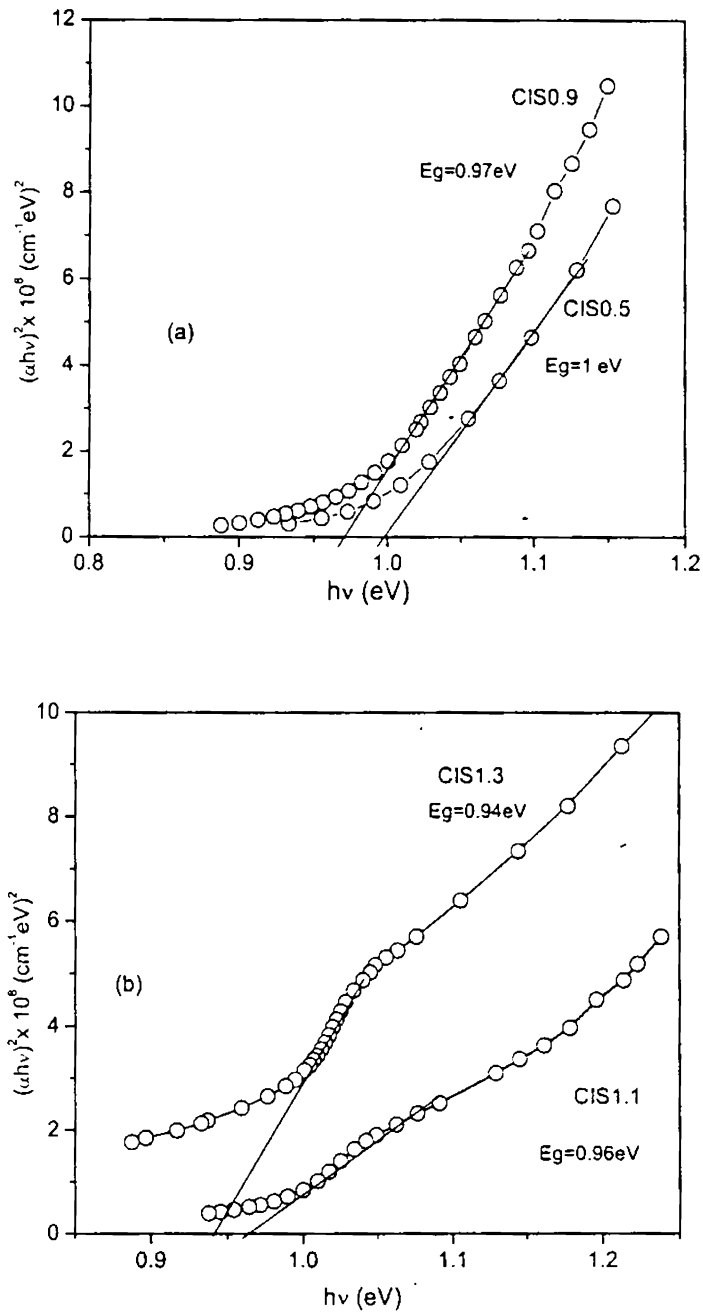


Figure 5.11: Variation of E_g value of CIS films with Cu/In ratio

5.2.2.6 Electrical characterization

The electrical parameters of CuInSe_2 films are dominated by native defects resulting from deviations from stoichiometric compositions. These defects may be interstitials and vacancies [14, 15,]. Recently, Rincon et al., reported detailed studies on theoretical approach of electrical activity and activation energy of various possible intrinsic defects in the material and compared with experimental data [16]. In other words, conductivity depends on composition of the films.

Electrical activity of the defects determines the type of conductivity. Various possible intrinsic defects in CuInSe_2 and their corresponding electrical activities are given in the table.5.2. p-type conductivity is achieved either by cation vacancies or anion interstitials. n-type conductivity is due to either anion vacancies or by cation interstitials. In general, $\text{Cu}/(\text{In}+\text{Se})$ ratio is the criteria, which determines the type of conductivity. If the selenium pressure is remained constant during formation of CuInSe_2 film, then, Cu/In ratio is the main parameter, which controls the conductivity of the films. Cu-rich films are generally p-type and In-rich films are n-type. In the former case, the antisitic defect Cu_{In} (copper in place of indium) and In vacancy (V_{In}) act as acceptor levels contributing holes for p-type conductivity. In the latter case, In_{Cu} is the major defect which act as donor level contributing n-type carriers.

Native point defect	Electrical Acivity
$\text{Cu}_i, \text{Se}_{\text{Cu}}, \text{In}_{\text{Se}}$	Single donor
$V_{\text{Se}}, \text{In}_{\text{Cu}}$	Double donor
In_i	Triple donor
$V_{\text{Cu}}, \text{Se}_{\text{In}}, \text{Cu}_{\text{Se}}$	Single acceptor
$\text{Se}_i, \text{Cu}_{\text{In}}$	Double acceptor
V_{In}	Triple donor

Table 5.2: Various possible native defects in CuInSe_2

Dark conductivity, photoconductivity and hall measurements were carried out to investigate the electrical parameters of CuInSe_2 film with various Cu/In ratios.

5.2.2.6.1 Dark conductivity

In the present study, temperature dependence of conductivity (σ) was measured in the range, 10-300 K. For that, CuInSe_2 films of various Cu/In ratio were prepared on glass substrate. Experimental details were described in sec.4.4.1.7. Ohmic nature of Ag contact was checked by measuring I-V characteristics. Then the cryostat was evacuated to vacuum of 10^{-5} mbar. The sample was cooled down to 50 K and then slowly heated to 300 K at a rate of 2.5 K/min. The current measurements were taken at different temperatures. Knowing the sample thickness ($0.4 \mu\text{m}$) and separation between electrodes (5 mm), conductivity at each temperature is calculated. Similar measurements were carried out for films having Cu/In ratio 0.9, 1.1 and 1.3.

i. Cu/In~0.9

Figure 5.13 shows the plot of variation of conductivity (σ) with inverse of temperature for film CIS0.9.

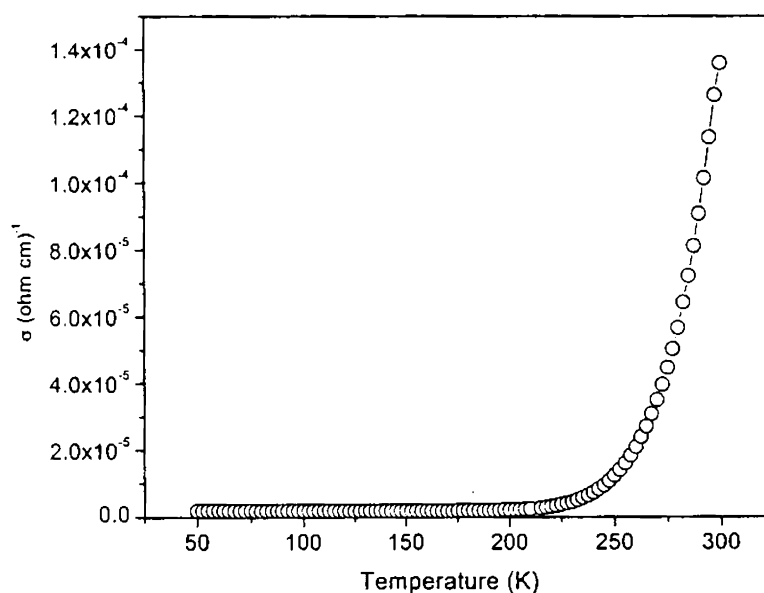


Figure 5.13: Variation of dark conductivity vs. temperature

It is clear that there are two distinct regions in the plot as in the case of indium selenide samples contributing different conduction mechanisms in the range 10-300 K. The two regions can be analysed separately as in the case of In_2Se_3 samples (sec. 4.4.1.7)

In the temperature ranges $T > 250$ K, the curve can be fitted to the expression,

$$\sigma = \sigma_0 \exp\left(-\frac{E_a}{kT}\right)$$

E_a is the activation energy and σ_0 is the pre-exponential conductivity [17]. This is clear from the fig. 5.14 (a) where σ Vs $1000/T$ is a straight line (log scale). Activation Energy, E_a is found out from the slope of the straight line as 300 meV. This activation energy is indicative of grain boundary limited diffusion process [18].

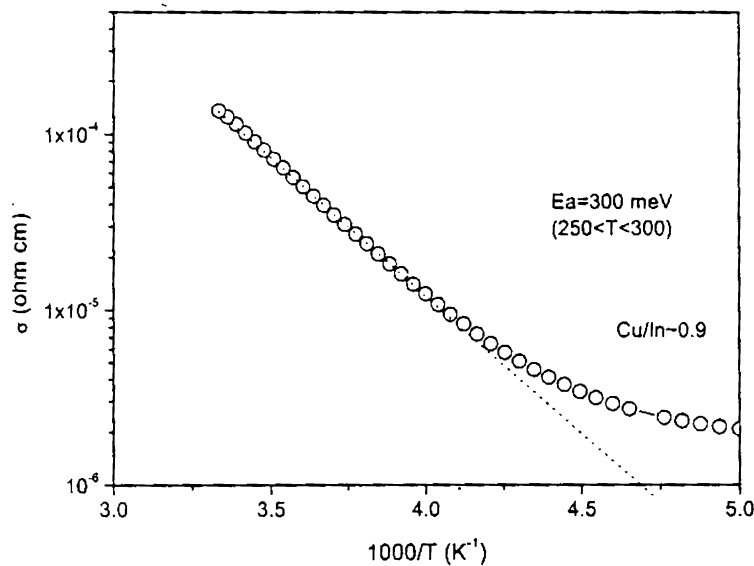


Figure 5.14 (a): Variation of dark conductivity with temperature of CIS0.9 film

In the low temperature range, $160 \text{ K} < T < 50 \text{ K}$, the weak dependence of conductivity on temperature is given in the plot (fig. 5.14(b)), curve can be approximated to the following expression which describes the impurity band conduction by hopping mechanism,

$$\sigma = \sigma_0 T^{-1/2} \exp - \left(\frac{T_0}{T} \right)^{1/2}$$

where $\frac{T_0}{T}$ is the parameter indicative of the hopping mechanism and T_0 is related to the disorder of the material. Hence at this temperature range, $(\sigma T^{1/2})$ vs. $(T^{-1/4})$ is a straight line as shown in the figure.

From the plot, T_0 is calculated as 720 K. This shows that $\frac{T_0}{T} > 1$ which is the criteria for the hopping mechanism and it is satisfied here [19].

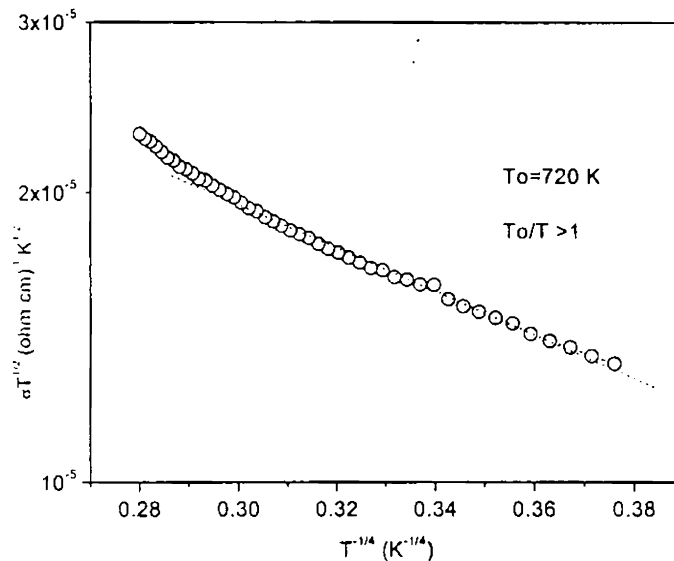


Figure 5.14 (b): $(\sigma T^{1/2})$ vs. $(T^{-1/4})$ plot of CuInSe₂ films with CIS0.9

ii. Cu/In~1.1

Variation of conductivity with temperature for sample CIS1.1 is shown in the fig. 5.15. In this case conductivity gradually increases as temperature increases. Figure.5.16 illustrates the semilogarithmic plot of conductivity vs. inverse of temperature. There are two activation energies obtained from the plot. 15 meV at temperature range $T > 160$ K and 7 meV for the range $T < 150$ K.

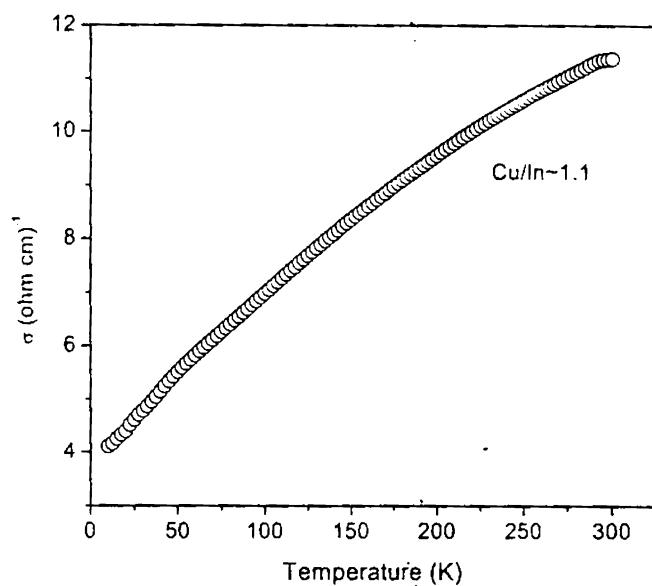


Figure 5.15: Variation of conductivity with temperature for CIS1.1

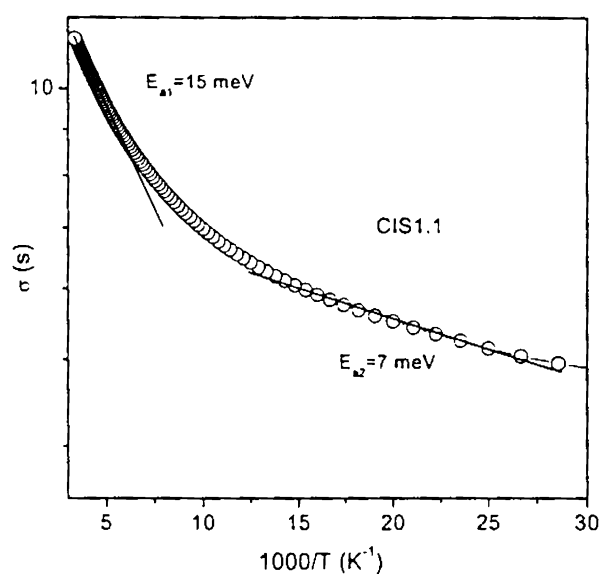


Figure 5.16: Variation of conductivity with inverse temperature for CIS1.1 (log scale)

ii. Cu/In ~1.3

The variation of conductivity with temperature in the range 50 -300 K for CIS1.3 is illustrated in the fig.5.17. From the graph, it is observed that, conductivity decreases with temperature. Hence, the films show pseudometallic nature. This can be attributed to the decrease of mobility due to phonon-assisted scattering occurring for the charge carriers [19, 20].

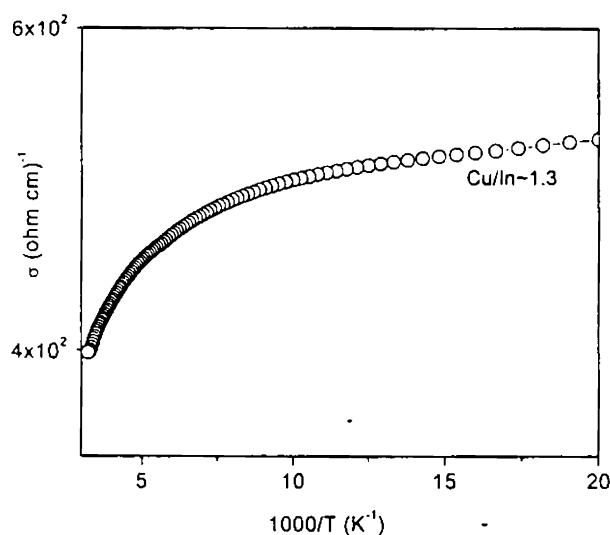


Figure 5.17: Conductivity vs. inverse temperature for CIS1.3

5.2.2.6.2 Hall Effect

Compositional dependence of electrical parameters such as resistivity (ρ), mobility (μ) and carrier concentration (n or p) studied by hall measurement data are given in table 5.4. Theoretical and experimental details are described in chapter 1. From the results, it is clear that when Cu/In ratio is 0.9, the films are slightly p-type. As the ratio increases, film becomes more p-type and finally when the ratio is 1.3 the films exhibit degenerate p-type nature. In the case of CIS0.9, p-type nature may be due to copper vacancies [18, 21]. For CIS1.1 and CIS1.3, possible acceptor levels are Cu_{In} and V_{In} . However, formation energy of V_{In} is larger compared to Cu_{In} [22].

Sample	resistivity (ρ) Ohm cm	mobility (μ) ($cm^2V^{-1}s^{-1}$)	Hall coeff. (cm^3C^{-1})	carrier density(cm^{-3})	Type of carriers
CIS0.9	1.15×10^4	8.23	1.95×10^6	1.74×10^{14}	P
CIS1.1	1.58×10^{-2}	0.05	2.3×10^{-2}	2.7×10^{19}	P
CIS1.3	5.0×10^{-3}	0.02	0.62×10^{-2}	10^{22}	P

Table 5.4: Hall measurement data on CIS of various compositions

5.2.2.6.3 Photoconductivity

Investigation of photoconductive properties is very important from both basic as well as application point of view. In the present study, conductivity due to illumination and decay after cutting off illumination are carried out for films with various compositions. For that, sample of same size as dark conductivity measurement was prepared. Sample was illuminated using a tungsten halogen lamp. Intensity of illumination was 80 mW/cm^2 . Conductivity under illumination and the decay pattern after illumination is plotted using SMU and ICS software as described in chapter 4.

Figure 5.18 depicts the photoresponse of the film, CIS0.9. The light is turned on at A and after 60 s of illumination the light is switched off at B. From the graph it is seen that during illumination current through the sample gradually increases and reaches a saturation value. At the instant of cutting off the illumination, current decays to its dark value. In this case, photocurrent (ΔI) is $0.5 \mu\text{A}$.

Photoresponse of the film CIS1.1 is illustrated in fig.5.19. Here, photocurrent is $6 \mu\text{A}$, which is one order in magnitude larger than that of Cu/In ratio 0.9. Also, decay is slower than that of film with Cu/In ratio 0.9.

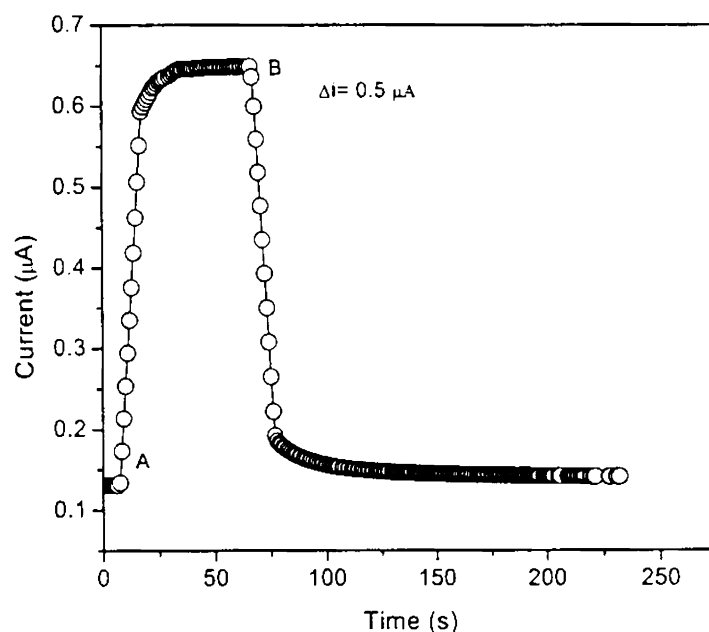


Figure 5.18: Photoresponse of CuInSe_2 film having Cu/In ratio 0.9

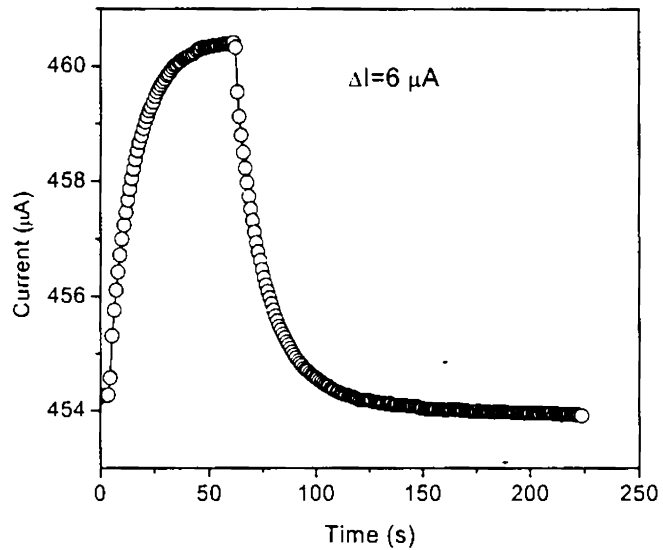


Figure 5.19: Photoresponse of CuInSe_2 film having Cu/In ratio 1.1

When the Cu/In ratio is 1.3, surprisingly the film shows negative photoconductivity. During illumination dark current gradually decreases and when illumination is cut off, current gradually rises to its dark value.

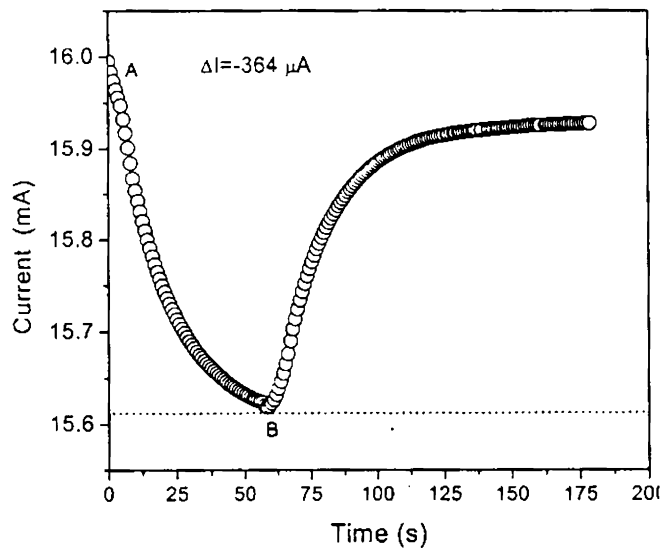


Figure 5.20: Photoresponse of CuInSe_2 film having Cu/In ratio 1.3

5.2.2.7 Analysis on NaCN treated films

Pal et al., and others [23, 24] reported that degeneracy of highly Cu-rich film is due to the formation of Cu_2Se as subphase in the grain boundary and surface of the film. Cu_2Se could be removed by dipping in NaCN solution so that the film becomes semiconducting.

On the basis of other reports for removing the semimetallic phases by chemical treatments using NaCN or KCN solutions, the same procedure is tried in the present work. The film with Cu/In ratio 1.3 was dipped in NaCN solution for 2 min and washed with distilled water and dried well in room temperature.

Visually a very few holes were present after the dipping process. XRD pattern of the NaCN treated films shows improvement in crystallinity. This is inferred from increased peak height and presence of weak reflections from (101) and (211) planes as clear from fig.5.20 in comparison with that of CIS1.3 (fig.5.4).

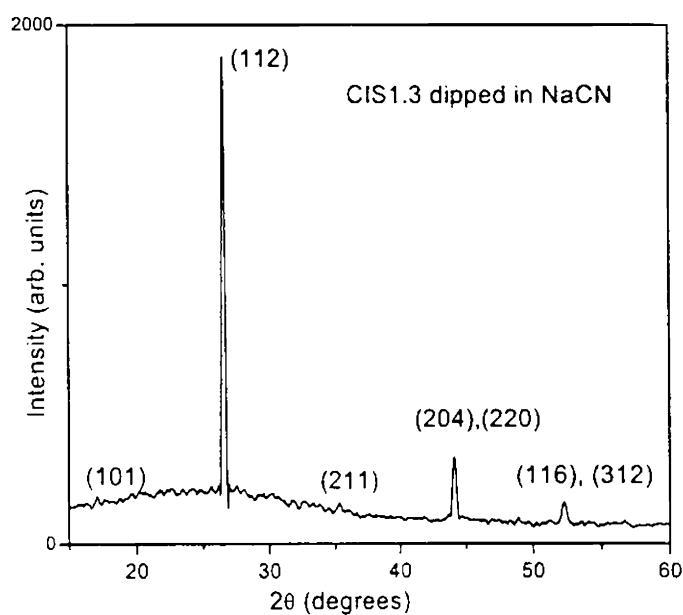


Figure 5.20: XRD pattern of NaCN treated CuInSe_2 film (Cu/In ratio~1.3)

Compositional analysis of dipped sample is done using XPS spectrum given in fig. 5.21(a) and (b) which show the profile montage and depthwise percentage of atomic concentration respectively. From these figures, it is found that copper layer near the surface (upto 5th cycle) is removed due to etching in NaCN solution. Towards the interior, the film is Cu-rich but Cu/In ratio is lesser than the as-prepared CIS1.3 and there is no change in ratio between In and Se in the film.

Optical transmittance spectrum of the dipped film compared to the as prepared film is shown in fig. 5.21. After dipping, the free carrier absorption is significantly decreased which shows the lowering of defect density. In the absorption spectrum, the band tailing is also reduced which again supports the reduced defect density. Band gap evaluated from the plot of $(\alpha h\nu)^2$ vs. $h\nu$ (fig. 5.22) is 0.96 eV.

Hall measurements give the carrier density $n=2.32 \times 10^{16} \text{ cm}^{-3}$, mobility $\mu = 10.4 \text{ cm}^2 \text{ V}^{-1} \text{ s}^{-1}$. Resistivity = 25.8 ohm cm. Temperature dependence of dark conductivity shows semiconducting behaviour, negative temperature coefficient, above 150 K as illustrated in fig.5.23. Activation energy is found out as 170 meV. Hence, semimetallic nature of the film when Cu/In ratio is 1.3, is removed by treatment with NaCN solution. Photoresponse of the film also confirms the same result as given in fig.5.24, which shows that conductivity increases under illumination.

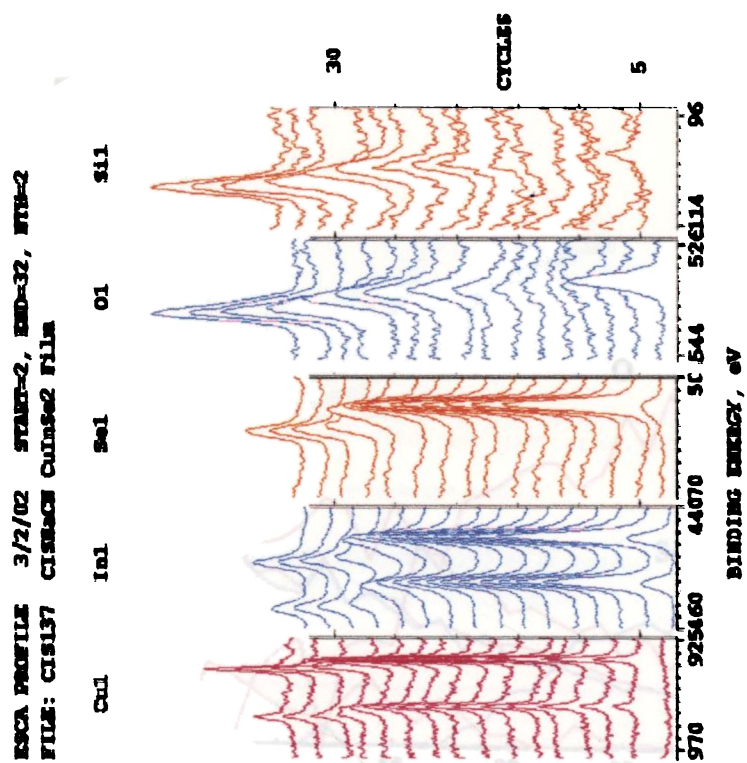


Figure 5.21(a): XPS profile montage of CIS1.3NaCN

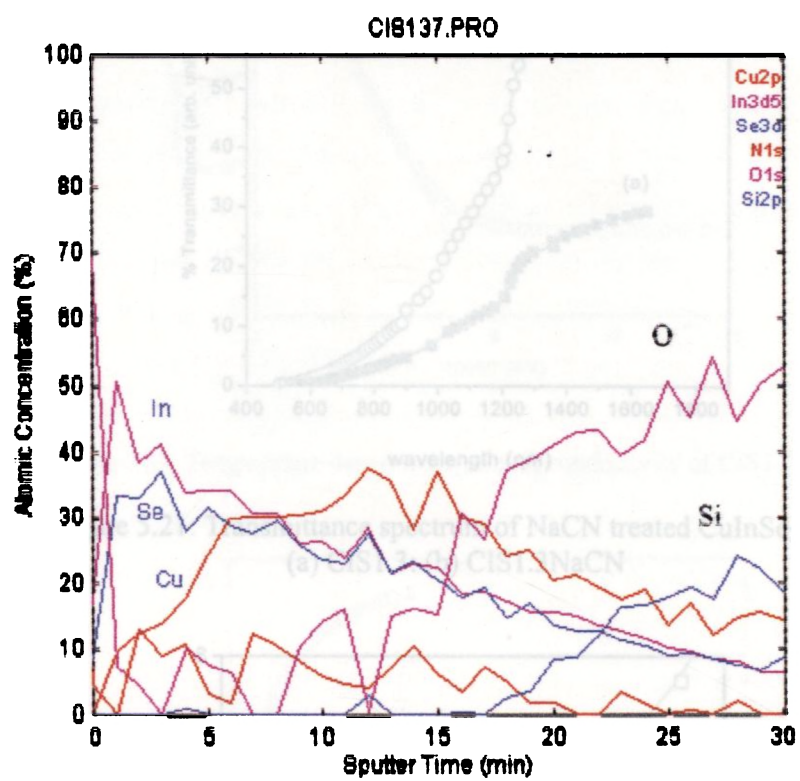


Figure 5.20(b): Depth profile of % atomic concentration of CIS1.3NaCN

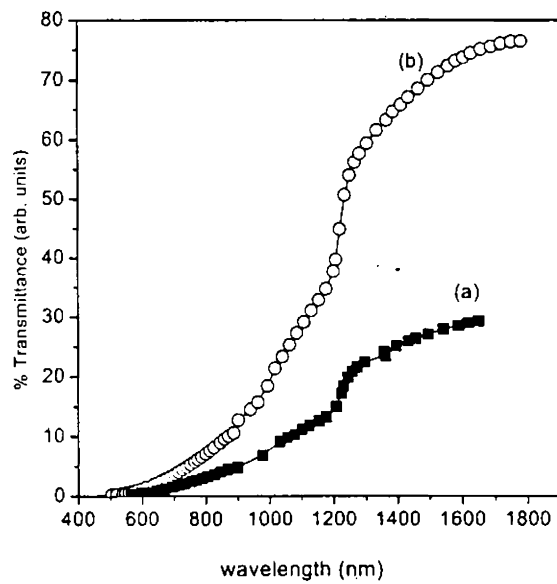


Figure 5.21: Transmittance spectrum of NaCN treated CuInSe_2 film
(a) CIS1.3: (b) CIS1.3NaCN

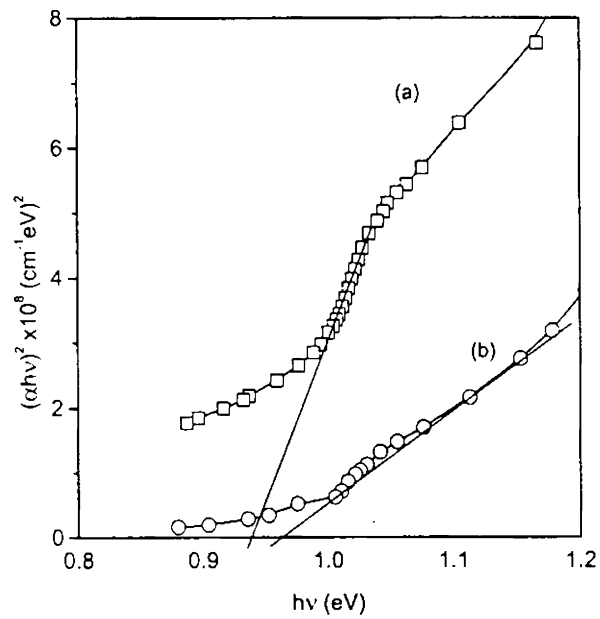


Figure 5.22: Plot of $(\alpha h\nu)^2$ vs. $h\nu$ of
(a) CIS1.3: (b) CIS1.3NaCN

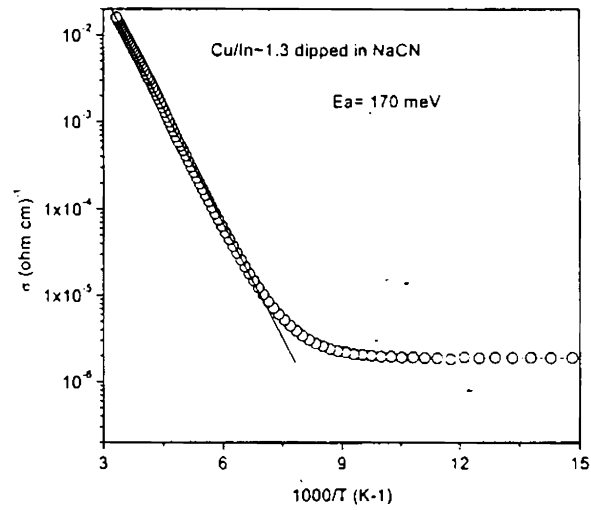


Figure 5.23: Temperature dependence of dark conductivity of CIS1.3NaCN

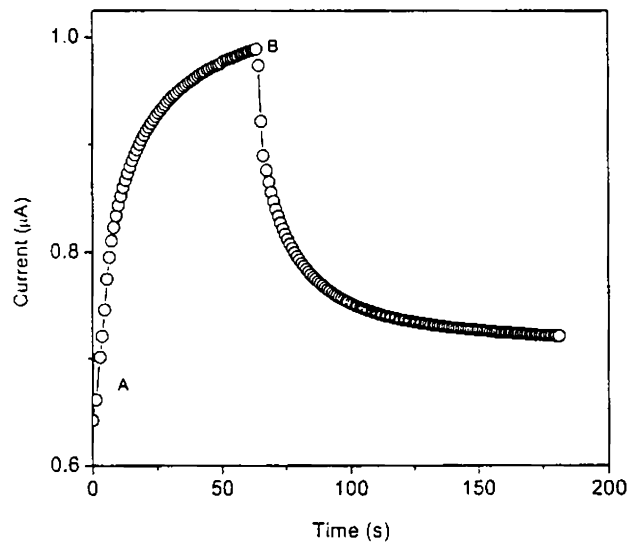


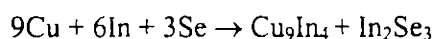
Figure 5.24: Photoresponse of NaCN treated films

5.2.3 Discussion

The SEM analysis shows granular type growth for CuInSe₂ films. Average grain size estimated from the graph is 0.2 μm. It can be inferred that surface of the film is uniform as only few lumps or distinct growths are observed in the micrograph.

Crystallographic studies reveal that polycrystalline CuInSe₂ films of chalcopyrite structure is formed due to annealing the Se/In/Cu stack layers at 673 K. From the XRD patterns of films formed at different temperatures, growth process is analysed. At 423 K, major phase is Cu-In alloy along with In₂Se₃, formed by diffusion of Cu into In melt and Cu-In alloy acts as precursor for selenisation to form CuInSe₂. CuInSe₂ growth starts at 473 K. Growth of the phase continues to result in improvement in crystallinity indicated by increase in peak height. The film grows such that (112) plane is perpendicular to the substrate. Typical chalcopyrite CuInSe₂ film is formed at 673 K annealing for 1h. Grain size of the sample (CIS400) is evaluated using Debye Scherrir formula, as 150 Å. This is different from the value obtained from the SEM. Such differences were observed by Khare et al., [25] explained this as assuming that each grain observed under the microscope is a cluster of submicroscopic crystallites [26]. From SEM we observe the surface morphology while XRD measurements give the average from the bulk of the film. The reaction kinetics can be written as-

At 423 K,



At 473 K,



At higher temperatures, the growth of CuInSe₂ continues until complete interlayer mixing of these binary compounds and metals leading to single phase CuInSe₂ at 673 K.

Growth of the film with compositional variation expresses that when Cu/In ratio is ~ 0.5, very small amount of CuInSe₂ is formed. As the ratio increases grain size increases and reaches saturation when the ratio is 1.6. Many authors reported

large grain size for Cu-rich films. When the ratio is 1.8, presence of far excess Cu-reduces the stoichiometry of the films resulting in reduced grain size.

XPS analysis of all the films with various composition show that the BE of Se $3d_{5/2}$ level has considerable shift from the elemental state which corresponds to that in CuInSe_2 phase. Interlayer mixing of Cu, In and Se diffusion is very effective by the annealing process [27]. This is very clear from the uniform distribution of Cu, In and Se in the depth profile of the films.

Optical transmittance of films formed at different annealing temperatures shows the growth process. Here, an onset of decrease of transmittance of films formed higher than 473 K shows that significant growth of CuInSe_2 film occurs above this temperature, which is in agreement with the XRD analysis. This type of growth analysis was reported by other groups [].

The increase in α with Cu concentration near the fundamental absorption edge may be understood as perturbation of the band structure due to the presence of defects. This perturbation is related to the quantity and nature of defects, which include vacancies and antisites in Cu-rich material [28]. In the present case, band gap decreases from 1 eV to 0.94 eV with increase in Cu/In ratio from 0.5 to 1.3. For, Cu rich films, significant band tailing effect observed in the absorption spectrum. The phenomenon is due to continuous distribution of defect states in grains and grain boundaries which produces gap-states near the band edge [28, 29].

Electrical conductivity and hall measurements show that carrier concentration increases due to which resistivity decreases, with increase of Cu/In ratio. Temperature dependence of dark conductivity reveals that the activation decreases with increase in Cu content. There is a possibility of incorporation of Cu inclusions at the grain boundaries which may passivate the charged states occupied at the grain boundaries [25]. Lower value of activation energy for Cu/In \sim 1.1 than that for Cu/In \sim 0.9 may be due to combined effect of increase in grain size and passivation of grainboundary mentioned above. Cu-deficient films are slightly p-type and Cu-rich films are strongly p-type and becomes degenerate when Cu/In

ratio is 1.3. Band tailing in absorption spectra for highly Cu-rich films supports the high carrier concentration in these films.

p-type conductivity in Cu-deficient films may be due to V_{Cu} . In Cu-rich films (Cu/In ratio 1.1) Cu_{In} antisites are the possible defects act as acceptor level. V_{Se} and Cu_i (Cu-inclusions) defects are also possible in Cu-rich films. However, since the films are p-type, these two defects are not significant. Further increase in Cu may result increase in Cu_{In} defect or hole density. At the same time the passivation of grain boundary by Cu_i may become prominent which enables the free carrier flow and the material becomes degenerate. This Cu can also act as recombination centers of carriers under illumination. Photoresponse is very sensitive to variation in Cu/In ratio. Photocurrent decay with time shows a persistence of photoconductivity (PPC). Potential barrier at the grain boundaries may separate the charges and delay the recombination process and thus causes the long-time relaxation. [30, 31]. Surprisingly, illumination of the film having Cu/In ratio 1.3 results in decrease in current. Sheinkman et al.,[33] described this phenomena as photoelectric fatigue or type II relaxation or negative photoconductivity. They explained this phenomenon generally as due to some photochemical reaction producing new recombination centers. Here, in highly Cu-rich films, presence of Cu inclusions in the grain boundary may act as recombination center for carriers photogenerated carriers [32].

After dipping in NaCN solution grain size decreases. Treatment of Cu-rich films removes the excess copper inclusions from the grain boundary, which increases the grain boundary potential. This may be the reason of increased activation energy for these films. The film becomes semiconducting and photoconducting property is regained.

5.3 Part B: Thermal diffusion of Cu into In_2Se_3 film

Another method for the preparation of $CuInSe_2$ films is developed which involved annealing the bilayer consists of Cu over In_2Se_3 . In 1996, Zweigart et al reported similar process for preparing CIS films leading to highly efficient solar cells. They achieved 14% efficiency for the cells fabricated using the films

prepared by this method. They referred this process as ‘inverted process’ because, in contrary to the traditional Cu-rich/Cu-poor sequences, this process starts with extreme Cu-poor precursor, i.e., In_2Se_3 [33].

5.3.1 Experimental details

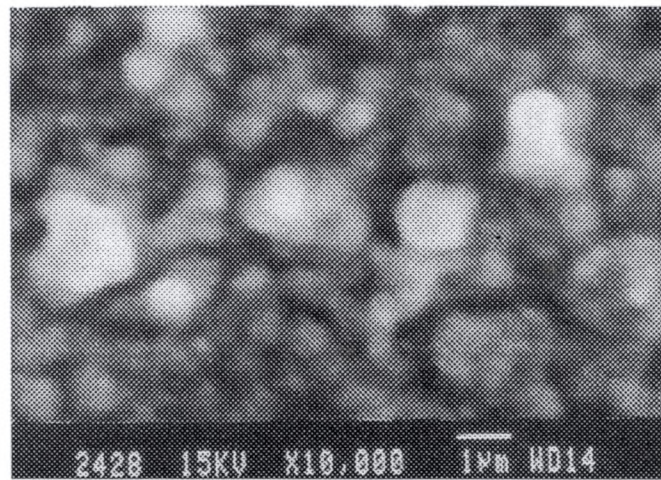
The overall process consists of three steps. In the first step, indium selenide films (IS100) were prepared on glass substrates as described in chapter 4. In the next step, Cu layer of thickness 200 Å was deposited on the In_2Se_3 layer using vacuum evaporation as described in sec. 5.2. Final step involved subsequent annealing of this multilayer, $\text{In}_2\text{Se}_3/\text{Cu}$ in vacuum for 1h at different temperatures viz., 473 K, 523 K, 573 K and 673 K. Annealing conditions were same as in SEL technique. Structural changes taking place in the multilayer, due to annealing at different temperatures was analysed using XRD, XPS and optical studies. The results are described the following sections. The rate of annealing was 3 K/min. Here, annealing was done directly to the final temperature unlike in the SEL technique. This type of samples are named hereafter as CISB200, CISB250, CISB300 and CISB400. At the optimized temperature films were prepared by diffusion of Cu layer thickness of 150 Å and 250 Å.

From structural studies of these films, annealing temperature was optimized as 673 K. Compositional and optical characterization of the films were carried out using XPS and optical transmission and absorption spectra. Growth process with increase in copper content were analysed using structural studies.

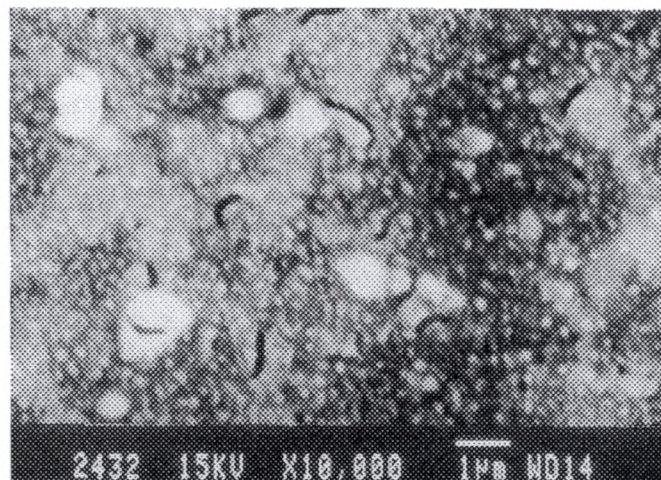
5.3.2 Characterization

5.3.2.1 Morphological studies

Morphology of un-annealed $\text{In}_2\text{Se}_3/\text{Cu}$ bilayer is shown in fig.5.25 (a). Surface nature of copper is not clear in the micrograph. Distinct microscopic Cu-crystallites are not distinguishable in the micrograph. In the annealed film, granular shaped grains are very clear (fig. 5.25 (b)).



(a)



(b)

Figure 5.25: SEM of (a) un-annealed $\text{In}_2\text{Se}_3/\text{Cu}$ (b) CISB

5.3.2.2 XRD

Structural analysis of the films obtained at different annealing temperatures was done using XRD to observe the growth process. Figure 5.26(a) shows the XRD pattern of un-annealed $\text{In}_2\text{Se}_3/\text{Cu}$ bilayer. In this graph, only one peak is present at $2\theta = 23.5^\circ$, $d = 3.82 \text{ \AA}$. This corresponds to $\gamma\text{-In}_2\text{Se}_3$ as described in section.4.3. On annealing at 473 K, a very weak peak is arising at $2\theta = 26.45^\circ$, $d = 3.34 \text{ \AA}$ as observed in fig.5.26(b). There is a strong peak of Cu-In alloy is present as in the SEL process.

As temperature increases from 473 K, three peaks of chalcopyrite CuInSe_2 are the only peaks present as depicted in graphs 5.26(c), (d) and (e). Also peak height increases with annealing temperature. This implies an increase in volume fraction of CuInSe_2 phase with (112) orientation being the most predominant. Again 673 K is found to be the optimum annealing temperature to get good crystallinity. The temperature, 673 K is thus optimized as in the case of SEL process and further studies were done on samples formed at this temperature.

Structural variations of films having various copper content are given in fig. 5.27. The peak height is minimum when the Cu thickness is 150 \AA as in fig. 5.27 (a) and increases with Cu thickness and it is maximum when Cu layer thickness is 250 \AA . From this, Cu layer thickness 250 \AA was selected as optimized thickness of the representative sample.

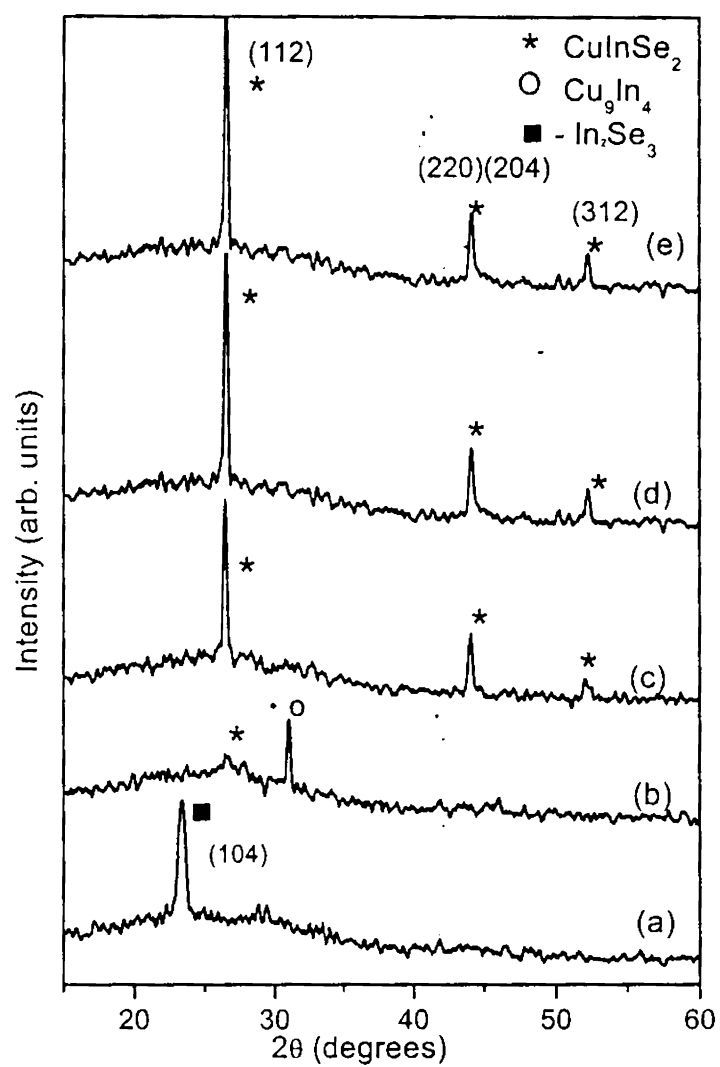


Figure 5.26: XRD patterns of $\text{In}_2\text{Se}_3/\text{Cu}$ samples (a) un-annealed (b) CISB200 (c) CISB250 (d) CISB300 (e) CISB400

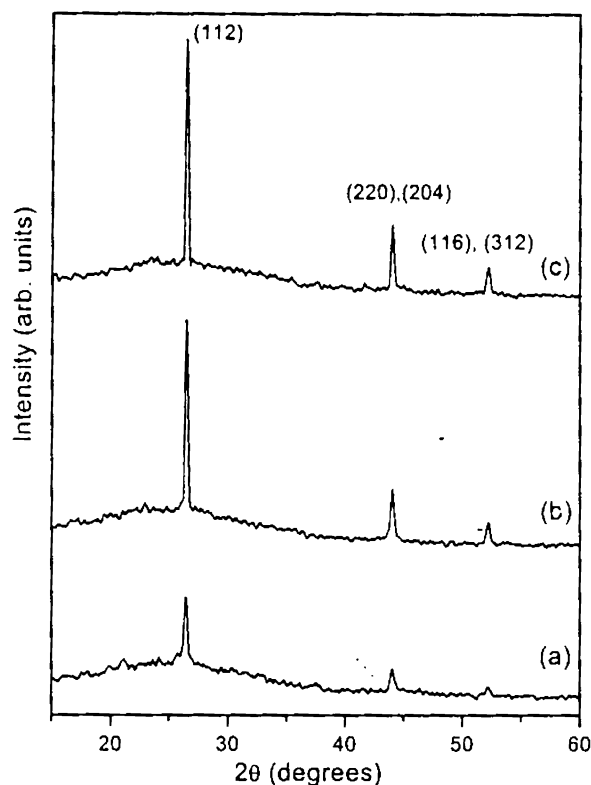


Figure 5.27: XRD patterns of CISB with various Cu thickness
 (a) Cu~150 Å (b) Cu~200 Å (c) Cu~250 Å

5.3.2. 3 XPS

XPS profile montage and depth profile of atomic concentration of un-annealed $\text{In}_2\text{Se}_3/\text{Cu}$ sample is given in figures 5.28 (a) and (b) respectively. These profiles clearly show two distinct layers, top one is Cu and bottom layer is In_2Se_3 layer. The profile montage and depth profile of atomic concentration of CISB sample are shown in fig.5.29(a) and (b) respectively. In fig.5.29(a) BE values of Cu and In do not show any shift from the elemental state, but Se $3d_{5/2}$ shows shift from the elemental state value of 55.5 eV to 54.5 eV. This value corresponds to BE of Se $3d_{5/2}$ level in CuInSe_2 . The figure reveals the uniform diffusion of Cu into In_2Se_3 from surface to substrate region. Depth profile of atomic concentration shows uniform ratio of Cu, In and Se and Cu/In ratio is ~ 1.3 .

ESCA PROFILE 4/12/01 START=2, END=32, NTH=3
 FILE: CIS095 No.2 In2Se3/Cu on Glass

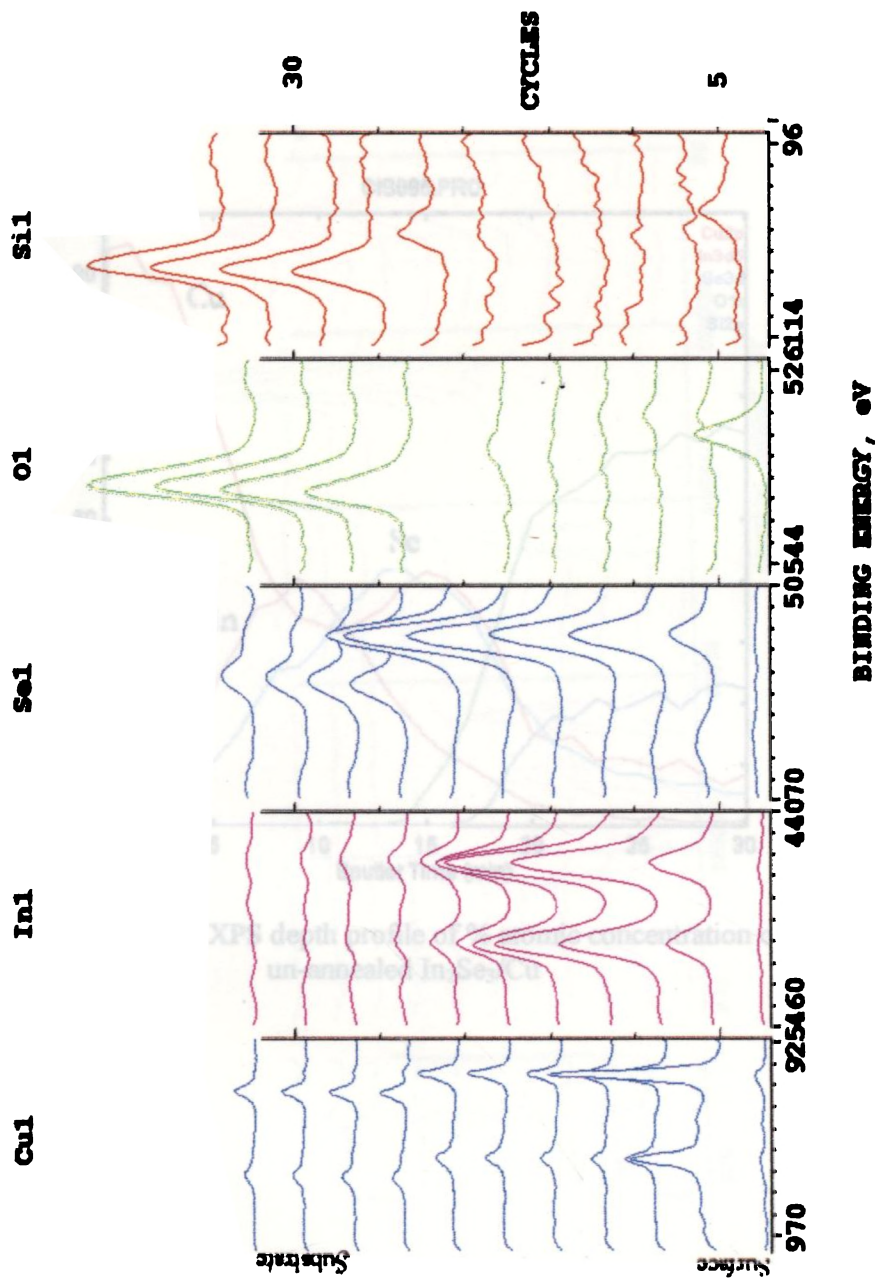


Figure 5.28 (a): XPS profile montage of un-annealed In₂Se₃/Cu

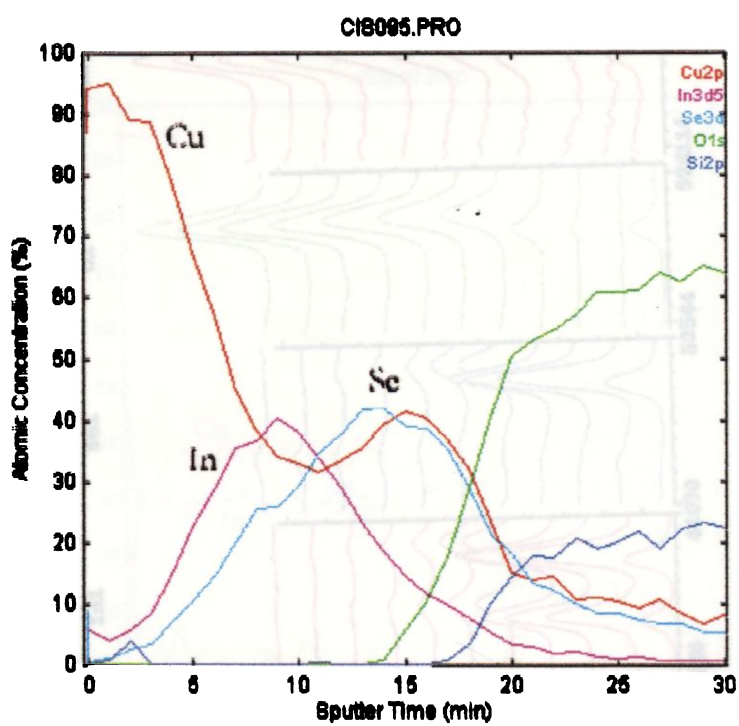


Figure 5.28(b): XPS depth profile of % atomic concentration of un-annealed $\text{In}_2\text{Se}_3/\text{Cu}$

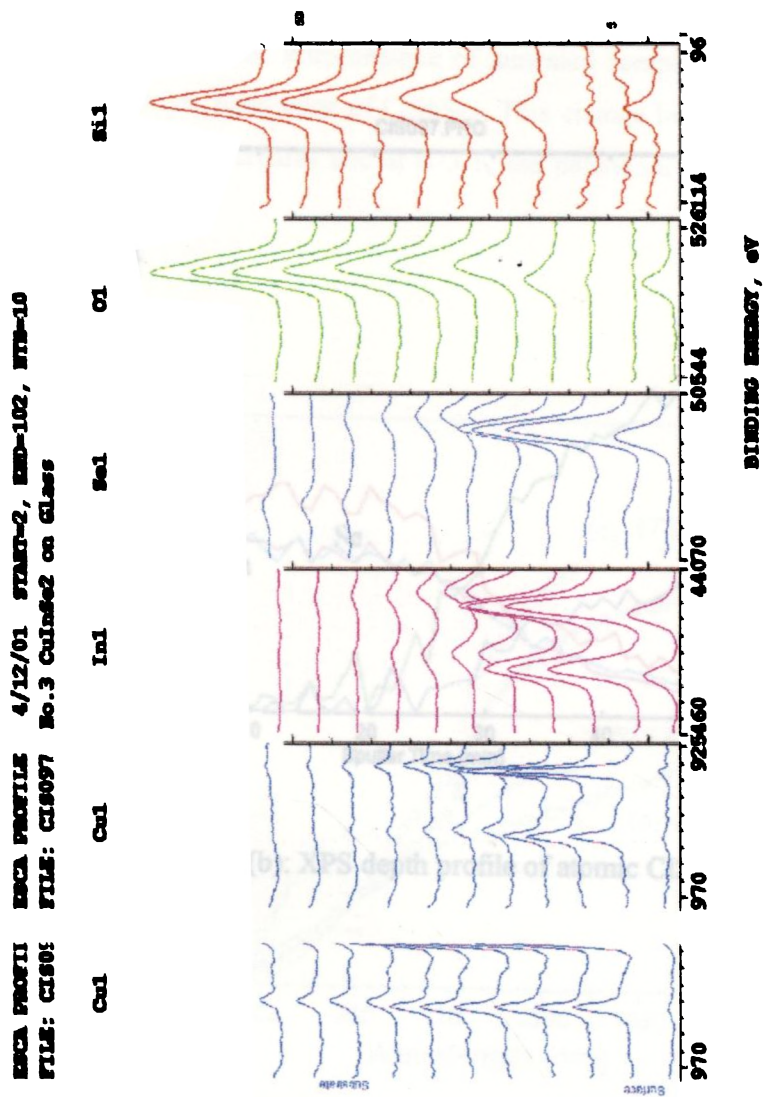


Figure 5.29(a): XPS profile montage of typical CISB

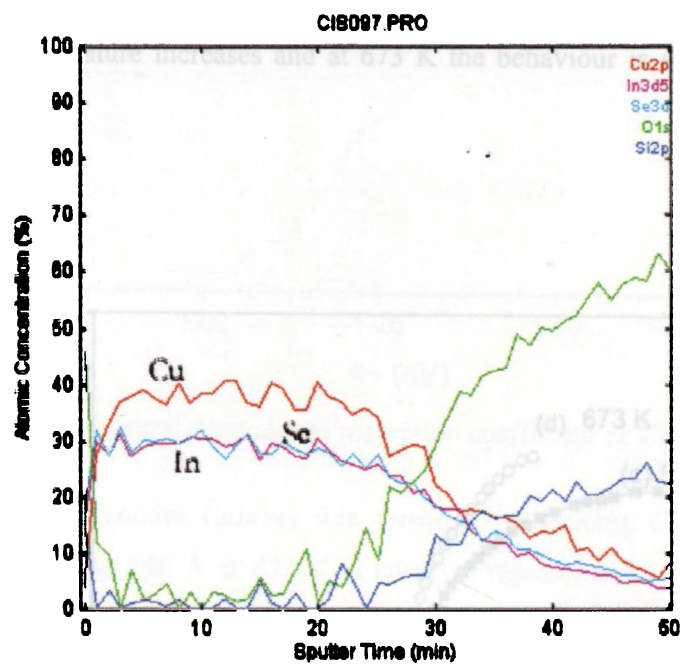


Figure 5.29 (b): XPS depth profile of atomic CISB

5.3.2.4 Optical Characterisation

Wavelength dependence of optical transmittance of CISB samples formed at different temperatures is illustrated in fig. 5.31. When compared with the as prepared $\text{In}_2\text{Se}_3/\text{Cu}$ bilayer, transmittance of annealed samples exhibit an abrupt change near 1200 nm, band edge of CuInSe_2 . This change becomes prominent as annealing temperature increases and at 673 K the behaviour is similar to that of CuInSe_2 .

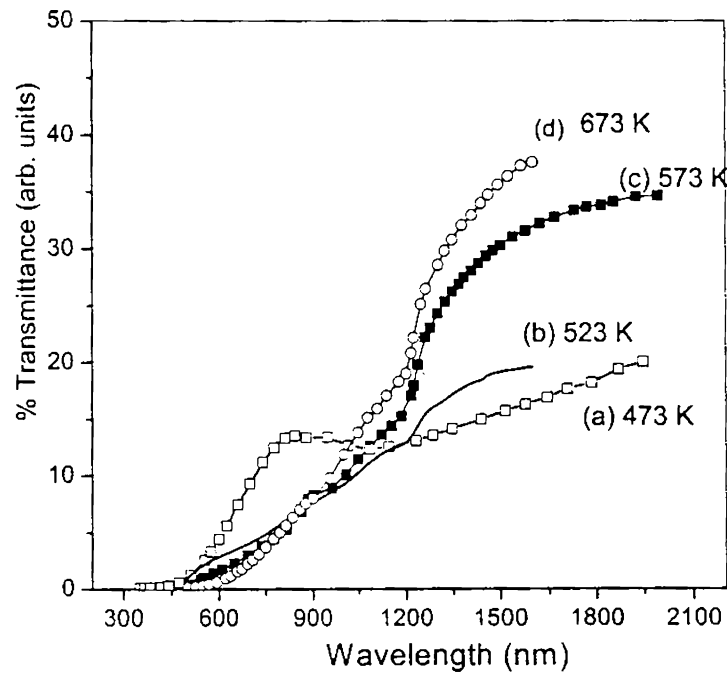


Figure 5.30: Transmittance spectra of $\text{In}_2\text{Se}_3/\text{Cu}$ stack layer
(a) un-annealed; (b) CISB200; (c) CISB250; (d) CISB300; (e) CISB400

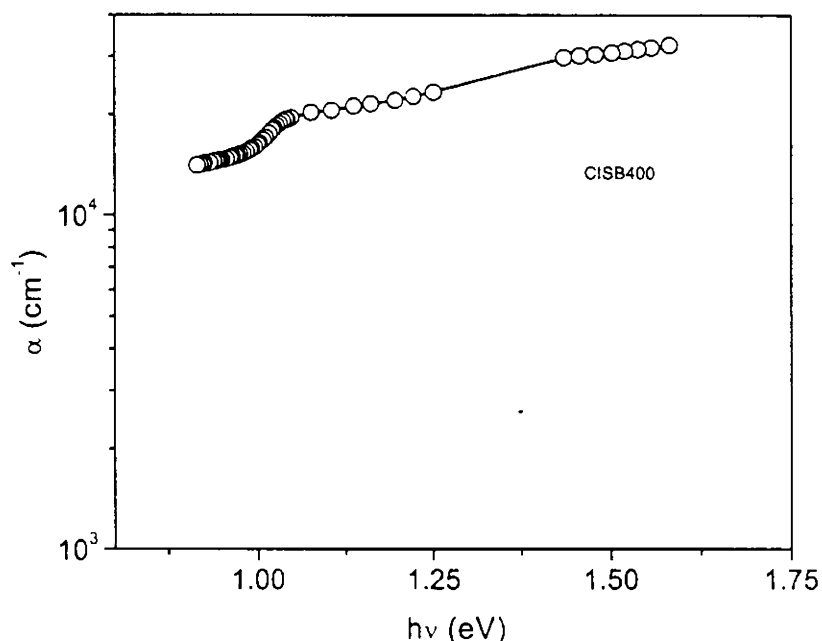


Figure 5.31: Spectral dependence absorption coefficient of CISB sample

From these studies CuInSe_2 film formed by annealing $\text{Cu/In}_2\text{Se}_3$ bilayer having Cu thickness 250 \AA at 673 K is taken as representative sample. Further analyses were done on these films.

Variation of absorption coefficient (α) with $h\nu$ for the sample CISB is depicted in the fig. 5.31. Band gap of the film is evaluated from the plot of $(\alpha h\nu)^2$ Vs $h\nu$ and is shown in fig. 5.32. The value obtained is 0.95 eV which is same as the Cu-rich film formed in the SEL process. Band tailing is also significant in this film.

5.3.2.5 Electrical characterisation

Hall measurements were carried out on CISB samples. The electrical parameters are resistivity = $1.23 \times 10^{-3} \text{ ohm cm}$, mobility = $0.8 \text{ cm}^2\text{V}^{-1}\text{s}^{-1}$, charge density = $1.23 \times 10^{21} \text{ cm}^{-3}$. The film showed p-type conductivity and since carrier concentration is very high, it behaves as degenerate semiconductor as in the case of CIS1.3 prepared by SEL process.

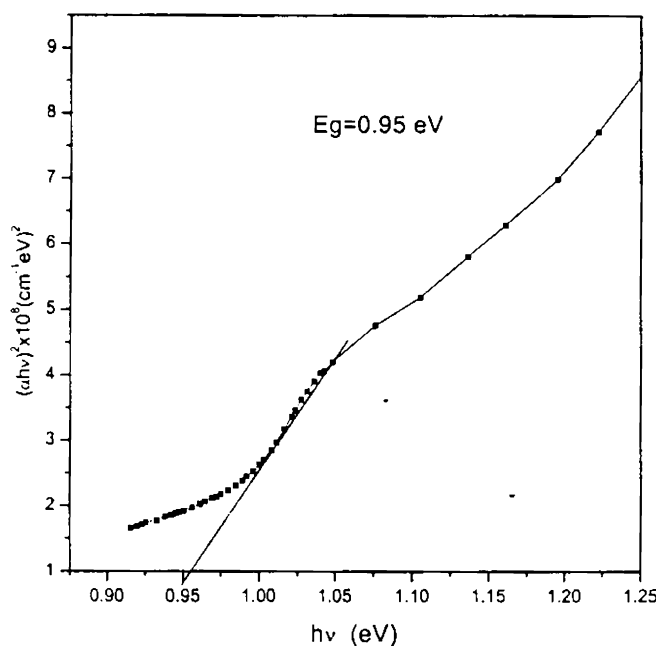


Figure 5.32: Plot of $(\alpha h\nu)^2$ vs. $h\nu$ of sample CISB400

5.3.3 Discussion

The growth process is almost similar as in the case of SEL process. Morphological studies show that the surface of CuInSe_2 films formed by annealing $\text{In}_2\text{Se}_3/\text{Cu}$ bilayer at 400°C is uniform without any lump-like structure. Grain size is of the order of $0.2\ \mu\text{m}$ as in the case of samples formed in SEL process. XRD analysis shows that the films are formed in chalcopyrite structure. Here also, diffusion of Cu into In_2Se_3 layer results in Cu-In precursor which undergoes selenisation by Se-layer. Films are growing with 112 preferred orientation. With increase in Cu layer thickness, film grows along the same orientation. Optical transmittance spectrum shows a gradual change in transmittance near band edge, $1200\ \text{nm}$. Band tailing is very clear in the absorption spectrum, which is due to the presence of high defect density. This results in high hole density. Further studies were not done in this type of sample as it exhibits same properties as that of CIS samples.

5.4 Conclusion

CuInSe₂ thin films were prepared using two different methods. First method was SEL technique which involves annealing process of the stacked layer of structure Glass/a:Se/In/Cu. Second process was thermal diffusion of Cu into In₂Se₃ in which In₂Se₃ films were prepared by annealing SEL structure of Glass/a:Se/In. Pollution free selenisation of Cu-In layer avoiding toxic gases such as Se vapour or H₂Se gas was developed to prepare CuInSe₂ films. Even though films obtained from both methods were having similar properties, first method was chosen as convenient. Probability for selenium loss was also less in this method.

References

- [1] F.O. Adurodija, M.J. Carter and R. Hill, *Sol. Energy Mater. and Sol. Cells*, 37 (1995) 203
- [2] Sandeep Verma, Nese Orbey, Robert W. Birkmire and T.W. Fraser Russell, *Prog. Photovolt. Res. Appl.*, 4 (1996) 341
- [3] Gary Hodes and David Cahen, *Solar Cells*, 16 (1986) 245
- [4] G. Masse and K. D. Jessas, *Thin Solid Films*, 237 (1994) 129,
- [5] L. L. Kazmerski, S. Ayyagari, G. A. Sanborn, F. R. White and A. J. Merrill, *Thin Solid Films* 37 (1976) 323
- [6] Sung Chan Park, Doo Youl Lee Ahn, Kyung Hoon Yoon, Jinsoo Song, *Sol. Energy Mater. Sol. Cells* 69 (2001) 99
- [7] J. F. Moulder, W. F. Stickle, P. E. Sobol and K. D. Bomben: Handbook of X-ray Photoelectron Spectroscopy, Perkin-ElmerCo., Eden Praire, MN, 1992
- [8] H. Sakata and H. Ogawa, *Sol. Energy Mater. Sol. Cells*, 63 (2000) 82
- [9] J. Herrero and C. Guillen, *J. Appl. Phys.* 69 (1991) 429
- [10] *J. Appl. Phys* J.R. Tuttle, D. Albin, R. J. Matson and R. Noufi, *J. Appl. Phys.*, 66 (1989) 4405.
- [11] L.Y. Sun, L.L. Kazmerski, A.H. Clark, P.J. Ireland and D.W. Morton. *J. Vac. Sci. Technol.*, 15 (1978) 265
- [12] S. M. Firoz Hasan, L. Quadir, Kh. S. Begum, M. A. Subhan, Kh. M. Mannan, *Sol. Energy Mater. Sol. Sells*, 58 (1999) 349
- [13] C. Guillen, E. Galiano and J. Herrero, *Thin Solid Films* 195 (1991) 137
- [14] R. Noufi, R. Axton, C. Herrington and S. K. Deb, *Appl. Phys. Lett.* 45 (1984) 668
- [15] H. Neumann and R. D. Tomlinson, *Solar Cells*, 28 (1990) 301
- [16] C. Rincon and R. Marquez, *J. Phys. Chem. Solids*, 60 (1999) 1865
- [17] J. Schmidt, H. H. Roscher, R. Labusch, *Thin Solid Films*, 251 (1994) 116
- [18] T. Datta, R. Noufi and S. K. Deb, *Appl. Phys. Lett.*, 47 (1985) 1102]
- [19] R. D. L. Kristensen, S. N. sahu and D. Hanemen, *Sol. Energy Mater.* 17 (1988) 329

-
- [20] S. M. Foroz Hasan, M. A. Subhan and Kh. M. Mannan, *J. Appl. Phys.*, 32 (1999) 1302
- [21] H. Neumann and R.D. Tomlinson, *Solar Cells*, 28 (1990) 301
- [22] S.W. Wasim, *Sol. Cells* 16 (1986) 289
- [23] R. Pal, K.K. Cattopadhyay, S. Chaudhuri and A.K. Pal, *Thin Solid Films*, 254 (1995) 111
- [24] N. Stratieva, E. Tzvetkova, M. Ganchev, K.K. Kochev and I. Tomov, *Sol. Energy Mater. Sol. Cells*, 45 (1997) 87
- [25] M. Varela, E. Bertrain and J. L. Morenza, *Thin Solid Films*, 130 (1985) 155
- [26] N. Khare, G. Razzini and L. Pera Ldo Bicelli, *Thin Solid Films*, 186 (1990) 113
- [27] Bindu. K, Lakshmi. M, Bini. S, Sudha Kartha. C, Vijayakumar. K.P, Abe. T, Kashiwaba.Y, National Symposium on Science and Tehnology of Vacuum and Thin films (IVSNS-2001)-PP33
- [28] J. R. Tuttle, D. Albin, R. J. Matson, and R. Noufi, *J. Appl. Phys.*, 66 (1989) 4408
- [29] I. Martil, J. Santamaria, E. Iborra, G. Gonzlalez-Diaz and F. Sanchez-Quesada, *J. Appl. Phys.*, 62 (1987) 4163
- [30] Y. G. Zhao, G. Zhao, J. L. Brebner, A. Bensaada and R. A. Masu, *Semicond. Sci. Technol.*, 7 (1992) 1359
- [31] M. K. Sheinkman and A. Ya. Shik, *Sov. Phys. Semicond.* 10 (1976) 128
- [32] Masayuki Tanda, Susumu Manaka, Akira Yamada, Makoto Konagai and Kiyoshi Takahashi, *Jpn. J. Appl. Phys.*, 32 (1993) 1913
- [33] S. Zweigart S. M. Sun, G. Bilger, H.W.Schock, *Sol. Energy Mater. Sol. Cells*, 41/42 (1996) 219

CHAPTER 6

RECOVERY AND REUSE OF SELENIUM PRECIPITATE FROM CHEMICAL BATH

6.1 Introduction

Real challenge in the optimization of a CBD technique for the deposition of thin films of a particular material is to reduce the precipitate in the bath to obtain high thin film yield. However even in the best optimized conditions, precipitate forms a major product of the condensation process for film formation. In the case of large area or large scale deposition, when one considers cost-effectiveness of the process also, this becomes a major problem. Moreover treatment of the precipitate as a waste especially in large scale process is another difficult problem when it contains materials like selenium or cadmium.

There are different ways in which the precipitate can be used as a precursor for other deposition techniques [1] as the compound formed in the bath is highly stoichiometric. M.T.S. Nair et al., used CdSe precipitate from the chemical bath to prepare CdSe/ZnO coatings by screen printing [2]. The same group used cupric sulfide precipitate from the bath for thin film deposition, to get composite coatings made of CuS dispersed in poly acrylic acid with propylene glycol used as a solvent [3]. Purity of the precipitate from chemical bath is superior to the initial chemicals in the bath because impurities whose concentrations are less than the required quantity to form solid precipitate, are left behind in the solution. P.K. Nair et al., also reported that it is possible to use dried precipitate of bismuth sulphide from the bath as source for vapour phase deposition [4]. In some cases, filtered precipitate is converted into starting chemical by reacting with acids.

In the present investigation, selenium precipitate from the reaction bath for the film deposition was recovered as to make starting solution for deposition of selenium film. Both copper selenide and copper indium selenide films were

prepared using these selenium films. Copper selenide films were prepared using selenium powder from the bath. All the films were characterized using different techniques and compared with those of films deposited using commercially obtained selenium pellets [5].

6.2 Experimental

The precipitate formed in the bath during selenium thin film was filtered, rinsed well in distilled water and dried in hot air oven. It was found that after drying, red colour of the fine powder was changed to dark gray. Then, 0.2 M Na_2SeSO_3 solution was prepared using this powder as described in chapter 3. During preparation of Na_2SeSO_3 solution, it was observed that the recovered selenium precipitate was easily soluble than the powdered commercially available pellets. Then selenium films were deposited using this solution as explained in section 3.2, from 0.0125 M 20 ml Na_2SeSO_3 solution at pH \sim 4.5. CuInSe_2 films were prepared by annealing the SEL structure, Se/In/Cu as explained in chapter 5. Hereafter the selenium film prepared using recovered precipitate is named, as a-SeR and those prepared using commercial Se powder as a-Se. CuInSe_2 films prepared using a-Se and a-SeR are named as CIS and CISR respectively.

With the intension of using the selenium precipitate from the reaction bath for preparation of binary selenides by CBD technique, copper selenide (Cu_2Se) was prepared from the reaction bath consisting of aqueous solution of CuSO_4 , Trisodium citrate and Na_2SeSO_3 described in chapter 2. Such copper selenide thin films are named as CSR.

6.3 Characterization

Structural, compositional and optical properties of all the films were analysed using XRD, XPS and UV-vis-NIR transmission and absorption spectral studies.

6.3.1 XRD

XRD patterns of powdered commercial selenium and selenium powder from the bath are shown in fig. 6.1(a) and (b) respectively. In fig. 6.1 (a) weak

peaks at 2θ values 20.75° , 23.2° , 24.8° , 28.8° , 29.5° and 31.5° and the respective d - values calculated are 4.27, 3.83, 3.58, 3.09, 3.02 and 2.83 Å. Strong peaks at 2θ values 24° , 30.2° , 41.6° , 44.1° , 45.85° , 51.95° and 56.15° corresponding to d - values of 3.70, 2.95, 2.16, 2.05, 1.97, 1.75 and 1.63 are present in fig. 6.1 (b). It is quite clear from the figure that, commercial powder exhibits monoclinic structure [JCPDS 24-714] while recovered precipitate from CBD has hexagonal structure [JCPDS 27-601]. Planes corresponding to the d -values are shown in the figure.

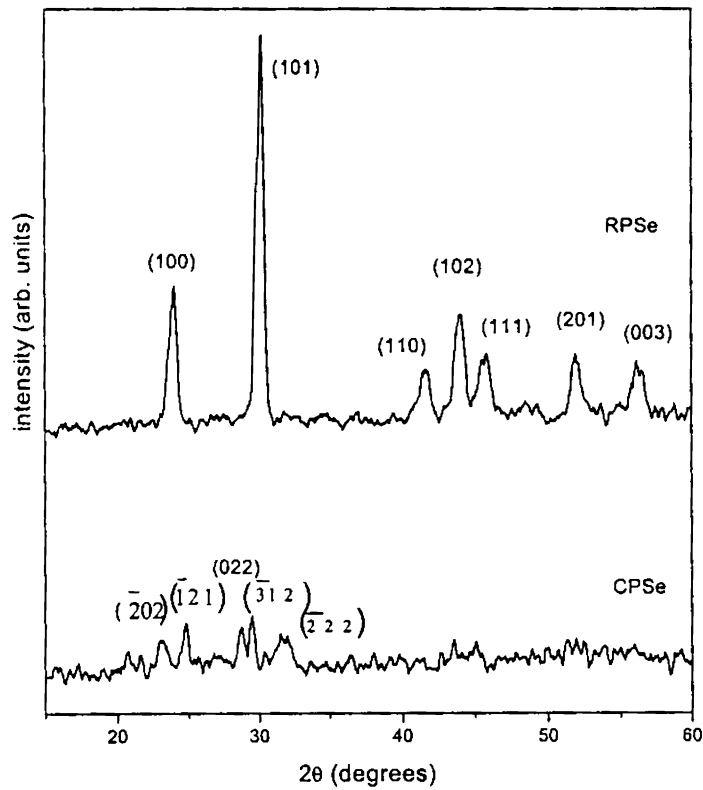


Figure 6.1: XRD patterns of selenium powder
(a) commercial; (b) dried precipitate from CBD
(drawn in same scale)

Crystallographic structure of CISR is illustrated in fig. 6.2 (a) in comparison with CIS. Both are identical having three distinct peaks corresponding to chalcopyrite phase as described in chapter 5. XRD of CSR is depicted in fig. 6.3 and this can be compared with that of CS sample depicted in chapter 2 (sec. 2.3.1, fig.2.1). Here also, film CSR has the same peaks as that of sample CS, as cited there.

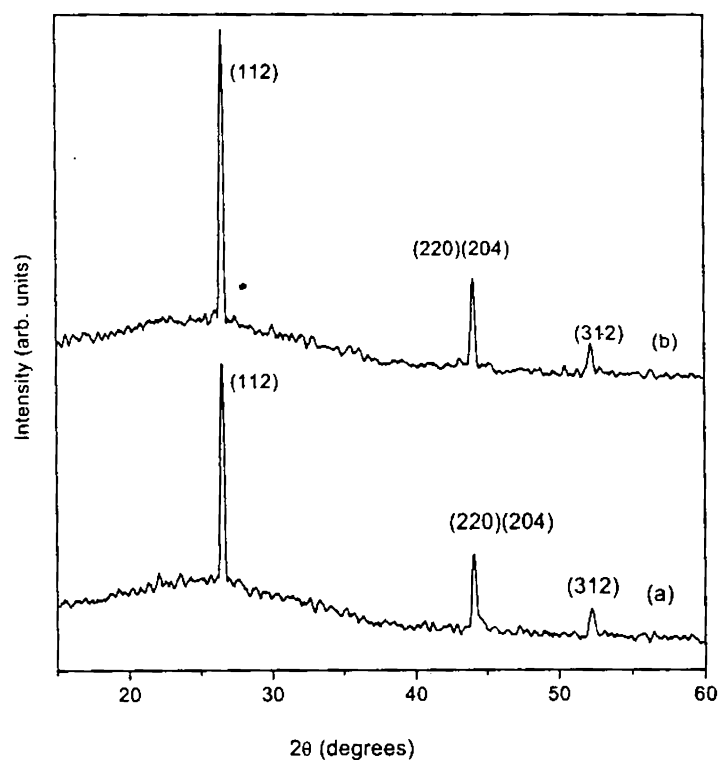


Figure 6.2: XRD pattern of (a) CIS (b) CISR
(same intensity scale)

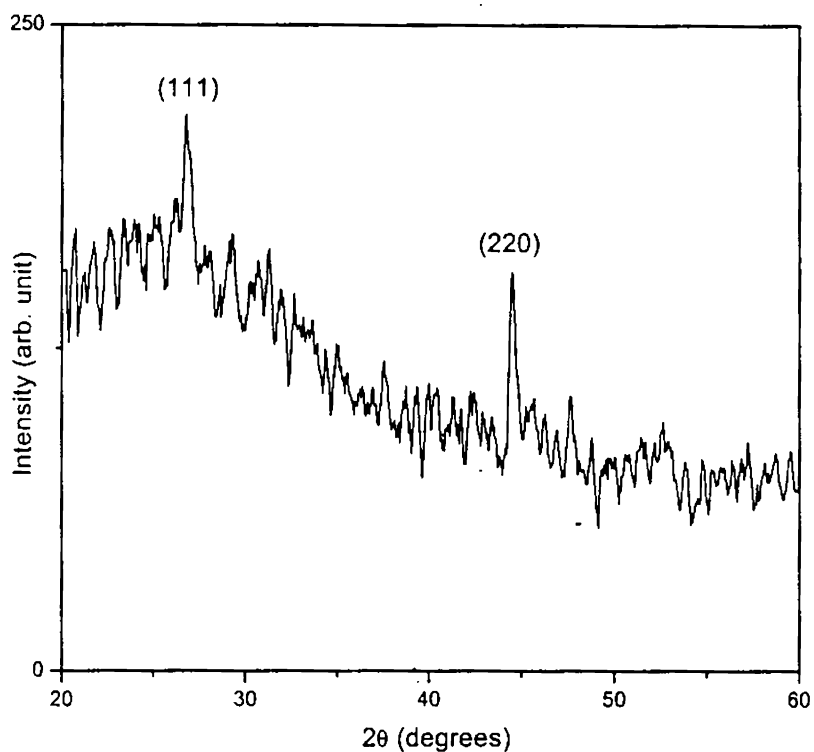


Figure 6.3: XRD pattern of CSR sample

6.3.2 XPS

XPS profile montage of SeR is given in fig. 6.4. The spectrum is similar with that of Se sample (up to 12th cycle) prepared using powdered selenium pellets (section 3.4.5). In the spectrum Binding energy (BE) of Se 3d_{5/2} (55.5 eV) coincides with that in elemental state. XPS profile of CISR sample is shown in fig. 6.5. BE of Cu, In and Se in fig. 6.5 corresponds to that of CIS samples described in chapter 5.

6.3.3 Optical properties

Wavelength dependence of optical absorption of Se and SeR are given in fig. 6.6. Band gap (E_g) of selenium films (Se and SeR) are evaluated as 2.12 eV from the plot of $(\alpha h\nu)^2$ vs. $h\nu$, as depicted in fig. 6.7. For CuInSe₂ films, (CIS and CISR), transmittance spectra (fig. 6.8) shows a rapid change near the absorption edge, $E_g \sim 1$ eV.

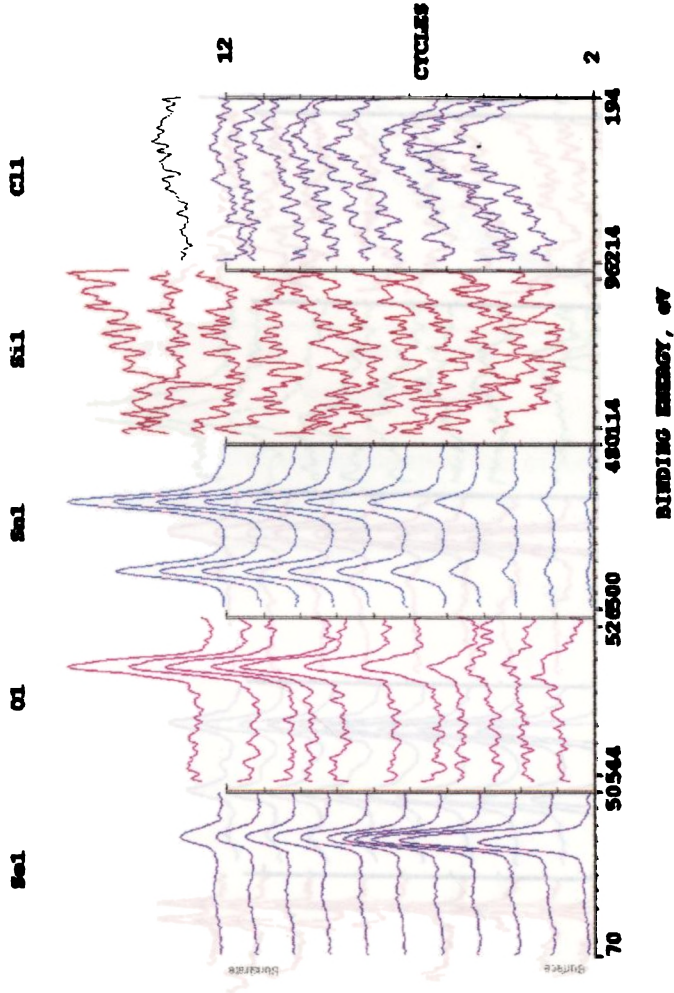


Figure 6.4: XPS profile montage of SeR

ESCA PROFILE 1/4/02 START=2, END=52, FWH=5
FILE: CIS131 2 CISR CuInSe2 Film

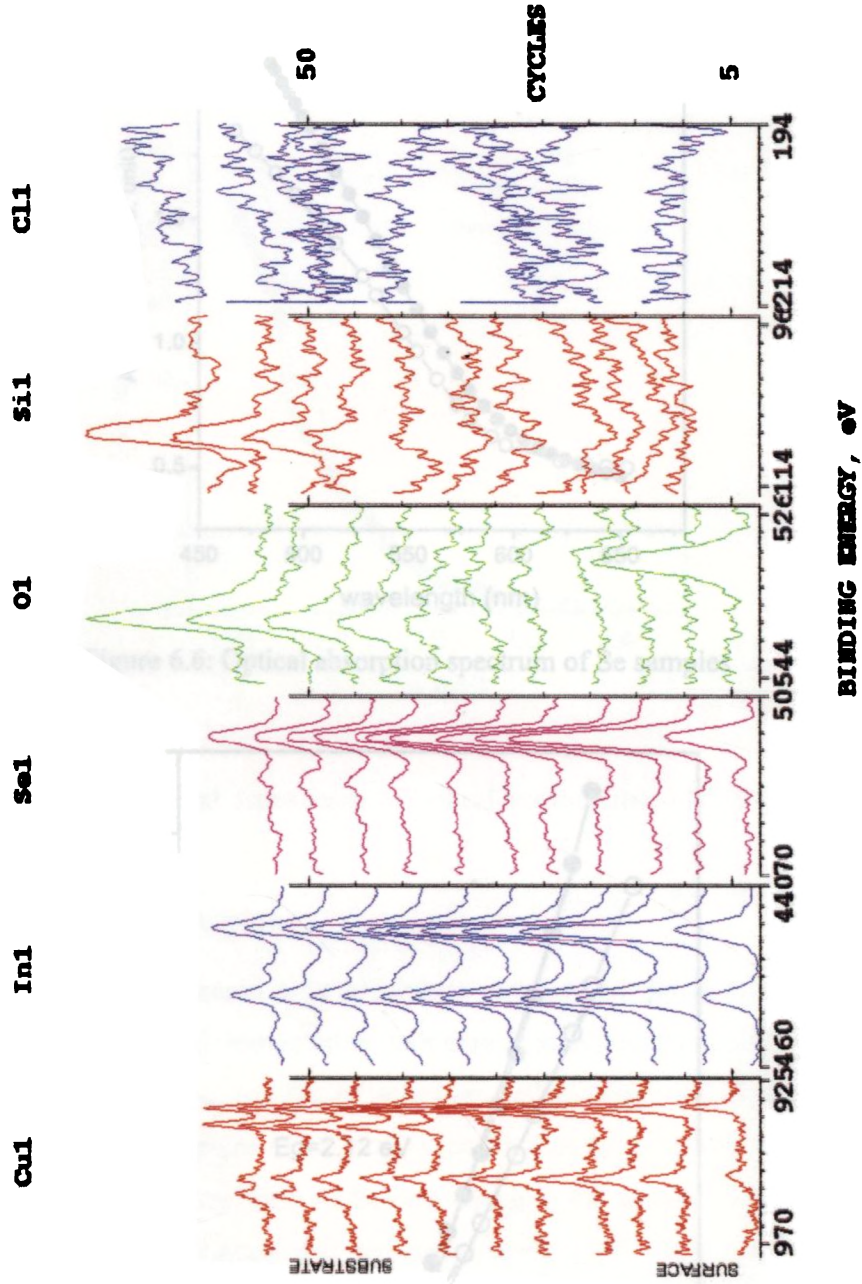


Figure 6.5: XPS depth profile of CISR

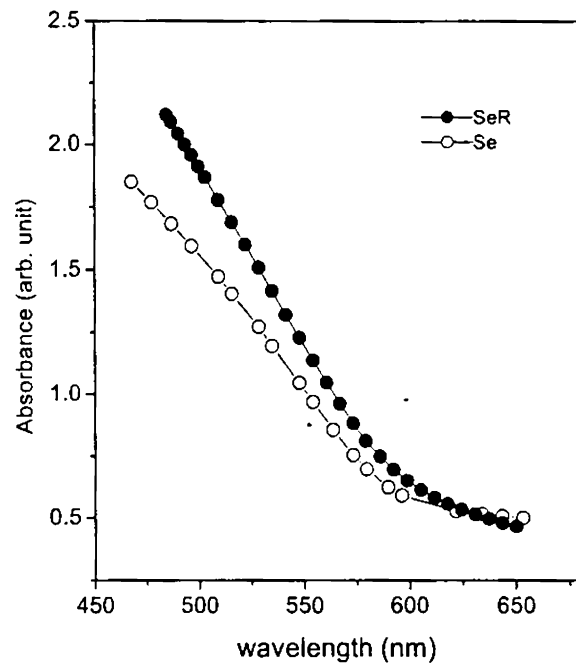
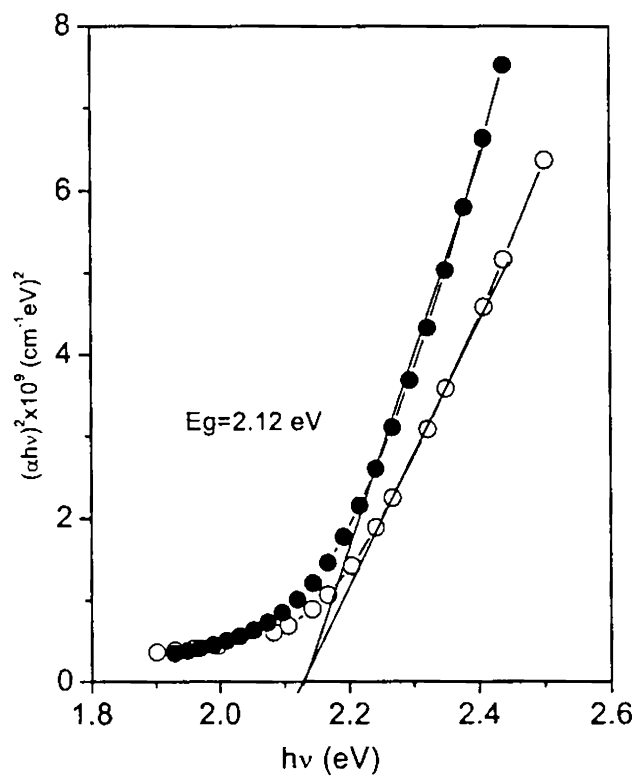


Figure 6.6: Optical absorption spectrum of Se samples

Figure 6.7: Plot of $(\alpha h\nu)^2$ vs. $h\nu$ of Se samples

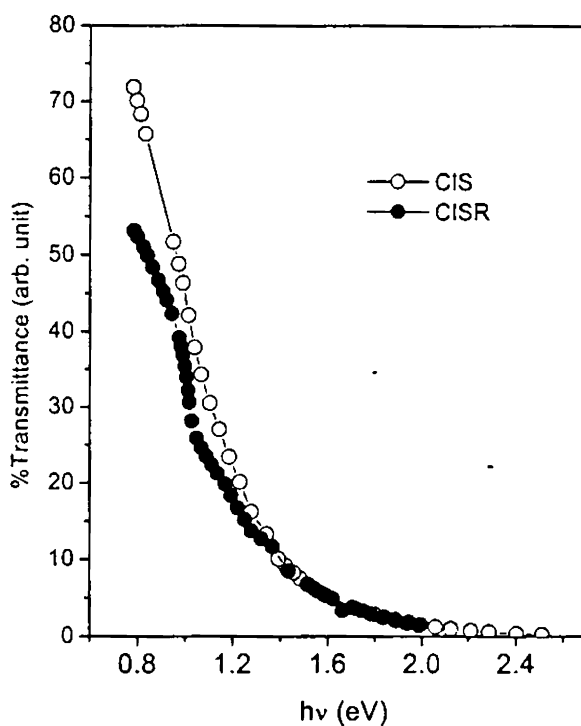


Figure 6.8: Spectral dependence of Optical transmittance of CIS samples

6.4. Results and discussions

Red coloured α -Se precipitate remained in the reaction bath after thin film deposition was converted to dark gray powder, during drying. The initial material for deposition, powder of selenium pellets were also gray in colour, having monoclinic structure. XRD studies reveals that the α -Se powder from CBD is converted to hexagonal form of Se on keeping in the ambient conditions. This type of phase transformation was reported elsewhere [6]. Also, the precipitate from CBD has better crystallinity compared to the powder of selenium pellets indicated by high intense and narrow peaks in fig. 6.1 (b). However, the selenium films formed using both types of powder by dissolving into aqueous Na_2SO_3 solution, exhibit amorphous nature. From this, it can be inferred that in the solution, $(\text{SeSO}_3)^{2-}$ behaves independent of crystallographic nature of Se in the solid phase. Optical properties of selenium films are also similar, having identical band gaps [5].

XRD patterns of copper indium selenide samples prepared using selenium precipitate as initial material are identical (fig. 6.2) to that formed using original selenium powder. Both are polycrystalline having chalcopyrite structure as indicated by planes corresponding to the d-values in the figure. These films have preferred orientation along (112) plane. Composition and purity of the films are also retained as that of the films formed from powdered selenium pellets as the starting material. Optical properties of the films are also similar with rapid decrease of transmittance near the fundamental absorption edge ~ 1 eV as evidenced from spectral dependence of optical transmittance.

Crystallographic studies of copper selenide thin films reveal that films prepared using selenium precipitate and powdered pellets are cubic Cu_{2-x}Se phase (fig. 6.3.)

6.6 Conclusion

Selenium precipitate remaining in the bath after the deposition of selenium film was recovered for the use as starting material for further deposition process. Composition and purity of selenium film prepared using selenium precipitate from the reaction bath was analysed using XPS and compared with that of the film prepared using powdered pellets. CuInSe_2 films were prepared by the SEL technique using selenium precipitate as initial material and structural, compositional and optical properties were analysed. Cu_{2-x}Se films were also prepared using the selenium precipitate by CBD technique and structure of the film was compared with that of Cu_{2-x}Se film deposited using commercial selenium powder..

From the above investigation it can be concluded that when selenium film is deposited using CBD technique the wastage of selenium can be minimized. This is achieved by reusing the selenium precipitate remaining in the solution.

References

- [1] P.K. Nair, M.T.S. Nair, V.M. Garcia, O.L. Arenas, Y. Pena, A. Castillo, I.T Ayala, O. Gomezdaza, A. Sanchez, J. Campos, H. Hu, R. Suarez and M.E. Rincon, *Solar Energy Materials and Solar Cells* 52 (1998) 313
- [2] M.T.S. Nair, P.K. Nair, H.M.K.K. Pathirana, R.A. Zingaro and E.A. Meyers, *J. Electrochem. Soc.* 140 (1993) 2987
- [3] P.K. Nair, V.M. Garcia, A.M. Fernandez, H.S. Ruiz and M.T.S. Nair, *J. Phys. D* 24 (1991) 441
- [4] M.T.S. Nair and P.K. Nair, *Semicond. Sci. Technol.* 6 (1991) 132
- [5] Bindu. K, Jayaprasad. A, Sudha Kartha. C, Vijayakumar. K.P, Abe. T and Kashiwaba.Y, Accepted for *World Renewable Energy Congress*, Cologne, June 29, 2002
- [6] S.G. Hansen and T.E. Robitaille, *Thin Solid Films* 151 (1987) 111

CHAPTER 7

SUMMARY AND CONCLUSIONS

Copper indium based solar cells are the most targeted device as it can replace the most widely used Si solar cells if low cost process are developed for large area and large scale fabrication. In this context, we developed an inexpensive, pollution free hybrid process for the preparation of CuInSe₂ films.

Of all methods, CBD is the most simple and low cost method for large area fabrication of thin films. In this method, to deposit device quality films, the parameters to be controlled are molarity of the reactants, pH and temperature of the bath. For the preparation of single phase ternary CuInSe₂ films control of these parameters is difficult as the formation of binary phases such as Cu₂Se is more probable. However, CBD is a well-suited technique for the deposition of binary films.

The first attempt was conversion of Cu₂Se prepared using CBD into CuInSe₂ by diffusing indium. Indium layer was deposited over Cu_{2-x}Se using vacuum evaporation and the resulting bilayer was annealed at 573 K in high vacuum (10⁻⁵ mbar). Indium layer of thickness up to 1300 Å was diffused into Cu_{2-x}Se film of thickness ~ 1 μ until Cu/In ratio ~1 as obtained from XPS analysis. Structural analysis using XRD revealed that the indium diffused film consists of mixed phases of unreacted Cu₂Se, In₂Se₃ and traces of CuInSe₂. Even though the optical absorption spectrum showed an increase in absorbance, XPS analysis revealed high deficiency of selenium in the film.

In order to compensate for the Se deficiency, we developed a novel selenisation technique using chemical bath deposited selenium thin film. However, instead of selenizing the indium diffused Cu₂Se film, we adopted Stacked Elemental Layer (SEL) technique to prepare binary and ternary selenides using the selenium thin film.

Deposition of selenium thin film through CBD was achieved by controlling pH value of the Na_2SeSO_3 solution. The optimized conditions were as follows: Well-leached glass substrates were dipped vertically in a 25 ml beaker containing 20 ml (0.025 M) Na_2SeSO_3 solution of pH ~ 4.5 , at room temperature. Orange red coloured selenium thin films of thickness 5000 Å were deposited after 3 h of deposition. XRD analysis showed that the films were amorphous in nature. Formation of elemental selenium thin films was confirmed using XPS, SIMS and ICP. Band gap evaluated was 2.10 eV from optical absorption spectrum and electrically the films were insulator.

Photovoltaic material, indium selenide In_2Se_3 thin films were prepared by annealing the stacked layer of structure Glass/a:Se/In in high vacuum in the range of temperature 373-723 K. The films formed at different temperatures were analysed using different techniques. Films formed at 373 K and above 673 K were hexagonal $\gamma\text{-In}_2\text{Se}_3$. For films formed at intermediate temperatures were amorphous in nature.

Depthwise compositional analysis using XPS showed that interlayer diffusion was uniform due to annealing and BE values of In and Se were coinciding with that of In_2Se_3 . Band gap values were estimated from optical absorption spectrum. For the films formed at 373 K, band gap was 1.8 eV and slight difference was observed for other films, which could be correlated to the structural change. Electrical conductivity was decreased with increase in annealing temperature. Both n-type and p-type films were obtained depending on annealing temperature. At room temperature maximum photosensitivity was observed for films formed at 423 K.

Copper selenide (Cu_{2-x}Se) films were prepared by annealing the SEL structure Glass/a:Se/Cu and characterized using XRD, XPS and optical absorption spectrum.

Copper indium selenide thin films were prepared by two different methods. First method was annealing the stacked layer structure of Glass/a:Se/In/Cu. Indium and copper layers were deposited using vacuum evaporation over selenium film. Preliminary analysis of reaction kinetics was analysed using XRD pattern of films formed at different temperatures in the range 423 K- 673 K. It was found that single-

phase (112) oriented chalcopyrite thin films were formed at 673 K. Growth of CIS film with increase in Cu/In ratio was studied using XRD. Band gap reduced with increase in Cu/In ratio and band tailing was observed for highly Cu-rich films. Electrical conductivity enhanced with Cu/In ratio and highly Cu-rich films showed semimetallic behaviour. Hall measurement studies revealed that the films were p-type and hole concentration increases with Cu/In ratio. Photosensitivity was found to be maximum for films having Cu/In ratio ~ 1 and decreases with increase in Cu/In ratio. Semimetallic copper rich films showed negative photoconductivity. When this type of films were treated with NaCN solution, it regained its semiconducting and photoconducting property.

Second method developed was diffused metallic Cu into In_2Se_3 film. Nature of growth of the films with temperature was similar as that of SEL technique except that formation of CuInSe_2 just begins at 473 K while in SEL technique significant growth was observed at 473 K. Also, pin holes were observed in films formed at 673 K. Optical properties were also similar to that of first technique. SEL technique is better than the second method, as the probability of escape of selenium is less in the first technique.

In order to avoid the wastage of material, selenium precipitate remained in the bath after deposition of the film was recovered for the use as starting material for further deposition process. Composition and purity of selenium film prepared using selenium precipitate from the bath was analysed using XPS and compared with that of the film prepared using powdered pellets. CuInSe_2 films were prepared by the SEL technique using selenium precipitate as initial material and structural, compositional and optical properties were analysed. Also, Cu_{2-x}Se films were prepared using the selenium precipitate by CBD technique and structure of the film was compared with that of original Cu_{2-x}Se film.

It is concluded that amorphous selenium thin film could be prepared using CBD. We developed a new pollution free selenisation technique using this selenium film. Indium selenide and copper indium selenide thin films were successfully

prepared using the above selenisation process. Reuse of selenium precipitate from the chemical bath minimized the wastage of material. This could be a promising option for developing much lower cost thin film technology for copper indium selenide and other selenides.

